Wastewater remediation using municipal solid waste-derived hydrochar

CT Dewah

orcid.org/0000-0002-1944-4045

Dissertation accepted in fulfilment of the requirements for the degree *Master of Science in Engineering Science with Chemical Engineering* at the North-West University

Supervisor: Prof S Marx

Co-supervisor: Dr R Venter

Graduation: May-June 2023

Student number: 37066498

DECLARATION

I, Christine Tambudzai Dewah, declare that I am the sole author of the dissertation entitled: **"Wastewater remediation using municipality solid waste-derived hydrochar."** This dissertation is submitted to fulfil the degree in Master of Science in Engineering Sciences with Chemical Engineering to the North-West University, Potchefstroom Campus, South Africa.

.

25/11/2021

C.T. Dewah Date

ABSTRACT

Industrialisation and population growth increase solid waste generation and the release of toxic pollutants into the environment. Therefore, novel approaches are necessary for both wastewater remediation and solid waste management. Current bio-waste adsorbents, such as bio-based activated carbon are expensive because of the high temperatures required for adequate preparation and activation. A promising alternative that can be chemically activated without high temperature is hydrochar, produced via hydrothermal liquefaction of the organic fraction of municipal solid waste. The comparative advantage of hydrochar over other bio-waste adsorbents is the high concentration of oxygen containing surface functional groups (COO-, -OH, -CO- and -C=O) that act as adsorption sites for heavy metals and phenolic components. This study explored the use of hydrochar as a bio-adsorbent in removing alkali and alkaline earth metals and phenolic components from a simulated wastewater stream of the hydrothermal liquefaction process. The simulated wastewater consisted of the five most abundant metals and four most abundant phenolics in the hydrothermal liquefaction aqueous product. These results were compared to adsorption using the real hydrothermal liquefaction aqueous product. Furthermore, the possibility of recovering adsorbed components and regenerating the hydrochar for multiple adsorption cycles was also investigated.

The hydrochar, prepared from hydrothermal liquefaction of the organic fraction of municipal solid waste, was activated by washing with KOH solutions of concentration 0.5 mol/L - 2.5 mol/L and an HCl solution with a concentration of 1.0 mol/L. The hydrothermal liquefaction aqueous phase was characterised to determine the concentrations of metals and phenolic compounds present. Based on the obtained results, the synthetic mixtures were prepared using five most abundant metals K^+ (3653.4 mg/L), Ca^{2+} (2512.9 mg/L), Na^+ (462.7 mg/L), Mg^{2+} (219.7 mg/L) and Fe^{2+} (12.5 mg/L) and four most abundant phenolic compounds vanillyl alcohol (0.59 g/L), resorcinol (0.26 g/L), phenol (0.24 g/L) and guaiacol (0.10 g/L). The adsorption experiments were performed using real wastewater and using the synthetic mixtures. After the adsorption experiments, the adsorption capacity was calculated as the amount of metal or phenolic compound adsorbed on a gram of hydrochar. The experiments were done in triplicates hence the values are averages from the three experiments. The obtained maximum adsorption capacities of hydrochar for metals in in the real wastewater were Ca^{2+} (156.2 mg/g), K^+ (121.3 mg/g), Na^+ (76.9 mg/g), Mg^{2+} (8.7 mg/g), Fe^{2+} (0.68 mg/g) and for phenolics vanillyl alcohol (62.8 mg/g), resorcinol (47.5 mg/g), phenol (27.6 mg/g) and guaiacol (6.1 mg/g). The removal efficiency decreased in the following order:

phenol (92 %) > Fe^{2+} (77 %) > guaiacol (73 %) > resorcinol (59 %) > Mg^{2+} (53 %) > vanillyl alcohol and Ca^{2+} (52 %) > Na^{+} (51 %) > K^{+} (47 %). Henry's law best described the adsorption of Ca^{2+} and Mg^{2+} adsorption, while the Freundlich isotherm best described the adsorption of Na^{+}, K^{+} and phenolic components. The adsorption mechanism for AAEMs and phenolic components proceeded through physical adsorption on the heterogeneous surface of the hydrochar, and the rate of adsorption was limited by intra-particle diffusion. The metal and phenolic component adsorption from the real HTL aqueous product dropped by 8 – 12 % compared to adsorption from the simulated wastewater due to the highly heterogeneous composition of hydrothermal liquefaction aqueous product.

More than 75 % of AAEM and 65 % of phenolic components could be recovered using a 1.0 mol/L HCl solution and a 1.0 mol/L KOH solution, respectively, to chemically re-activate the hydrochar for a further adsorption cycle. The study showed that the hydrochar could be re-used for up to four adsorption cycles before its removal efficiency dropped below 80 %. This study highlights the opportunity to produce a low-cost bio-adsorbent from the organic fraction of municipal solid waste, thereby providing a cost-effective alternative to fossil-based or expensive bio-waste adsorbents. Furthermore, the valorisation of municipal solid waste for wastewater treatment contributes positively to the United Nations Sustainable Goal 6 (Clean water and sanitation). Additionally, through application of proper separation and purification techniques, the recovered phenolic components can supplement or replace fossil-based phenolic platform chemicals currently used in the pharmaceutical and food industries, thus lowering dependence on fossil-based resources, and supporting UN Sustainable Development Goal 12.

Keywords: wastewater remediation, hydrochar, hydrothermal liquefaction, adsorption, metal, phenolics

ACKNOWLEDGEMENTS

"Have I not commanded you? Be strong and of good courage; do not be afraid, nor be dismayed, for the Lord your God *is* with you wherever you go." – Joshua1:9

- Firstly, I want to thank myself for taking this journey walk through it until the end, pushing myself, not giving up.
- Appreciative to my supervisor Professor Sanette Marx for her patience, supervision, assistance throughout the study.
- My co-supervisor, Dr Roelf Jacobus Venter, thank you for your guidance, advice, and support.
- Many thanks to Biofuel's laboratory manager Rene Bekker, for your assistance with ICP-OES, IC, phenolic and sugar HPLC sample analysis, Dr Okolo thank you for assistance with the BET and Mr Shuro thank you for assistance with SEM analysis.
- Grateful to NRF for financial assistance.
- Much love and gratefulness to my mum, Grace Dewah, and my late uncle Obiot Shoko my biggest support system.
- Delighted to my dad, Master Dewah, and sister Carol for their encouragement.
- Lastly, many thanks to friends that supported me throughout this journey.

TABLE OF CONTENTS

DECLARATION IX
ABSTRACT X
ACKNOWLEDGEMENTS XII
TABLE OF CONTENTS XIII
LIST OF TABLES XIX
LIST OF FIGURES XXI
ABBREVIATIONS XXIV

1 INTRODUCTION 1

1.1 BACKGROUND AND MOTIVATION 1
1.2 STATEMENT OF THE PROBLEM AND HYPOTHESIS 5
1.2.1 Statement of the problem 5
1.2.2 Hypothesis 5
1.3 AIM AND OBJECTIVES 5
1.3.1 Research aim 5
1.3.2 Research objectives 6
1.3.3 Project scope 7
1.4 PROJECT OUTLINE 8
REFERENCES 9

2 LITERATURE REVIEW 14

2.1 WASTEWATER, POLLUTION, AND CONTAMINATION 14
2.1.1 Pollutants 15
2.1.2 Metals 17
2.1.2.1 Bio-importance and bio-toxicity of inorganic compounds 17
2.1.3 Phenolic compounds 19
2.1.3.1 Detected valuable phenolics 19
2.1.3.2 Phenolic compound toxicity 20
2.1.4 Multi-component systems 21
2.2 WATER REMEDIATION 21
2.2.1 Conventional methods 22
2.2.1.1 Chemical precipitation 22
2.2.1.2 Chemical oxidation 23

2.2.1.3 Electrochemical oxidation 24
2.2.1.4 Distillation technologies 25
2.2.2 Established recovery processes 25
2.2.2.1 Membrane filtration 25
2.2.2.2 Membrane technologies 27
2.2.2.3 Ion exchange 27
2.2.2.4 Advanced oxidation processes (AOPs) 28
2.2.2.4.1 Photochemical oxidation 28
2.2.2.4.2 Fenton and Fenton like processes 28
2.2.2.4.3 Photo-catalytic oxidation 29
2.2.3 Emerging technologies 29
2.2.3.1 Biosorption 29
2.2.3.2 Adsorption 30
2.2.3.2.1 Adsorbents 32
2.3 BIOCHAR 32
2.3.1 Biochar engineering 33
2.3.1.1 Pyrolysis 33
2.3.1.2 Hydrothermal processes 33
2.3.1.3 Hydrothermal liquefaction (HTL) 34
2.3.2 HTL feedstock 35
2.3.2.1 Agricultural and forest residues 36
2.3.2.2 Industrial by-products and non-conventional materials 36
2.3.3 Municipal solid waste 37
2.3.4 Applications of hydrochar 38
2.3.4.1 Carbon sequestration 38
2.3.4.2 Soil amendment and fertility 38
2.3.4.3 Fuels 39
2.3.4.4 Hydrochar a Catalyst during Heterogeneous Oxidation 39
2.3.5 Hydrochar as an adsorbent 40
2.3.5.1 Mechanisms for hydrochar- adsorption 40
2.3.5.1.1 Physical or surface sorption 41
2.3.5.1.2 Ion exchange 41
2.3.5.1.3 Precipitation and complexation 42

2.3.5.1.4 Electrostatic attraction / repulsion 42
2.3.5.1.5 Electron donor and acceptor interaction 43
2.3.5.1.6 Partitioning 43
2.3.5.1.7 Hydrophobic interactions 44
2.3.5.2 Hydrochar activation 44
2.4 BATCH ADSORPTION 45
2.4.1 Performing adsorption experiments 45
2.4.2 Hydrochar regeneration and reusability 46
2.4.3 Factors affecting adsorption 47
2.4.3.1 Contact time 47
2.4.3.2 Adsorbent Dosage 47
2.4.3.3 Temperature 47
2.4.3.4 pH 48
2.4.3.5 Initial concentration 48
2.5 ADSORPTION KINETIC MODELS 49
2.5.1 Pseudo-1st order model 49
2.5.2 Pseudo 2nd order model 49
2.5.3 Elovich model 50
2.6 MASS TRANSFER 51
2.6.1 Intraparticle diffusion model 51
2.6.2 Boyd intraparticle diffusion model 51
2.6.3 Mass considerations with Biot number 52
2.7 ADSORPTION ISOTHERMS 53
2.7.1 Henry's law 53
2.7.2 Langmuir isotherm 53
2.7.3 Freundlich isotherm 55
2.7.4 Temkin isotherm 55
2.7.5 Dubinin-Radushkevich (D-R) isotherm 56
2.8 THERMODYNAMIC PARAMETERS 58
2.9 CONCLUSION 59
REFERENCES 60
3 EXPERIMENTAL MATERIALS AND METHODS 84

3.1 MATERIALS USED 84
3.1.1 Preparation of glassware 84
3.1.2 Chemicals used 84
3.2 ANALYTICAL TECHNIQUES AND INSTRUMENTATION USED 86
3.2.1.1 Metal identification and quantification: ICP-OES 87
3.2.1.2 Identification and quantification of phenolic components 88
3.2.1.2.1 Total phenol analysis of HTL aqueous phase using Folin-Ciocalteu assay .. 88
3.2.1.2.2 Monomeric phenolics analysis of HTL aqueous phase using HPLC (high-performance liquid chromatography) 88
3.2.1.3 Identification and quantification of organic acids and monomeric sugars in HTL aqueous phase 90
3.2.1.4 Anion and cation identification and quantification using Ion chromatography (IC) 91
3.3 HTL PRODUCTS 91
3.4 ACTIVATION AND CHARACTERISATION PROCEDURES OF HYDROCHAR 92
3.4.1 Activation of hydrochar 92
3.4.2 Characterisation of hydrochar 92
3.4.2.1 Proximate analysis 92
3.4.2.2 Elemental analysis 93
3.4.2.3 Calorific value analysis (HHV) 93
3.4.2.4 Point of zero charge 93
3.4.2.1 Functional group analysis 94
3.4.2.2 Surface topography analysis using scanning electron microscopy (SEM) 94
3.4.2.3 Surface area, pore volume and diameter using Brunauer-Emmett-Teller (BET) 94
3.5 PREPARATION OF SYNTHETIC WASTEWATER 94
3.6 BATCH ADSORPTION EXPERIMENTS 95
3.6.1 Experimental method 96
3.6.2 Fitting with mathematical models 97
3.6.3 Desorption experiments. 97
3.7 ADSORPTION AND DESORPTION EXPERIMENTS WITH HTL AQUEOUS PHASE 98
3.7.1 Adsorption of metals and phenolics from HTL aqueous phase 98
3.7.2 Regeneration and reusability of the hydrochar 98

REFERENCES 99

4 RESULTS AND DISCUSSION 101

4.1 HTL YIELDS 101

4.2 COMPOSITION OF HTL AQUEOUS PHASE (WASTEWATER) 102

4.2.1 Metals present in the wastewater 102

4.2.2 Phenolic compound analysis 103

4.2.3 Organic acids and sugars present in wastewater 104

4.3 RESULTS FOR ACTIVATION AND CHARACTERISATION OF HYDROCHAR 105

4.3.1 Effect of hydrochar activation on the hydrochar and adsorption of metal and phenolic compounds 105

4.3.2 Composition of filtrates from activation of hydrochar 107

4.3.3 Characterisation of unwashed and washed hydrochar 109

4.3.4 The pH point of zero charge (pH_{pZc}) of unwashed and washed hydrochar 110

4.3.5 Hydrochar surface topography before and after adsorption 111

4.3.6 Hydrochar surface properties before and after adsorption 114

4.3.7 Hydrochar surface functional groups 116

4.4 FACTORS AFFECTING THE ADSORPTION OF METALS AND PHENOLS ONTO HYDROCHAR 119

4.4.1 Effect of contact time on the adsorption of metals and phenolics on hydrochar 119

4.4.2 Effect of the initial concentration on the adsorption of metals and phenolic compounds 122

4.4.3 Effect of hydrochar dose on the adsorption of metals and phenolics 126

4.4.4 Effect of temperature on the adsorption of metals and phenolics on hydrochar 128

4.4.5 Effect of pH on the adsorption of metals and phenolics on hydrochar 131

4.4.6 Effect of combining metals and phenols on their adsorption on hydrochar 133

4.5 DESORPTION OF ADSORBED METALS AND PHENOLICS 135

4.6 FITTING THE METALS AND PHENOLICS ADSORPTION DATA WITH KINETIC MODELS 135

4.6.1 Fitting with the pseudo-first-order kinetic model 136

4.6.2 Fitting with the pseudo-second-order kinetic model 138

4.6.3 Fitting with the Elovich kinetic model 141

4.7 MASS TRANSFERS DURING ADSORPTION OF METALS AND PHENOLICS 144

4.7.1 Fitting with Weber and Morris intraparticle diffusion model 144

4.7.2 Fitting with Boyd intraparticle diffusion model 148

4.7.3 Mass transfer behaviour using Biot number 152
4.8 FITTING METAL AND PHENOLIC ADSORPTION DATA WITH ADSORPTION ISOTHERMS 153
4.9 FITTING WITH HENRY'S LAW 153
4.9.1 Fitting with Langmuir isotherm 155
4.9.2 Fitting with Freundlich isotherm 157
4.9.3 Fitting with Temkin isotherm 158
4.9.4 Fitting with Dubinin-Radushkevich isotherm 159
4.9.5 The isotherm fitting curves 161
4.10 THERMODYNAMICS OF METAL AND PHENOLICS ADSORPTION 165
4.10.1 Calculated Enthalpy Change (ΔH), Gibbs Free Energy (ΔG) and Entropy Change (ΔS) from the adsorption data 165
4.10.2 Activation energy 168
4.11 ADSORPTION EXPERIMENTS USING HTL AQUEOUS PHASE (WASTEWATER) 169
4.11.1 Adsorption of metals and phenolics from real wastewater 169
4.11.2 Recovery of adsorbed metals and phenolics 172
4.11.3 Reusability of the hydrochar 174
REFERENCES 178
5 CONCLUSIONS AND RECOMMENDATIONS 181
5.1.1 Conclusion 181
5.1.2 Recommendations 182
ANNEXURE A: CALIBRATION DATA 183
ANNEXURE B: FACTORS AFFECTING ADSORPTION PROCESS RAW DATA 183
ANNEXURE C: ADSORPTION WITH REAL WASTEWATER (HTL-AQ) 215

LIST OF TABLES

Table 2.1: Main features of pressure-driven membrane procedures (adopted from *(Figoli and Criscuoli, 2017)* 26
Table 2.2: The prediction of the n values in Freundlich isotherm 55
Table 3.1: Chemicals used throughout the project 84
Table 3.2: Analytical techniques and instruments used in the study 86
Table 4.1:The metal present in the HTL aqueous phase (wastewater) 102
Table 4.2:Monomeric phenolics detected in HTL aqueous phase by HPLC 103
Table 4.3: The organic acids present in HTL aqueous phase determined by HPLC 104
Table 4.4:The effect of washing hydrochar with 0.5 mol/L, 1.0 mol/L, 1.5 mol/L, 2.0 mol/L, 2.5 mol/L KOH and 1 mol/L HCl on the adsorption capacity (qe(mg/g) and removal efficiency (%) of metals 105
Table 4.5:The effect of washing hydrochar with 0.5 mol/L, 1.0 mol/L, 1.5 mol/L, 2.0 mol/L, 2.5 mol/L KOH and 1.0 mol/L HCl on the adsorption capacity (qe (mg/g) and removal efficiency for phenolics 106
Table 4.6: Composition of filtrates from base and acid activation of hydrochar 107
Table 4.7: Proximate analysis, elemental analysis, and higher heating value (HHV) of the hydrochars 109
Table 4.8: Surface properties of hydrochar before and after adsorption of both metals and phenolics 114
Table 4.9: Desorption of adsorbed metals and phenolics (with both 1.0M HCl and KOH) 135
Table 4.10: Pseudo 1st order kinetic model calculated parameters at a differing initial concentration 137
Table 4.11: Pseudo-second-order calculated parameters 140
Table 4.12: Elovich kinetic model calculated parameters 143
Table 4.13: Weber and Morris' intraparticle diffusion calculated parameters 147
Table 4.14:Boyd's intraparticle diffusion calculated parameters 151
Table 4.15: The dimensionless Biot number parameters 152
Table 4.16:Isotherm calculated parameters 160
Table 4.17: Thermodynamic parameters for the adsorption of metals and phenolic compounds on hydrochar 167
Table 4.18: Activation energy of metals and phenolic compounds on bWHc. 169
Table 4.19: Desorption of metals 173

Table 4.20:Desorption of phenolic compounds 173

LIST OF FIGURES

Figure 1.1:The distribution of water across the globe (Joseph *et al.,* 2019). 2
Figure 1.2: Project scope 7
Figure 1.3:Structure of the dissertation 8
Figure 2.1: Pollutants from various industrial segments collects in a water resource, A1: pharmaceuticals, A2: dyes, A3: agriculture, A4: mines and energy generation, A5: consumer emerging pollutants and A6 sewage. 16
Figure 2.2: Water remediation technologies currently used (Figoli and Criscuoli, 2017; Rodriguez-Narvaez et al., 2017; Sirkar, Singh and Li, 2017) 22
Figure 2.3: Oxidation of phenolic compounds using permanganate with bisphenol A as an example (Zhang et al., 2013) 24
Figure 2.4: Adsorption process at a microscopic level (Singh *et al.,* 2012). 31
Figure 2.5: Fate of feedstock macromolecules subjected to HTL (a) hydrolysis; (b) decomposition; (c) dehydration; (d) polymerization; (e) deamination; (f) Maillard reaction; (g) decarboxylation; (h) aminolysis; (i) cyclization; (j) halogenations; (k) dehydrohalogenation; (l) condensation pyrolysis (adopted from Watson et al., 2020) 36
Figure 2.6: Adsorption mechanism for both organic and inorganic pollutants onto hydrochar. (M_{ad}- metal adsorbed, M_{ex}- exchangeable metal ion)(Oliveira et al., 2017) 41
Figure 3.1: Inductively coupled plasma- optical emission spectrometer (ICP-OES) 87
Figure 3.2: Phenolic High-Performance Liquid Chromatography 89
Figure 3.3: Sugar High-Performance Liquid Chromatography 90
Figure 3.4: Ion chromatography (IC) 91
Figure 3.5: Batch adsorption experiment set up 96
Figure 4.1. The products from HTL of OFMSW 102
Figure 4.2: The pH point of zero charge (pH_{pZc}) of raw/ unwashed, and base- and acid-washed hydrochars 111
Figure 4.3 The SEM images of hydrochar at x10 000 magnification, before and after adsorption 114
Figure 4.4: The FTIR spectra of the before adsorption and after adsorption hydrochars 118
Figure 4.5:The effect of contact time on metal adsorption on hydrochar 120
Figure 4.6: The effect of contact time on phenolic adsorption on hydrochar 121
Figure 4.7: Effect of initial metal concentration on metal adsorption on hydrochar 124
Figure 4.8: Effect of initial phenolics concentration on phenolics adsorption 125

Figure 4.9: Effect of hydrochar dose on metal adsorption..... 126
Figure 4.10: Effect of hydrochar dose on phenolics adsorption 128
Figure 4.11: Effect of temperature on metal adsorption on hydrochar..... 129
Figure 4.12: Effect of temperature on adsorption of phenolics on the hydrochar 130
Figure 4.13: Effect of pH (2-12) on qe (A) and removal efficiency (B) of metals by adsorption. 131
Figure 4.14: Effect of pH (2-12) on qe (A) and removal efficiency (B) of adsorption of phenolic compounds on hydrochar..... 133
Figure 4.15: Effect of combining metals and phenolics on adsorption of metals and phenolics on hydrochar 134
Figure 4.16:Psuedo-first-order kinetic model plots of metals and phenolic compounds at a differing initial concentration 137
Figure 4.17 Pseudo-second-order kinetic model plots of metals and phenolic compounds at a differing initial concentration 140
Figure 4.18: Elovich model plots of the adsorption of metals and phenolics at a different initial concentration..... 143
Figure 4.19: adsorption data fitted with Weber and Morris intraparticle diffusion model at different initial adsorbate concentrations (shown in the legends). 147
Figure 4.20: Boyd's intraparticle diffusion plots at different concentrations of metals and phenolic compounds. 151
Figure 4.21: The Henry isotherm plots of metals (A) and phenolics (B) 154
Figure 4.22:Linearised Langmuir plots of 1/qe vs 1/Ce for (A) phenolics and (B) metals. 156
Figure 4.23: Linearised Freundlich plots of ln qe vs ln Ce for (A) phenolics and (B) metals. .. 158
Figure 4.24: Fitted isotherms to experimental equilibrium adsorption data of phenolic components 164
Figure 4.25: Van't Hoff plot w.r.t. Ke for both metal adsorption and phenolics adsorption..... 166
Figure 4.26:The plot of Gibbs free energy vs temperature to show the feasibility of the adsorption process of the metal and phenolic compounds..... 167
Figure 4.27: Arrhenius plots w.r.t k_1 for metals and phenolic compounds 169
Figure 4.28: Removal efficiency of metals present in HTL aqueous phase 170
Figure 4.29: Adsorption capacity of hydrochar on the metals present in HTL aqueous phase .. 171
Figure 4.30: Removal efficiency of phenolic compounds present in HTL aqueous phase 172
Figure 4.31: Adsorption capacity of the phenolic compounds present in HTL aqueous phase.. 172

Figure 4.32: Percentages of metal adsorbed (A) and desorbed (B) per given cycle..... 175
Figure 4.33: Percentages of phenolic compounds adsorbed (A) and desorbed (B) per given cycle
..... 176

ABBREVIATIONS

BET	Brunauer-Emmett-Teller
CSM	Combined Synthetic Mixtures
DNA	Deoxyribonucleic Acid
EPA	Environmental Protection Agency
FTIR	Fourier-Transform Infrared Spectroscopy
HPLC	High Performance Liquid Chromatography
HTC	Hydrothermal Carbonisation
HTL	Hydrothermal Liquefaction
HTL-AQ	Hydrothermal Liquefaction Aqueous Phase
HHV	Higher Heating Value
IC	Ion Chromatography
ICP-OES	Inductively Coupled Plasma-Optical Emission Spectroscopy
MSM	Metal Synthetic Mixtures
OFGs	Oxygen Functional Groups
OFMSW	Organic Fraction Of Municipal Solid Waste
PFO	Pseudo Second Order
PSM	Phenolics Synthetic Mixture
PSO	Pseudo Second Order
SANAS	South African National Accreditation System
SEM	Scanning Electron Microscope
SSM	Separate Synthetic Mixtures
WHO	World Health Organisation

CHAPTER 1

1 INTRODUCTION

This chapter contextualises the research problem and justifies the need for such a study on wastewater remediation using municipal solid waste-derived hydrochar. Section 1.1 outlines the background on water concerns, water remediation processes, and the novel hydrochar adsorbent. The statement of the research problem and hypothesis of the study is presented in Section 1.2. Section 1.3 states the aim, objectives, and scope of the study. Section 1.4. specifies the project outline, while Section 1.5 presents the literature reviewed and cited in this chapter.

1.1 Background and motivation

One of the largest challenges of the 21st century is an adequate supply of safe drinking water and sanitation (United Nations, 2018). Water is needed in industrial processes to sustain and grow economies for the benefit of the citizens, but it also needs to be available for domestic consumption. An increasing depletion of safe and clean water is thus a global concern. Analysis of Figure 1.1 shows that usable water is not as abundant as it seems (Joseph *et al.*, 2019). Most industrial processes use huge amounts of water; small percentages are incorporated in their products, while large amounts of water are lost through evaporation. Water and Environmental laws necessitate water treatment at all industrial plants and sanitary treatment facilities. A large fraction of used water (greywater) still finds its way into watercourses and dams. Recently, global public health and ecological concerns associated with pollution have increased dramatically, calling for urgent remedial action (Shakoor *et al.,* 2013). Remediation of wastewater is challenging as there could be various pollutants present with a range of chemical combinations and at varying concentrations (Inyang *et al.*, 2012; Taghipour *et al.*, 2019).

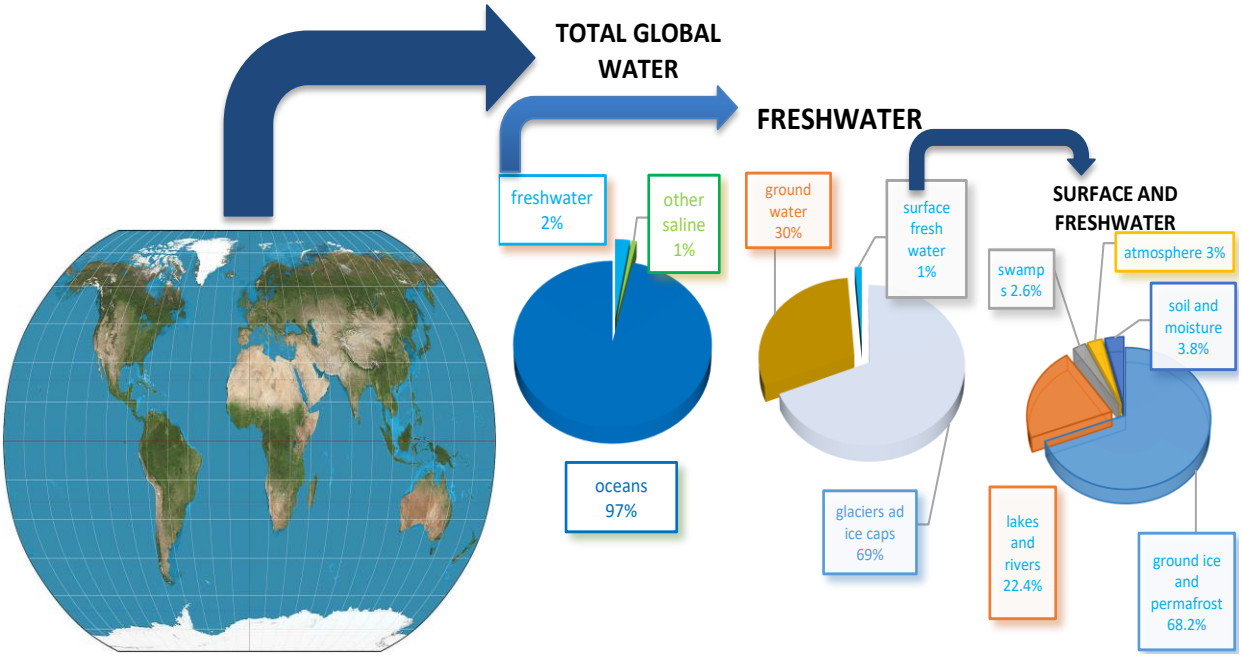

Figure 1.1:The distribution of water across the globe (Joseph *et al.*, 2019).

In developing countries like South Africa, concurrent resource exploitation and industrialisation have improved economies and living standards. These developments have, however, also introduced toxic and hazardous compounds to the environment, most of which end up in rivers and dams from which domestic water supply in informal settlements is sourced, leading to a significant increase in water pollution (Crini *et al.*, 2019; Dlamini *et al.*, 2019). Pollutants can be organic or inorganic compounds mainly from fossil-based power generation, agriculture activity, chemical manufacturing (e.g. pharmaceutical, resins, plastics, explosives, and transportation fuels), mining, and building and construction operations (Crini *et al.*, 2019). Heavy metals and phenolic compounds (phenolics) are the world's most concerning water pollutants; removing these is an urgent requirement (Mohammed *et al.*, 2011; Mu'azu *et al.*, 2017). Both heavy metals and phenolics damage biomolecules like DNA and proteins, thereby affecting their optimal functioning (David and Hazel, 1998). Heavy metals and phenolics accumulate in living organisms, triggering countless diseases and disorders. Since these pollutants are non-biodegradable, they need to be removed through water treatment and remediation processes (Parthasarathy and Narayanan, 2014).

Water remediation is a major element in the control and regulation of pollution. It reduces or removes the specific pollutants present that cause adverse effects on the environment and equally pose a threat to human life (Joseph *et al.*, 2019). Suitable wastewater remediation through both

chemical and biological approaches is employed to limit the effect of wastewater pollutants on community health and the environment (Lv *et al.*, 2018). At present, many conventional and non-conventional wastewater treatment processes (like membrane technologies, ion exchange, biosorption, chemical and electrochemical oxidation) have been proposed and applied. However, most of these are expensive on a large scale; they generate a high-density concentrated sludge; or they are only applicable to biodegradable pollutants. The heterogeneous nature of wastewater treatment sludge is due to various metals, metalloids, organic and anionic components, making it a challenge to dispose of safely (Braghiroli *et al.*, 2018; Liu and Zhang, 2018; Wang and Wang, 2019; Yoon *et al.*, 2017). Membrane technologies are some of the most effective separation methods, but membrane fouling is a significant problem, especially in the presence of high concentrations of pollutants (Peydayesh *et al.*, 2019). The largest biological and membrane purification plant for industrial wastewater in South Africa is situated in Secunda in South Africa, and it forms part of the wastewater treatment facilities of a large petrochemical company (Jacobs and Sanderson, 1987).

Adsorption seems to be simple, affordable, environmentally friendly, and effective. Due to reversibility and desorption capabilities, adsorption is regarded as the most effective and economically viable option for removing metals and phenol derivatives from aqueous solutions (Ge *et al.*, 2018; Mahdi *et al.*, 2019). The efficiency of adsorption is dependent upon the types of adsorbents used. Activated carbon (AC), activated alumina (AA), zeolites, chitosan, and chitin are some of the adsorbents recommended in the water remediation adsorption process (Joseph *et al.*, 2019; Wang *et al.*, 2020). Most commercially available adsorbents have demonstrated high adsorption efficiency, but their synthesis may compromise the cost-effectiveness of the remediation process. As a result, research in this field focuses on developing novel low cost and effective adsorbents from renewable sources like biomass. A viable source of biomass that does not compromise food security and contribute to the development of a circular economy is the organic fraction of municipal solid waste (OFMSW). Solid waste refers to the refuse, litter, sludge, and other unwanted materials from industrial, commercial, mining, and agricultural operations and community activities and are usually disposed of at landfill sites (Landsberger, 2019). Poor management of the OFMSW leads to landfill sites containing heavy metal and non-degradable components that causes both soil and water pollution. This soil and water pollution is a global problem for both developed and third world countries (Van der Bruggen *et al.*, 2017; Mendoza-Castillo, 2017). Studies on the use of biomass in fuels suggest that accumulating OFMSW could

be employed to generate renewable sources of energy (Yang *et al.,* 2019). OFMSW can also be used to produce cheap and efficient biochar-based adsorbents that can be successfully employed in wastewater treatment (Ayeleru *et al.,* 2011; Kantakanit *et al.,* 2018). According to Wang *et al.* (2019), biochar is a solid product obtained from the thermochemical conversion of biomass in a limited oxygen environment. The thermochemical conversion includes gasification, pyrolysis, and hydrothermal liquefaction (HTL). Biochar from the HTL is referred to as hydrochar.

Hydrochar characteristics such as oxygen-containing surface functional groups make it a recommended adsorbent in removing heavy metals and phenolics. The composition of the biomass used has a great influence on characteristics and properties of hydrochar which impact its adsorption abilities (Gollakota et al., 2018). In this study, synthetic mixture of the OFMSW was made according to the composition of OFMSW in the South African State of Waste report (2018). The use of OFMSW to produce low-cost adsorbents addresses both wastewater treatment and solid waste accumulation by reducing solid waste and improving the quality of recycled wastewater.

Furthermore, the recovered pollutants are of high value as platform chemicals in industrial processes, thereby contributing to the recycling of non-biodegradable components. Ortho-methoxy phenols are used in chemical and biochemical applications in the manufacturing of drugs and chemical diagnostics. Phenol derivatives with antioxidant properties are also used to produce disinfectants (Lapierre, 2019). For instance, vanillin has great anti-inflammatory properties and is used to formulate anti-inflammatory drugs (Van Holme and De Meester, 2019). Similarly, 3-methoxyphenyl has dual functions as catalysts and building blocks in the synthesis of antioxidants. All these are lignin degradation products when subjected to thermochemical processes like HTL and accumulate in wastewater (HTL aqueous phase). Pharmaceuticals, fragrance companies, and industries use phenolic compounds like vanillin, catechol, syringol, and guaiacol in their production processes, 95 % of which are produced from petroleum-based phenols (Thomas, 1995). The rapid depletion of fossil-based resources necessitates an urgent search for alternatives that could lessen the dependence of production companies on fossil-based chemicals and fuels (Koley *et al.,* 2018; Nazari *et al.,* 2015; Zhang, *et al.,* 2018). In order to have more biobased phenolics lignin containing biomass should be considered. If hydrochar can remove both phenolics and heavy metals from wastewater, valuable compounds can also potentially be recovered and recycled to replace fossil-based chemicals.

1.2 Statement of the problem and hypothesis

1.2.1 Statement of the problem

Anthropogenic and industrial activities generate large volumes of greywater that contains heavy metals and non-biodegradable components which subsequently accumulate in the environment (Pan and Chen, 2018; Mohammed *et al.,* 2011; Crini and Lichtfouse, 2019; Dai *et al.*, 2019). Adsorption is a viable means of recovering heavy metals and non-biodegradable phenolic components from wastewater. Adsorbents are generally expensive, and more cost-effective adsorbents could significantly lower the cost of wastewater treatment processes. Hydrochar-based adsorbents produced from accumulating municipal solid waste are a promising alternative because this is a simple and affordable approach to wastewater treatment. To date, most recent studies focus on analysis and understanding of one adsorbate (Saidi *et al.,* 2014; Batool *et al.,* 2017; Lee *et al.,* 2017; Ni *et al.,* 2019), yet multi-component solutions are relevant for designing, optimising and operating of real-life systems for wastewater and industrial effluents. Based on this requirement, it is necessary to explore a multi-component solution with organic and inorganic pollutants. Studies have shown that pollutants adsorbed on the hydrochar can be desorbed (Bogusz *et al.*, 2015; Tong *et al.*, 2011). The same phenomenon is applicable in recovering valuable compounds from wastewater, e.g., phenolics from HTL aqueous phase. Therefore, there is an urgent need to study OFMSW-derived hydrochar that simultaneously removes metallic and organic pollutants in a multi-component wastewater stream.

1.2.2 Hypothesis

Heavy metals and phenolic components from contaminated wastewater streams can be co-adsorbed onto hydrochar derived from the HTL of the OFMSW.

1.3 Aim and Objectives

1.3.1 Research aim

This project aims to evaluate the use of hydrochar produced by hydrothermal liquefaction (HTL) of municipal solid waste as an adsorbent in the concurrent removal of alkali and alkaline earth metals (AAEM) and phenolic components from wastewater streams.

1.3.2 Research objectives

The following research objectives have been formulated to meet the aim of the study:

- Characterisation of hydrochar as an adsorbent and HTL aqueous phase as the wastewater stream to be remediated;
- Determine the efficiency of hydrochar as an adsorbent for removal of both phenolic compounds and heavy metals from an HTL aqueous phase product;
- Determine the mechanism of co-adsorption of heavy metals and phenolic components on hydrochar using appropriate adsorption isotherm and adsorption kinetic models;
- Determine the recovery of adsorbed heavy metals and phenols;
- Determine the regeneration reusability of hydrochar as a cost-effective adsorbent.

1.3.3 Project scope

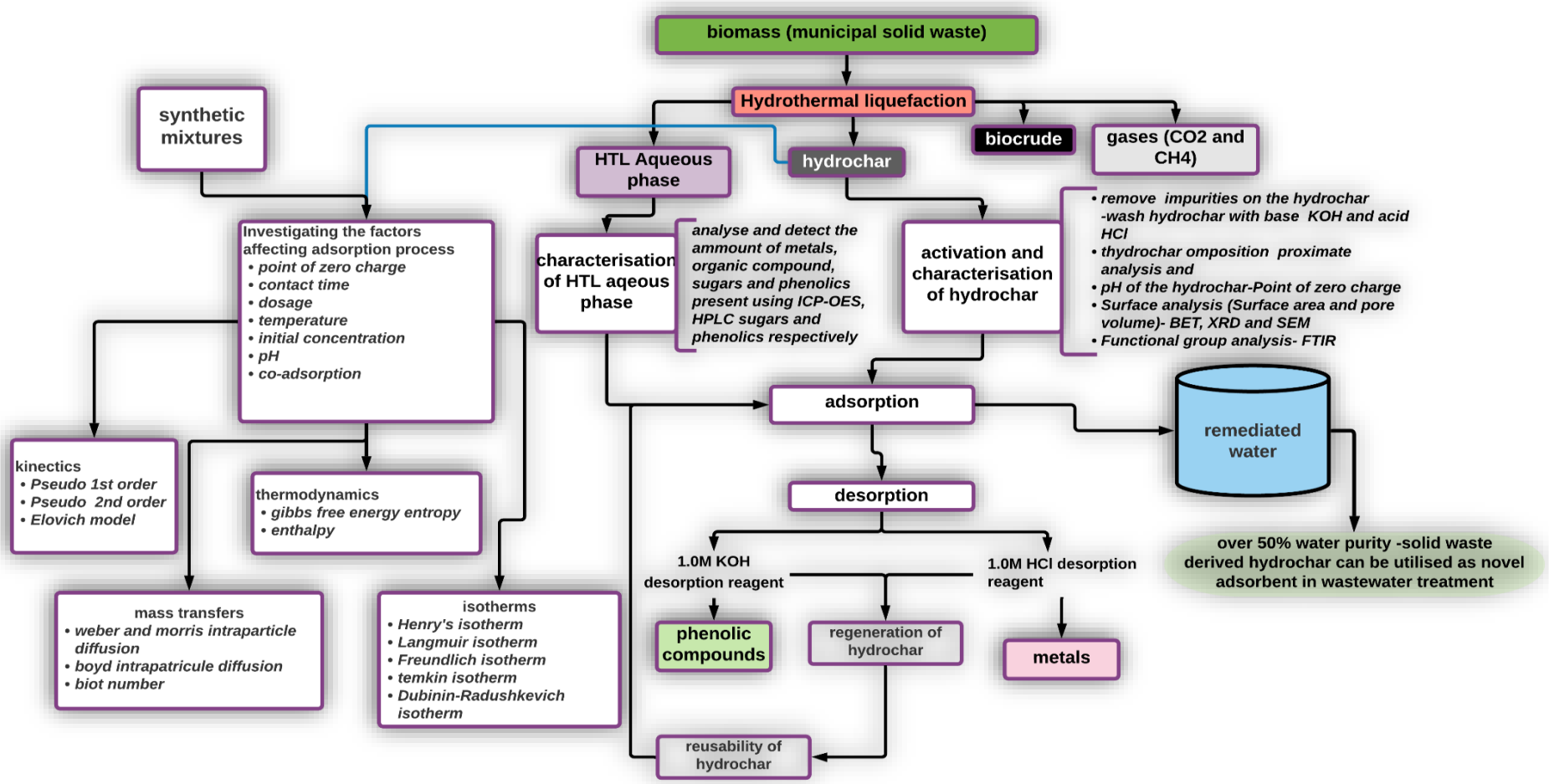

Figure 1.2: Project scope

1.4 Project outline

The project is divided into five chapters to satisfy the aim and objectives stipulated in Section 1.3;

Chapter 1: Introduction	Chapter 2: Literature Reviews	Chapter 3: Material and Methodology	Chapter 4: Results and Discussion
•The background motivation of the research •Problem statement and study hypothesis •Research aim and objectives •The outline of the dissertation	•Wastewater and wastewater treatment •Adsorption •Adsorbent biochar •Municipality solid waste •Theorems, kinetics, mass transfers and thermodynamics.	•Collecting hydrochar and HTL aqueous phase •Activation and characterisation of hydrochar • Characterisation of HTL aqueous phase •Adsorption at various conditions e.g., temperature, ph, initial concentration, dosage •Adsorption and desorption experiments •Regeneration of the hydrochar •Reusability of the char	•Characterisation of hydrochar and HTL aqueous phase (wastewater) •Factors affecting the adsorption process •Adsorption isotherms •mass transfers •Interpretation and disscusions of the of the results

Figure 1.3:Structure of the dissertation

REFERENCES

Ayeleru, O.O., Ntuli, F. and Mbohwa, C. 2011. Utilisation of Organic Fraction of Municipal Solid Waste (OFMSW) as Compost: *A Case Study of Florida, South Africa.*

Batool, S., Idrees, M., Hussain, Q. and Kong, J. 2017. Adsorption of copper (II) by using derived-farmyard and poultry manure biochars: Efficiency and mechanism. *Chemical Physics Letters*. 689:190–198.

Bogusz, A., Oleszczuk, P. and Dobrowolski, R. 2015. Application of laboratory prepared and commercially available biochars to adsorption of cadmium, copper and zinc ions from water. *Bioresource Technology*. 196:540–549.

Braghiroli, F.L., Bouafif, H., Hamza, N., Neculita, C.M. and Koubaa, A. 2018. Production, characterisation, and potential of activated biochar as adsorbent for phenolic compounds from leachates in a lumber industry site. *Environmental Science and Pollution Research*. 25(26):26562–26575.

Crini, G. and Lichtfouse, E. 2019. Advantages and disadvantages of techniques used for wastewater treatment. *Environmental Chemistry Letters*. 17(1):145–155.

Crini, G., Lichtfouse, E., Wilson, L.D. and Morin-Crini, N. 2019. Conventional and non-conventional adsorbents for wastewater treatment. *Environmental Chemistry Letters*. 17(1):195–213.

Dai, Y., Zhang, N., Xing, C., Cui, Q. and Sun, Q. 2019. The adsorption, regeneration and engineering applications of biochar for removal organic pollutants: A review. *Chemosphere*. 223:12–27.

David, H. and Hazel, P. 1998. Analytical Biochemistry. Pearson Education Limited, ed. 3rd ed. London, England: Addison Wesley Longman Limited.

Department of Environmental Affairs **State of Waste Report South Africa - Second Draft Report** (2018)

Dlamini, S., Simatele, M.D., Serge Kubanza, N. and Kubanza, N.S. 2019. Municipal solid waste management in South Africa: from waste to energy recovery through waste-to-energy technologies in Johannesburg. *Local Environment*. 24(3):249–257.

Ge, M., Wang, X., Du, M., Liang, G., Jahangir, A. and Hu, G. 2018. Adsorption analyses of phenol from aqueous solutions using magadiite modified with organo-functional groups: Kinetic and equilibrium studies. *Materials*. 1(13):203–216.

Inyang, M., Gao, B., Yao, Y., Xue, Y., Zimmerman, A.R., and Cao, X. 2012. Removal of heavy metals from aqueous solution by biochars derived from anaerobically digested biomass. *Bioresource Technology*. 110:50–56.

Jacobs, E.P. and Sanderson, R.D. 1987. Membrane Development and Fabrication for Reverse Osmosis and Ultrafiltration, Cape Town, South Africa. (172).

Joseph, L., Jun, B.M., Flora, J.R.V., Park, C.M. and Yoon, Y. 2019. Removal of heavy metals from water sources in the developing world using low-cost materials: A review. *Chemosphere*. 229:142–159.

Kantakanit, P., Tippayawong, N., Koonaphapdeelert, S. and Pattiya, A. 2018. Hydrochar Generation from Hydrothermal Carbonization of Organic Wastes. In: Vol. 159. IOP Conference Series: *Earth and Environmental Science. Institute of Physics Publishing*.

Koley, S., Khadase, M.S., Mathimani, T., Raheman, H. and Mallick, N. 2018. Catalytic and non-catalytic hydrothermal processing of Scenedesmus obliquus biomass for bio-crude production – A sustainable energy perspective. *Energy Conversion and Management*. 163(February):111–121.

Landsberger, S. 2019. 2 The Circular Economy in China. Beijing *Garbage*. 53–76.

Lapierre, C. 2019. Lignin structure and its engineering. Current Opinion in *Biotechnology*. 56:240–249.

Liu, Y. and Zhang, Z. 2018. Preparation of Polymeric Adsorbent and Study of Its Adsorption of Heavy Metal Ions in Water. *Journal of Coastal Research*. 83(sp1):414.

Lv, Z., Yang, S., Liu, Y., Zhou, J., Xing, L. and Chen, L. 2018. The novel PEI-modified biochars and their application for the efficient elimination of Cr (VI) from aqueous solutions. *Water Science and Technology*. 77(8):2045-2056

Mahdi, Z., Hanandeh, A. El and Yu, Q.J. 2019. Preparation, characterisation, and application of surface-modified biochar from date seed for improved lead, copper, and nickel removal from aqueous solutions. *Journal of Environmental Chemical Engineering*. 7(5):103379.

Mendoza-castillo, D.I. 2017. Adsorption Processes for Water Treatment and Purification. H. Elizabeth and Reynel-Ávila, eds. 1st ed. Cham, Switzerland: Springer International Publishing.

Mohammed, A.S., Kapri, A. and Goel, R. 2011. Heavy Metal Pollution: Source, Impact, and Remedies. In: M.S. Khan, A. Zaidi, R. Goel, and J. Musarrat, eds. *Bio management of Metal-Contaminated Soils.* Dordrecht: Springer Netherlands 1–28.

Mu'azu, N.D., Jarrah, N., Zubair, M. and Alagha, O. 2017. Removal of phenolic compounds from water using sewage sludge-based activated carbon adsorption: A review. International *Journal of Environmental Research and Public Health*. 14(10):1–34.

Nazari, L., Yuan, Z., Souzanchi, S., Ray, M.B. and Xu, C. (Charles). 2015. Hydrothermal liquefaction of woody biomass in hot-compressed water: Catalyst screening and comprehensive characterisation of bio-crude oils. *Fuel*. 162:74–83.

Ni, B.J., Huang, Q.S., Wang, C., Ni, T.Y., Sun, J. and Wei, W. 2019. Competitive adsorption of heavy metals in aqueous solution onto biochar derived from anaerobically digested sludge. *Chemosphere*. 219:351–357.

Parthasarathy, P. and Narayanan, S.K. 2014a. Hydrogen production from steam gasification of biomass: influence of process parameters on hydrogen yield. *A review in Renewable energy*. 66(1):570–579.

Peydayesh, M., Pauchard, M., Bolisetty, S., Stellacci, F. and Mezzenga, R. 2019. Ubiquitous aluminium contamination in water and amyloid hybrid membranes as a possible sustainable solution. *Chemical Communications*. 55(74):11143–11146.

Saidi, M., Samimi, F., Karimipourfard, D., Nimmanwudipong, T., Gates, B.C. and Rahimpour, M.R. 2014. Upgrading of lignin-derived bio-oils by catalytic hydrodeoxygenation. *Energy and Environmental Science*. 7(1):103–129.

Taghipour, A., Ramirez, J.A., Brown, R.J. and Rainey, T.J. 2019. A review of fractional distillation to improve hydrothermal liquefaction biocrude characteristics; future outlook and prospects. *Renewable and Sustainable Energy Reviews*. 115.

Thomas, J. V. 1995. Petroleum and Coal. Coal. *Analytical Chemistry*. 67(12):317–319.

Tong, X.J., Li, J.Y., Yuan, J.H. and Xu, R.K. 2011. Adsorption of Cu (II) by biochars generated from three crop straws. *Chemical Engineering Journal*. 172(2–3):828–834.

United Nations. 2018. United Nations Sustainable Development goals. Water Action Decade, 2018-2028. https://www.un.org/sustainabledevelopment/water-and-sanitation/ Date of access: 03 Aug. 2021.

Van der Bruggen B., Canbolat Ç.B., Lin J., Luis P. (2017) The Potential of Membrane Technology for Treatment of Textile Wastewater. In: Figoli A., Criscuoli A. (eds) Sustainable Membrane Technology for Water and Wastewater Treatment. Green Chemistry and Sustainable Technology. Springer, Singapore pp 349–380.

Van Holme, R. and De Meester, B. 2019. Lignin biosynthesis and its integration into metabolism. Current Opinion in *Biotechnology*. 56:230–239.

Wang, J. and Wang, S. 2019. Preparation, modification and environmental application of biochar: A review. *Journal of Cleaner Production*. 227:1002–1022.

Wang, Z., Zhang, J., Wen, T., Liu, X., Wang, Y., and Sun, J. 2020. Highly effective remediation of Pb (II) and Hg (II) contaminated wastewater and soil by flower-like magnetic MoS2 nanohybrid. *Science of The Total Environment*. 699.

Yang, J., He, Q. (Sophia), Corscadden, K., Niu, H., Lin, J. and Astatkie, T. 2019. Advanced models for the prediction of product yield in hydrothermal liquefaction via a mixture design of biomass model components coupled with process variables. *Applied Energy*. 233–234(September 2018):906–915.

Yoon, K., Cho, D.W., Tsang, D.C.W., Bolan, N., Rinklebe, J. and Song, H. 2017. Fabrication of engineered biochar from paper mill sludge and its application into removal of arsenic and cadmium in acidic water. *Bioresource Technology*. 246:69–75.

Zhang, B., He, Z., Chen, H., Kandasamy, S., Xu, Z., and Guo, H. 2018. Effect of acidic, neutral and alkaline conditions on product distribution and biocrude oil chemistry from hydrothermal liquefaction of microalgae. *Bioresource Technology*. 270:129–137.

CHAPTER 2

2 LITERATURE REVIEW

This chapter reviews recent literature and discusses in detail the importance of industrial wastewater treatment. Section 2.1 focuses on the composition of industrial residual wastewater and its impact on human health and the environment. Section 2.2 discusses the conventional methods currently employed and further examines established and emerging technologies and their shortcomings. The currently used adsorbents and their disadvantages are discussed in Section 2.2.3.2 as well the need to find a low-cost adsorbent. A detailed discussion is provided in Section 2.3 on the synthesis of alternative and more cost-effective adsorbents from biomass feedstock. The Section also explains the adsorbent properties of hydrochar, possible hydrochar-adsorption mechanisms, and suggestion on improving the hydrochar adsorption process. The focus of Sections 2.4, 2.5, 2.6, 2.7 and 2.8 is on preferred batch adsorption and essential parameters for adsorption, such as processing conditions, isotherm and kinetic models, and the potential mechanisms relating to the adsorption process, respectively. Finally, conclusions from this literature review are given in Section 2.9.

2.1 Wastewater, pollution, and contamination

Wastewater is the effluent from anthropogenic and industrial activities, making it unsuitable for a particular direct use, domestic or otherwise (Ge *et al.*, 2018). Wastewater can be either polluted or contaminated. Contaminated water contains constituents present in higher concentrations than permitted by law, whereas polluted water contains substances that accumulate in living organisms and adversely affect humans and the environment. In other words, all pollutants are contaminants, but not all contaminants are pollutants (Crini *et al.*, 2019). Wastewater originates from factories, industries, domestic sources, and mines (Shakoor *et al.*, 2013). As much as anthropogenic and industrial activities are desirable for human development and welfare, a wide spectrum of chemicals and pathogens of different physical chemistry and detectable ranges are accumulating in nature. This can be a malignant problem for human survival on earth in the future. Wastewater from multiple sources collects in water sources such as dams and streams.

2.1.1 Pollutants

Pollutants can be organic or inorganic. Pollutants include phenolics, nitrates, phosphates, detergents, pesticides, heavy, alkali and alkaline earth metals (for example potassium, calcium, iron, lead, mercury, chromium, cadmium, arsenic dyes). Benzene, bisphenol, mineral derivatives (particularly arsenic and cyanides), microorganisms, volatile organic compounds (VOC) (Lei *et al.*, 2018), polycyclic aromatic hydrocarbons (PAHs)(Dieguez-Alonso *et al.*, 2018; Nguyen *et al.*, 2007), polychlorobiphenyls (PCBs), bromine-containing flame-retardants (çaglar *et al.*, 2018), are some of the water pollutants. Anthropogenic chemicals constitute some persistent pollutants which are characterised by a wide range of physiochemical properties and toxicological profiles. Some of these are toxic to biota at low concentrations ($1 \cdot 10^{-3}$ to $1 \cdot 10^{-9}$ g/L) (David and Hazel, 1998). Their toxicity depends, of course, on their composition, which in turn depends on their industrial origin (Wang *et al.*, 2013). Figure 2.1 below shows some of the pollutants found in wastewater.

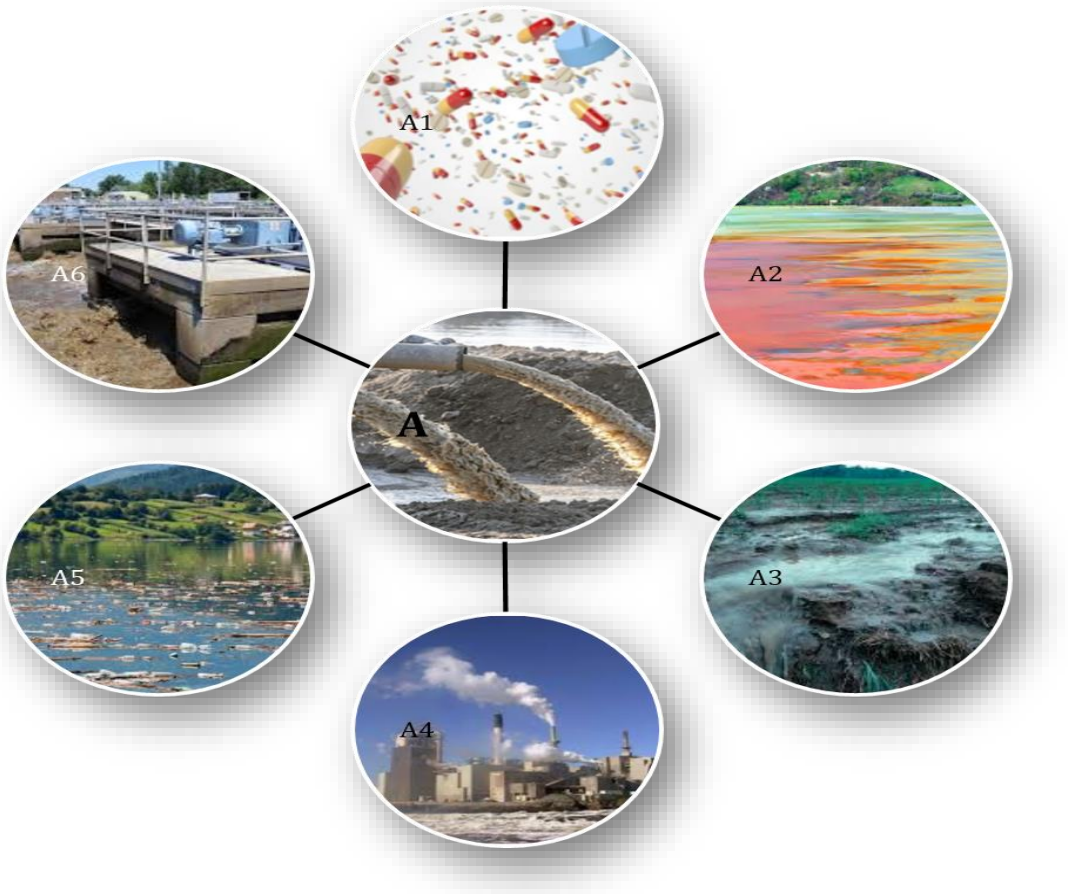

Figure 2.1: Pollutants from various industrial segments collects in a water resource, A1: pharmaceuticals, A2: dyes, A3: agriculture, A4: mines and energy generation, A5: consumer emerging pollutants and A6 sewage.

Pharmaceuticals (like antibiotics) are hazardous aquatic pollutants. Studies by Awad *et al.* (2020) and Mestrea *et al.* (2012) for example, reported pharmaceuticals in trace amounts in the ground, surface and drinking water. Living body tissues like the liver and kidneys absorb antibiotics, analgesics, anti-inflammatories, and hormones. These pharmaceuticals obstruct other metabolic processes through hormone receptor inhibition (WHO, 2011) even at trace amount levels. Conventional sewage treatments do not effectively eliminate trace pollutants like pharmaceuticals, causing their continuous accumulation in water sources. This unchecked accumulation poses environmental risks to both ecosystems and humanity. Adsorbents such as activated carbons, zeolites and silica showed satisfactory results on the adsorption of diclofenac, ibuprofen, erythromycin, carbamazepine and naproxen (Parthasarathy and Narayanan, 2014b).

Agriculture is an advancing industry and a major contributor to the economy, and the use of agricultural chemicals improves harvest yields and product quality. Agricultural effluent containing fertilisers accumulates in water reservoirs where it causes algae blooms and eutrophication that depletes the oxygen supply for aquatic organisms (Papadopoulos *et al.*, 2014). Pesticides and herbicides increase toxicity directly or indirectly to untargeted organisms. The damage to ecological balance and human health can be minimised by eliminating products from water using adsorption with biochar. Thiacloprid was successfully removed by maize straw biochar (produced at 300-700 °C) (Zhang, Sun, *et al.*, 2018), and imidacloprid was successfully removed using broiler litter derived hydrochar (Uchimiya *et al.,* 2013). Zheng *et al.,* (2010) removed pesticides such as triazine and atrazine (451-1158 mg/g) and simazine (243-1066 mg/g) using green waste biochar.

Dyes are water pollutants characterised by colour, high molecular weight, complex structures with persistent and recalcitrant properties originating from textile, paper, cosmetics, food, and rubber industries. Dyes can be acidic, basic, reactive, and dispersive, toxic, mutagenic, and carcinogenic to living organisms. Several adsorption studies have reported the adsorption of different dyes like methylene blue on several adsorbents (çaglar *et al.*, 2018; Lei *et al.*, 2018). Naphthol and Congo red are some of the dyes that are found in textile industry wastewater. 2-Naphthol is also used as a bactericide and is a more corrosive aromatic compound than phenol. Exposure to naphthol contaminated water causes poor human blood circulation and kidney dysfunction (Lin and Xing,

2008). An anionic azo-dye, Congo red, degrades to benzidine, a well-established carcinogen (Li *et al.*, 2016). Such pollutants are resistant to aerobic and anaerobic digestions and moderate oxidising agents, making them difficult to remove (Cheng *et al.*, 2015; Zhang *et al.*, 2011). Li *et al.*, (2016) investigated the removal of Congo red and naphthol using bamboo-derived hydrochar. The adsorption capacities of Congo red and 2-naphthol on the hydrochars were found to be 6.0–33.7 mg/g and 3.0–12.2 mg/g at 25 °C and 0.1 mg/mL, respectively.

Emerging pollutants are not routinely monitored, and synthetic or natural pollutants require technically advanced analytical techniques for their detection. They can be hormones, steroids, phytoestrogens, hydrocarbons, disinfectants, by-products, and personal care products based on their origin. They may all end up in the water, as shown in Figure 2.1, A5. With their increasing accumulation, they impose adverse effects on biota and human health, and some may cause cancer. Most emerging pollutants are endocrine-disrupting, and their trace concentrations remain a challenge to conventional pollutant removal methods. However, some studies show that adsorption with activated carbons or zeolites could be applied in their removal (Gong *et al.*, 2016; Rodriguez-Narvaez *et al.*, 2017). Therefore, removing these pollutants from wastewater using hydrochar is possible.

2.1.2 Metals

Metals and their respective ions are considered inorganic pollutants because of their non-biodegradability. Among the metals, heavy metals are of major concern. They have become a major research topic because of the global public health and ecological concerns attributed to these heavy metals. Heavy metals are elements with a high atomic weight and a density of at least five times water (Manahan, 2003). Examples include copper (Cu), cadmium (Cd), cobalt (Co), manganese (Mn), nickel (Ni), chromium (Cr), iron (Fe), and zinc (Zn) (Ebenebe *et al.*, 2018; Pan and Chen, 2018). These toxic metals accumulate in living organisms, triggering countless diseases and disorders (Parthasarathy and Narayanan, 2014a). Some metal species are essential for human health at lower concentrations but are toxic at higher concentrations.

2.1.2.1 Bio-importance and bio-toxicity of inorganic compounds

An essential element is essential if its absence is associated with a defect, or its presence relieves a defect. Life essential elements and are classified into four categories, namely:

- bulky element (C, H, N, O, P and S),
- macro minerals and ions (Ca^{2+}, K^{+}, Mg^{2+}, Cl, phosphates, and sulphates),
- trace element (Fe, Zn and Cu),
- and ultra-trace elements (F, I, Se, Si, As).

Group 1 and Group 2 elements are structural elements; they maintain osmotic balance (Frasch, 2015; Mohammed *et al.,* 2011). Single oxidation state trans-elements, such as zinc II form superoxide dismutase and participate in gene regulation. They are also co-factors of various enzymes (anhydrases, peptidases and oxidases) (Artelle and Odgers, 2010). Metals can also stimulate protein activity, e.g. calcium in calmodulin can stimulate the formation of extra Troponin C (Campbell and Farrell, 2006). Transition elements in multiple oxidation states are electron carriers, e.g. iron in cytochromes or copper in plastocyanins (Crichton, 2001; de la Rosa *et al.,* 2019). Iron is found in haemoglobin, myoglobin, tryptophan 2,3-dioxygenase cytochromes catalase, succinate dehydrogenase, aldehyde oxidase aconitase, peroxidases, and many more proteins (Komkiene and Baltrenaite, 2016). Iron and copper facilitate oxygen transport in haemoglobin and haemocyanins (Crichton, 2001).

As much as metals are important, their bio-toxic effects at higher concentrations are potentially life-threatening, and therefore their presence in wastewater cannot be overlooked. The bio-toxic effects of heavy metals refer to the harmful effects of heavy metals on the body when consumed above the bio-recommended limits. The nature of such effects could be toxic, neurotoxic, carcinogenic, mutagenic, or teratogenic. There is no understanding of the role of lead, cadmium and mercury in human physiology and biochemistry, and these heavy metals do not occur naturally in living organisms (Campbell and Farrell, 2006). Therefore, when taken orally, they accumulate in different organs and become harmful (WHO, 2011). Cadmium toxicity has been linked to renal dysfunction, characterised by tubular proteinuria (Duruibe, Ogwuegbu, and Egwurugwu, 2007). Lead is highly toxic and teratogenic when ingested in food, water, or inhaled, and it inhibits haemoglobin synthesis, leading to chronic damage to the nervous system and permanent brain damage (Duruibe *et al.*,2007; Kim *et al.,* 2019). The WHO (2011) reported that lead causes poor brain development in children, specifically the grey matter and high calcium and zinc favour its absorption.

2.1.3 Phenolic compounds

Phenolics refer to compounds with a hydroxyl functional group directly bonded to an aromatic ring (Carey and Sundberg, 2007). Phenolics are secondary plant metabolites but can also be artificially synthesised. In the 1860s, phenolics were initially used as antiseptics. Later on, in the 19th century, their use was extended to manufacture of dyes, plastics, and petrochemicals, thereby significantly increasing the concentration of phenolics in wastewater (Braghiroli *et al.*, 2018). The main types of phenolics are phenolic acids and polyphenols. Lignin is a natural polymer of phenolics, and Singh *et al.*, (2019) investigated its degradation of lignin and oligomers to its respective monomers. Changjun *et al.*, (2013) successfully obtained value-added chemicals like guaiacol (2-methoxy phenol) from the degradation of lignin's β–O–4 bond. The cleavages of other functional groups, including hydroxyl, aromatic, and carbonyl, resulted in an increased phenolic –OH content. Studies on advanced biofuels from thermochemical processing of biomass are continually expanding. Hydrothermal liquefaction (HTL), one of the thermochemical processes that convert lignocellulosic biomass into biofuels related products produces an aqueous product that was found to contain some valuable chemicals (Elliott *et al.*, 2015; Schuler *et al.*, 2017). Bulky high value-added chemical compounds found in the hydrolysate include phenolic compounds, saccharides, ketones, organic acids and furfurals (Ruiz *et al.*, 2013; Wu *et al.*, 2013). These compounds are valuable in the food industry, chemical synthesis, and pharmaceuticals since they provide platform chemicals that produce various high value-added derivatives (Ruiz *et al.*, 2013; Wu *et al.*, 2013).

2.1.3.1 Detected valuable phenolics

HTL of barley husks produced several lignin-derived products such as benzoic acid, gallic acid and cinnamic acid (Leja *et al.*, 2013). Gallic acid helps in protecting the skin from UV sun rays and other skin cancer-causing compounds. Cheng et al. (2017) obtained syringaldehyde, hydroxytyrosol, tyrosol, vanillyl alcohol, oleuropein and 3, 4-dihydroxybenzaldehyde from the HTL of barley husks. In recent work, (Sandquist *et al.*, 2019) performed HTL on tea residues and reported that vanillin, dihydroconiferyl alcohol, vanillic acid, and guaiacol were the main phenolics present in the aqueous product. Vanillin has great anti-inflammatory properties hence useful in the manufacture of anti-inflammatory drugs (Van Holme and De Meester, 2019).

Similarly, 3-methoxy phenol has dual functions as a catalyst and building block in the synthesis of antioxidants. Phenolics e.g., polyphenols are natural antioxidants with potential in food

industries as food additives (Xiong *et al.,* 2020). Furthermore, the phenolic-rich extract contains various potentially valuable compounds with antimicrobial and biological activities comparable to synthetic antioxidants. Conde et al., (1998) and Nazari *et al.,* (2015) identified low molecular weight phenolics: gallic acid, 3,4-dihydroxybenzaldehyde, vanillic acid, syringic acid, vanillin and p-coumaric acid from HTL of birch wood sawdust biomass. Ortho-methoxy phenol has been detected by $–OCH_3$ in an NMR spectrum and has chemical and biochemical applications in manufacturing drugs and chemical diagnostics. It also has antioxidant properties, and it is therefore applied in the production of perfumes and disinfectants.

Furthermore, ortho-methoxy phenol has been reported to be a raw material in synthesising guaiacol derivatives (Lapierre, 2019). Simple phenolics like oleuropein and hydroxytyrosol have benefited human health, such as preventing cardiovascular diseases (Schuler *et al.,* 2017). Hydroxytyrosol, vanillin, vanillic acid, caffeic acids have also been found to suppress the spread of tumoral diseases (Schuler *et al.,* 2017). P-coumaric acid, caffeic acid, and ferulic acid minimise the oxidation of low-density lipoproteins (LDL) lipoprotein oxidation (Lapierre, 2019). The complex composition of HTL aqueous products hinders its application. Therefore, it is necessary to study the recovery of some of these platform chemicals from this complex wastewater stream.

2.1.3.2 Phenolic compound toxicity

Phenolic derivatives are also categorised into a group of common environmental contaminants. Phenolic compounds can be either harmful or useful. Phenol is categorised as a harmful pollutant since it is poisonous to microorganisms, animals and humans even at low concentrations (Gholizadeh *et al.,* 2013; Villegas *et al.,* 2016). The Environmental Protection Agency set 0.1 mg/L as the phenol limit in wastewater (Environmental Protection Agency accessed 2021). South African National Standards (SANS) limits phenol in portable water to 0.01mg/L (SANS 241-2015) whereas WHO (2011) is stricter on phenol regulation and has a 0.001 mg/L phenol limit in potable water. It also has derivatives that could be even more toxic than phenol itself. The derivatives can have substitutes on the ortho, para and meta position, and examples of these include chlorophenols, aminophenols, chlorocatechols, nitrophenols, and methyl phenols (Wang *et al.,* 2013). Bisphenol and alkylphenols tend to alter the development of mammary glands hence induce endocrine defects to exposed animals (Acero *et al.,* 2005; Marais *et al.,*2019). Toxic phenols and their derivatives readily oxidise to quinone radicals which cause DNA damage or acylation. The damaged DNA is then transcribed into default proteins, e.g., the energy transducing membrane protein thus

disrupting the conveyance of electrons in energy transducing membranes. And this can be fatal. The consumption of phenol contaminated water causes protein degeneration, tissue erosion and paralysis of the nervous system (de la Rosa *et al.,* 2019). It is confirmed that phenol is extremely lethal and carcinogenic; hence the WHO limits its concentration in consumable water to 0.001 mg/L (WHO, 2011)The recovery of phenolic components supplies bio-based chemicals to existing industrial processes and removes toxic pollutants in wastewater.

2.1.4 Multi-component systems

Previous studies established that conditions required to improve adsorbent performance of one pollutant could be contradictory to another (Shipley *et al.,* 2013; Lee *et al.,* 2017; Awad *et al.,* 2020). To date, most studies focus on the analysis and understanding of one adsorbate. Yet, a multi-component solution is relevant for designing, optimising, and operating real-life systems for waste, groundwater and industrial effluents (Mendoza-castillo, 2017). Several synergic, non-interaction and antagonistic effects are noticed using multi-components adsorbate solutions. Hence, the multi-component systems continue to challenge water remediation as far as adsorption is concerned (Gunarathne *et al.,* 2018). This study investigates the co-adsorption of metals and phenols from a multi-component system composed of AAEM, phenolics, sugars, and organic acids e.g., lactic acid.

2.2 Water remediation

Water remediation is a major process in pollution control as it reduces or removes the concentration of specific pollutants that cause adverse effects and threats on the environment and human beings (Joseph *et al.,* 2019). The methods utilised have to be technologically effective and economically feasible. Permissible pollution concentrations, the self-purification capacity of the water source, and industry and municipality economic interests govern to enhance or impede the water remediation process. Methods of removing contaminants are shown in Figure 2.2 below. The complexity of the composition of most industrial and municipal wastewater and stringent discharge limits often requires a combination of different treatment methods. Water remediation processes currently used on an industrial scale rely on conventional technologies like degradation, neutralisation, biological treatment, and physical and chemical treatments. Figure 2.2 below shows the classification of some of the methods currently used in wastewater remediation.

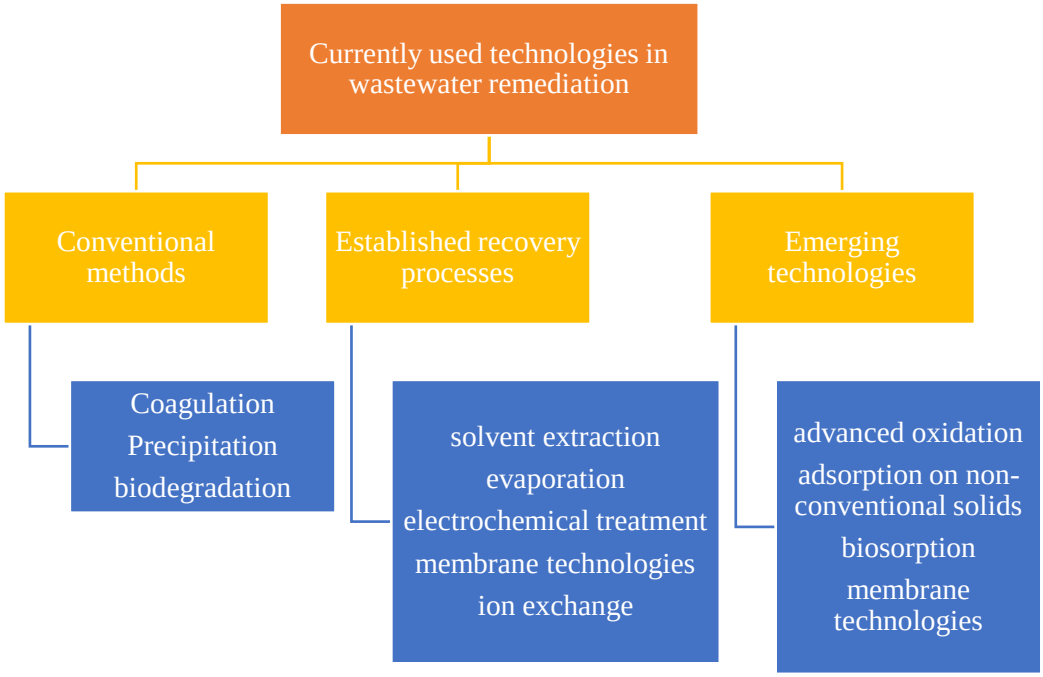

Figure 2.2: Water remediation technologies currently used (Figoli and Criscuoli, 2017; Rodriguez-Narvaez et al., 2017; Sirkar, Singh and Li, 2017).

2.2.1 Conventional methods

2.2.1.1 Chemical precipitation

This process uses pH transition, electro-oxidation or co-precipitation potential with coagulants to eliminate dissolved impurities in water (Escudero *et al.*, 2019). The most common alkaline reagents used for sequential removal of metals are limestone ($CaCO_3$), caustic soda (NaOH), soda ash (Na_2CO_3), quicklime (CaO), slaked lime ($Ca(OH)_2$), magnesium hydroxide ($Mg(OH)_2$ (Figoli and Criscuoli, 2017; Rodriguez-Narvaez et al., 2017). The addition of counter ions reduces metal solubility (Villegas *et al.*, 2016b; Mendoza-Castillo, 2017). Additionally, metal solubility decreases with increased pH, and they precipitate out of solution as heavy metal carbonates, hydroxides, and sulphides. Hydroxide precipitation with lime is considered the most cost-effective in metal removal. Its addition increases the pH, and heavy metals precipitate out of solution as heavy metal hydroxides at varying pH values (Tünay *et al.*, 2010). The process is represented by equation 2.1 below:

$$M^{n+} + Ca(OH)_2 \rightarrow M(OH)_n + Ca^{2+} \qquad 2.1$$

Where M is the metal.

Carbonate precipitation is another method and is represented by equations 2.2 and 2.3 below

$$M^{n+} + nN_aCO_3 \rightarrow nMCO_3 + nNa_{\cdot}^{+} \quad 2.2$$

$$nMCO_3 + H_2O \rightarrow CO_2 + M(OH)_n \quad 2.3$$

Sulphide precipitation has higher removal efficiency than hydroxide precipitation but finding the correct dosage could be challenging. Any overdose results in excessive residual sulphate and malodour, while insufficient dosage surges amount of Zinc in the affluent (Gong *et al.,* 2016; Purwanto, 2016). Equation 2.4 below is the general equation of the process:

$$M^{n+} + S^{2-} \rightarrow M_nS \quad 2.4$$

Some processes have recovered metals at varying pH regimes and synthesised commercially valuable materials such as pigments and magnetite (Gong *et al.,* 2016). Some minerals are recovered and sold to metallurgical industries, offsetting treatment costs (Fu, 2011). Precipitation and coagulation are currently used to reduce heavy metals in aqueous solutions; however, these processes generate a low-density aerated sludge with dewatering and disposal problems. Ion exchange, reverse osmosis, electrodeposition, and adsorption have been proposed as plausible alternative processes in heavy metal removal.

2.2.1.2 Chemical oxidation

Chemical oxidation is a destructive technique utilised in aqueous phenolic treatment (Tünay, 2010). The most common chemicals used in this process include ozone, chlorine, chloramines ferrate and permanganate (Zhang *et al.,* 2013). The oxidation process operates at mild temperatures and pH with a relatively low energy cost. The oxidation treatment mainly uses ferrate and permanganate due to their high reduction potential (E_o ($KMnO_4$) = 1.68V, E_o (K_2FeO_4) = 2.2V), and removes up to 80 % of contaminants (Hadjltaief *et al.,* 2015). The immediate advantages include that permanganate is fairly economical. It is also easy to handle since the produced manganese dioxide sludge is highly stable and does not form chlorinated or brominated by-products. Peings et al. (2015) investigated the oxidation mechanism of phenol by sulfatoferrate (VI) and compared it with permanganate and hypochlorite. The results indicated that excess oxidant is required for complete degradation. Zhang *et al.* (2013) and Wang *et al.* (2021) reported that over 99 % of 5 μmol/L bisphenol A was degraded using 100 μmol/L $KMnO_4$ at pH 7. Hence, they concluded that oxidation using permanganate effectively degrades this endocrine-disrupting

chemical namely bisphenol-A. The degradation mechanism is not fully understood, but Figure 2.3 below shows some of the intermediates detected in the degradation of bisphenol A using permanganate.

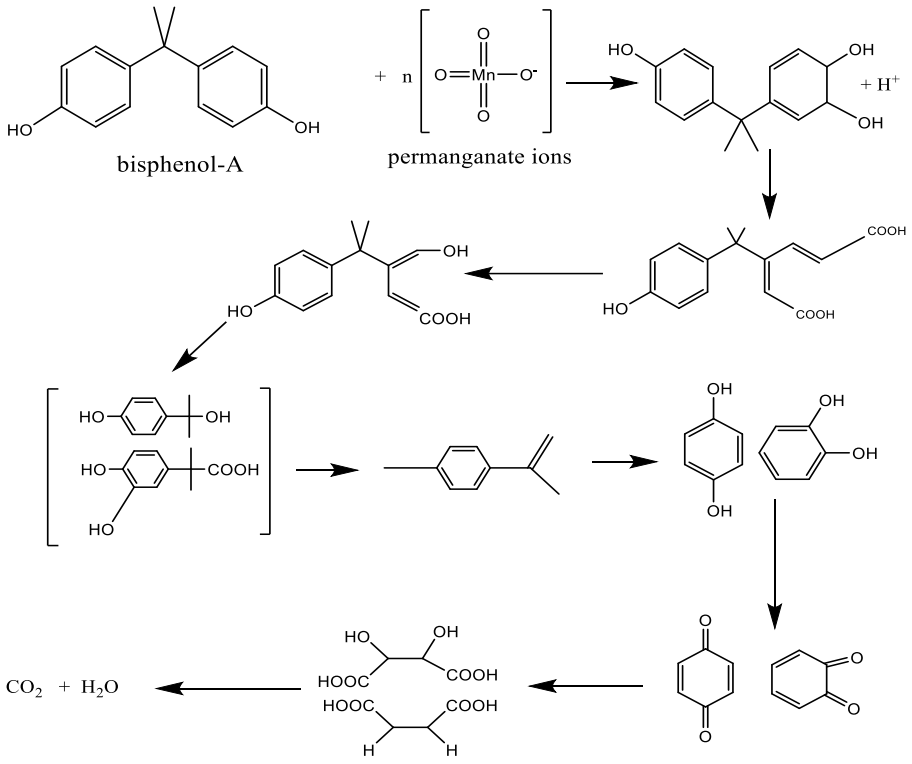

Figure 2.3: Oxidation of phenolic compounds using permanganate with bisphenol A as an example (Zhang et al., 2013)

2.2.1.3 Electrochemical oxidation

Electrochemical oxidation is an alternative treatment for removing phenolics in aqueous media that requires no direct or indirect reagents. Removal occurs on Pt, PbO_2, IrO_2, and boron-doped diamond electrodes (Komtchou *et al.*, 2017; McBeath and Graham, 2021). Doped boron anodes generate hydroxyl radicals, which then participate in the oxydegradation of organic compounds. The treatment efficacy is influenced by parameters like current density, pH, anode material, and electrolytes. Indirect oxidation limits pollutant electrode fouling by the use of intermediary redox reagents for electron transfer. Elimination of organic pollutants with special interest to phenol is prominent in the presence of Cl^- forming Cl_2 or ClO^-. Electrochemical oxidation of o-nitrophenol using a boron-doped diamond anode was studied and showed that 96 % mineralisation was attained after 8 hrs at 60 mA/cm^2 and pH 3 (Rodriguez-Narvaez *et al.*, 2017). The author suggested that the pathway is via hydroxyl radicals from carboxylic acids followed by conversion of organic

nitrogen to ammonium and nitrate ions. It was also concluded that in sodium sulphate electrolytes, O-nitrophenol degrades more efficiently at low pH, unlike in sodium or potassium chloride electrolytes. In other studies, Tünay (2010) and Hadjltaief *et al.,* (2015) examined the oxidation of 2,4-dinitrophenol in batch and continuous-flow reactors using steel coated PbO_2 electrodes. Their results indicated total conversion of organic nitrogen to NH_4^+ and NO_3^- ions at pH 6.6, 1.1 g/L sodium chloride concentration and 1.4 mA/cm^2 current. Based on Lin (2019) results, oxidation with Ti/SnO_2-Sb_2O_5-IrO_2 as an anode and a porous carbon polytetrafluoroethylene (PTFE) composite as a cathode improves the oxidation of m-cresol. However, the process depends on the hydroxyl radicals generated via the Fenton reaction. In as much as the treatment is effective for targeted compounds, the cost of electrodes and energy consumption remains a major concern (Gurung *et al.*, 2018; Rao *et al.*, 2001).

2.2.1.4 Distillation technologies

Distillation technologies are either destructive or constructive and are generally energy-intensive for high-boiling components or components forming azeotropes. Azeotropic distillation purifies phenolic contaminated water based on the relative volatility of phenolic components (Frascari *et al.,* 2016). Researchers (Frascari *et al.,* 2016; Villegas *et al.,* 2016b) introduced phenolic contaminated water to a steam plasma jet, and the results showed that the hydroxyl radicals degraded the phenolic compounds. The main liquid phase intermediates were pyro catechol, hydroquinone, and muconic acid, while the major gaseous products were hydrogen, carbon dioxide and carbon monoxide (Villegas *et al.,* 2016a). However, the process is highly energy demanding and some of the products, e.g., CO, and CO_2 are not eco-friendly.

2.2.2 Established recovery processes

2.2.2.1 Membrane filtration

Membrane filtration have seen significant adoption in wastewater treatment due to their ease of use and flexibility in plant design and operation (Awad *et al.*, 2019; Fosso-kankeu *et al.*, 2018). The process can remove pollutants of different sizes and is more effective at high pollutant concentrations (Yu *et al.,* 2018). Table 2.1 below gives the main pressure-dependent membrane processes and their respective properties and applications in wastewater treatment (Sikdar and Criscuoli, 2017).

Table 2.1: Main features of pressure-driven membrane procedures (adopted from *(Figoli and Criscuoli, 2017)*

Membrane operations	Pore size (µm)	Pressure (bar)	Rejected species	Main applications
Microfiltration	1.0–0.1	0.5–2	Particles, colloids, bacteria	Clarification and sterilisation
Ultrafiltration	0.1–0.01	1–5	All the above plus viruses and macromolecules	Macromolecular recovery and fractionation
Nanofiltration	0.01–0.001	3–30	All the above plus divalent ions	Water softening
Reverse Osmosis	<0.001	10–100	All the above plus monovalent ions	Desalination

The use of membrane processes for water purification is very attractive as there are no chemicals required, and all the operations are done at ambient temperature. The permeate obtained can be rinsed or washed, allowing it to be reusable in other industrial plant processes (Acero *et al.*, 2005; Peydayesh *et al.*, 2019). Furthermore, membrane processes can also be used as an efficient pre-treatment process for downstream chemical oxidation treatment processes. However, membranes are disadvantaged by reducing permeate flux due to membrane fouling caused by concentration polarisation, adsorption of solute on the membrane pores and blocking of pores by rejected solutes (Huang *et al.*, 2020). Various alternatives that reduce fouling have been proposed, including the pre-treatment of feed solutions, adjustment of membrane material properties, membrane cleaning, and improvement by operating conditions. With these adjustments, the membrane processes have become one of the most efficient in low scale water remediation (Assayie *et al.*, 2017).

Ghasemi and Nematollahzadeh (2018) used a polysulfone polymer to synthesise molecularly imprinted membranes to remove polycyclic aromatic hydrocarbons from petrochemical wastewater. The results indicated that the imprinted membranes have a higher affinity for naphthalene molecules. An acetyl-sulphate and styrene modified polyvinylidene fluoride membrane was prepared for oil and water separation (Yan *et al.*, 2018). The results showed that water was preferentially permeated, resulting in pure water permeate.

2.2.2.2 Membrane technologies

Membrane technologies provide substantial advantages over other water remediation processes, including low energy consumption, high-quality effluent, compact footprint and simple scaling of membrane components, but the use of membranes for wastewater streams with a complex mix of pollutants remains a challenge (Wei *et al.,* 2019). Some membranes are used as extractive membrane bioreactors, and hollow fibre membranes can be used as photo-catalytic membrane reactors for high-pressure membrane processes like nanofiltration, reverse osmosis and membrane distillation. Extractive membrane bioreactors (EMBR) and hollow fibre membranes used in aqueous-aqueous extractive membrane processes suggest a high capacity for disposal of phenol in wastewater (Peydayesh *et al.,* 2019). Praveen and Loh, (2013) employed hollow fibre membranes impregnated with trioctylphosphine oxide to extract phenol. Both findings Peydayesh et al., (2019) and Praveen and Yo., (2013) indicated a minimum of 85 % phenol removal. Photo-catalytic Membrane Reactors are hybrid reactors that provide a buffer for photocatalysis and a preferential barrier to the oxidation of contaminants. Rao *et al.,* (2001) also examined the oxidation of organic matter found in tannery wastewater utilising an undoped industrial TiO_2 catalyst, Degussa P25, and N-doped titanium nanoparticles under UV or visible light irradiation, respectively. P25 was only active with UV light, while N-doped titanium was potent in processing tannery wastewater with visible LED light.

2.2.2.3 Ion exchange

Ion exchange involves an exchange of ions between two or more electrolyte solutions. High cation exchange capacity clay and resins are commonly used to uptake metals from aqueous solutions (Mohammed *et al.*,2011; Li *et al.*, 2018). However, this method is labour intensive, limited to a finite concentration of metals in the solution, and sensitive to temperature and pH. Natural and synthetic clays, zeolites, and synthetic resins have been used to remove and attenuate metals from wastewater (Chen *et al.,* 2017). Different adsorbents and membrane filtrations have been applied to separating target products in the HTL aqueous product (Frascari *et al.,* 2019). Anion exchange resin Amberlyst A21 (Cl^- and OH^-) recovered 80 % and 88 % of glucose and acetic acid with the purity of 87 % and 98 %, respectively (Chen *et al.,* 2017; Frascari *et al.,* 2019). Amberlite IR-120 (Na^+ and Ca^{2+}) 97 % acetic acid and 87 % phenol were separated by this cation exchange resin. Anion exchange resins can thus be used to recover monosaccharides and organic acids in HTL

wastewater effectively. Cation exchange resin was applied to recover organic acids and phenolic compounds in high-temperature hydrolysates.

2.2.2.4 Advanced oxidation processes (AOPs)

These advanced oxidation processes are a promising technique that utilises radicals to degrade non-biodegradable and recalcitrant organic constituents from industrial and municipal wastewater. The AOPs are characterised by radical reactions using combinations of chemical agents (e.g. ozone, hydrogen peroxide, metal and or their oxides) and supplementary energy sources (e.g. ultraviolet-visible (UV-Vis) irradiation, electronic current, γ-radiation, and ultrasound) (Tünay *et al.,* 2010). The AOPs vary with how the radicals are formed, and formed radicals initiate radical chain reactions with the organic compounds, thus oxidatively degrading the organic contaminants (Villegas *et al.,* 2016b; Han *et al.,* 2018). The advantages of AOPs include no sludge generation, and radicals are non-selective and hence are compatible with all organic compounds and some inorganic compounds (Wang and Wang, 2007). The reaction is relatively fast hence less retention time is required. However, the high capital and operational costs remain challenging when considering both energy and the chemicals used (Villegas *et al.*, 2016b). Again, there are problems associated with peroxide residual or bromate formation (Han *et al.,* 2018). Hence, their removal should also be considered.

2.2.2.4.1 Photochemical oxidation

Photochemical oxidation involves radical formation using a combination of UV and O_3, H_2O_2, transition metals or metal oxides. H_2O_2 is preferred as an oxidising agent as it is easy to store, safe and efficient (Rodriguez-Narvaez *et al.*, 2017). Benzene, toluene, ethylbenzene, and xylenes were 100% degraded by UV/H_2O_2 and UV/H_2O_2/O_3 when used to treat petroleum refining and petrochemical wastewater (Koley *et al.*, 2018).

2.2.2.4.2 Fenton and Fenton like processes

In Fenton (Fe^{2+}/H_2O_2) and Fenton-like processes (Fe^{3+}/H_2O_2), Fe^{2+} reacts with H_2O_2 forming Fe^{3+} (which regenerates Fe^{2+} under acidic condition) and hydroxyl radicals (Hadjltaief *et al.,* 2015; Komtchou *et al.,* 2017) as shown in the equation below:

$$Fe^{2+} + H_2O_2 \rightarrow Fe^{3+} + \cdot OH + OH^- \quad 2.5$$

The ultraviolet wavelength is crucial in the photo Fenton process; hence in Hadjltaief et al. (2015), a wavelength of 365 nm degraded 100% phenol in only 30 % while 254 nm did the same in one hour. In the same study, the Fenton process removed more phenolics at pH 2 than at pH 5.

2.2.2.4.3 Photo-catalytic oxidation

In recent studies, zeolites (Thomas *et al.*, 2021), active coal (Drumm *et al.*, 2019), structured clay (Hadjltaief *et al.*, 2015) and silica textures (Mahy *et al.*, 2020) have been used as support structures for photo-catalytic catalysts (Beauchet *et al.*, 2012; Rodriguez-Narvaez *et al.*, 2017). In wastewater, the elimination of phenol was studied using ZnO/TiO_2 anchored on a reduced graphene oxide nanocomposite (Wei *et al.*, 2019). Graphene has photo-catalytic properties due to increased surface area and a lower electron-hole recombination rate (Tünay *et al.*, 2010). Microwave-assisted catalytic wet peroxide oxidation catalysed by activated carbon was explored to remove benzene, toluene, xylene, and naphthalene (Mudhoo *et al.*, 2019). The process involves two steps, i.e., pollutant adsorption onto activated carbon, followed by adsorbed compound oxidation. Wastewater particles significantly lowers the catalytic oxidation reaction, hence increasing ozone consumption during catalytic ozonation of petrochemical secondary effluent (Koley *et al.*, 2018; Thomas, 1995; Yang *et al.*, 2019). 4-Chlorophenol degradation was explored using a combination of UV and MnO_2 nanoparticles for peroxymonosulfate activation (Chen *et al.*, 2019). Complete degradation was achieved in the first 30 minutes, and the leaching of Mn was negligible.

2.2.3 Emerging technologies

2.2.3.1 Biosorption

Bio-sorption involves using biological molecules or biomass materials to remove contaminants from wastewater (Jaman *et al.*, 2009; Al-Qahtani, 2016). Bio-sorption includes absorption, adsorption, ion exchange and surface complexation. The process can be economically efficient depending on the selectivity, effectiveness at low solute concentrations, and life-cycle of the bio-sorbents (Li *et al.*, 2018; Manahan, 2003). The advantages of this process include its ease of use and the fact that low-cost adsorbents are readily available. Micro-algae and seaweed, bacteria, fungi, crop residues and plant-immobilised have successfully removed heavy metals and other organic pollutants from wastewater (Chalenko *et al.*, 2012; Ding *et al.*, 2020; Escudero *et al.*, 2019; Ilva *et al.*, 2017). *Ulmus carpinifolia* and *Fraxinus excelsior* tree leaf bio-adsorbents indicate

high removal efficiencies of Pb^{2+} (201.1 and 172.0 mg/g), Cd^{2+} (80.0 and 67.2 mg/g) and Cu^{2+} (69.5 and 33.1 mg/g) respectively. It was achieved at high Na^{+}, K^{+}, Ca^{2+}, and Mg^{2+} concentrations typically found in wastewaters (Gollakota *et al.*, 2017). Bio-sorption setbacks are the released organic compounds from the bio adsorbent itself that contribute to secondary environmental pollution and decrease dissolved oxygen in the water.

2.2.3.2 Adsorption

Adsorption describes the action of an adsorbate (most often in an aqueous solution) binding to the surface of an adsorbent (most often a solid) through either chemical or Van der Waals forces (Weideman *et al.*, 2019). Adsorption can occur from either the gas phase onto a solid or liquid phase onto a solid, for example the adsorption of organic and inorganic species from solution onto activated carbons (ACs) (Li *et al.*, 2019; Zhang *et al.*, 2020). According to Chen *et al.*, (2015), the adsorption process is technologically simple and economically feasible, yielding high-quality water. There are five major steps taking place in series in any adsorption process, i.e.

- External or bulk diffusion of the adsorbate to the boundary film interface of the adsorbent;
- Film diffusion of the adsorbate across the film boundary interface;
- Adsorption of the adsorbate on the outer surface of the adsorbent;
- Internal diffusion of adsorbate from the outer surface of the adsorbent particle to internal adsorption sites;
- Chemical or physical adsorbate adsorption onto active sites within the pores of the adsorbent (Singh *et al.*, 2012).

The adsorption process steps are visually presented in Figure 2.4

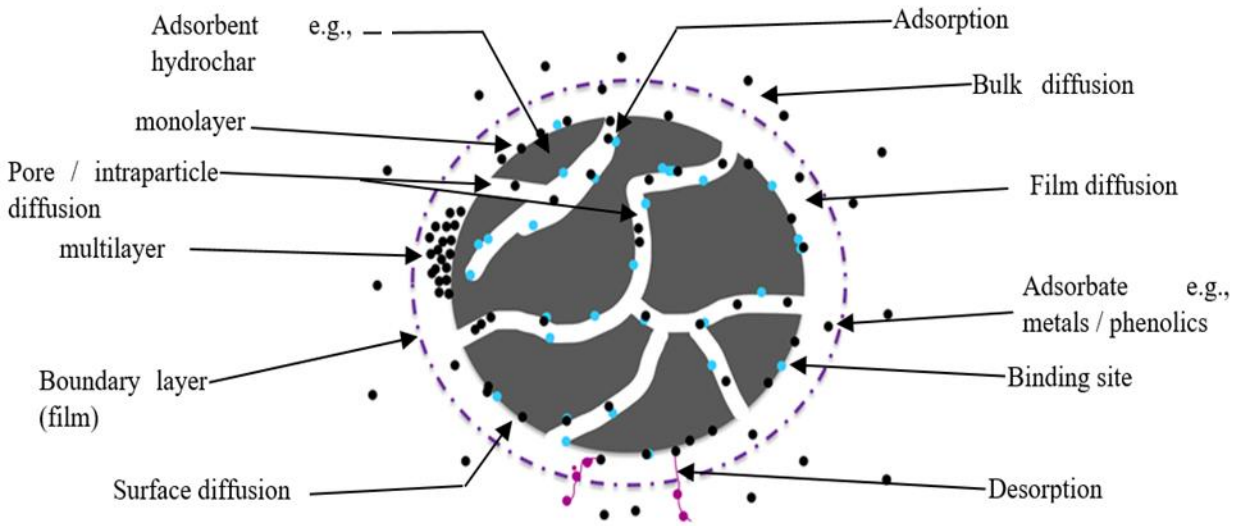

Figure 2.4: Adsorption process at a microscopic level (Singh *et al.,* 2012).

Atoms, ions or molecules adhere to the adsorbent surface physically (physisorption) or chemically (chemisorption) (Rashed, 2013; Thomas, 1995). Physisorption is when the adsorbate binds to the active sites on the surface of the adsorbent through weak interactions such as Van der Waals forces, hydrogen bonds, and dipole-dipole interactions (Dai *et al.*, 2019; Wang *et al.*, 2019). These intermolecular forces negate the significant changes in electron orbital patterns of species and are therefore easily reversible by desorption processes. Chemisorption involves strong adsorbate-adsorbent interactions whereby the specific functional group of an adsorbate forms a chemical bond with the adsorbent through electron exchange (Sangi *et al.,* 2008; Wang *et al.,* 2019). The process is irreversible and difficult to recover both adsorbent and the once adsorbed material through desorption processes. Adsorption is a potential innovation that could be used to remediate wastewater at a reasonable expense. By understanding the process, it is possible to design and develop more effective adsorbents and processes. Adsorption has significant advantages over other conventional water treatment systems. These advantages include minimal running costs, highly efficient operating procedures, absence of hazardous by-products, regenerating capacity, reversibility, and desorption capabilities (Mendoza-Castillo, 2017; Ni *et al.*, 2019). However, the economic and technical feasibility of desorption depends on the adsorbent type and the pollutant targeted for removal.

2.2.3.2.1 Adsorbents

Zeolites, clay, chitosan and chitin are some of the adsorbents currently used to remove pharmaceuticals, metals, phenolic and aromatic derivatives, pesticides, and dyes (Li *et al.*, 2016). The adsorption capacity is influenced by the physical nature of the adsorbent, its pore structure, and functional groups. The adsorbate functional groups, polarity, molecular weight, size, and solution conditions such as pH and ionic strength all in combination influence adsorption capacity. Activated carbons (ACs) have exceptionally high surface areas (500-5000 mg), well-established internal micro-porosity and a spectrum of oxygen functional groups (OFGs) (Artelle and Odgers, 2010; Ding *et al.*, 2020). Crini *et al.* (2011) and Ghobashy *et al.* (2018) obtained high adsorption affinities for organic pollutants using cross-linked polystyrene organo-gel prepared via tetrachloroethylene radiolysis and use of Co-60 gamma rays. The polystyrene organogel indicated reusability and good stability for up to five cycles. Nitroaniline was removed from wastewater using raw and oxidized multiwalled carbon nanotubes mixed with H_2SO_4/HNO_3. The results indicated that the material is a good adsorbent with high chances of recovery (Li *et al.*, 2009) Despite its excellent performance, activated carbon remains an expensive commodity; hence, this is not a viable option (Yangui *et al.*, 2017). For that reason, this research focuses on the development of non-conventional solid materials as a low cost-efficient and green adsorbent that eliminate pollutants even at trace levels like biochar.

2.3 Biochar

Biochar is a dark carbonaceous solid material from the thermal decomposition of biomass at high temperatures and pressure in the absence of oxygen (Tian *et al.*, 2020; Wang *et al.*, 2019). Naturally, it is usually found in the soil due to vegetation fires and historic soil management practices (Yang, Zhang, *et al.*, 2019). Biomass for biofuels studies also confirmed that pyrolysis, gasification, hydrothermal carbonization (HTC) and hydrothermal liquefaction (HTL) of lignocellulose material produce biochar (Valdez *et al.*, 2012; Wang and Wang, 2019). Hydrochar is biochar from the HTL process. Many mechanisms clarify the hydrochar physiochemical properties. Fuertes, (2010) suggests hydrochar as a polyaromatic lignin type material built on a hydrophobic core of stable oxygen groups like ether, pyrone or quinones and hydrophilic shell of oxygen functional groups (OFGs), hydroxyl, phenolics, carboxyl or carbonyls. The second one confirms that hydrochar has most of its carbon cross-linked via sp^3 and sp^2 hybrid bonds and such features contribute to the sorption of positively charged species like heavy metals. The char has

physicochemical properties that influence its potential application in wastewater pollution remediation, bioenergy production and soil enrichment (Peydayesh *et al.,* 2019). Although hydrochar is a promising adsorbent, characterisation is only beginning; hence for effective utilisation of the hydrochar, the structure and underlying mechanisms should be investigated. This study focused on applying hydrochar as an adsorbent of heavy metals and phenolics in an aqueous solution, emphasising relevant hydrochar characteristics.

2.3.1 Biochar engineering

2.3.1.1 Pyrolysis

Pyrolysis uses temperatures ranging from 300-1200 ˚C, forming a solid residue (biochar), liquid bio-oil from condensed vapours, and non-condensable gases (Lee *et al.,* 2019). Examples of pyrolysis processes include torrefaction, slow, fast intermediate, flash, or microwave pyrolysis. The pyrolysis methods differ in reaction conditions, such as how fast the heat is transferred, resident time, and product quality and distribution (Garcia-Perez *et al.*, 2011). Depending on the desired products, different forms of pyrolysis are used. Slow and intermediate pyrolysis have moderate heating and long residence times that yield 30-35 % of gases and vapours and approximately 40 % of char (Arán *et al.,* 2016). Fast pyrolysis with rapid heating and fast cooling of the generated gases is preferred when liquid products are prioritised. The liquid yield increases to 75 % (Panisko *et al.,* 2015). Most biomass materials are wet, have a moisture content of up to 95 wt. %, and require drying before pyrolysis (Gollakota *et al.*, 2017). This process has high operation and investment costs and produces gases and ashes that potentially harm the environment.

2.3.1.2 Hydrothermal processes

Hydrothermal carbonization (HTC) and hydrothermal liquefaction (HTL) involve solid heating materials in an aqueous solution under high pressures in high-pressure reactors (HTC (180-280 ^{o}C) and HTL (200- 450 ^{o}C) (Gollakota *et al.*, 2017). Most solid raw materials used in the hydrothermal processes are native plants, municipality solid waste, algae. An amount ranging from 60-86 % of biomass is converted to solids in HTC, while pyrolysis only produces 50 % (Ferrentino *et al.*, 2020) Out of the 60-86 %, 50 % of that carbon is aromatic (Arán *et al.,* 2016). Thus, HTC has high carbon conversion efficiency, for it has low /C and O/C ratios. The aromaticity of the biomass brings about several oxygen-containing functional groups (OFG) like carboxyl, hydroxyl,

and carbonyl carbons to the hydrochar. Compared to pyrolysis, hydrothermal processes are done at moderate conditions, lower temperatures in the range of 180 – 450 ^{o}C and pressures from 4 to 22 MPa (Yang *et al.*, 2019)

2.3.1.3 Hydrothermal liquefaction (HTL)

Hydrothermal liquefaction (HTL) converts wet organic biosolids into bio-crude oil for fuel or other biochemical products at elevated temperatures (200–450 ^{o}C) and pressures (10–15 MPa) (Gollakota *et al.*, 2017). Four products are produced (1) bio-crude oil, (2) biochar solid residue, (3) CO_2-rich gas, and (4) aqueous post-HTL wastewater (PHWW) (Gollakota *et al.*, 2018; Pipitone *et al.*, 2019; Fan *et al.*, 2020). The process yields very little gas (1-5 %), and the organic compounds remaining contribute to the liquid and solid products as shown in Figure 2.5. Hydrochar is biochar from the HTL process. HTL is advantageous over pyrolysis due to the following reasons:

- The biomass does not require drying before treatment since water is a solvent and reactant, and some researchers contend that it also has a catalytic function in the process.
- Gaseous sulphur oxides and nitrogen oxides solubilize, reducing the emission of these toxic gases during the hydrothermal biomass conversions.
- Heating under very high pressures improves the thermal efficiency of the process as it reduces latent heat loss when liquid water is vaporising.
- The process uses relatively lower temperatures as compared to pyrolysis because water participates as a reactant.
- Water is supercritical at high temperatures and pressure and exhibits an organic solvent nature.

Therefore, considering the above reasons, pyrolysis consumes much energy through biomass drying and can release harmful gases; hence, this project opts for HTL. One needs to understand the overview of the HTL process, mainly the type of biomass used and the reaction conditions. These two enable one to predict the components of the aqueous phase and the quality of the biochar; hence the better the adsorption (Maddi *et al.*, 2016; Schuler *et al.*, 2017; Gollakota *et al.*, 2018).

2.3.2 HTL feedstock

Hydrochar is synthesised from numerous feed stocks, mainly plant matter from agriculture and forest remains and municipal solid waste materials, e.g., sewage sludge, and industrial waste, e.g., paper and pulp industries. They all contain a fraction of hemicellulose, cellulose, lignin, lipids and protein (Han, Qian, *et al.*, 2016). Cellulose is a complex long, linear chain of glucose joined together by β glycosidic linkages and denoted by $(C_6H_{10}O)_n$ (Schuler *et al.*, 2017). Hemicellulose is a branched heteropolymer with an amorphous structure embracing pentose and hexose monomeric units, namely D-xylose, D-galactose, and uronic acid (Schuler *et al.*, 2017). Lignin is a more complex structure than cellulose and hemicellulose composed of paracoumaryl, confieryl and sinapyl alcohol cross-linked by ethers hence resistant to biological degradation (Elliott *et al.*, 2015; Schuler *et al.*, 2017). Lipids and fats are non-polar compounds immiscible in water or hydrophobic, for example, triacylglycerides (TAGs). During HTL, the glycerol further degrades into acetaldehyde, ethanol, acrolein, aldehydes, propionaldehyde, CO, CO_2 and H_2 (Gai *et al.*, 2014). Proteins consist of several chains of peptide polymers of amino acids and are the major constituency in microbial and algal biomass. Figure 2.5 below shows the fate of these macromolecules when subjected to the HTL process. The amount of these macromolecules varies with the type of feedstock.

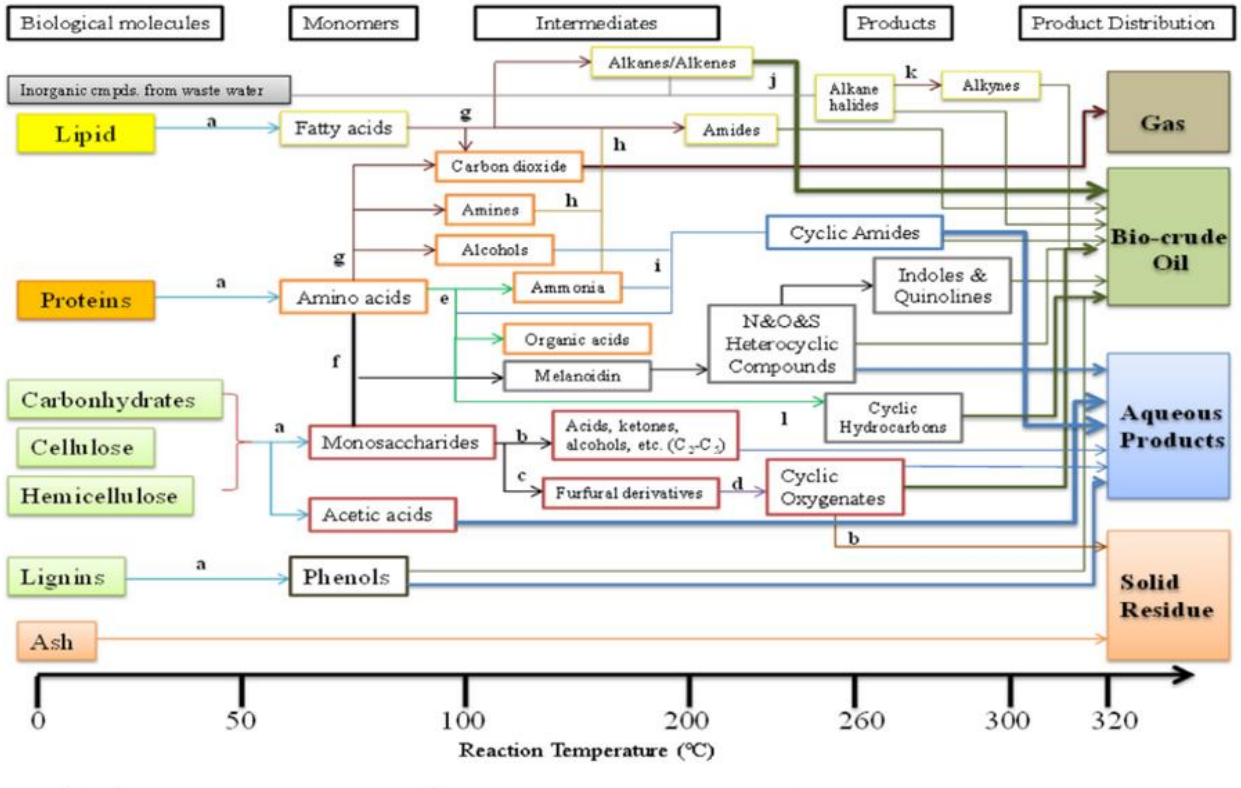

Figure 2.5: Fate of feedstock macromolecules subjected to HTL (a) hydrolysis; (b) decomposition; (c) dehydration; (d) polymerization; (e) deamination; (f) Maillard reaction; (g) decarboxylation; (h) aminolysis; (i) cyclization; (j) halogenations; (k) dehydrohalogenation; (l) condensation pyrolysis (adopted from Watson et al., 2020)

2.3.2.1 Agricultural and forest residues

An estimated 500 million tons of plant waste are produced globally and annually from agricultural and forest residue (Duku *et al.*, 2011). The majority of the residues generated are scarcely utilised; hence they can serve as feedstock for biochar production. The biochars produced from agricultural feedstock show large surface areas, which lead to the sorption of aqueous chromium, Cr (VI) (Sun *et al.*, 2014; Wang *et al.*, 2015).. Biochars produced from poultry waste and dairy manure was successfully used to remove heavy metals (Al-Anber, 2011; Ding *et al.*, 2020; Uchimiya *et al.*, 2013).

2.3.2.2 Industrial by-products and non-conventional materials

The use of industrial waste and by-products in the synthesis of biochar is currently of significant interest. Sun *et al.* (2014) investigated the use of digested residues from bioenergy facilities and

sewage sludge from wastewater treatment plants, and results show 70 % removal of metal pollutants. The production of carbon adsorbents from non-conventional materials such as waste tyres, algae, newspaper scraps, plastics, bones, bio-energy residues, and food waste have also been examined for producing carbon sorbents (Purevsuren *et al.,* 2004; Green Cape, 2019; Fu *et al.,* 2019). These studies have concluded that bone biochars are heterogeneous sorbents (Purevsuren *et al.,* 2004).

2.3.3 Municipal solid waste

Municipal solid waste (MSW) encompasses all the feedstock from various sectors. Solid waste refers to the refuse, litter, sludge, and other unwanted materials generated by industrial, commercial, mining, agricultural operations and community activities (Landsberger, 2019). A million tonnes of solid waste are generated annually in South Africa. About 32 % of this solid waste can be recycled, mostly paper, bottles, plastics, and metals (Landsberger, 2019).The rest of the waste is exposed to old waste management practices like dumping, incineration, composting and landfill. However, these practices cause environmental pollution through greenhouse gas emissions from landfill sites and leakage of landfill leachate into the soil and groundwater resources (Braghiroli *et al.,* 2018). The generation of municipal solid waste is directly linked to population and industrial developments (Braghiroli *et al.,* 2018). Waste emanates from South Africa's very own industries, poor management of this solid waste results in mixed landfill sites and heavy metal, leaching causing both soil and water pollution. Urbanisation concentrates people in certain places resulting in the accumulation of solid waste and polluted wastewater and this is a global problem for both developed and third-world countries. Hence it is necessary to find solutions for these circumstances from within. One of the waste management practices that has gained interest in the past few decades is energy generation (Dlamini *et al.,* 2019). Biomass for biofuels studies proposed that accumulating Organic Fraction Municipal Solid Waste (OFMSW) can be employed to generate renewable sources of energy (Yang, He *et al.,* 2019). Studies also show that OFMSW produces cheap, efficient adsorbent biochar that can be successfully employed in wastewater treatment (Ayeleru *et al.,* 2011; Kantakanit *et al.,* 2018). Therefore, the MSW is anticipated to generate hydrochar and used in wastewater treatment, addressing soil waste accumulation and wastewater problems, thus protecting human health and the environment.

2.3.4 Applications of hydrochar

Biochar is unique among resource technologies. It has the potential to address several problems at once: soil quality, water quality, crop health, carbon sequestration, energy production, and greenhouse gas emissions. Getting the most out of any biochar system requires the creativity and cooperation of multiple players across agriculture, government, and related industries. Current evidence suggests that the type of biomass used in HTL has a major impact on hydrochar characteristics (Yin and Tan, 2012; Gollakota *et al.*, 2018). The biomass composition determines concentrations of elemental constituents, density, porosity, and pH of the hydrochar that is ultimately produced. The properties of hydrochar influence its use for various applications.

2.3.4.1 Carbon sequestration

Hydrochar/biochar has a high carbon content, thus a good material carbon sequestration for climate change mitigation, reducing the emission of greenhouse gases like CO_2, and CH_4 from the soil. Fang *et al.,* (2017), carried out adsorption of CO_2 and N_2O on beet, corn, and bark hydrochars from the soil. The results show that they were able to adsorb N_2O from the soil thus reducing N_2O emission, and the corn hydrochar reduced the CO_2 emission. However, beet chip hydrochar increased CO_2 emission because there was no CO_2 adsorbed on to the hydrochar. In the studies of Brewer (2012), biochar soil treatment decreases nutrient leaching, ammonia volatilization, and denitrification. Hence, these nutrients are less likely to end up in water or the atmosphere. Biochar also increases the soil's cation exchange capacity as it tends to hold beneficiary potassium and calcium for plant use (Fuertes *et al.,* 2010). Studies indicate a decrease in methane and nitrous oxide emissions; in some cases, up to 70 % of the N_2O is noticed in biochar amended soils compared to the control soils (Wang and Wang, 2019).

2.3.4.2 Soil amendment and fertility

Despite hydrochar having a low nutritional content for use as a fertiliser, it can boost fertiliser effects by reducing fertiliser loss through leaching or runoff. It absorbs the nutrients using its porous surface and slowly releases them to the soil for plant uptake. Fang *et al.,* (2017) and Xiong *et al.,* (2020) recorded harvest improvement for beans and barley upon adding the char to the soil. However, a decrease in the growth and yield of sugar beetroot is linked to the decomposition of hydrochar-immobilised nitrogen in the soil (Gai *et al.*, 2014; Marta *et al.*, 2019). Therefore, hydrochar can upgrade the soil quality in agricultural sectors by slowing down nutrient

decomposition from the soil. Lastly, hydrochar improved physiochemical properties like water holding capacity, pH, cation, and anion exchange capacity of the soil, thus having a synergic effect with fertilizers on enhancing plant growth (Gai *et al.*, 2014). Water retention using hydrochar was significant in sandy soils with a low available water capacity (AWC) and is attributed to hydrochar porous structure, which decreases the bulk soil density and increases pore volume; thus, more water is retained. Therefore, hydrochar has a potentially useful contribution to the future of agriculture.

2.3.4.3 Fuels

Gas, solid and liquid fuels are all products of both HTL and HTC. With hydrochar having low ash content, it is considered a potential solid fuel (Demirbas *et al.*, 2018; Reza *et al.*, 2013). Besides, the lower ash content products burn cleaner and more efficiently than the high ash content ones. In recent research, studies show that the higher heat value is in the range of 15- 32 MJ/kg (Koley *et al.*, 2018; Saqib *et al.*, 2018). In another study, pinewood hydrochar pellets were found to have a mass density of 1468.2 kg/m^3 and the higher heating value (HHV) of 26.4 MJ/kg (Zhang *et al.*, 2017). The significant dehydration and decarboxylation reactions during the thermal chemical process are responsible for the energy density. Therefore, hydrochar with high carbon content can be applied in power generation industries as a fuel.

2.3.4.4 Hydrochar a Catalyst during Heterogeneous Oxidation

Catalytic ozonation processes, Fenton-like reactions, and photocatalytic systems use hydrochar based catalysts in water remediation. Reza *et al.*, (2013); and Gene *et al.*, (2015) tested the catalytic potential pistachio hull biomass-derived biochar for catalytic potential. The microporous structure and surface functional groups of hydrochar were beneficiary in the ozonation of red 198 dye. Recent studies concluded that the carbon material are capable stimulating various oxidants during water remediation. (Fang *et al.*, 2017; Lei *et al.*, 2018) demonstrated that pine needles, wheat, and maize straw consequent biochars encourage synthesis hydroxyl radicals (OH•) upon exposure to oxygen. Wu *et al.*, (2013) reported that biochar free radicals lose electrons to oxygen, forming superoxide radicals and H_2O_2, which further generate OH•. These radicals are efficient in organic pollutants degradation.

2.3.5 Hydrochar as an adsorbent

Hydrochar characteristics, including high surface area, surface functional groups and porosity, complement its use as an adsorbent in removing pollutants (Lee *et al.*, 2019; Wu *et al.*, 2013).These adsorptive properties suggest that biochar may be especially beneficial in the containment step of the remediation process, perhaps not as effective as purpose-made activated carbons but potentially more cost-effective. Hydrochar made from rice husk pyrolysis has a large surface area of 132.86 m^2/g, rapidly increasing to 1818.45 m^2/g when activated with KOH, resulting in increased phenol adsorption 309 mg/g with a removal percentage of 96 % (Fu *et al.*, 2019). The porosity of the hydrochar from HTC of sawdust and pinewood significantly increase both adsorption capacity of 1,2,4 trichlorobenzene (49.78 mg/g) and methylene blue (556.36 mg/g) and removal percentage to over 85 % from aqueous solutions. FTIR of various hydrochar confirmed the presence of surface functional groups (–COOH, -OH, $-CH_3$, -C=O and C-O), which significantly improve adsorption of metals, organic compounds, dyes and pharmaceuticals (Barrera-zapata, 2017; Del Bubba *et al.*, 2020; çaglar *et al.*, 2018; Zhou *et al.*, 2019). Like activated carbons, hydrochar has the potential as an adsorbent for many metals organic molecules, including polycyclic aromatic hydrocarbons (PAHs) and phenolic compounds (Lei *et al.*, 2018; Mu'azu *et al.*, 2017). However, hydrochar is more beneficial, for it is a low-cost material, eco-friendly and can be synthesised from a spectrum of feedstock (Ding *et al.*, 2020; Reza *et al.*, 2013). Moreover, its mechanical and thermal stability remains advantageous to its application in heavy metal and phenolic sorption (Ding *et al.*, 2020; Mohan *et al.*, 2014). Therefore, it can be employed in wastewater treatment reducing solid waste accumulation and improving recycled wastewater quality.

2.3.5.1 Mechanisms for hydrochar- adsorption

Sorption mechanisms explain biochar adsorption systems, which vary considerably with biochar properties and the target pollutants (Joseph *et al.*, 2019). Figure 2.6 below illustrates adsorption mechanisms associated with organic and inorganic compounds on adsorbent hydrochar (Oliveira et al., 2017).

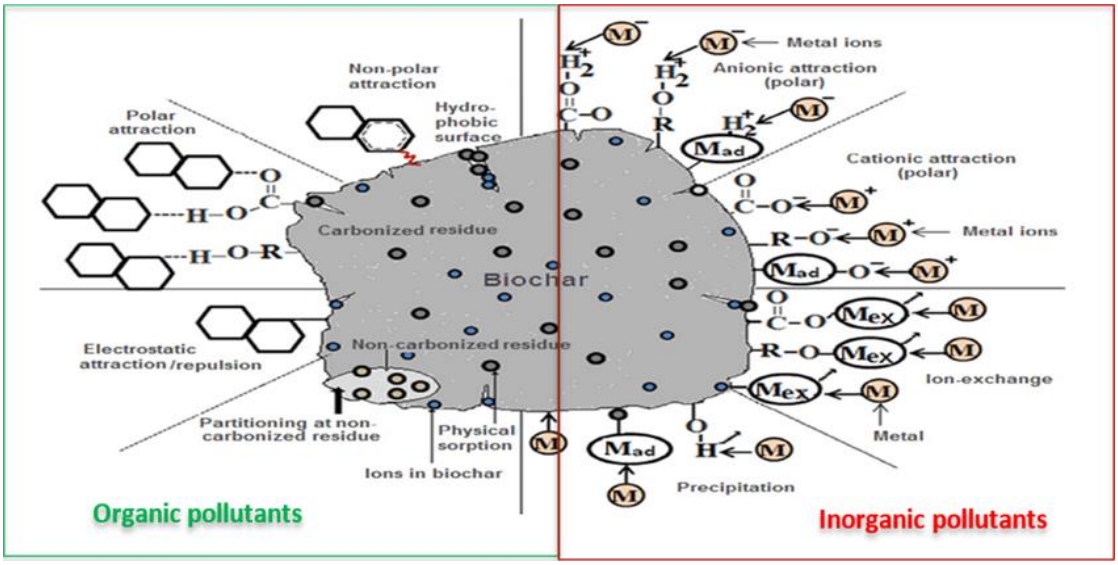

Figure 2.6: Adsorption mechanism for both organic and inorganic pollutants onto hydrochar. (M_{ad}- metal adsorbed, M_{ex}- exchangeable metal ion)(Oliveira et al., 2017)

2.3.5.1.1 Physical or surface sorption

Physical or surface sorption is the binding of adsorbates on the hydrochar surface without forming a chemical bond. Increasing carbonisation temperatures above 300 ^{o}C promote biochar pore volume and surface area (Ferrentino *et al.*, 2020; Reza *et al.*, 2013). Uranium and copper were effectively removed from aqueous solutions using biochar from switchgrass (300 ^{o}C) and pinewood (700 ^{o}C), and the process was concluded to be surface diffusion (Jin *et al.*, 2018). (Purevsuren *et al.*, 2004) reported animal bone derived hydrochar to remove 0.54 mmol/g of Cd in their pore networks, and the process was adequately controlled by film diffusion.

2.3.5.1.2 Ion exchange

Ion exchange is a chemical process whereby unwanted dissolved ions exchange for other ions with a similar charge. In cation exchange water treatment, positively charged ions such as Hg^{2+}, Pb^{2+}, and Ag^{+} interact with positively charged ions on the resin surface, primarily $Na^{+}/K^{+}/Ca^{2+}$. Sulphates, arsenic, nitrates, and fluorides are all negatively charged ions exchanged with negatively charged ions, generally chloride (Frascari *et al.*, 2019). Several transition elements show a strong binding ability to surface functional groups, as shown in Figure 2.6 above. Accordingly, rice husk biochar produced at 175–180 ^{o}C indicates strong sorption capacity for Zn and Hg due to the deprotonation of C-H followed by subsequent exchange for Zn_2C and HgC (Mohamed *et al.*, 2017). Cation exchange was a dominant mechanism in the enhanced removal of

Pb and Cd using wheat straw, plum stone and grape husks (Trakal *et al.,* 2016). Lu *et al.,* 2012's FTIR analysis suggested the possible ion exchange between the metals and the cationic containing functional groups, e.g. R-O-M^+ or R-COO-M^+ where M is metal (Flora *et al.,* 2013; Penido *et al.,* 2019). Regmi et al., (2012) recommended the mechanism though he strongly believes that the cationic ∏- interactions cannot be neglected.

2.3.5.1.3 Precipitation and complexation

In adsorption processes, precipitation refers to the establishment of solids on the adsorbent surface. Outer and inner-sphere complexation forms multiatom structures with specific metal-ligand interactions. This binding mechanism is potential to transition metals with partially filled d-orbitals and high affinity for ligands like carboxyl, phenolic, and lactonic that effectively bind with heavy metals, as shown in Figure 2.6 (Escudero *et al.,* 2019; Inyang *et al.,* 2016). Wang *et al.,* (2015) concluded that precipitation was the dominant mechanism in the Cd adsorption through the formation of insoluble Cd compounds. Inyang *et al.,* (2011) reported that hydro cerussite from bagasse biochar was responsible for precipitating Pb ions [Pb_3 $(CO_3)_2(OH)_2$]. Similarly, Elaigwu and Greenway, (2016) established 45.3 mg/g and 38.3 mg/g for Pb^{2+} and Cd^{2+} removal, respectively, using the hydrochar prepared from *Prosopis afficana* shells. Scanning electron microscopy analysis of the biochar also shows that insoluble complexes appear on the biochar surface after the adsorption of heavy metals (Fu, Shen, *et al.*, 2019; Lee *et al.*, 2019). In complexation, the metal with multiple oxidation states complexes with specific metal-ligand interaction, usually with the adsorbent OFGs. çaglar *et al.,* (2018) reported that complexation and cation-∏ bonding increased the adsorption of Cd ions from 1.76 mg/g to 101.0 mg/g and Cu ions from 1.63 mg/g to 64.9 mg/g. Similarly, some animal waste-derived chars with phosphate ligands form pyromorphite, a complex with Pb ions (Han,*et al.*, 2016) .Some of the metal complexes that were intercalated in the hydrochar carbon matrix include carbon sylvite (KCl), calcite ($CaCO_3$), hydroxyapatite ($Ca_{10}PO_4)_6(OH)_2$), and calcium anhydrite ($CaSO_4$).

2.3.5.1.4 Electrostatic attraction / repulsion

According to Wang and Kaskel (2012), high temperatures favour graphene production, a structure vital for removing pollutants via electrostatic attraction/repulsion, as shown in Figure 2.6. The researcher reported that the electrostatic interaction between the positive biochar and negatively charged CrO_4^{2-} were responsible for removing chromium ions. Electrostatic interaction between surface charged biochars pollutants is a prevalent mechanism and depends on the pH of a solution

and the hydrochar point of zero charges (pH_{PZC}). The two are responsible for the hydrochar metal immobilization (Gai *et al.*, 2014; Pan *et al.*, 2010; Xia *et al.*, 2019). The cationic Pb is attracted to anionic hydrochar derived from rice and wheat, resulting in high removal efficiency of Pb (Qiu *et al.,* 2008. Similarly, Lin and Xing, 2008), observed Pb retention on *Oryza sativa* and *Triticum aestivum* derived chars.

2.3.5.1.5 Electron donor and acceptor interaction

Similar to Figure 2.6 above (polar attraction), electron donor and acceptor interactions are dominant in the sorption of aromatic compounds with graphene-like biochar surfaces. At less than 500 ^{o}C biochar synthesis temperature, irregular charge sharing between the biochar aromatic rings generates ∏ electron enriched or deficient mediums (Fuertes *et al.,* 2010; Wang and Kaskel, 2012). Therefore, the ∏ aromatic biochar system acts as either an electron acceptor or electron donor in the sorption of organic pollutants. Liu and Zhang, (2009) and Villegas *et al.*, (2016a) reported sorption of sulfamethoxazole on ∏-electron enriched reed biochar due to the interaction between the aniline protonated rings and the biochar aromatic compounds. The ∏- electron donor and acceptor interaction between the aromatic char and the chlorine were accounted for the atrazine sorption.

2.3.5.1.6 Partitioning

Carbonised (graphene and crystalline-like fractions) and non-carbonised (non-crystalline, amorphous and organic carbon) fractions of biochar control the sorption of organic pollutants (Wang *et al.,* 2013). In partitioning, the sorbates diffuse into either the pores or matter of organic carbon. The diffused organic compounds solubilize with the biochar matrix and enhance their adsorption (Kasozi *et al.,* 2010). At high solute concentration and or volatile matter content, enriched biochar partitioning is the dominant mechanism (Han *et al.*, 2016). Flora *et al.,* (2013) reported atrazine sorption on organic carbon of dairy and swine-derived hydrochar and concluded partitioning as the mechanism. Kasozi *et al.,* (2010) suggested a pore-filling mechanism as the dominant mechanism in catechol sorption using oak, gamma grass-derived biochar. The hydrochar surface micropores assisted in the sorption of 1.4 dichlorobenzenes and 1, 2, 4 trichlorobenzenes.

2.3.5.1.7 Hydrophobic interactions

This mechanism consists of both partitioning and hydrophobic mechanisms in the sorption of hydrophobic and neutral organic compounds. Deng *et al.,* (2015) reported that the high hydrophobicity of perfluorooctane facilitated its adsorption on bamboo-derived char. Similarly, perfluorooctane sulfonate showed similar results on its adsorption on corn-straw derive hydrochar.

2.3.5.2 Hydrochar activation

Recent studies indicate that modifying the hydrochar chemical structure and surface structure enhances its efficiency as heavy metal and phenolic adsorbent (Zhang *et al.,* 2018). Hydrochar surface modification is currently via thermal and (or) chemical treatments. Chemical treatments use acids, bases, acids and bases, surfactants, ozone or biological modification (Sangi *et al.,* 2008; Regmi *et al.,* 2012; Sun *et al.,* 2015a; Yoon *et al.,* 2017). Regmi *et al.* (2012) proposed cold alkali activation. The outcomes of the experiments suggested that 2 mol/L KOH increased the hydrochar porous structure and adsorption capability. The activated switch grass hydrochar exhibited high adsorption of 34 and 31 mg/g for Cd and Cu, respectively, compared to 1.5 and 1.8 mg/g for untreated chars. An investigation on sawdust, wheat straw and corn stalk by (Sun *et al.,* 2015) illustrated that KOH treatment increased the OFG and aromatic quality of the char, which doubled the Cd removal efficiency in aqueous solutions from 13.92- 14.51 mg/g in untreated chars to 30.40-41.09 mg/g in KOH treated chars (Deng *et al.,* 2017).

Another modification method that has been applied is impregnation with organic and inorganic compounds (Maddi *et al.,* 2016; Trakal *et al.,* 2016; Wang and Wang, 2019). The selection of the modification method greatly influences the cost efficiency of the hydrochar as a whole (Bogusz *et al.,* 2015; Yangui *et al.,* 2017). CO_2 activation of chars from pyrolysis of pinewood and rice husks significantly increased their Cu^{2+} adsorption capacities to 25.18 and 22.62 mg/g from the 4 mg/g of untreated chars (Liu and Zhang, 2009; Zhu *et al.*, 2015). Tong *et al.,* (2011) conducted batch experiments, investigating the effect of 10 % H_2O_2 treated peanut hull-derived hydrochar on heavy metal adsorption. Acquired results indicated 22.82 mg/g Pb^{2+} sorption ability; thus, 20 times that of the untreated char (0.88 mg/g). In some of his work, the H_2O_2 activation also shows efficient adsorption of Cu^{2+}, Cd^{2+}, and Ni^{2+}. Ifthikar *et al.,* (2017) mention that although the hydrochar has excellent sorption, its separation after treatment remains a problem due to its small-sized particles and lower density and recommended modification with magnetic material.

Generally, the greater the surface area and porosity, the better the adsorption performance of the adsorbent. In an XRD (x-ray diffraction) study of the crystalline biochar structure and phase composition, the $CaCO_3$ and KCl disappeared when biochar was modified with the acid and base, which resulted in the increased surface area hence maximal equilibrium adsorption of As (V) and Cd (II) of 22.8 and 41.6 mg/g, respectively. SEM images of chitosan-pyromellitic anhydride treated hydrochar exhibited a rough exterior morphology and a higher number of tiny and fine pores than untreated hydrochar, resulting in a 30 % increase in Pb^{2+}, Cd^{2+}, and Cu^{2+} adsorption. Thus modification improved the surface area from 32.1 to 62.6 m^2/g and the pore size 0.038 to 0.096 cm^3/g, respectively (Donar *et al.,* 2016; Yoon *et al.,* 2017). In this study, hydrochar is activated using an alkali KOH and acid HCl because, unlike some treatments, the procedure is done at room temperature, yielding a char with excellent adsorption capacity for both heavy metals and phenolics (Mihajlovic *et al*.,2017; Fu *et al.,* 2019).

2.4 Batch adsorption

2.4.1 Performing adsorption experiments

A continuous column or a batch system are typically used in adsorption experiments. In batch operation, a fixed amount of adsorbent is added to a predetermined volume of adsorbate solution at a specific pH, temperature, contact time, and agitation speed. The samples are withdrawn at different time intervals, and the remaining adsorbate concentration is measured (Sangi *et al.,* 2008). The column system involves packing a column with adsorbent and running an adsorbate solution through it at a set flow rate (Negrea *et al.,* 2020). The amount of adsorbate bound to the adsorbent is then calculated from the eluted samples. For both processes, the adsorbate adsorbed on the biochar q_e (mg/g) is determined using the Equation 2.6 below while the % removal (removal efficiency) is determined by equation 2.7 below (Duan *et al.*, 2017; Mohamed *et al.*, 2017);

$$qe = \frac{(C_o - C_e)V}{m} \qquad 2.6$$

$$\% \text{ removal} = \frac{(C_o - C_e)}{C_o} \times 100 \qquad 2.7$$

where C_0 (mg/L) is the initial concentration of the phenolic compound or heavy metal, C_e (mg/L) is the equilibrium concentration of the phenol, or heavy metal, m (g) is the mass of the adsorbent used, and V (L) is the volume of the solution used. Kausar et al. (2017) and Negrea *et al.* (2020) investigated the adsorption of arsenate ions on laterite and radioactive elements on rice husk waste.

A high adsorption capacity and removal efficiency were reported using the batch method. Unlike the column, the batch is simply executed in a controlled environment which is challenging with the column. Therefore, batch experiments are an excellent approach in determining adsorption rates, maximum adsorption capacity, analysis of adsorbate and adsorbate interaction, and thermodynamic parameters.

2.4.2 Hydrochar regeneration and reusability

Reusability is critical in determining the commercial viability of hydrochar as an adsorbent, while the regeneration of pollutant-saturated adsorbent is critical in determining the economic feasibility of adsorption in water treatment (Chen *et al.,* 2015; Lee *et al.,* 2019). Adsorbent performance degrades due to excessive adsorbate accumulation, and investigation of this phenomena aids in the recovery of adsorbates. Both regeneration and reusability rely on the adsorbent–adsorbate interaction (Sangi *et al.*, 2008). The regeneration agent influences the adsorption capacity recovery of an adsorbent, adsorbent physiochemical properties, pollutants and reaction conditions (Ifthikar *et al.,* 2017). Similar to modification techniques, thermal, chemical, biological, and vacuum regeneration are some of the classes of regeneration techniques. The techniques imply pH variation, heating, chemical reaction and degradation (Dai *et al.*, 2019; Yangui *et al.*, 2017; Yoon *et al.*, 2017). Deionized water, 0.1 mol/L HCl, 0.1 mol/L $CaCl_2$ or a mixture of 0.1 mol/L HCl 1:1 and 0.1 mol/L $CaCl_2$ are the most used desorption reagents (Zhang *et al.*, 2019). The results obtained by (Lin 2019; Takaya *et al.*, 2016) showed that washing hydrochar with acids introduces acidic functional groups on biochar's surface, thus desorbing the adsorbed metals. The desorption efficiency and percentage is calculated as follows:

$$\text{Desorption efficiency} = \frac{amount\ of\ metal\ or\ phenolics\ desorbed}{amount\ of\ metal\ and\ phenolics\ adsorbed} \quad 2.8$$

$$\%\ \text{Desorption} = desorption\ efficiency\ X\ \ 100 \quad 2.9$$

Optimising the regeneration conditions improves adsorbent lifetime, thus more cycles (Mendoza-castillo, 2017). Therefore, in this study, the reusability of hydrochar and recovery of adsorbed heavy metals and phenolics is ultimately evaluated by conducting a series of desorption experiments with acidic mixtures on one hydrochar sample. Each of these series of experiments were done in triplicates and the average was recorded.

2.4.3 Factors affecting adsorption

2.4.3.1 Contact time

The minimum time required to saturate an adsorbent with an adsorbate or to reach an equilibrium is contact time, and it exerts significant influence on the adsorbent use and commercialisation in water remediation (Al-Qahtani, 2016; Anayurt *et al.*, 2009). In the studies conducted by Ifthikar *et al.*, (2017) and Wang *et al.*, (2015), adsorption of Pb ions on sludge derived hydrochars was achieved within the first 60 minutes, with rapid lead removal in the first 30 minutes. Phenolic compounds tend to take longer, at least 120mins. Lee *et al.*, (2019) achieved adsorption of phenol on food waste-derived hydrochars within the first 30 minutes, and the phenol remains bound to the char for a further 24 hrs. In this study, the batch experiment was allowed to run until equilibrium was achieved, approximately 24 hrs.

2.4.3.2 Adsorbent Dosage

The dosage of an adsorbent effectively impacts its adsorption efficiency, and optimum hydrochar dosage influences its cost-effectiveness in remediation (Begum *et al.*, 2021). A rise in adsorbent dosage increases the available surface area and thereby the functional groups. Therefore, there is an increase in the adsorbent-adsorbate interactions that, in turn, increase the removal of pollutants. According to Abbas *et al.* (2018), the rise in the removal percentages is ascribed to increased pores, unsaturated sites and surface area. The removal of Pb and Cd increased from 12.9-95.1 % and 28.6-94.1 %, respectively, upon the biochar dosage increase from 0.2 g/L-2 g/L. The key mechanism involved in this experiment was pore filling and diffusion. The application of 0.5-2 % rice hull-derived-biochar enhances the removal of flubendiamide by 60-89 %, safranin by 32 % and the herbicide fomesafen by 87 % (Schuler *et al.*, 2017). In my study, I investigated the effect of dose (0.1-2 g) on phenolics and metals adsorption on the hydrochar.

2.4.3.3 Temperature

The effect of temperature on adsorption is a fairly commonly studied parameter as it increases molecules' kinetic energy, hence more chances of the adsorbate finding an active site. However, the same increase in adsorbate mobility can cause desorption of the already adsorbed adsorbate, reducing adsorption (Li *et al.*, 2019; Mu'azu et al.,2017). Wasewar, 2010) studied the adsorption of Ni on the tea factory waste (TFW), an increase in temperature (20-60 ^{o}C), raised the adsorption

yield from 88.3-100 % and suggested that temperature increased the mobility of metals, swelling effect on the TFW internal structure, and increased the number of active sites through bond rupture. Begum *et al.*, (2021), concluded increasing temperature from 15-45 ^{o}C was beneficial for the maximum removal of NH_4^+. Therefore, in this study, the effect of temperature was investigated using washed hydrochar at 25, 35 and 45 ^{o}C.

2.4.3.4 pH

Largely, adsorption onto the hydrochar depends on pH as pH affects the degree of ionisation of the species (Liu and Zhang, 2009; Mu'azu et al.,2017). Under acidic conditions, the hydrochar oxygen-containing functional groups are protonated making them inaccessible to positively charged ions like heavy metal ions Pb^{2+} and Hg^{2+}. By increasing pH, deprotonation of the oxygen functional groups occurs, providing a chance for the metals to adhere to the surface. Hence, as the proton concentration decreases with increased pH, the positively charged species effectively bind to the adsorbent and increase the adsorption capacity. However, at pH 6 and above, the removal rate is expected to decrease due to the formation of metal hydroxyl complexes which significantly lowers the metal removal efficiency (Komkiene and Baltrenaite, 2016; Liu and Zhang, 2009). Phenol removal as a function of pH indicated that phenol adsorption decreased gradually from 10 to 8 mg/g as the solution pH increased from 3 to 10. This drop results from the continuous ionization of phenolics and increased electrostatic repulsions with an increase in pH. Related behaviours have been observed in the adsorption of phenol onto biochar from *H. fusiformis* and rice husk hydrochar (Lee *et al.*, 2019).

2.4.3.5 Initial concentration

Initial concentration is important in applying hydrochar in remediation. It provides information about the efficiency of the adsorbent on different wastewaters with varied pollutant concentrations (Villegas *et al.*, 2016b; Bardestani *et al.*, 2019; Elkhaleefa *et al.*, 2020). The Zn^{2+} and Cr^{3+} adsorption decrease with an increase in initial concentration due to increased competition of ions in solution (Al-Qahtani, 2016; Wasewar, 2010). Kumar and Kirthika, (2009) and Regmi *et al.*,)2012) studied nickel removal on Bael leaves powder and lead on switchgrass derived char, respectively decreasing with increases in initial concentration. In the removal of Rhodamine dye using perlite, an increase in initial concentration raises the adsorption of the dye. The effect of initial concentration is investigated by scaling phenols and metals wastewater concentration by factors 3 and 10.

2.5 Adsorption kinetic models

Many mathematical models have been established to define the adsorption of pollutants on carbon-based adsorbents (Qiu *et al.,* 2009). Adsorption kinetics enables the design of adsorption operating equipment and defines their performance in batch and continuous systems by providing knowledge of the mechanisms, characteristics, and prospective applications (Mendoza-castillo, 1999; Gollakota *et al.,* 2018). Several adsorption kinetic models have been recognised, including the pseudo-first-order model, the pseudo-second-order model and the Elovich model (Lengauer, 2018), to comprehend the kinetics and the rate-controlling steps.

2.5.1 Pseudo-1st order model

Lagergren proposed the pseudo-first-order model, which assumes that the rate of change in solute uptake with time is directly proportional to the difference in saturation concentration (Li *et al.*, 2009; Wu *et al.,* 2009). The amount of solute uptake with time is applied over the first stage of the adsorption process. It is given by the equation (adopted from Li *et al.,* 2009):

$$qt = qe\ (1 - e^{k_1 t}) \qquad 2.10$$

which is reduced and linearised to:

$$ln(qe - qt) = qe - kt \qquad 2.11$$

where *qe* is the [adsorbate] at equilibrium, *qt* is the [adsorbate] at a given time, mg/g, k_1 is the rate constant (min^{-1}), and *t* is the time in minutes. The pseudo-first-order rate constant, correlation coefficients can be determined from linear plots of log (*qe-qt*) vs *t*. Despite its limitations, thus mostly valid for initial stages of the adsorption process which can be very fast, it was applied successfully in the sorption of the kinetics of heavy metals on various hydrochars. The kinetic model describes the adsorption kinetics of heavy metals on hydrochar adsorbents that occur within 30 minutes hence making this order more applicable (Yang *et al.*,2019; Kumar and Kirthika, 2009; Vijayakumar *et al.*, 2011)

2.5.2 Pseudo 2nd order model

The pseudo-second-order model was developed by Ho and McKay (McKee, 2003). It describes a kinetic process involving ion exchange, usually the one that involves divalent ions and is expressed by the following equation:

$$\frac{dqt}{dt} = k_2(qe - qt)^2 \quad 2.12$$

By defining the integral followed by the application of initial conditions t=0, q=0 and t=t and q=q, the equation becomes:

$$\frac{1}{q_e - q_t} = \frac{1}{q_e} + k_2 t \quad 2.13$$

which is reduced and linearised to:

$$\frac{1}{q_t} = \frac{1}{q^2{}_e k_2 t} + \frac{1}{qe} \quad 2.14$$

where q_e is the equilibrium adsorption capacity and q_t are the adsorption capacity at a given time, and k_2 is the adsorption constant in g/min. A plot *t/qt* vs time gives a straight line where *qe*, k_2 and h_0 are calculated from the intercept and the slope. The pseudo-second-order kinetic model correlated with copper and zinc exclusion sorption data using corn straw and hardwood-derived hydrochars with R^2 above 0.9 (Chen *et al.,* 2011).

2.5.3 Elovich model

Initially, the Elovich model was established to define chemisorption kinetic processes on adsorbents with heterogeneous surfaces (Wu *et al.*, 2009; Rincón-Silva *et al.*,2016). The model is essential in assessing the adsorbent homogeneity though out the adsorption process. Therefore, deviation from the linearity of the linearized equation indicates a change in reactivity of the surface (Chien and Clayton, 1980). The Elovich kinetic model is often used to interpret adsorption kinetics and successfully describe second-order kinetics, assuming that the surface is energetically heterogeneous. The Elovich or Roginsky-Zeldovich equation is generally expressed as follows:

$$dqt = \propto e^{\beta qt} \quad 2.15$$

It is assumed that $\alpha\beta t > 1$ and on applying the boundary conditions $qt = 0$ at $t = 0$ and $qt = qt$ at $t = t$, the equation becomes:

$$qt = \frac{1}{\beta} ln \propto \beta + \frac{1}{\beta} lnt \quad 2.16$$

where *qt* = the amount of adsorbate adsorbed mg/g, at time *t*, α = the initial adsorbate sorption rate, mg/g.min, β = the desorption constant, g/mg. The constant was attained from the slope and

intercept of the linear plot of *qt* versus ln *t*. The model has been applied in the sorption of Pb on digested whole sugar-derived biochar. The results indicated that the Elovich model correlates better than either the first- or second-order models (Xue *et al.*, 2012; Inyang *et al.*, 2012,2016).

2.6 Mass transfer

Diffusion models are applied mainly if the initial sorption process is restricted by diffusional mass transfer rate (Ahmed and Theydan, 2012). Formerly, diffusion models have been widely applied to describe the removal of organics and dyes from wastewaters (Ahmed and Theydan, 2012; Mendoza-castillo, 2017).

2.6.1 Intraparticle diffusion model

This intraparticle diffusion model, also known as the Weber and Morris model, is applied to examine the rate-limiting step. The adsorption of metals generally follows the order: film diffusion, intraparticle diffusion into either the inner or the outer adsorbent pores or a combination of both (Kara and Demirbel, 2012). The intra-particle diffusion equation can be written as:

$$qt = K_{ipd} t^{\frac{1}{2}} + C \qquad 2.17$$

where *qt* is the amount of dye adsorbed onto the adsorbent at time *t* (mg/g), *C* is the intercept, and K_{ipd} is the intra-particle diffusion rate constant (mg /g. min). The intraparticle diffusion equation is demonstrated by plotting *qt* against the square root of time ($t^{1/2}$). If the straight line passes through the origin, it can be concluded that the adsorption process is controlled by intraparticle diffusion. However, if the linear fitting multiple linear sections then more than one processes influence the adsorption process. (Luter *et al.*, 2012). In my study, this model was applied, and the R^2 value was used to determine the best fit and explain the kinetics governing the adsorption process.

2.6.2 Boyd intraparticle diffusion model

Boyd developed a single-resistance model that was applied to understand if the film diffusion is the rate-controlling step. The model assumes that the adsorbent's boundary layer has a greater effect on solute diffusion (Karthikeyan *et al.*, 2010). The effect is determined by applying the following equation:

$$\mathrm{F} = 1 - \frac{6}{\pi^2}\sum_{1}^{\infty}\left(\frac{1}{\mathrm{n}^2}\right)\mathrm{e}^{-\mathrm{n}^2\mathrm{Bt}} \quad 2.18$$

where *F* is the fraction of solute adsorbed at time *t* and *Bt* is the mathematical function of *F*

$$F = \frac{q_t}{q_\infty} \quad 2.19$$

where *qt* is mass adsorbed at a given time and q_e is solute adsorbed at an infinite time (*t*>24 hrs). It is difficult to calculate the values of *Bt* using the equation above but easy from the integrated Fourier transformation of equation 2.18 and equation 2.19 and the following given conditions

$$0 \leq F \leq 0 \cdot 85;\ \ Bt = 2\pi - \frac{\pi^2 F}{3} - 2\pi\sqrt{1 - \frac{\pi F}{3}} \quad 2.20$$

$$0.86 \leq F \leq 1: B_t = -0.4977 - ln(1 - F) \quad 2.21$$

Plotting the graph of *Bt* vs *t* helps to predict the rate-limiting step. The rate-limiting step is intraparticle diffusion if the curve approximates y=mx+0; otherwise, the film diffusion model governs the process (Viegas *et al.*, 2014).

2.6.3 Mass considerations with Biot number

The dimensionless Biot number (Bi) gives the relationship between the transfer from the liquid and intraparticle transfer. Thus, it is the ratio of the transport rate across the liquid layer to the rate of intraparticle mass transfer. It is given by the equation:

$$B_i = \frac{k_f\,\mathrm{d}_p}{D\mathrm{e}} \quad 2.22$$

where k_f (m/s) is the film mass transfer constant and is obtained as a slope of $\frac{C_t}{C_i}$ (fractional adsorbate content) vs time *t*, d_p (m) is the average hydrochar particle, and D_e (m^2/s) is the effective intraparticle diffusion coefficient and is calculated from slope from the plot of $-\mathrm{In}\left(1 - \left(\frac{\mathrm{q_t}}{\mathrm{qe}}\right)^2\right)$ vs time *t*. Girish and Murty, (2016) argue that film diffusion is dominant when *Bi* < 100 while internal diffusion is dominant when Bi >100.

2.7 Adsorption isotherms

The adsorption data at equilibrium is a fundamental requirement in designing systems. Adsorption isotherms are mathematical models based on equilibrium data used to determine the mechanism of adsorption (Kołodyńska *et al.*, 2012; Mendoza-castillo, 2017). These models are based on assumptions correlated to:

- Adsorbent homogeneity or heterogeneity
- Surface coverage either monolayer or multilayer
- Interaction of adsorbed sorbates (Li *et al.*, 2018).

Several adsorption isotherms have been proposed and applied to demonstrate how the adsorbate is distributed on absorbent at equilibrium. This study uses the most applied isotherms, namely Henry's law, Langmuir, Freundlich, Temkin and Dubinin Radushkevich isotherm (Baccar and Yangui, 2013; Edet and Ifelebuegu, 2020; Kara and Demirbel, 2012).

2.7.1 Henry's law

Henry's law is the simplest form of adsorption, usually applied in gas-solid adsorption. It states that the partial pressure of gas adsorbed is proportional to the amount of surface adsorbate. An appropriate fit is possible at low concentrations where all the adsorbates are secluded from their closest neighbours (Al-Ghouti and Da'ana, 2020). The law is given by the equation:

$$q_e = k_{HE} c_e \qquad 2.23$$

where q_e is amount of absorbate adsorbed, C_e is the adsorbate concentration at equilibrium, K_{HE} is Henry's constant.

2.7.2 Langmuir isotherm

The isotherm is based on the following assumptions:

- the adsorption sites are identical, equivalent in energy and thermodynamically one site only holds one adsorbate (Komkiene and Baltrenaite, 2016).
- the maximum adsorption corresponds to a saturated monolayer of solute molecules on the surface of the adsorbent,
- adsorption is reversible (Tran *et al.*, 2017)

- no transmigration of adsorbed molecules on the surface of the adsorbent, and no lateral interaction between the adsorbed molecules (Chou *et al.,* 2010).

The following equation describes this isotherm:

$$qe = \frac{q_{max}\, K_L\, C_e}{1+K_L C_e} \qquad 2.24$$

And is linearised to

$$\frac{1}{q_e} = \frac{1}{k_L q_{max} C_e} + \frac{1}{q_{max}} \qquad 2.25$$

where q_e amounts of adsorbate adsorbed, C_e is the adsorbate concentration at equilibrium, K_L is Langmuir's constant which shows the degree of adsorption affinity, q_{max} (l/g) is the constant related to the overall solute adsorptivity. From the linearized equation, the parameters are calculated from the plot of $\frac{1}{qe}$ vs $\frac{1}{Ce}$ where intercept = $\frac{1}{qm}$, and $C = \frac{1}{qm.KL}$. R_L is an essential or valuable feature in the Langmuir isotherm as it is used to predict the favourability of a system (Jaman *et al.,* 2009; Baccar and Yangui, 2013). The R_L value indicates the shape of the isotherm and is given by the equation

$$R_L = \frac{1}{1+bC_i} \qquad 2.26$$

where C_i is the metal ion initial concentration mg/l, b is the Langmuir's constant mg/ml. The Table below shows the prediction of R_L value from equation 2.21

RL value	Prediction	References
0 < RL< 1	Favourable	(Inyang et al., 2012; Tran et al., 2017)
RL > 1	Unfavourable	(Tran et al., 2017)
RL = 1	Linear	(Tran et al., 2017)
RL = 0	Irreversible	(Tran et al., 2017)

Several researchers have successfully applied the isotherm and yielded meaningful results (Tong *et al.,* 2011; Inyang *et al.,* 2012; Lee *et al.,* 2019). Therefore, in this study, Langmuir isotherm was assessed in describing the distribution of metals and phenolics between the char and the solution.

2.7.3 Freundlich isotherm

The isotherm assumes

- heterogeneous adsorbent's surfaces,
- a multilayer surface coverage and associated with strong adsorbate-adsorbate interaction
- adsorption sites are distributed exponentially to adsorption energy (Ahmed and Theydan, 2012).

The Freundlich isotherm is described by the equation below:

$$qe = K_F C_e^{\frac{1}{n}} \quad 2.27$$

And linearised to

$$ln\, qe = lnk_f + \frac{1}{n} lnCe \quad 2.28$$

where q_e is amount of adsorbate adsorbed, C_e is the adsorbate concentration at equilibrium, K_F adsorption capacity, $\frac{1}{n}$ is adsorption intensity, and value n indicates how favourable the adsorption process is. And the prediction of the adsorption process based on the calculated n value is illustrated in the Table 2.2 below:

Table 2.2: The prediction of the n values in Freundlich isotherm

n value	Prediction	References
1 < n < 10	favourable	(Komkiene and Baltrenaite, 2016 Kumar *et al.*,2006a)
n = 1	linear	(Tran *et al.*,2017)
n < 1	unfavourable	(Dada *et al.*, 2012).

Therefore, in this study, the isotherm is applied to describe the heterogeneity of the char surface and the favourability of the adsorption.

2.7.4 Temkin isotherm

This isotherm

- considers the adsorbent–adsorbate interactions.

- assumes that all the molecules in the layered heat of adsorption decrease linearly rather than logarithmic with coverage (Dada *et al.*,2012; Elkhaleefa *et al.,* 2020; Taşar and Özer, 2020).

Temkin isotherm derivation is characterised by the uniform distribution of binding energies and is given by the following non-linearised 2.29 and linearised equations 2.30 below:

$$qe = \frac{RT}{b_T} ln(A_T C_e) \quad 2.29$$

$$q\mathrm{e} = BlnA_T + BlnC_e \quad \text{with } B = \frac{RT}{b_T} \quad 2.30$$

where A_T =Temkin isotherm equilibrium binding constant (L/g), b_T = Temkin isotherm constant related to heat of sorption (J/mol), *R*= universal gas constant (8.314 J/mol/K) *T*= Temperature at 298K. *B* = Constant. The slope and intercept can be obtained from the plot *qe* against *lnCe*, and the constants were determined.

The Temkin isotherm is also applied to differentiate between chemical and physical sorption (Sharma *et al.*,2016). The process is physisorption when the heat of adsorption is less than 1kcal/mol (4.184 kJ/mol), chemisorption when it is 20-50 kcal (80-210 kJ/mol) (Ionel *et al.,* 2003; Kara and Demirbel, 2012). Al-Ghouti and Da'ana., (2020), argued that the isotherm is more appropriate in the gas adsorption process than complex adsorption systems, including aqueous phase adsorption. Despite this limitation, Tounsadi *et al.,* (2015) applied the isotherm on the adsorption studies of Cd and Co on biosorbents *Diplotaxis harra* and *Glebionis coronaria* and concluded evidence of chemisorption process with B (kJ/mol) of Cd (550 and 480) and Co (1128 and 535), with all the R^2 values above 0.91 respectively. Similar results were obtained in the studies of Kumar and Kirthika, (2009) and Dada *et al.,* (2012) for the adsorption of nickel and zinc respectively. Therefore, in this study, the data will be fit with the Temkin isotherm.

2.7.5 Dubinin-Radushkevich (D-R) isotherm

The isotherm is a semi-empirical equation that follows the pore filling process, unlike Langmuir and Freundlich isothermal models. The isotherm

- assumes a multi-layered character involving Van der Waal forces implying physical adsorption processes.

- high soluting behaviours are applied to the intermediate range of adsorbate concentrations due to the unrealistic asymptotic actions on the characteristic However, in the case of low pressure, the law of Henry does not predict the Dubinin-Radushkevich model.
- contemplates that adsorption equilibrium relation for a given adsorbate-adsorbent combination is expressed independently of temperature using the adsorption potential (ε)(Ding *et al.*, 2020)

$$\varepsilon = RT\ ln\left(1 + \frac{1}{Ce}\right) \qquad 2.31$$

where *R*, *T* and *Ce* represent the gas constant (8.314 J/mol K), absolute temperature (K) and adsorbate equilibrium concentration (mg/L), respectively.

The D-R estimates the energy of adsorption. It assumes the Gaussian distribution for characteristic curve and is expressed by the equation below;

qe= qs exp -Kε^2 that is linearised to

$$Inqe = ln\, q_{DR} - K\varepsilon^2 \qquad 2.32$$

where q_e = amount of adsorbate in the adsorbent at equilibrium (mg/g); q_s is theoretical isotherm saturation capacity (mg/g); *K* is Dubinin–Radushkevich isotherm constant (mol^2/kJ^2)

The isotherm is not only proposed for constant adsorption potential or homogeneous adsorbents but also heterogeneous ones. Free sorption energy E_s is used to determine whether the adsorption was physisorption (less than 8.0 (kJ/mol) or chemisorption (8.0-16.0 (kJ/mol), and the equation 2.28 expresses it

$$E_S = \frac{1}{\sqrt{2B}}. \qquad 2.33$$

where *B* is denoted as the isotherm constant (-*K*).

Recent studies applied the isotherm in the adsorption of Zn on bio sorbents and hydrochars, and the R^2 value in the range 0.74-0.88 and q_m (mg/g) agrees with q_m obtained from the Langmuir isotherm fit. The E_s (kJ/mol) were all below the 8.0 hence concluding physisorption. Therefore, applying data to this isotherm can help determine the occurrence of chemical or physical

adsorption. In the adsorption of Ni on corncob derived hydrochar, the E_s value was determined as 2.24 kJ/mol concluding a physisorption process (Elkhaleefa *et al.,* 2020).

2.8 Thermodynamic parameters

The nature of adsorption can be fully understood by calculating the thermodynamic parameters like enthalpy change ΔH, Gibbs free energy ΔG and entropy change ΔS using the equilibrium constants under several conditions (Lee *et al.,* 2019). According to Chowdhury (2017), solid-liquid system adsorption is a combination of desorption of the water molecules, the solvent, metals and phenolic compounds. The total energy absorbed in bond breaking is less than the total energy released in the bond making between adsorbate and adsorbent, resulting in extra energy in the form of heat hence an exothermic reaction, and the opposite is true for endothermic reactions. Entropy (ΔS) measures inaccessible energy (system disturbance) in a closed thermodynamic system and is strongly influenced by reversible system heat and temperature changes. The following equation is used to estimate these thermodynamic parameters.

$$K_e = \frac{q_e}{C_e} \qquad 2.34$$

$$ln\,Ke = \frac{\Delta S}{R} - \frac{\Delta H}{RT} \qquad 2.35$$

where q_e (mg/g) is the amount of adsorbate adsorbed onto the biochars from the solution at equilibrium, C_e (mg/L) the equilibrium concentration of lead in the solution, R (J/mol K) the gas constant 8.314, T (K) the absolute temperature and K_e (L/g) is the adsorption equilibrium constant. ΔS and ΔH are determined from the intercept and the slope of lnK_e vs. $\frac{1}{T}$. The value of ΔG suggests the spontaneous nature of the adsorption process and gives information about the type of adsorption: chemical or physical adsorption (Ahmed and Theydan, 2012; Lee *et al.*, 2019). It was investigated, and the hydrochar sorption capacity of biochar was obtained from the equation below.

$$\Delta G = \Delta H - T\Delta S \qquad 2.36$$

Liu and Zhang (2009) explained that higher temperature gives Pb ions sufficient energy to diffuse into the inner pores of pine and rice husk biochars. Therefore, with the positive enthalpy values of 41.10 (kJ/mol). The removal efficiency of Pb increased with rising temperatures. Similarly, an endothermic process was concluded for the adsorption of copper and zinc on corn straw and

hardwood derived hydrochars (Jiang *et al.*, 2019). Therefore, the thermodynamics of both the adsorption of phenolics and heavy metals can be determined; hence the reactions can be manipulated and optimised. The thermodynamic parameters are investigated to show the exothermicity or endothermicity, and the spontaneity of the adsorption mechanism of both metals and phenols.

Chemisorption is associated with bond breaking, and bond formation activation is mostly high above 40 kJ/mol, while that of physisorption is less than 40 kJ/mol (Chowdhury, 2017). The activation energy is calculated using the Arrhenius equation below:

$$ln\, k = \frac{E_a}{RT} + ln\, A \qquad 2.37$$

where k is the adsorption rate constant from the kinetic models, A is a constant called the frequency factor, and E_a is the activation energy (kJ/mol), R is the gas constant (8.314 J/mol. K), and T is the temperature(K). By plotting $ln\, k$ versus $1/T$ and from the slope and the intercept, values of E_a and A can be obtained.

2.9 Conclusion

Wastewater treatment, contaminated water with multiple pollutants increases with technological and industrial advances; hence water remediation becomes a priority. Adsorption is both technologically simple and economically feasible, yielding high-quality water. It is the subject of interest to many researchers evaluating ways to improve adsorbents' prices and the efficiency of the adsorption process. The characteristics, surface area, surface functional groups, and porosity of hydrochar from the HTL of biomass complement its use as an adsorbent in removing pollutants like heavy metals and phenolics. Only a few studies have explored the use of hydrochar produced from municipal solid waste and sewage as a viable bio-waste adsorbent. Furthermore, the adsorption mechanisms for simultaneous adsorption of metals and phenolic components are not yet well understood but could be useful for industrial design and application.

REFERENCES

Acero, J.L., Benítez, F.J., Leal, A.I. and Real, F.J. 2005. Removal of phenolic compounds in water by ultrafiltration membrane treatments. *Journal of Environmental Science and Health - Part A Toxic/Hazardous Substances and Environmental Engineering*. 40(8):1585–1603.

Ahmed, M.J. and Theydan, S.K. 2012. Equilibrium isotherms, kinetics and thermodynamics studies of phenolic compounds adsorption on palm-tree fruit stones. *Ecotoxicology and Environmental Safety*. 84:39–45.

Al-Anber, M.A. 2011. Thermodynamics Approach in the Adsorption of Heavy Metals. *Chemosphere*.2013.08-027.

Al-Ghouti, M.A. and Da'ana, D.A. 2020. Guidelines for the use and interpretation of adsorption isotherm models: A review. *Journal of Hazardous Materials*. 393(November 2019):122383.

Al-Qahtani, K.M. 2016. Water purification using different waste fruit cortexes for the removal of heavy metals. *Journal of Taibah University for Science*. 10:700–708.

Al-Senani, G.M. and Al-Fawzan, F.F. 2018. Adsorption study of heavy metal ions from aqueous solution by nanoparticle of wild herbs. *Egyptian Journal of Aquatic Research*. 44(3):187–194.

Anayurt, R.A., Sari, A. and Tuzen, M. 2009. Equilibrium, thermodynamic and kinetic studies on biosorption of Pb (II) and Cd (II) from aqueous solution by macrofungus (Lactarius scrobiculatus) biomass. *Chemical Engineering Journal*. 151(1–3):255–261.

Arán, D., Antelo, J., Fiol, S. and Macías, F. 2016. Influence of feedstock on the copper removal capacity of waste-derived biochars. *Bioresource Technology*. 212:199–206.

Artelle, L.Y.H.W. and Odgers, J.A.E.R. 2010. Immobilization of Heavy Metal Ions (Cu II, Cd II, Ni II, and Pb II) by Broiler Litter-Derived Biochars in Water and Soil. *Bioresource Technology*. 212: 538–544.

Assayie, A.A., Gebreyohannes, A.Y. and Giorno, L. 2017. Municipal Wastewater Treatment by Membrane Bioreactors. *Journal of Water Supply: Research and Technology - AQUA*. 70(1).265–294.

Awad, A.M., Jalab, R., Benamor, A., Nasser, M.S., Ba-Abbad, M.M., and Mohammad, A.W. 2020. Adsorption of organic pollutants by nanomaterial-based adsorbents: An overview. *Journal of Molecular Liquids*. 301:112335–112366.

Awad, A.M., Shaikh, S.M.R., Jalab, R., Gulied, M.H., Nasser, M.S., and Adham, S. 2019. Adsorption of organic pollutants by natural and modified clays: A comprehensive review. *Separation and Purification Technology*. 228:115719–115748.

Ayeleru, O.O., Ntuli, F. and Mbohwa, C. 2011. *Utilization of Organic Fraction of Municipal Solid Waste (OFMSW) as Compost: A Case Study of Florida, South Africa*.

Baccar, R. and Yangui, E. 2013. Removal of some water contaminants by adsorption on activated carbon prepared from olive-waste cakes and biological treatment using fungi. *Chemical Engineering Journal* 283 (2016) 293–303

Bardestani, R., Roy, C. and Kaliaguine, S. 2019. The effect of biochar mild air oxidation on the optimization of lead (II) adsorption from wastewater. *Journal of Environmental Management*. 240:404–420.

Barrera-zapata, R. 2017. Morphological and physicochemical characterization of biochar produced by gasification of selected forestry species Caracterización morfológica y fisico-química de biocarbones producidos. *Revista Facultad de Ingeniería (Rev. Fac. Ing.)* 26(46):123–130.

Beauchet, R., Monteil-Rivera, F. and Lavoie, J.M. 2012. Conversion of lignin to aromatic-based chemicals (L-chems) and biofuels (L-fuels). *Water, Air, and Soil Pollution*. 121(3):328–334.

Begum, S.A., Golam Hyder, A.H.M., Hicklen, Q., Crocker, T. and Oni, B. 2021. Adsorption characteristics of ammonium onto biochar from an aqueous solution. *Journal of Water Supply: Research and Technology - AQUA*. 70(1).

Bogusz, A., Oleszczuk, P. and Dobrowolski, R. 2015. Application of laboratory prepared and commercially available biochars to adsorption of cadmium, copper and zinc ions from water. *Bioresource Technology*. 196:540–549.

Braghiroli, F.L., Bouafif, H., Hamza, N., Neculita, C.M. and Koubaa, A. 2018. Production, characterization, and potential of activated biochar as adsorbent for phenolic compounds from leachates in a lumber industry site. *Environmental Science and Pollution Research*. 25(26):26562–26575.

Brewer, C.E. 2012. Biochar characterization and engineering. Iowa state University. https://lib.dr.iastate.edu/etd/12284.

çaglar, E., Donar, Y.O., Sinag, A., Biro Gul, I., Bilge, S., and Pliekhov, O. 2018. Adsorption of anionic and cationic dyes on biochars, produced by hydrothermal carbonization of waste biomass: Effect of surface functionalization and ionic strength. *Turkish Journal of Chemistry*. 42(1):86–99.

Campbell, M.K. and Farrell, S.O. 2006. *Biochemistry*. Jay Campbell, ed. 5th edition, Ed. Belmont Carlifonia: David Harris.

Carey, F.A. and Sundberg, R.J. 2007. *Advanced Organic Chemistry*. Springer, ed. 5th ed. New York.: Springer New York LLC.

Chalenko, Y., Shumyantseva, V., Ermolaeva, S. and Archakov, A. 2012. Biosensors and Bioelectronics Electrochemistry of Escherichia coli JM109: Direct electron transfer and antibiotic resistance. *Biosensors and Bioelectronics*. 32(1):219–223.

Changjun, L., Xiao, Y., Zhe, Z., Dong, Z., Liang, Z., and Jianmin, C. 2013. Hydrothermal Liquefaction of Desert Shrub Salix psammophila to High Value-added Chemicals and Hydrochar with Recycled Processing Water. *BioResources*. 8(2):2981–2997.

Chen, J., Qi, Y., Pan, X., Wu, N., Zuo, J., … Chen, Z. 2019. Mechanistic insights into the reactivity of Ferrate (VI) with phenolic compounds and the formation of coupling products. *Water Research*. 158:338–349.

Chen, K., Hao, S., Lyu, H., Luo, G., Zhang, S. and Chen, J. 2017. Ion exchange separation for recovery of monosaccharides, organic acids and phenolic compounds from hydrolysates of lignocellulosic biomass. *Separation and Purification Technology*. 172:100–106.

Chen, K., Lyu, H., Hao, S., Luo, G., Zhang, S. and Chen, J. 2015. Separation of phenolic compounds with modified adsorption resin from aqueous phase products of hydrothermal liquefaction of rice straw. *Bioresource Technology*. 182:160–168.

Chien, S.H. and Clayton, W.R. 1980. Application of Elovich Equation to the Kinetics of Phosphate Release and Sorption in Soils. *Soil Science Society of America Journal*. 44(2):265–268.

Chowdhury, Z.Z., Adebisi, G.A., Bee, S. & Hamid, A. 2017. Studies of Divalent Cation Adsorption onto Calamus gracilis Sawdust-Based Activated Carbon. *Environmental Chemistry Letters*. 12(2):2872–2898.

Crichton, R., Crichton, R.R., and Boelaert J.R. 2001. *Inorganic Biochemistry of Iron Metabolism from molecular mechanisms to clinical consequences.* John Wiley and Sons, Ltd Baffins Lane, Chichester, West Sussex PO19 1UD, England

Crini, G., Lichtfouse, E., Wilson, L.D. and Morin-Crini, N. 2019. Conventional and non-conventional adsorbents for wastewater treatment. *Environmental Chemistry Letters*. 17(1):195–213.

Dada, A.., Olalekan, A. and Olatunya, A.M. 2012. Langmuir, Freundlich, Temkin and Dubinin–Radushkevich Isotherms Studies of Equilibrium Sorption of Zn 2+ Unto Phosphoric Acid Modified Rice Husk. *IOSR Journal of Applied Chemistry*. 3(1):38–45.

Dai, Y., Zhang, N., Xing, C., Cui, Q. and Sun, Q. 2019. The adsorption, regeneration and engineering applications of biochar for removal organic pollutants: A review. *Chemosphere*. 223:12–27.

de la Rosa, L.A., Moreno-Escamilla, J.O., Rodrigo-García, J. and Alvarez-Parrilla, E. 2019. *Phenolic Compounds*. *Postharvest Physiology and Biochemistry of Fruits and Vegetables*. Elsevier Inc.

Del Bubba, M., Anichini, B., Bakari, Z., Bruzzoniti, M.C., Camisa, R., and Orlandini, S. 2020. Physicochemical properties and sorption capacities of sawdust-based biochars and commercial activated carbons towards ethoxylated alkylphenols and their phenolic metabolites in effluent wastewater from a textile district. *Science of the Total Environment*. 708:135217.

Demirbas, A., Ak, N., Aslan, A. and Sen, N. 2018. Calculation of higher heating values of hydrocarbon compounds and fatty acids. *Petroleum Science and Technology*. 36(11):712–717.

Deng, J., Liu, Y., Liu, S., Zeng, G., Tan, X. and Huang, B. 2017. Journal of Colloid and Interface Science Competitive adsorption of Pb (II), Cd (II) and Cu (II) onto chitosan-pyromellitic dianhydride modified biochar. *Journal of Colloid and Interface Science*. 506:355–364.

Deng, S., Nie, Y., Du, Z., Huang, Q., Meng, P., and Yu, G. 2015. Enhanced adsorption of perfluorooctane sulfonate and perfluorooctanoate by bamboo-derived granular activated carbon. *Journal of Hazardous Materials*. 282:150–157.

Dieguez-Alonso, A., Funke, A., Anca-Couce, A., Rombolà, A.G., Ojeda, G., and Behrendt, F. 2018. Towards biochar and hydrochar engineering-influence of process conditions on surface physical and chemical properties, thermal stability, nutrient availability, toxicity and wettability. *Energies*. 11(3).

Ding, Z., Hu, X., Wan, Y., Wang, S. and Gao, B. 2020. Removal of lead, copper, cadmium, zinc, and nickel from aqueous solutions by alkali-modified biochar: Batch and column tests. *Journal of Industrial and Engineering Chemistry*. 102(2):406–433.

Dlamini, S., Simatele, M.D., Serge Kubanza, N. and Kubanza, N.S. 2019. Municipal solid waste management in South Africa: from waste to energy recovery through waste-to-energy technologies in Johannesburg. *Local Environment*. 24(3):249–257.

Donar, Y.O., Çağlar, E. and Sinağ, A. 2016. Preparation and characterization of agricultural waste biomass based hydrochars. *Fuel*. 183:366–372.

Drumm, F.C., Grassi, P., Sulkovski, A.A., Franco, D.S.P., Georgin, J., and Jahn, S.L. 2019. Applicability of Coal Bottom Ash from Thermoelectric Power Plant as an Alternative Heterogeneous Catalyst in Photo-Fenton Reaction. *Water, Air, and Soil Pollution 2019 230:12*. 230(12):1–12.

Duan, S., Ma, W., Pan, Y., Meng, F., Yu, S. and Wu, L. 2017. Synthesis of magnetic biochar from iron sludge for the enhancement of Cr (VI) removal from solution. *Journal of the Taiwan Institute of Chemical Engineers*. 80:835–841.

Duruibe, J. O.1, Ogwuegbu, M. O. C.2 and Egwurugwu, J.N. 2007. Heavy metal pollution and human biotoxic effects. *International Journal of Physical Sciences Vol.* 2(5):112–118.

Ebenebe PC, Shale K, Sedibe M, et al. South African Mine Effluents: Heavy Metal Pollution and Impact on the Ecosystem. *International Journal of Chemical Science.* 2017;15(4):198

Edet, U.A. and Ifelebuegu, A.O. 2020. Kinetics, isotherms, and thermodynamic modeling of the adsorption of phosphates from model wastewater using recycled brick waste. *Processes*. 8.(1)563-591

Elaigwu, S.E. and Greenway, G.M. 2016. Chemical, structural and energy properties of hydrochars from microwave-assisted hydrothermal carbonization of glucose. *International Journal of Industrial Chemistry*. 7(4):449–456.

Elkhaleefa, A., Ali, I.H., Brima, E.I., Elhag, A.B. and Karama, B. 2020. Efficient removal of Ni (II) from aqueous solution by date seeds powder biosorbent: Adsorption kinetics, isotherm and thermodynamics. *Processes*. 8(8):6–9.

Elliott, D.C., Biller, P., Ross, A.B., Schmidt, A.J. and Jones, S.B. 2015. Hydrothermal liquefaction of biomass: Developments from batch to continuous process. *Bioresource Technology*. 178:147–156.

Escudero, L.B., Quintas, P.Y., Wuilloud, R.G. and Dotto, G.L. 2019. Recent advances on elemental biosorption. *Environmental Chemistry Letters*. 17(1):409–427.

Fan, Y., Hornung, U., Raffelt, K. and Dahmen, N. 2020. The influence of lipids on the fate of nitrogen during hydrothermal liquefaction of protein-containing biomass. *Journal of Analytical and Applied Pyrolysis*. (October 2019):104798-104809

Ferrentino, R., Ceccato, R., Marchetti, V., Andreottola, G. and Fiori, L. 2020. sewage sludge hydrochar: an option for removal of methylene blue from wastewater. *Applied Sciences*. 10(10):3445.

Figoli, A. and Criscuoli, A. 2017. Green Chemistry and Sustainable Technology Sustainable Membrane Technology for Water and Wastewater Treatment. Springer Nature Singapore Pte Ltd. 2017

Flora, J.F.R., Lu, X., Li, L., Flora, J.R.V. and Berge, N.D. 2013. The effects of alkalinity and acidity of process water and hydrochar washing on the adsorption of atrazine on hydrothermally produced hydrochar. *Chemosphere*. 93(9):1989–1996.

Fosso-kankeu, E., Weideman, R., Moyakhe, D. and Waanders, F. 2018. Adsorption of metal ions from fine coal tailings dump wastewater using biochar. *Chemical Engineering Journal*. 363:436–443.

Frascari, D., Bacca, A.E.M., Zama, F., Bertin, L., Fava, F. and Pinelli, D. 2016. Olive mill wastewater valorisation through phenolic compounds adsorption in a continuous flow column. *Chemical Engineering Journal*. 283:293–303.

Frascari, D., Rubertelli, G., Arous, F., Ragini, A., Bresciani, L., and Pinelli, D. 2019. Valorisation of olive mill wastewater by phenolic compounds adsorption: Development and application of a procedure for adsorbent selection. *Chemical Engineering Journal*. 360:124–138.

Fu, M.M., Mo, C.H., Li, H., Zhang, Y.N., Huang, W.X. and Wong, M.H. 2019. Comparison of physicochemical properties of biochars and hydrochars produced from food wastes. *Journal of Cleaner Production*. 236:167-176

Fu, Y., Shen, Y., Zhang, Z., Ge, X. and Chen, M. 2019. Activated bio-chars derived from rice husk via one- and two-step KOH-catalyzed pyrolysis for phenol adsorption. *Science of the Total Environment*. 646:1567–1577.

Fuertes, A.B., Arbestain, M.C., Sevilla, M., MacIá-Agulló, J.A., Fiol, S., and MacIas, F. 2010. Chemical and structural properties of carbonaceous products obtained by pyrolysis and hydrothermal carbonisation of corn stover. *Australian Journal of Soil Research*. 48:618–626.

Gai, C., Zhang, Y., Chen, W.-T., Zhou, Y., Schideman, L., and Dong, Y. 2014. Characterization of aqueous phase from the hydrothermal liquefaction of Chlorella pyrenoidosa. *Bioresource technology*. 184.157-169

Garcia-Perez, M., Lewis, T. and Kruger, C.E. 2011. Methods for Producing Biochar and Advanced Biofuels in Washington State Part 1: Literature Review of Pyrolysis Reactors. *Department of Ecology Washington State University*. 1(April):137.

Ge, M., Wang, X., Du, M., Liang, G., Jahangir, A. and Hu, G. 2018. Adsorption analyses of phenol from aqueous solutions using magadiite modified with organo-functional groups: Kinetic and equilibrium studies. *Materials*. 1(13):203–216.

Geldenhuys, A.J.M. 2004. Water treatment technologies for removal of acid, sulphates and metals. North-west University Potchefstroom campus. South Africa.

Gene, P., Chabi, K., Kefela, T., Adoukonou-sagbadja, H., Ahoton, L., and Gachomo, E.W. 2015. A simple and ef fi cient genomic DNA extraction protocol for large scale genetic analyses of plant biological systems. *PLGENE*. 1:43–45.

Ghasemi, S. and Nematollahzadeh, A. 2018. Molecularly imprinted polymer membrane for the removal of naphthalene from petrochemical wastewater streams. *Advances in Polymer Technology*. 37(6):2288–2293.

Gholizadeh, A., Kermani, M., Gholami, M. and Farzadkia, M. 2013. Kinetic and isotherm studies of adsorption and biosorption processes in the removal of phenolic compounds from aqueous solutions: Comparative study. *Journal of Environmental Health Science and Engineering*. 11(1).

Girish, C.R. and Murty, V.R. 2016. Mass transfer studies on adsorption of phenol from wastewater using Lantana camara, forest waste. *International Journal of Chemical Engineering*. 2016.

Gollakota, A.R.K., Kishore, N. and Gu, S. 2017. A review on hydrothermal liquefaction of biomass. *Renewable and Sustainable Energy Reviews*. 43(13):111–131.

Gollakota, A.R.K., Kishore, N. and Gu, S. 2018a. A Review on Hydrothermal Liquefaction of Biomass A review on hydrothermal liquefaction of biomass. *Renewable and Sustainable Energy Reviews*. (March):1–15.

Gollakota, A.R.K., Kishore, N. and Gu, S. 2018b. A review on hydrothermal liquefaction of biomass. *Renewable and Sustainable Energy Reviews*. 81(May 2017):1378–1392.

Gong, Y., Wang, L., Liu, J., Tang, J. and Zhao, D. 2016. Removal of aqueous perfluorooctanoic acid (PFOA) using starch-stabilized magnetite nanoparticles. *Science of the Total Environment*. 562:191–200.

Green Cape. 2019. Waste: Market Intelligence Report 2019. *Waste*. 1–64.

Gunarathne, V., Ashiq, A., Ginige, M.P., Premarathna, S.D., de Alwis, A., and Vithanage, M. 2018. Municipal waste biochar for energy and pollution remediation., In Green adsorbents for pollutant removal Gregorio Crini · Eric Lichtfouse Ed, Springer Nature Switzerland AG 2018

Gurung, K., Ncibi, M.C., Shestakova, M. and Sillanpää, M. 2018. Removal of carbamazepine from MBR effluent by electrochemical oxidation (EO) using a Ti/Ti_2O_5-SnO_2 electrode. *Applied Catalysis B: Environmental*. 221:329–338.

Hadjltaief, H.B., Zina, M. Ben, Galvez, M.E. and Da Costa, P. 2015. Photo-Fenton oxidation of phenol over a Cu-doped Fe-pillared clay. *Comptes Rendus Chimie*. 18(10):1161–1169.

Hairuddin, M.N., Mubarak, N.M., Khalid, M., Abdullah, E.C., Walvekar, R. and Karri, R.R. 2019. Magnetic palm kernel biochar potential route for phenol removal from wastewater. *Environmental Science and Pollution Research*. 26(34):35183–35197.

Han, L., Qian, L., Yan, J. and Chen, M. 2016. Contributions of different biomass components to the sorption of 1,2,4-trichlorobenzene under a series of pyrolytic temperatures. *Chemosphere*. 156:262–271.

Han, L., Ro, K.S., Sun, K., Jin, J., Libra, J.A., and Han, L. 2016. New Evidence for High Sorption Capacity of Hydrochar for Hydrophobic Organic Pollutants New Evidence for High Sorption Capacity of Hydrochar for Hydrophobic Organic Pollutants. *Environmental. Science Technology* 50(24):13274–13282.

Han, L., Ro, K.S., Wang, Y., Sun, K., Sun, H., and Xing, B. 2018. Science of the Total Environment Oxidation resistance of biochars as a function of feedstock and pyrolysis condition. *Science of the Total Environment*. 616–617:335–344.

Huang, B., Gu, H., Xiao, K., Qu, F., Yu, H. and Wei, C. 2020. Fouling mechanisms analysis via combined fouling models for surface water ultrafiltration process. *Membranes*. 10(7):1–12.

Ifthikar, J., Wang, T., Khan, A., Jawad, A., Sun, T., and Jawad, A. 2017. Highly Efficient Lead Distribution by Magnetic Sewage Sludge Biochar: Sorption Mechanisms and Bench Applications. *Bioresource Technology*. 238:399–406.

Ilva, W.S.I.D.S., Erera, M.M.N.P., Erera, K.L.N.S.P. and Ickramasuriya, A.M.W. 2017. ScienceDirect In silico Analysis of osr40c1 Promoter Sequence Isolated from Indica Variety Pokkali. 24(4):228–234.

Inyang, M., Gao, B., Ding, W., Pullammanappallil, P., Zimmerman, A.R. and Cao, X. 2011. Enhanced lead sorption by biochar derived from anaerobically digested sugarcane bagasse. *Separation Science and Technology*. 46(12):1950–1956.

Inyang, M., Gao, B., Yao, Y., Xue, Y., Zimmerman, A.R., Cao, X. 2012. Removal of heavy metals from aqueous solution by biochars derived from anaerobically digested biomass. *Bioresource Technology*. 110:50–56.

Inyang, M.I., Gao, B., Yao, Y., Xue, Y., Zimmerman, A. 2016. Technology A review of biochar as a low-cost adsorbent for aqueous heavy metal removal. *Critical Reviews in Environmental Science and Technology*. 46(4):406–433.

Jaman, H., Chakraborty, D. and Saha, P. 2009. A study of the thermodynamics and kinetics of copper adsorption using chemically modified rice husk. *Clean - Soil, Air, Water*. 37(9):704–711.

Jin, J., Li, S., Peng, X., Liu, W., Zhang, C., and Wang, X. 2018. HNO_3 modified biochars for uranium (VI) removal from aqueous solution. *Bioresource Technology*. 4:678-684

Joseph, L., Jun, B.M., Flora, J.R.V., Park, C.M. and Yoon, Y. 2019. Removal of heavy metals from water sources in the developing world using low-cost materials: A review. *Chemosphere*. 229:142–159.

Kantakanit, P., Tippayawong, N., Koonaphapdeelert, S. and Pattiya, A. 2018. Hydrochar Generation from Hydrothermal Carbonization of Organic Wastes. In: Vol. 159. *IOP Conference Series: Earth and Environmental Science*. Institute of Physics Publishing.

Kara, A. and Demirbel, E. 2012. Kinetic, isotherm and thermodynamic analysis on adsorption of Cr (VI) ions from aqueous solutions by synthesis and characterization of magnetic-poly (divinylbenzene-vinylimidazole) microbeads. *Water, Air, and Soil Pollution*. 223(5):2387–2403.

Karthikeyan, S., Sivakumar, B. and Sivakumar, N. 2010. Film and Pore Diffusion Modeling for Adsorption of Reactive Red 2 from Aqueous Solution onto Activated Carbon Prepared from Bio-Diesel Industrial Waste. *E-Journal of Chemistry*. 7(S1):175–184.

Kasozi, G.N., Zimmerman, A.R., Nkedi-Kizza, P. and Gao, B. 2010. Catechol and humic acid sorption onto a range of laboratory-produced black carbons (biochars). *Environmental Science and Technology*. 44(16):6189–6195.

Kim, J.J., Kim, Y.S. and Kumar, V. 2019. Heavy metal toxicity: An update of chelating therapeutic strategies. *Journal of Trace Elements in Medicine and Biology*. 54(November 2018):226–231.

Koley, S., Khadase, M.S., Mathimani, T., Raheman, H. and Mallick, N. 2018. Catalytic and non-catalytic hydrothermal processing of Scenedesmus obliquus biomass for bio-crude production – A sustainable energy perspective. *Energy Conversion and Management*. 163(February):111–121.

Kołodyńska, D., Wnętrzak, R., Leahy, J.J., Hayes, M.H.B., Kwapiński, W. and Hubicki, Z. 2012. Kinetic and adsorptive characterization of biochar in metal ions removal. *Chemical Engineering Journal*. 197:295–305.

Komkiene, J. and Baltrenaite, E. 2016. Biochar as adsorbent for removal of heavy metal ions [Cadmium (II), Biochar as adsorbent for removal of heavy metal ions [Cadmium (II), Copper

(II), Lead (II), Zinc (II)] from aqueous phase. *International Journal of Environmental Science and Technology*. 3:13-18.

Komtchou, S., Dirany, A., Drogui, P., Robert, D. and Lafrance, P. 2017. Removal of atrazine and its by-products from water using electrochemical advanced oxidation processes. *Water Research*. 125:91–103.

Kumar, P.S. and Kirthika, K. 2009. Equilibrium and kinetic study of adsorption of nickel from aqueous solutions onto Bael tree leaf powder. *Journal of Engineering Science and Technology* 4(4)351-363

Landsberger, S. 2019. 2 The Circular Economy in China. *Beijing Garbage*. 53–76.

Lapierre, C. 2019. Lignin structure and its engineering. Current Opinion in *Biotechnology*. 56:240–249.

Lee, C.G., Hong, S.H., Hong, S.G., Choi, J.W. and Park, S.J. 2019. Production of Biochar from Food Waste and its Application for Phenol Removal from Aqueous Solution. *Water, Air, and Soil Pollution*. 230(3).

Lei, Y., Su, H., Tian, F. and Deng. 2018. Chemosphere Chemically activated hydrochar as an effective adsorbent for volatile organic compounds. *Bioresource Technology*. 218(March):680–686.

Leja, M., Kamińska, I., Kramer, M., Maksylewicz-Kaul, A., Kammerer, D., and Baranski, R. 2013. The Content of Phenolic Compounds and Radical Scavenging Activity Varies with Carrot Origin and Root Color. *Plant Foods for Human Nutrition*. 68(2):163–170.

Lengauer, C.L. 2018. Production, characterization and adsorption studies of bamboo-based biochar / montmorillonite composite for nitrate removal. *Waste Management.* 79(385–394).

Li, B., Guo, J., Lv, K. and Fan, J. 2019. Adsorption of methylene blue and Cd (II) onto maleylated modified hydrochar from water. *Environmental Pollution*. 254.

Li, K., Zheng, Z., Huang, X., Zhao, G., Feng, J. and Zhang, J. 2009. Equilibrium, kinetic and thermodynamic studies on the adsorption of 2-nitroaniline onto activated carbon prepared from cotton stalk fibre. *Journal of Hazardous Materials*. 166(1):213–220.

Li, Q., Tang, L., Hu, J., Jiang, M., Shi, X., and Pan, X. 2018. Removal of toxic metals from aqueous solution by biochars derived from long-root Eichhornia crassipes. *Royal Society Open Science*. 5(10).

Li, Y., Meas, A., Shan, S., Yang, R. and Gai, X. 2016. Production and optimization of bamboo hydrochars for adsorption of Congo red and 2-naphthol. *Bioresource Technology*. 207:379–386.

Lin, D. and Xing, B. 2008. Adsorption of phenolic compounds by carbon nanotubes: Role of aromaticity and substitution of hydroxyl groups. *Environmental Science and Technology*. 42(19):7254–7259.

Lu, H., Zhang, W., Yang, Y., Huang, X., Wang, S. and Qiu, R. 2012. Relative distribution of Pb2+ sorption mechanisms by sludge-derived biochar. *Water Research*. 46(3):854–862.

Luter, L., Julius, A., Henry, D.T., Ikyenge, B.A., Sesugh, A. and Okoronkwo, M.U. 2012. Adsorption kinetics of Pb (II) and Zn (II) ions unto carbonized groundnut shells and Maize cobs. *European Journal of Scientific Research*. 84(3).

Maddi, B., Panisko, E., Albrecht, K. and Howe, D. 2016. Qualitative Characterization of the Aqueous Fraction from Hydrothermal Liquefaction of Algae Using 2D Gas Chromatography with Time-of-flight Mass Spectrometry. (March):1–11.

Mahy, J.G., Hermans, S., Tilkin, R.G. and Lambert, S.D. 2020. Influence of nucleating agent addition on the textural and photo-Fenton properties of Fe (III)/SiO2 catalysts. *Journal of Physics and Chemistry of Solids*. 144 (November 2019).

Manahan, S.E. 2003. Toxicological Chemistry and Biochemistry. C.P. LLC, ed. 3rd edition ed. Boca Raton London New York Washington, D.C. Copyright: Lewis Publishers.

Marais, H.B., Marx, S. and Venter, R.J. 2019. Valorisation of waste lignin for phenolic derivative compounds using hydrothermal liquefaction. 27th European Biomass Conference and Exhibition, 27-30 May 2019, Lisbon, Portugal

Marta, J., Rorat, A. and Grobelak, A. 2019. Enzymatic assays confirm the toxicity reduction after manure treatment of heavy metals contaminated soil. *South African Journal of Botany*. 124:47–53.

McBeath, S.T. and Graham, N.J.D. 2021. In-situ electrochemical generation of permanganate for the treatment of atrazine. *Separation and Purification Technology*. 260:237-244.

Mendoza-castillo, D.I. 2017. *Adsorption Processes for Water Treatment and Purification*. H. Elizabeth and Reynel-Ávila, eds. 1st ed. Cham, Switzerland: Springer International Publishing.

Mestrea, A.S., Tyszkoa, E., Andradea, M.A., Galhetasa, M., Freireb, C. and Carvalhob, A.P. 2012. Sustainable activated carbons prepared from a sucrose-derived hydrochar: remarkable adsorbents for pharmaceutical compounds. *Royal Society of Chemistry Advances* (25)19696-19707

Mihajlovic, M.L., Kragovic, M. and Stojanovic, M. 2017. Effect of KOH activation on hydrochar surface: FT-IR analysis. *Radiation and Applications*. 2(1):65–67.

Mohamed, G.M., El-shafey, O.I. and Fathy, N.A. 2017. Preparation of Carbonaceous Hydrochar Adsorbents from Cellulose and Lignin Derived from Rice Straw. *Egyptian Journal of Chemistry* 60(5):793–804.

Mohammed, A.S., Kapri, A. and Goel, R. 2011. Heavy Metal Pollution: Source, Impact, and Remedies. In: M.S. Khan, A. Zaidi, R. Goel, and J. Musarrat, eds. *Biomanagement of Metal-Contaminated Soils*. Dordrecht: Springer Netherlands. pp. 1–28.

Mohan, D., Sarswat, A., Sik, Y. and Pittman, C.U. 2014. Organic and inorganic contaminants removal from water with biochar, a renewable, low cost and sustainable adsorbent – A critical review. *Bioresource Technology*. 160:191–202.

Mu'azu, N.D., Jarrah, N., Zubair, M. and Alagha, O. 2017. Removal of phenolic compounds from water using sewage sludge-based activated carbon adsorption: A review. *International Journal of Environmental Research and Public Health*. 14(10):1–34.

Mudhoo, A., Gautam, R.K., Ncibi, M.C., Zhao, F., Garg, V.K. and Sillanpää, M. 2019. Green synthesis, activation and functionalization of adsorbents for dye sequestration. *Environmental Chemistry Letters* 17(1)157-193.

Nazari, L., Yuan, Z., Souzanchi, S., Ray, M.B. and Xu, C. (Charles). 2015. Hydrothermal liquefaction of woody biomass in hot-compressed water: Catalyst screening and comprehensive characterization of bio-crude oils. *Fuel*. 162:74–83.

Negrea, A., Mihailescu, M., Mosoarca, G., Ciopec, M., Duteanu, N., and Minzatu, V. 2020. Estimation on fixed-bed column parameters of breakthrough behaviors for gold recovery by adsorption onto modified/functionalized amberlite xad7. *International Journal of Environmental Research and Public Health*. 17(18):1–14.

Nguyen, T.H., Cho, H.H., Poster, D.L. and Ball, W.P. 2007. Evidence for a pore-filling mechanism in the adsorption of aromatic hydrocarbons to a natural wood char. *Environmental Science and Technology*. 41(4):1212–1217.

Ni, B.J., Huang, Q.S., Wang, C., Ni, T.Y., Sun, J. and Wei, W. 2019. Competitive adsorption of heavy metals in aqueous solution onto biochar derived from anaerobically digested sludge. *Chemosphere*. 219:351–357.

Oliveira, F.R., Patel, A.K., Jaisi, D.P., Adhikari, S., Lu, H. and Khanal, S.K. 2017. Environmental application of biochar: Current status and perspectives. *Bioresource Technology*. 246(February 2018):110–122.

Păcurariu, C., Mihoc, G., Popa, A., Muntean, S.G. and Ianoş, R. 2013. Adsorption of phenol and p-chlorophenol from aqueous solutions on poly (styrene-co-divinylbenzene) functionalized materials. *Chemical Engineering Journal*. 222:218–227.

Pan, C. and Chen, J. 2018., Advances on Absorption of Heavy Metals in the Wastewater by Biochar A Review: IOP Conf. Series: *Materials Science and Engineering* 301 (2018) 012160

Pan, Y.X., Liu, C.J., Mei, D. and Ge, Q. 2010. Effects of hydration and oxygen vacancy on CO2 Adsorption and activation on β-Ga2O3(100). *Langmuir*. 26(8):5551–5558.

Panisko, E., Wietsma, T., Lemmon, T., Albrecht, K. and Howe, D. 2015. Characterization of the aqueous fractions from hydrotreatment and hydrothermal liquefaction of lignocellulosic feedstocks. *Biomass and Bioenergy*. 74:162–171.

Papadopoulos, E., Arsenos, G., Ptochos, S., Katsoulos, P., Oikonomou, G., and Καρατζιάς, X. 2014. Pollutants in wastewater Effluents impacts. *International Journal of Environmental Research and Earth Science*. 3(3):50–59.

Parthasarathy, P. and Narayanan, S.K. 2014a. Hydrogen production from steam gasification of biomass: influence of process parameters on hydrogen yield. *A review in Renewable energy*. 66(1):570–579.

Peings, V., Frayret, J. and Pigot, T. 2015. Mechanism for the oxidation of phenol by sulfatoferrate (VI): Comparison with various oxidants. *Journal of Environmental Management*. 157:287–296.

Penido, E.S., Melo, L.C.A., Guilherme, L.R.G. and Bianchi, M.L. 2019. Cadmium binding mechanisms and adsorption capacity by novel phosphorus/magnesium-engineered biochars. *Science of The Total Environment*. 671:1134–1143.

Peydayesh, M., Pauchard, M., Bolisetty, S., Stellacci, F. and Mezzenga, R. 2019. Ubiquitous aluminium contamination in water and amyloid hybrid membranes as a possible sustainable solution. *Chemical Communications*. 55(74):11143–11146.

Pipitone, G., Zoppi, G., Bocchini, S., Maria, A. and Chiaramonti, D. 2019. Aqueous phase reforming of the residual waters derived from lignin-rich hydrothermal liquefaction: investigation of representative organic compounds and actual biorefinery streams. *Catalysis Today.* 345:237-250.

Praveen, P. and Loh, K.C. 2013. Trioctylphosphine oxide-impregnated hollow fiber membranes for removal of phenol from wastewater. *Journal of Membrane Science*. 437:1–6.

Purevsuren, B., Avid, B., Narangerel, J., Gerelmaa, T. and Davaajav, Y. 2004. Investigation on the pyrolysis products from animal bone. *Journal of Materials Science*. 39(2):737–740.

Purwanto, M.G.M. 2016. The Role and Efficiency of Ammonium Sulphate Precipitation in Purification Process of Papain Crude Extract. *Procedia chemistry*.18:127–131.

Rao, N.N., Somasekhar, K.M., Kaul, S.N. and Szpyrkowicz, L. 2001. Electrochemical oxidation of tannery wastewater. *Journal of Chemical Technology and Biotechnology*. 76(11):1124–1131.

Rashed, M.N. 2013. Adsorption Technique for the Removal of Organic Pollutants from Water and Wastewater. *Organic Geochemistry*. 3:29-34.

Regmi, P., Garcia Moscoso, J.L., Kumar, S., Cao, X., Mao, J. and Schafran, G. 2012. Removal of copper and cadmium from aqueous solution using switchgrass biochar produced via hydrothermal carbonization process. *Journal of Environmental Management*. 109:61–69.

Reza, M.T., Lynam, J.G., Uddin, M.H. and Coronella, C.J. 2013. Hydrothermal carbonization: Fate of inorganics. *Biomass and Bioenergy*. 49:86–94.

Rincón-Silva, N.G., Moreno-Piraján, J.C. and Giraldo, L. 2016. Equilibrium, kinetics and thermodynamics study of phenols adsorption onto activated carbon obtained from lignocellulosic material (Eucalyptus Globulus labill seed). *Adsorption*. 22(1):33–48.

Rodriguez-Narvaez, O.M., Peralta-Hernandez, J.M., Goonetilleke, A. and Bandala, E.R. 2017. Treatment technologies for emerging contaminants in water: A review. *Chemical Engineering Journal*. 323(April):361–380.

Ruiz, H.A., Rodríguez-Jasso, R.M., Fernandes, B.D., Vicente, A.A. and Teixeira, J.A. 2013. Hydrothermal processing, as an alternative for upgrading agriculture residues and marine biomass according to the biorefinery concept: A review. *Renewable and Sustainable Energy Reviews*. 21:35–51.

Sandquist, J., Tschentscher, R. and del Alamo Serrano, G. 2019. Hydrothermal liquefaction of organic resources in biotechnology: how does it work and what can be achieved? *Applied Microbiology and Biotechnology*. 103(2):673–684.

Sangi, M.R., Shahmoradi, A., Zolgharnein, J., Azimi, G.H. and Ghorbandoost, M. 2008. Removal and recovery of heavy metals from aqueous solution using Ulmus carpinifolia and Fraxinus excelsior tree leaves. *Journal of Hazardous Materials*. 155(3):513–522.

Saqib, N.U., Baroutian, S. and Sarmah, A.K. 2018. Physicochemical, structural and combustion characterization of food waste hydrochar obtained by hydrothermal carbonization. *Bioresource Technology*. 266:357–363.

Schuler, J., Hornung, U., Kruse, A., Dahmen, N. and Sauer, J. 2017. Hydrothermal Liquefaction of Lignin. *Journal of Biomaterials and Nanobiotechnology*. 8(1):96–108.

Shakoor, M., Ali, S., Farid, M., Farooq, M.A., Tauqeer, H.M., and Bharwana, S. 2013. Heavy metal pollution, a global problem and its remediation by chemically enhanced phytoremediation: A Review. *Journal of Biodiversity and Environmental Sciences*. 3:12–20.

Sharma, P.K., Ayub, S. and Tripathi, C.N. 2016. Isotherms describing physical adsorption of Cr (VI) from aqueous solution using various agricultural wastes as adsorbents. *Cogent Engineering*. 3(1).

Sikdar, S.K. and Criscuoli, A. 2017. Sustainability and how Membrane Technologies in Water Treatment Can Be a Contributor. In sustainable membrane technology for water and wastewater treatment pp. 1–21. Springer, Singapore.

Singh, A., Aggrawal, S. and Lal, D. 2019. Effect of formaldehyde to phenol ratio in phenolic beads on pore structure, adsorption and mechanical properties of activated carbon spheres. *Defence Science Journal*. 69(1):46–52.

Sirkar, K.K., Singh, D. and Li, L. 2017. Membrane Distillation in Desalination and Water Treatment. In sustainable membrane technology for water and wastewater treatment pp. 201–219. Springer, Singapore.

Sun, K., Ro, K., Guo, M., Novak, J., Mashayekhi, H. and Xing, B. 2011. Sorption of bisphenol A, 17 a -ethinyl estradiol and phenanthrene on thermally and hydrothermally produced biochars. *Bioresource Technology*. 102(10):5757–5763.

Sun, K., Tang, J., Gong, Y. and Zhang, H. 2015. Characterization of potassium hydroxide (KOH) modified hydrochars from different feedstocks for enhanced removal of heavy metals from water. *Environmental science and pollution research*. 22(21),16640-16651

Sun, Y., Gao, B., Yao, Y., Fang, J., Zhang, M., and Yang, L. 2014. Effects of feedstock type, production method, and pyrolysis temperature on biochar and hydrochar properties. *Chemical Engineering Journal*. 240:574–578.

T McKee and R, J. 1998. Biochemistry The Molecular Basis of Life (No. 01 QD415, M2 1998) -149.

Takaya, C.A., Fletcher, L.A., Singh, S., Anyikude, K.U. and Ross, A.B. 2016. Chemosphere Phosphate and ammonium sorption capacity of biochar and hydrochar from different wastes. *Chemosphere*. 145:518–527.

Taşar, Ş. and Özer, A. 2020. A thermodynamic and kinetic evaluation of the adsorption of Pb (II) ions using peanut (Arachis hypogaea) shell-based biochar from aqueous media. *Polish Journal of Environmental Studies*. 29(1).

Thomas, J. V. 1995. Petroleum and Coal. Coal. *Analytical Chemistry*. 67(12):317–319.

Thomas, N., Dionysiou, D.D. and Pillai, S.C. 2021. Heterogeneous Fenton catalysts: A review of recent advances. *Journal of Hazardous Materials*. 404:124082.

Tian, Y., Wang, F., Djandja, J.O., Zhang, S.L., Xu, Y.P. and Duan, P.G. 2020. Hydrothermal liquefaction of crop straws: Effect of feedstock composition. *Fuel*. 265(2001).

Tong, X.J., Li, J.Y., Yuan, J.H. and Xu, R.K. 2011. Adsorption of Cu (II) by biochars generated from three crop straws. *Chemical Engineering Journal*. 172(2–3):828–834.

Tounsadi, H., Khalidi, A., Abdennouri, M. and Barka, N. 2015. Biosorption potential of Diplotaxis harra and Glebionis coronaria L. biomasses for the removal of Cd (II) and Co (II) from aqueous solutions. *Journal of Environmental Chemical Engineering*. 3(2):822–830.

Trakal, L., Veselská, V., Šafařík, I., Vítková, M., Číhalová, S. and Komárek, M. 2016. Lead and cadmium sorption mechanisms on magnetically modified biochars. *Bioresource Technology*. 203:318–324.

Tran, H.N., You, S.J., Hosseini-Bandegharaei, A. and Chao, H.P. 2017. Mistakes and inconsistencies regarding adsorption of contaminants from aqueous solutions: A critical review. *Water Research*. 120:88–116.

Tünay, O., Kabdaşlı, I., Arslan-Alaton, I. and Ölmez-Hancı, T. 2010. *Chemical Oxidation Applications for Industrial Wastewaters*. 1st ed. London, England: IWA publishing. https://iwaponline.com/ebooks/book-pdf/521267/wio9781780401416.pdf Date of access: 31 Jan. 2021.

Uchimiya, M., Ohno, T. and He, Z. 2013. Pyrolysis temperature-dependent release of dissolved organic carbon from plant, manure, and biorefinery wastes. *Journal of Analytical and Applied Pyrolysis*. 104:84–94.

Valdez, P.J., Nelson, M.C., Wang, H.Y., Lin, X.N. and Savage, P.E. 2012. Hydrothermal liquefaction of Nannochloropsis sp.: Systematic study of process variables and analysis of the product fractions. *Biomass and Bioenergy*. 46:317–331.

Van Holme, R. and De Meester, B. 2019. Lignin biosynthesis and its integration into metabolism. *Current Opinion in Biotechnology*. 56:230–239.

Viegas, R.M.C., Campinas, M., Costa, H. and Rosa, M.J. 2014. How do the HSDM and Boyd's model compare for estimating intraparticle diffusion coefficients in adsorption processes. *Adsorption*. 20(5–6):737–746.

Vijayakumar, G., Tamilarasan, R. and Dharmendirakumar, M. 2011. Adsorption, Kinetic, Equilibrium and Thermodynamic studies on the removal of basic dye Rhodamine-B from aqueous solution by the use of natural adsorbent perlite. *J. Mater. Environ. Sci*. 3(1):157–170.

Villegas, L.G.C., Mashhadi, N., Chen, M., Mukherjee, D., Taylor, K.E. and Biswas, N. 2016a. A Short Review of Techniques for Phenol Removal from Wastewater. *Current Pollution Reports*. 2(3):157–167.

Villegas, L.G.C., Mashhadi, N., Chen, M., Mukherjee, D., Taylor, K.E. and Biswas, N. 2016b. A Short Review of Techniques for Phenol Removal from Wastewater. *Current Pollution Reports*. 2(3):157–167.

Wang, H., Liu, W., Yao, W., Zhang, K., Zhong, J. and Chen, R. 2013. Quaternary ammonium salts intercalated α-ZrP compounds for adsorption of phenolic compounds. *Applied Surface Science*. 268:179–187.

Wang, J. and Kaskel, S. 2012. KOH activation of carbon-based materials for energy storage.*Journal of Materials Chemistry*. 22(45):23710–23725.

Wang, J. and Wang, S. 2019. Preparation, modification and environmental application of biochar: A review. *Journal of Cleaner Production*. 227:1002–1022.

Wang, L., Wang, Y., Ma, F., Tankpa, V., Bai, S., and Wang, X. 2019. Mechanisms and reutilization of modified biochar used for removal of heavy metals from wastewater: A review. *Science of The Total Environment*. 668:1298–1309.

Wang, Y., Wei, X., Qi, Y. and Huang, H. 2021. Efficient removal of bisphenol-A from water and wastewater by Fe2O3-modified graphene oxide. *Chemosphere*. 263.

Wang, Z., Liu, G., Zheng, H., Li, F., Ngo, H.H., and Xing, B. 2015. Investigating the mechanisms of biochar's removal of lead from solution. *Bioresource Technology*. 177:308–317.

Wasewar, K.L. 2010. Adsorption of metals onto tea factory waste: A review. *IJRRAS*. 3(3):303–322. https://www.researchgate.net/publication/45627731 Date of access: 23 Mar. 2021.

Watson, J., Wang, T., Si, B., Chen, W.T., Aierzhati, A. and Zhang, Y. 2020. Valorization of hydrothermal liquefaction aqueous phase: pathways towards commercial viability. *Progress in Energy and Combustion Science*. 77:100819.

Wei, X., Zhang, S., Han, Y. and Wolfe, F.A. 2019. Treatment of petrochemical wastewater and produced water from oil and gas. *Water Environment Research* 91: 1025–1033, 2019

Weideman, R., Moyakhe, D., Wanders, F.B., Roux, M. Le and Campbell, Q.P. 2019. Hydrothermal preparation of biochar from spent coffee grounds and its application for the removal of cadmium from coal tailings leachate. 119(July):607–612.

World Health Organization. 2011. Summary World Report on Disability. *World Health*. 1–24.

Wu, F.C., Tseng, R.L. and Juang, R.S. 2009. Characteristics of Elovich equation used for the analysis of adsorption kinetics in dye-chitosan systems. *Chemical Engineering Journal*. 150(2–3):366–373.

Wu, S.Y., Peng, W.C., Wu, Y.Q., Gao, J.S., Qin, X.G. and Nie, L. 2013. Characteristics of liquid products from hydrothermal liquefaction of typical crop straws under CO atmosphere. *Journal of the Energy Institute*. 86(3):134–139.

Xia, Y., Yang, T., Zhu, N., Li, D., Chen, Z., and Jiao, W. 2019. Enhanced adsorption of Pb (II) onto modified hydrochar: Modeling and mechanism analysis. *Bioresource Technology*. 288.

Xiong, Y., Zhang, P., Johnson, S., Luo, J. and Fang, Z. 2020. Comparison of the phenolic contents, antioxidant activity and volatile compounds of different sorghum varieties during tea processing. *Journal of the Science of Food and Agriculture*. 100(3):978–985.

Xue, Y., Gao, B., Yao, Y., Inyang, M., Zhang, M., and Ro, K.S. 2012. Hydrogen peroxide modification enhances the ability of biochar (hydrochar) produced from hydrothermal carbonization of peanut hull to remove aqueous heavy metals: Batch and column tests. *Chemical Engineering Journal*. 200–202:673–680.

Yan, W., Zhang, H., Sheng, K., Mustafa, A.M. and Yu, Y. 2018. Evaluation of engineered hydrochar from KMnO4 treated bamboo residues: Physicochemical properties, hygroscopic dynamics, and morphology. *Bioresource Technology*. 250:806–811.

Yang, J., (Sophia) He, Q. and Yang, L. 2019. A review on hydrothermal co-liquefaction of biomass. *Applied Energy*. 250:926–945.

Yang, J., He, Q. (Sophia), Corscadden, K., Niu, H., Lin, J. and Astatkie, T. 2019. Advanced models for the prediction of product yield in hydrothermal liquefaction via a mixture design of biomass model components coupled with process variables. *Applied Energy*. 233–234(September 2018):906–915.

Yang, X., Zhang, S. and Ju, M. 2019. Preparation and Modification of Biochar Materials and their Application in Soil Remediation. *Applied sciences*.9(7), 1365.

Yangui, A., Abderrabba, M. and Sayari, A. 2017. Amine-modified mesoporous silica for quantitative adsorption and release of hydroxytyrosol and other phenolic compounds from olive mill wastewater. *Journal of the Taiwan Institute of Chemical Engineers*. 70:111–118.

Yin, S. and Tan, Z. 2012. Hydrothermal liquefaction of cellulose to bio-oil under acidic, neutral and alkaline conditions. *Applied Energy*. 92:234–239.

Yoon, K., Cho, D.W., Tsang, D.C.W., Bolan, N., Rinklebe, J. and Song, H. 2017. Fabrication of engineered biochar from paper mill sludge and its application into removal of arsenic and cadmium in acidic water. *Bioresource Technology*. 246:69–75.

Yu, W., Liu, T., Crawshaw, J., Liu, T. and Graham, N. 2018. Ultrafiltration and nanofiltration membrane fouling by natural organic matter: Mechanisms and mitigation by pre-ozonation and pH. *Water Research*. 139:353–362.

Zhang, B., He, Z., Chen, H., Kandasamy, S., Xu, Z., and Guo, H. 2018. Effect of acidic, neutral and alkaline conditions on product distribution and biocrude oil chemistry from hydrothermal liquefaction of microalgae. *Bioresource Technology*. 270:129–137.

Zhang, J., Sun, B. and Guan, X. 2013. Oxidative removal of bisphenol A by permanganate: Kinetics, pathways and influences of co-existing chemicals. *Separation and Purification Technology*. 107:48–53.

Zhang, P., Sun, H., Min, L. and Ren, C. 2018. Biochars change the sorption and degradation of thiacloprid in soil: Insights into chemical and biological mechanisms. *Environmental Pollution*. 236:158–167.

Zhang, S., Li, Z., Yang, Y., Jian, W., Ma, D. and Jia, F. 2020. Kinetics and thermodynamics of SO2adsorption on metal-loaded multiwalled carbon nanotubes. *Open Physics*. 18(1):1201–1214.

Zhang, X., Gao, B., Fang, J., Zou, W. and Dong, L. 2019. Chemosphere Chemically activated hydrochar as an effective adsorbent for volatile organic compounds. Chemosphere. 218:680–686.

Zhang, X., Zhang, L. and Li, A. 2017. Hydrothermal co-carbonization of sewage sludge and pinewood sawdust for nutrient-rich hydrochar production: Synergistic effects and products characterization. *Journal of Environmental Management*. 201:52–62.

Zheng, W., Guo, M., Chow, T., Bennett, D.N. and Rajagopalan, N. 2010. Sorption properties of green waste biochar for two triazine pesticides. *Journal of Hazardous Materials*. 181(1–3):121–126.

Zhou, Y., He, Y., He, Y., Liu, X., Xu, B., and Luo, L. 2019. Analyses of tetracycline adsorption on alkali-acid modified magnetic biochar: Site energy distribution consideration. *Science of the Total Environment*. 650.

Zhu, X., Liu, Y., Qian, F., Zhang, S. and Chen, J. 2015. Investigation on the Physical and Chemical Properties of Hydrochar and Its Derived Pyrolysis Char for Their Potential Application: Influence of Hydrothermal Carbonization Conditions. *Energy and Fuels*. 29(8):5222–5230.

CHAPTER 3

3 EXPERIMENTAL MATERIALS AND METHODS

A comprehensive description of experimental procedures, instrumentation and chemicals used in the experimental work is provided in this chapter. Section 3.1 provided chemicals and instrumentation used, and their uses and suppliers are listed in Table 3.1 and Table 3.2. Section 3.2 describes the characterisation of the wastewater (HTL aqueous phase), while Sections 3.3 and 3.4 describe the activation and characterisation of hydrochar. Section 3.5 explains the preparation of synthetic mixtures used in Section 3.6 for batch experimental procedures to measure the effect of contact time, dosage, pH, initial concentration, temperature and combining metals and phenolics on the adsorption of metals and phenolics. The results were fitted with mathematical models described in Sections 2.5, 2.6 and 2.7. The batch desorption experiment is also presented in Section 3.6. Lastly, the adsorption and desorption on HTL aqueous phase and regeneration and reusability of hydrochar experiments are presented in Section 3.7.

3.1 Materials used

3.1.1 Preparation of glassware

Laboratory glassware, e.g., volumetric flasks, reagent bottles, conical flasks, Büchner funnels, HPLC vials, IC and ICP-OES tubes, measuring cylinders and beakers were used in this project. All glassware was washed with soap and water, followed by rinsing with distilled water, rinsing with acetone and finally with deionized water. After washing and rinsing, the glassware was dried in a Series 2000 Scientific oven at 105 °C and then removed and allowed to cool to room temperature before use in experimentation. This cleaning and drying procedure was followed to ensure that all glassware used in this study was clean and contaminant free.

3.1.2 Chemicals used

All chemicals used in this study are listed in Table 3.1.

Table 3.1: Chemicals used throughout the project

Chemicals	Purity%	Supplier	Use

Hydrochar	-	Van der Merwe, 2021 and Nel, 2021	Adsorbent
HTL -aqueous phase	-	Van der Merwe, 2021 and Nel, 2021	Wastewater
Vanillyl alcohol	>99%	Sigma-Aldrich	Preparation of stock solution
Resorcinol	>99%	Sigma-Aldrich	Preparation of stock solution
Phenol	>99%	Sigma-Aldrich	Preparation of stock solution
Guaiacol	>99%	Sigma-Aldrich	Preparation of stock solution
$CaCl_2.2H_2O$	>99%	ACE Chemicals	Preparation of stock solution
$FeSO_4.7H_2O$	>99%	Sigma-Aldrich	Preparation of stock solution
KCl	>99%	ACE Chemicals	Preparation of stock solution
$MgCl_2.6H_2O$	>99%	ACE Chemicals	Preparation of stock solution
NaCl	>99%	ACE Chemicals	Preparation of stock solution
NaOH	>99%	ACE Chemicals	pH adjustment solution
HCl	>99%	Sigma-Aldrich	Hydrochar activating reagent (1.0 mol/L) Desorbing reagent (1.0 mol/L) pH adjustment solution (0.1 mol/L)
Deionized water	-	North-west University, Faculty of Engineering Biofuels laboratory	Preparation of stock solution
Acetone	>99%	Sigma-Aldrich	Cleaning of glassware
Ethanol	>99%	Sigma-Aldrich	Cleaning of glassware
Citric acid Monohydrate	HPLC grade	Sigma-Aldrich	Calibration of HPLC
L (+) Lactic Acid	HPLC grade	Sigma-Aldrich	Calibration of HPLC
Formic Acid	HPLC grade	Sigma-Aldrich	Calibration of HPLC
Acetic Acid	HPLC grade	Sigma-Aldrich	Calibration of HPLC
Glucose	HPLC grade	Sigma-Aldrich	Calibration of HPLC
Xylose	HPLC grade	Sigma-Aldrich	Calibration of HPLC
Galactose	HPLC grade	Sigma-Aldrich	Calibration of HPLC
Arabinose	HPLC grade	Sigma-Aldrich	Calibration of HPLC
Gallic acid	HPLC grade	Sigma-Aldrich	Calibration of HPLC

Hydroquinone	HPLC grade	Sigma-Aldrich	Calibration of HPLC
Vanillyl alcohol (p-VA)	HPLC grade	Sigma-Aldrich	Calibration of HPLC
Resorcinol	HPLC grade	Sigma-Aldrich	Calibration of HPLC
Vanillic acid	HPLC grade	Sigma-Aldrich	Calibration of HPLC
Catechol	HPLC grade	Sigma-Aldrich	Calibration of HPLC
3-Hydroxy-2Methoxy Benzyl Alcohol	HPLC grade	Sigma-Aldrich	Calibration of HPLC
Vanillin	HPLC grade	Sigma-Aldrich	Calibration of HPLC
Phenol	HPLC grade	Sigma-Aldrich	Calibration of HPLC
Guaiacol	HPLC grade	Sigma-Aldrich	Calibration of HPLC
Syringol	HPLC grade	Sigma-Aldrich	Calibration of HPLC
4-Nitrophenol	HPLC grade	Sigma-Aldrich	Calibration of HPLC
p-Cresol	HPLC grade	Sigma-Aldrich	Calibration of HPLC
o-Cresol	HPLC grade	Sigma-Aldrich	Calibration of HPLC
2-Nitrophenol	HPLC grade	Sigma-Aldrich	Calibration of HPLC
2-Naphthol	HPLC grade	Sigma-Aldrich	Calibration of HPLC
ICP-OES and IC standard are described in their method section			

3.2 Analytical techniques and instrumentation used

Analytical techniques and instruments used to analyse and characterise hydrochar and wastewater samples are listed in Table 3.2.

Table 3.2: Analytical techniques and instruments used in the study

Instrument	Use	Model and Supplier
Elemental analyser	To determine the elemental composition of hydrochar	CE-440 Elemental Analyser –Exeter Analytical
Bomb calorimeter	To determine the HHV of hydrochar	C5003 bomb calorimeter IKA
Fourier Transform Infrared Spectrometer (FTIR)	To identify functional groups, present on the hydrochar	IR- Affinity -1S-Shimadzu

Platform shaker	To maintain the desired temperature and uniform mixing during adsorption	Platform form S/N 21048-Labex
pH meter	To measure the pH of a solution	Metrohm 713 series Metrohm
Scanning electron microscope	To analyse the surface structure of hydrochar	FEI QUANTA 250 FEG SEM
BET	Measure surface area and porosity	Micromeritics 3 Flex 5.02 – Agilent technologies
Furnace	Used in proximate analysis	CWF 1300 furnace - Carbolite

3.2.1.1 Metal identification and quantification: ICP-OES

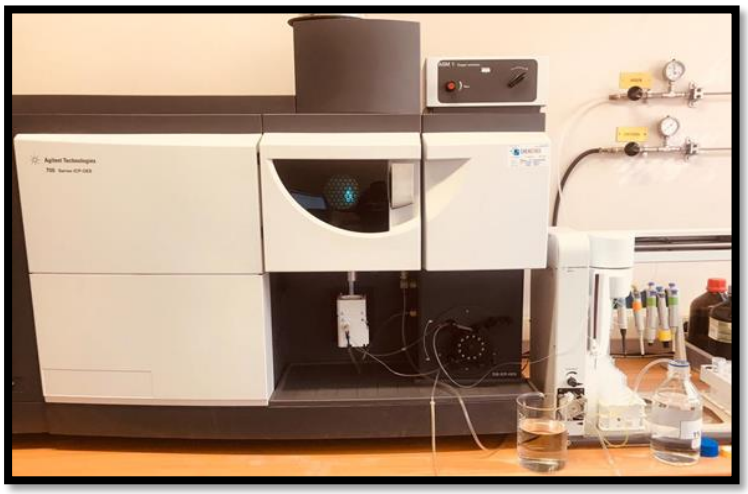

Figure 3.1: Inductively coupled plasma- optical emission spectrometer (ICP-OES)

The residual concentration of inorganic components and metals present in wastewater samples were quantified using an Agilent Technologies 725-ES ICP-OES instrument equipped with a radical torch, as shown in Figure 3.1. The argon flow to the plasma was 15 L/min with auxiliary and nebuliser flow rates of 1.50 L/min and 0.75 L/min, respectively and a viewing height of 12 mm. A 1 % nitric acid solution was used as the mobile phase for analysis. The 10 ppm and 100 ppm standards for Mg^{2+}, Na^{+}, Ca^{2+} and K^{+} were obtained from Chemetrix. From these standards the 1ppm, 2 ppm, 5 ppm, 10 ppm or 50 ppm were prepared depending on the concentration of the wastewater samples. With the help of the machine manual and the prepared standard the machine was calibrated with obtaining the limit of detection as 1 ppm. From that Ca^{2+}, K^{+}, Mg^{2+}, Na^{+}, Si, Zn^{2+}, Ag^{+}, Al^{3+}, As^{3+}, Ba^{2+}, Be^{2+}, Cd^{2+}, Co^{2+}, Cr^{3+}, Cu^{2+}, Fe^{2+}, Mn^{2+}, Ni,$^{2+}$ Pb^{2+}, Se^{4+}, Ti^{3+}/Ti^{4+} and

VO_3^-/VO_2^+ ions in the sample were identified and quantified. Before analysis, a blank sample with deionised water is also to cater for the dilutions. The preparation of the sample involved the detection and quantification of a tenfold dilution of each sample in a centrifuge tube, which was then carefully mixed before each analysis.

3.2.1.2 Identification and quantification of phenolic components

3.2.1.2.1 Total phenol analysis of HTL aqueous phase using Folin-Ciocalteu assay

The total phenolic content of HTL aqueous phase (wastewater) was determined using an electron transfer-based assay (Folin-Ciocalteu assay) and gives reducing capacity, which is expressed as phenolic content. The external calibration was done using different concentrations of gallic acid (Sigma Aldrich) dissolved in 80% ethanol *i.e.*, 0.5 mg/L, 1.3 mg/L, 2.6 mg/L, 5.1 mg/L, 7.6 mg/L and 12.8 mg/L. 200 μL of wastewater and 2.0 mL of solution A (a mixture of 10 mL of 2 % Na_2CO_3 with 0.1 mL of $CuSO_4$ and 0.1 mL of sodium and potassium tartrate) were mixed. After 4 mins., 0.4 mL of 0.5 mol/L sodium hydroxide (NaOH) was added. After 10 min., 0.2 mL of Folin-Ciocalteu reagent (1:1 v/v with water) was added. The solution was left for 30 min., and its absorbance was measured using a UV Vis spectrophotometer at 765 mm. The total phenolic content was calculated as mg/L gallic acid equivalent (mg/L GAE) using gallic acid calibration (Singleton *et al*.,1999).

3.2.1.2.2 Monomeric phenolics analysis of HTL aqueous phase using HPLC (high-performance liquid chromatography)

The monomeric phenolic components in the aqueous product (wastewater) and adsorption mixtures were identified and quantified by an Agilent Technologies 1260 Infinity II HPLC, as shown in Figure 3.2 below:

Figure 3.2: Phenolic High-Performance Liquid Chromatography

The HPLC has an Infinity Lab Poroshell 120 EC-C18 4.6 x 100 mm column and a diode array detector with a wavelength of 275 nm and bandwidth of 4 nm. Two formic acid solutions were used to make up mobile phases for analysis, i.e., a 1 % Formic acid in water (solution A) and 1 % Formic acid in acetonitrile (solution B). A mobile phase consisting of 92 % of solution A and 8 % of solution B was used during the first 10 minutes of analysis, after which the mobile phase was switched to a mixture containing 70 % of solution A and 30 % of solution B. The column temperature was set at 40 °C with an injection volume of 10 µL, and gallic acid was used as an internal standard for calibration. The HPLC instrument was quantitatively calibrated as described by Seal, (2016) with the standards hydroquinone, resorcinol, catechol, guaiacol, syringol, vanillyl alcohol, vanillic acid, vanillin, and phenol in Table 3.1 to identify and quantify hydroquinone, resorcinol, catechol, guaiacol, syringol, vanillyl alcohol, vanillic acid, vanillin, and phenol in the synthetic or real wastewater. The detailed calibration information that includes standards concentrations, standard curves and calculations are provided in the link in annexure 1. HPLC samples were prepared for analysis by mixing 100 µL of wastewater samples with 800 µL 0.1 mol/L formic acid and 100 µL of gallic acid in ethanol.

3.2.1.3 Identification and quantification of organic acids and monomeric sugars in HTL aqueous phase

The organic acids in the HTL Aqueous phase were identified and quantified Agilent Technologies 1200 HPLC by HPLC sugars Agilent as shown in Figure 3.3 below.

Figure 3.3: Sugar High-Performance Liquid Chromatography

The HPLC was fitted with an Aminex HPX-87P column and refractive index detector (RID) detector. For acids and alcohols, 10 µL sample volume was analysed with 0.005 % H_2SO_4 as mobile phase with a flow rate of 0.6 mL/min at a column temperature of 65 °C. For sugars, 10 µL sample volume was analysed with water 0.005 µS/cm as the mobile phase with a flow rate of 0.6 mL/min at a column temperature of 80 °C for 35 min run time. The instrument was calibrated using standard sugars (glucose, xylose, galactose, and arabinose) and organic acids (citric acid, lactic acid, formic acid, and acetic acid) (Seal, 2016) with the standards glucose, xylose, galactose, arabinose, citric acid, lactic acid, formic acid, and acetic acid. The detailed calibration information that includes standards concentrations, standard curves, limit of detections and calculations are provided in the link in Annexure 1. The limit of detection was obtained to be 0.0001 g/L. HPLC sugar and acid analysis samples were prepared by mixing 100 µL of the wastewater sample with 900 µL of the appropriate mobile phase.

3.2.1.4 Anion and cation identification and quantification using Ion chromatography (IC)

The cations and anions in the wastewater samples before and after adsorption were identified and quantified using a Metrohm 930 Compact IC series instrument (see Figure 3.4) equipped with an autosampler and an 858 professional sampler processor operating at a conductivity of between 0 and 15000 µS/cm and a UV/Vis detector, with a full loop injection (20 µL). A solution of 4.2 mM Na_2CO_3 and 1.0 mM $NaHCO_3$ in water was used as the mobile phase, and the instrument was calibrated to detect and quantify F^-, Cl^-, NO_2^-, Br^-, NO_3^-, SO_4^{2-}, PO_4^{2-}, Li^+, Na^+, NH_4^+, K^+, Mg^{2+} and Ca^{2+}. The limit of detection was set at 1ppm.

Figure 3.4: Ion chromatography (IC)

3.3 HTL products

The hydrochar and HTL aqueous phase were collected from an M. Eng. Student (van der Merwe, 2021) and was prepared as follows: A synthetic municipal solid waste mixture (dry basis) containing municipal sewage (112 g), green apples (2.10 g), bananas (1.20 g), blackberries (0.10 g), red apples (1.30 g), oranges (1.60 g), carrots (1.10 g), cauliflower (0.50 g), lettuce (0.10 g), red pepper (0.70 g), tomatoes (0.30 g), protein (3.40 g), fat (1.50 g), milk powder (1.40 g), sorghum (42.30 g), oil (4.90 g), potatoes (3.00 g), grass clippings (8.90 g), newspapers (0.46 g), printing paper (9.00 g), and corrugated paper (2.90 g) were used as feed to an SS316 stainless steel autoclave batch reactor. HTL was performed at 300^{o}C for a residence time of 20 minutes and a

volume loading of 50 %. Details of HTL product recovery and purification can be found in the dissertation of van der Merwe (2021). The HTL aqueous phase (approximately 2 L) was stored in an air-tight glass reagent bottle container at 4 °C until used in the experiments. The hydrochar (500 g) was sieved through a 75-micron sieve and labelled unwashed/raw hydrochar (RHc). The hydrochar was stored in airtight glass container at room temperature until used in the series of experiments.

3.4 Activation and characterisation procedures of hydrochar

3.4.1 Activation of hydrochar

The RHc samples (15 ± 0.005 g) were washed with 250 mL of a 1.0 mol/L HCL solution in water or 0.5, 1.0, 1.5, 2.0, or 2.5 mol/L KOH solution with shaker 1.9 Hz at 25 ± 2 ºC for 2 hours. The solutions were then filtered through non-sterile hydrophilic polytetrafluoroethylene (PTFE) 0.2 µm (diameter 25 mm) syringe filters from Grafiltech to recover the solids. The filtrates were placed in clean reagent bottle for characterisation with HPLC, ICP-OES, total phenols analysis and elemental analysis. The recovered solids were continually washed with deionised water to remove excess acid or base until the pH of the filtrate remained constant. The filtered hydrochars were dried at 60 ºC in an oven overnight and placed in air-tight containers labelled as acid-washed hydrochar aWHc, and base washed hydrochar (bWHc): 0.5 mol/L bWHc, 1.0 mol/L bWHc, 1.5 mol/L bWHc, 2.0 mol/L bWHc and 2.5 mol/L bWHc, respectively.

3.4.2 Characterisation of hydrochar

Physicochemical analyses were performed on the RHc, 1.0 mol/L aWHc, 0.5 mol/L, 1.0 mol/L, 1.5 mol/L, 2.0 mol/L and 2.5 mol/L KOH bWHc samples. Chemical characterisation was done using proximate analysis, elemental analysis, and Fourier-transform infrared spectroscopy (FTIR) analysis. The point of zero charge for each adsorbent was also determined. The physical characterisation was done by performing Brunauer-Emmett-Teller (BET) and scanning electron microscopy (SEM) analysis.

3.4.2.1 Proximate analysis

The proximate analysis is a scientific test that determines the moisture, volatile, ash and fixed carbon content of the washed and unwashed hydrochars. Proximate analysis was performed according to SANS 17246:2011 in conjunction with SANS 589 and SANS 50 to determine the

moisture content using volatile matter content. The ash content was determined as follows: 1 g of a hydrochar sample was added to a clean porcelain crucible and placed in a Lenton muffle furnace NREL/TP-510-42622 at 250 ^{o}C for 30 minutes. With the samples still in the furnace, the temperature was adjusted to 500 ^{o}C, at exactly 500 ^{o}C started counting the 30 minutes. The temperature was adjusted to 850 ^{o}C, and at exactly 850 ^{o}C, the sample was left overnight (16 hrs). After 16 hours, the sample was left to cool on the bench at room temperature until sample mass was constant (approximately 20 minutes), and the mass residual mass in the crucible was recorded. The procedures were done in triplicate and the mean value was recorded.

3.4.2.2 Elemental analysis

The carbon, hydrogen, and nitrogen content of the hydrochar samples were analysed with an Exeter CE-440 Elemental Analyser based on the ISO 12902 – CHN Instrumental method. Sample preparation was done according to IDO 13909-4: 2001, and the percentage difference was assigned to oxygen, the metals identified by ICP-OES

3.4.2.3 Calorific value analysis (HHV)

The calorific value (higher heating value (HHV)) of hydrochar was conducted on a model MC1 0 bomb calorimeter supplied by Energy Instrumentation. The bomb calorimeter was calibrated by combusting a benzoic acid pellet in the calorimeter and then adjusting the correction factor until the calorimeter yielded the appropriate calorific value. The calorific values of the different samples were determined by measuring 2 g of hydrochar followed by combusting it inside the bomb calorimeter. The acquired calorific value data in KJ/Kg were recorded on a computer coupled to the machine.

3.4.2.4 Point of zero charge

The point of zero charge (pH_{pZc}) of the different hydrochar samples was determined using 2.5 g of each sample and 100 mL of deionised water at different pH levels. The pH of the deionised water was adjusted using solutions of 0.1 mol/L HCl or NaOH in deionised water. The samples were mixed in a shaker at 1.9 Hz and 25 ± 2 °C overnight. The final pH of each solution was measured and recorded. The point of zero charge of each hydrochar was then obtained as the intersection at the x-axis of the pH profile when plotting the change observed in pH with mixing (ΔpH) against the starting pH.

3.4.2.1 Functional group analysis

Hydrochar surface functional group analysis was done using FTIR with an IR Affinity-1S from Shimadzu with a spectral range of 4000 – 400 cm^{-1}. For the analysis, a mass of approximately 20 mg of a hydrochar sample was mixed with approximately 200 mg of potassium bromide (KBr) using a mortar and pestle to form a fine powder.

3.4.2.2 Surface topography analysis using scanning electron microscopy (SEM)

The surface morphology and topography of hydrochar were analysed using SEM analysis. An FEI QUANTA 250 FEG SEM with integrated OXFORD X-max electron dispersive spectrometer (EDS) system, using a backscattered electron compositional signal, operating with a 5 kV electron beam at a working distance of 10 mm, 300 ns scan speed and magnification of x10 000 was used to acquire the SEM micrographs (Fuertes *et al.*, 2010). Six micrograph images were captured for every sample, and the best images representing the topography were chosen.

3.4.2.3 Surface area, pore volume and diameter using Brunauer-Emmett-Teller (BET)

The porosity and surface area of the hydrochar samples were determined using Micrometrics 3 Flex 5.02. A Micrometrics 3 Flex 5.02 surface area and porosity analyser instrument was used. The samples (0.50 g) were degassed under vacuum (10 µmHg) at 90 ^{o}C for 2880 min on the degassing port of the equipment before adsorption analysis (0 ^{o}C in an ice bath for CO_2 and at 77 K in liquid nitrogen for N_2 adsorption measurements, respectively). The adsorption data were automatically acquired by the 3 Flex 5.02 software in the relative pressure range: $0 < P/P0 < 0.032$ for CO_2 and $0 < P/P0 < 0.30$ for N_2 analyses, respectively. The Dubinin-Radushkevich equation and the Brunauer-Emmett-Teller equation were used to calculate micro and mesoporous surface area, respectively. In contrast, the Dollimore-Heal Adsorption (D-H) and Barrett-Joyner-Halenda (BJH) method were used to calculate average micropore and average mesopore diameter, respectively (Okolo *et al.*, 2015).

3.5 Preparation of synthetic wastewater

A synthetic wastewater mixture that resembled the composition of the HTL aqueous product was prepared from a detailed analysis of the AAEM (Alkali and Alkaline Earth Metals) and phenolic components present in the HTL aqueous product. Only AAEMs and metals with an average

concentration higher than 10 mg/L were included as constituents of the synthetic wastewater mixture and included Ca^{2+}, Mg^{2+}, K^{+}, Na^{+} and Fe^{2+}. The synthetic AAEM and metal synthetic mixture (MSM) was prepared by dissolving 230.8 mg, 513.1 mg, 3596.1 mg, 12.7 mg, and 2670 mg of $MgCl_2.6H_2O$, NaCl, KCl, $FeSO_4.7H_2O$ and $CaCl_2.H_2O$ into 1 L of deionised water, respectively.

The synthetic mixture containing phenolic components (PSM) in the highest concentration in the HTL aqueous phase was prepared by dissolving 501.3 mg, 303.3 mg, 201.3 mg, and 11.29 µL of vanillyl alcohol, resorcinol, phenol and guaiacol, respectively, in 1 L of deionised water.

A synthetic mixture containing both AAEM, and phenolic components (CMS) was prepared by dissolving 230.8 mg, 513.1 mg, 3596.1 mg, 12.7 mg, 2670.4 mg, 501.3 mg, 303.3 mg, 201.3 mg and 11.29 µL of $MgCl_2.6H_2O$, NaCl, KCl, $FeSO_47H_2O$, $CaCl_2.2H_2O$ vanillyl alcohol, resorcinol, phenol and guaiacol, respectively in 1 L of deionised water. The latter mixture is called the stock solution throughout the rest of this dissertation.

3.6 Batch adsorption experiments

A hydrochar sample was added to 100 mL of stock solution. It was mixed well through shaking by hand, after which it was placed in a platform shaker and continuously shaken at 2.5 Hz at a constant temperature of 25 ± 2 ^{o}C for 120 minutes. Aliquots of 5 mL were taken at regular intervals and filtered through non-sterile hydrophilic polytetrafluoroethylene (PTFE) 0.2 µm (diameter 25 mm) syringe filters from Grafiltech to remove all solids before analysis. The aliquot filtrates were then analysed with ICP-OES (metals) and HPLC (phenolics). The procedures were done in triplicate, and the results were recorded as mean values, and the precision was recorded as a standard deviation.

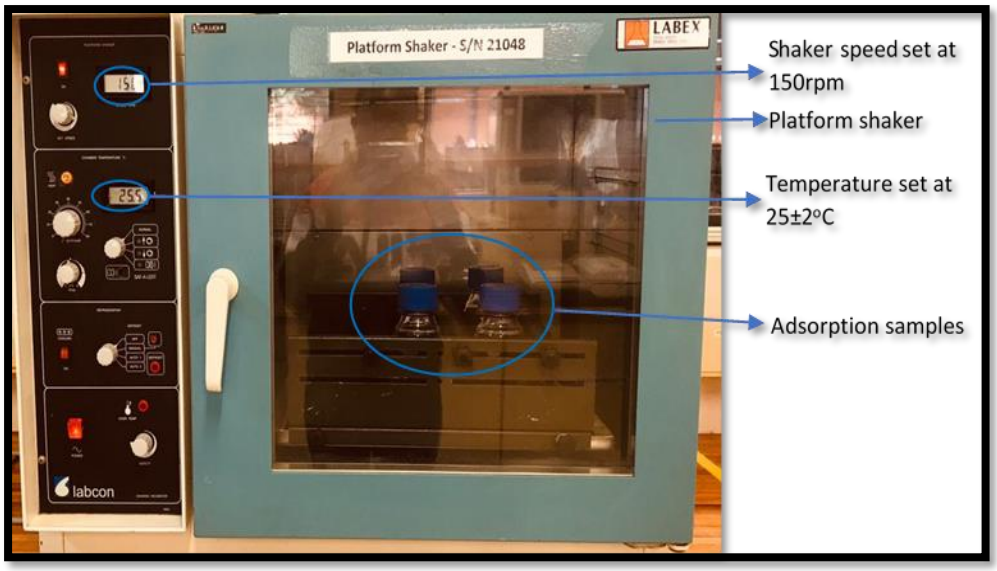

Figure 3.5: Batch adsorption experiment set up

Adsorption capacity calculations: The adsorption capacity of the hydrochar at a given time (qt) was calculated using equation 2.1 below:

$$qe = \frac{(C_o - C_e)V}{m} \qquad 3.1$$

where C_0 (mg/L) is the initial concentration of the phenolic components or heavy metal, C_e (mg/L) is the concentration at equilibrium, V (L) is the volume of the solution used and m (g) is the mass of the adsorbent used.

The maximum removal efficiency was determined as the point where the concentration of individual components reached a constant value (around 120 min), and the removal efficiency at any given time was calculated using equation 2.2 below:

$$\% \text{ removal} = \frac{(C_o - C_e)}{C_o} \times 100 \qquad 3.2$$

where C_0 (mg/L) is the initial concentration of the phenolic type of heavy metal, C_e (mg/L) is the equilibrium concentration of the adsorbate.

3.6.1 Experimental method

Adsorbent dosage, contact time, temperature and pH ranges were selected to achieve the set of objectives for the project as these variables were shown to have a significant impact on the

adsorption process (Ahmed and Theydan, 2012; Kausar *et al.*, 2017; Lu *et al.*, 2012b; Nacke *et al.*, 2016; Saeed and Ahmed, 2006). As such, adsorbent dosage (0.1 g, 0.5 g, 0.75 g, 1.0g and 2.0g), contact time (0 – 48 hrs), pH (2-12) and temperature (298K, 308K and 318K) were varied using a traditional linear experimental design where one variable was varied between the minimum and maximum chosen values. In contrast, the other variables were kept constant.

3.6.2 Fitting with mathematical models

The data obtained from Section 3.6.1 was fitted with adsorption kinetic models, mass transfer models, adsorption isotherm and thermodynamic parameters described in Sections 2.5, 2.6 and 2.7 to determine the mechanism of co-adsorption of metals and phenolic components on hydrochar. The data obtained at varying temperatures were fitted with thermodynamic equations described in Section 2.8 to understand the nature of adsorption. The correlation coefficient was calculated using the regression function in Microsoft Excel.

3.6.3 Desorption experiments.

Desorption of adsorbed components was done by washing the loaded hydrochar samples with both 10 mL of 1.0 mol/L HCl and 1.0 mol/L KOH consecutively. This is to determine the number of adsorbed metals and phenolics that can be desorbed from the hydrochar. The loaded hydrochar was mixed well with the 10 mL of 1.0 mol/L HCl through shaking by hand after which it was placed in a platform shaker and continuously shaken at 1.9 Hz at a constant temperature of 25 ± 2 ^{o}C for 120 minutes. After the 120 mins solid were filtered with 7.5 diameter hydrophilic polytetrafluoroethylene (PTFE) filter paper and rinsed both the filter from Grafiltech and the hydrochar with water until the pH remains constant. The process is then repeated with 10 mL of 1.0 mol/L KOH. The aliquot filtrates were then analysed with ICP-OES (metals) and HPLC (phenolics) to determine the amount of the metals and phenolics desorbed. The procedures were done in triplicate, and the results were recorded as mean values, and the precision was recorded as a standard deviation. The desorption efficiency and % desorption were calculated using the equations below:

$$\text{Desorption efficiency} = \frac{\text{amount of metal or phenolics desorbed}}{\text{amount of metal and phenolics adsorbed}} \quad 3.3$$

Therefore, % Desorption = Desorption efficiency x 100

3.7 Adsorption and desorption experiments with HTL aqueous phase

3.7.1 Adsorption of metals and phenolics from HTL aqueous phase

Adsorption of components present in the HTL aqueous product was done by adjusting the pH of 100 mL of the wastewater to the point of zero charge (pH_{pZc}) determined for the hydrochar used in the hydrochar activation experiments, i.e., a pH of 10.6 for the hydrochar activated with a 1.0 mol/L KOH solution in water. A dosage of 1.0 g of hydrochar activated using 1.0 mol/L KOH (BWHc). Once the hydrochar was added to the HTL wastewater, the mixture was shaken well by hand and then placed in a platform oven and shaker and continuously shaken at 2.5 Hz and 25 ± 2 °C for 24 hours. Aliquots of 5 mL were drawn at different time intervals and filtered immediately through a 0.2 µm syringe filter to remove any solids before analysis. The concentration of metals (ICP-OES) and phenolic components in the aliquots were determined as described previously in Sections 3.2.1.1 and 3.2.1.2

3.7.2 Regeneration and reusability of the hydrochar

The regeneration and reusability of the hydrochar were determined by subjecting approximately 10.2 g of BWHc to consecutive adsorption and desorption cycles. The HTL aqueous phase (100 mL) was adjusted to the determined pH_{pZc} of the BWHc hydrochar. A dosage of 10.2 g of BWHc was added to the HTL wastewater, shaken by hand, then placed in an oven shaker, and continuously shaken at 2.5 Hz and 25 ± 2 °C for 24 hours. Aliquots of 5 mL were drawn from the adsorption solution at time t = 0 and t = 120 min. The aliquots were immediately filtered through a 0.2 µm syringe filter to remove solids before analysis. The concentration of AAEM and phenolic components in the aliquot's filtrates were determined using ICP-OES, IC and HPLC as described previously in Sections 3.2.1.1 and 3.2.1.2, respectively. After 120 minutes of adsorption, the adsorption solution was filtered from the hydrochar using vacuum filtration with 0.22 µm filter paper. The filter paper and hydrochar were dried in an oven at 100 ^{o}C for 30 minutes. Desorption of adsorbed components from the adsorbent hydrochar done using 50 mL of 1 mol/L HCL in waste and 1 mol/L KOH in water consecutively. The hydrochar was finally recovered from the desorption mediums using vacuum filtration, rinsed with deionised water, and dried in an oven at 100 ^{o}C. The residual cleaned 9.2 g was then used in a second adsorption cycle using a fresh volume of 100 mL of HTL wastewater. This cycle was repeated until the no there was nothing desorbing

REFERENCES

Ahmed, M.J. and Theydan, S.K. 2012. Equilibrium isotherms, kinetics and thermodynamics studies of phenolic compounds adsorption on palm-tree fruit stones. *Ecotoxicology and Environmental Safety*. *Elsevier*. 84:39–45.

Fuertes, A.B., Arbestain, M.C., Sevilla, M., MacIá-Agulló, J.A., Fiol, S., López, R., Smernik, R.J., Aitkenhead, W.P., Arce, F., and MacIas, F. 2010. Chemical and structural properties of carbonaceous products obtained by pyrolysis and hydrothermal carbonisation of corn stover. *Australian Journal of Soil Research*. 32:618–626.

Kausar, A., Bhatti, H.N., Iqbal, M., and Ashraf, A. 2017. Batch versus column modes for the adsorption of radioactive metal onto rice husk waste: Conditions optimization through response surface methodology. *Water Science and Technology*. 76(5):1035–1043.

Lu, H., Zhang, W., Yang, Y., Huang, X., Wang, S., and Qiu, R. 2012. Relative distribution of Pb2+ sorption mechanisms by sludge-derived biochar. *Water Research*. *Elsevier Ltd*. 46(3):854–862.

Nacke, H., Gonçalves, A.C., Campagnolo, M.A., Coelho, G.F., Schwantes, D., Dos Santos, M.G., Briesch, D.L., and Zimmermann, J. 2016. Adsorption of Cu (II) and Zn (II) from Water by Jatropha curcas L. as Biosorbent. *Open Chemistry* 14(1):103–117.

Okolo, G.N., Everson, R.C., Neomagus, H.W.J.P., Roberts, M.J., and Sakurovs, R. 2015. Comparing the porosity and surface areas of coal as measured by gas adsorption, mercury intrusion and SAXS techniques. *Fuel*. *Elsevier Ltd*. 141:293–304.

Saeed, M.M. and Ahmed, M. 2006. Effect of temperature on kinetics and adsorption profile of endothermic chemisorption process: -Tm(III)-PAN loaded PUF system. *Separation Science and Technology*. 41(4):705–722.

Seal, T., 2016. Quantitative HPLC analysis of phenolic acids, flavonoids and ascorbic acid in four different solvent extracts of two wild edible leaves, Sonchus arvensis and Oenanthe linearis of North-Eastern region in India. *Journal of Applied Pharmaceutical Science*. 6 (02): pp. 157-166, February,

van der Merwe, J., 2021. Biodiesel production from municipal solid waste using lipase catalysis, DSI/NRF Research Chair in Biofuels and Other Clean Alternative Fuels, Centre of Excellence Carbon-based Fuels, Faculty of Engineering, North-West University, Potchefstroom, South Africa.

CHAPTER 4

4 RESULTS AND DISCUSSION

This chapter discusses and interprets the experimental results obtained in the study. Section 4.1 describes hydrothermal liquefaction products of municipal solid waste used in this study, while Section 4.2 explains the composition analysis of the HTL aqueous phase. The hydrochar activation with acid and base solutions and characterisation of the hydrochars is given in Section 4.3. Section 4.4 focuses on factors affecting the adsorption of alkali and alkaline earth metals (AAEMs) and phenolic compounds from a synthetic aqueous phase wastewater solution. The fitting with adsorption kinetics, mass transfer phenomena adsorption isotherms, and determination of adsorption thermodynamics, are discussed in Sections 4.5, 4.6, 4.7 and 4.8, respectively. Section 4.9 discusses the desorption of adsorbed metals and phenolics. The performance of hydrochar as an adsorbent for the removal of AAEMs and phenolic compounds from the real HTL aqueous phase is presented and discussed in Section 4.9. Lastly, the recovery and reusability of the hydrochar as a bio-waste adsorbent is explained in Section 4.10. Supplementary data for this chapter can be found in Appendix B as indicated in the text where appropriate.

4.1 HTL yields

The details of the municipal solid waste used to prepare the hydrochar and HTL aqueous phase in this study can be found in van der Merwe (2021). In short, a synthetic mixture representing a typical organic fraction of municipal solid waste (OFMSW) was subjected to HTL at 300 ^{o}C, 100 bars and yielded the HTL aqueous phase, hydrochar, biocrude and gas. Figure 4.1 below shows three of the four products.

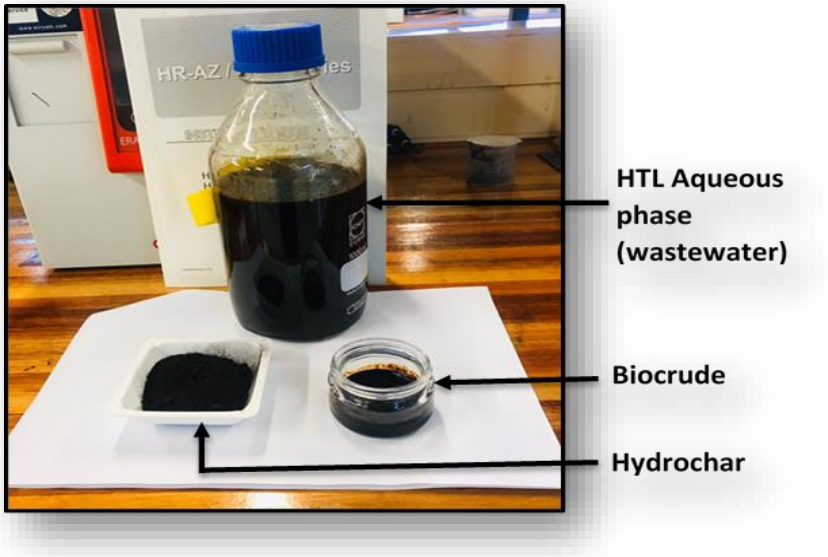

Figure 4.1. The products from HTL of OFMSW

The hydrochar obtained is dark brown; hence it is similar to the lignite coal, which is brown.

4.2 Composition of HTL aqueous phase (wastewater)

4.2.1 Metals present in the wastewater

Table 4.1 gives the metals present in the HTL aqueous determined by ICP-OES with the standard deviation as from the replicates. The results show that the wastewater contains a high concentration of AAEMs than heavy metals with potassium (K^+) (3653.4 mg/L) as the most abundant mineral. The AAEM originated from plant matter, fruits in food residues, cleaning reagents and sewage water that form OFMSW Heavy metals were found in lower quantities with iron (Fe^{2+}) (12.5 mg/L) as the most abundant heavy metal present in the wastewater. These are attributed to accumulation over time hence relatively low.

Table 4.1:The metal present in the HTL aqueous phase (wastewater)

Metal	Concentration (mg/L)
K^+	3653.4±93.04
Ca^{2+}	2512.9±111.26
Na^+	462.7±32.58
Mg^{2+}	219.7±8.07
Fe^{2+}	12.5±0.57

Mn^{2+}	4.1±0.21
Ba^{2+}	2.8±0.23
Zn^{2+}	2.3±0.62
Co^{2+}	1.9±1.29
Sr^{2+}	1.3±0.09
Pb^{2+}	1.1±0.52
Al^{3+}	1.1±0.08

4.2.2 Phenolic compound analysis

Phenolic derivatives and aromatic ethers are formed from the degradation of plant polymer lignin during HTL, resulting in polymeric and monomeric phenols (total phenols). The total phenol content (g/L) in the HTL aqueous phase was determined to be 2.27 g/L (average) using the Folin-Calteau method.

Table 4.2 below shows the monomeric phenolics (mg/L) detected using HPLC. The polymeric phenolics were calculated to be 0.85 g/L as the difference between the total phenols and the monomeric phenolics; hence 63 % of the total phenols in the wastewater are monomeric phenolics, and the remaining 37 % is polymeric phenolics. Therefore, the HTL process degrades lignin into both polymeric and monomeric phenolics.

Table 4.2:Monomeric phenolics detected in HTL aqueous phase by HPLC

Monomeric phenolics	Concentration (g/L)
Vanillyl alcohol	0.59±0.10
Resorcinol	0.26±0.04
Phenol	0.24±0.02
Guaiacol	0.10±0.02
Vanillic acid	0.07±0.01
Catechol	0.07±0.06
Vanillin	0.05±0.02
4-Nitrophenol	0.04±0.03
Total monomeric phenolics	1.42

Vanillyl alcohol (0.59 g/L), resorcinol (0.26 g/L), phenol (0.24 g/L), guaiacol (0.10 g/L), vanillic acid (0.07 g/L), catechol (0.07 g/L), vanillin (0.05 g/L) and 4-nitrophenol (0.04 mg/L), are detected phenolic compounds in the HTL aqueous phase. The phenolic content can be affected by

their solubility in either water or the extractive solvent hexane (Marais *et al.,* 2019; Wu *et al.,* 2013). Compounds more soluble in water are found mostly in the aqueous phase, and the opposite is true with respect to organic solvents. The hexane solvent extraction at 40 ^{o}C was found to lower the phenol content in the HTL Aqueous phase (Marx *et al.,* 2019). During thermochemical conversion, HTL parameters like pH and temperature affect the phenolic components formed. Marais *et al*. (2019) found phenolic components such as vanillin, catechol, cresol and guaiacol in the aqueous phase from HTL of technical lignosulphonate under alkaline conditions. Zou *et al.* (2014) used base catalysts like K_2CO_3 to enhance catechol formation at the expense of guaiacol. Gollakota *et al.,* (2018) found out that HTL temperature affects the individual phenolic compounds formed, and an increase in temperature above 350 ^{o}C favours the formation of guaiacol products while minimising vanillin production. In this study, no catalyst was used, and an HTL temperature of 300 ^{o}C was used; hence the aqueous phase contains guaiacol and vanillin. Therefore, the HTL of OFMSW yields more phenolics than the detected above that may be distributed in the different HTL products, e.g., on the hydrochar (detected on the filtrate from the wash with KOH). Despite all the limitations (equipment, solvents used in the separation process, separation process steps etc.) the monomeric phenolics detected using HPLC are above the recommended values for potable water (0.001 g/L) (Environmental Protection Agency, 2021), hence, remediation is required.

4.2.3 Organic acids and sugars present in wastewater

Table 4.3: The organic acids present in HTL aqueous phase determined by HPLC

Organic acids	Concentration (g/L)
Lactic acid	17.18±0.27
Acetic acid	9.84±0.56
Citric acid	5.03±0.07
Formic acid	2.67±0.03

The simple sugars glucose, galactose, xylose, and arabinose were absent because the monosaccharides were further degraded into acids and ketones. The organic acids were abundant in the HTL aqueous phase, as shown in Table 4.3 above, because under hydrothermal conditions, carbohydrates are hydrolysed into monosaccharides, which are then further degraded into various oxygenated hydrocarbons like organic acids. Hence, the observation agrees with the processes a, b and e in Figure 2.5 proposed by (Watson *et al.,* 2020). The lactic has the highest concentration

of 17.18 g/L, which is due to the base catalytic role of subcritical water in the degradation of both polysaccharides and monosaccharides. Acetic acid (9.84 g/L) is mainly from hydrolysis of carbohydrates, decomposition of glucose or fructose and deamination of amino acids (Campbell and Farrell, 2006).The citric acid (5.03 g/L) originates from fruits in the biomass and degradation of fructose or glucose. The carbohydrate and protein derivatives tend to dissolve in the aqueous phases preferentially hence are abundant in the HTL aqueous phase.

4.3 Results for activation and characterisation of hydrochar

4.3.1 Effect of hydrochar activation on the hydrochar and adsorption of metal and phenolic compounds

Table 4.4 and Table 4.5 below shows the effect of washing the hydrochar with HCl and KOH on the adsorption of metals and phenolics, respectively. The experimental conditions are given below the tables. OFMSW-derived hydrochar still contains metals and phenolic components in its pore structures or attached with weak bonds to the surface of the hydrochar. Therefore, washing the hydrochar with acid and base removes some residual components on the hydrochar surface, significantly increasing the removal efficiencies and adsorption capacity for both metals and phenolics. The wash activated hydrochar binding sites and emptied hydrochar pores, thus increasing the adsorption of metals and phenolics. However, no trend was observed in terms of changes in removal efficiency and the concentration of KOH; hence the adsorption capacity (mg/g) was analysed for individual adsorbates. The adsorption capacity for Ca^{2+} increased from 155.2 to 167.3-187.9 mg/g, K^{+} from 595.8 to 644.8 - 759.6 mg/g, Mg^{2+} from 6.7 to 7.7 - 11.4 mg/g and Na^{+} from 53.4 to 64.1 - 89.5 mg/g. Overall, all the metals have large adsorption with the acid and 1.0 mol/L KOH wash in hence the 1.0 mol/L HCl aWHc and the 1.0 mol/L KOH bWHc are best for metal adsorption.

Table 4.4:The effect of washing hydrochar with 0.5 mol/L, 1.0 mol/L, 1.5 mol/L, 2.0 mol/L, 2.5 mol/L KOH and 1 mol/L HCl on the adsorption capacity (qe(mg/g) and removal efficiency (%) of metals

Activation	Removal efficiency %				Adsorption capacity (mg/g)			
agent	Ca^{2+}	K^{+}	Mg^{2+}	Na^{+}	Ca^{2+}	K^{+}	Mg^{2+}	Na^{+}
STDEV	±0.96	±0.32	±0.65	±0.45	±0.74	±5.67	±01.89	±1.79
Not activated	49	48	33	40	155.2	595.8	6.7	53.4
1.0 mol/L HCl	59	62	57	67	187.9	759.6	11.4	89.5

0.5 mol/L KOH	52	55	39	48	167.3	676.8	7.7	64.1
1.0 mol/L KOH	58	53	47	64	183.6	649.8	9.4	84.4
2.0 mol/L KOH	55	52	42	53	175.9	644.8	8.5	70.8
2.5 mol/L KOH	57	55	48	51	181.1	676.8	9.6	67.1

Experimental conditions: total volume of solution 100 mL, solution pH: 10.6; hydrochar dose: 1g, temperature: 273 K; shaker 2.5 Hz; initial metal concentration Ca^{2+} 2652 mg/L, K^{+} 3586 mg/L, Mg^{2+} 230 mg/L and Na^{+} 510 mg/L for 120 minutes

Like metals, phenolics show no overall trend between the adsorption capacities and washes. A higher adsorption capacity change is noticed in vanillyl alcohol (from 154.2 to 156.0- 261.5 mg/g) and guaiacol (from 3540.6 to 2884.1-5922.9 mg/g) compared to resorcinol (from 106.1 to 109.9 - 177.8 mg/g), and phenol (from 7.75 to 8.32-18.69 mg/g) due to their methoxy attaches functional group, stabilising the whole structure resulting in less electrostatic repulsion. Table 4.5 shows maximum adsorption capacity with the 1.0 mol/L KOH bWHc washed hydrochar is enough to remove the already bound phenolics but not too high to ionise phenolics and cause electrostatic repulsion to the adsorbing phenolics. Therefore, the 1.0 mol/L KOH bWHc is ideal for phenolic adsorption.

Table 4.5:The effect of washing hydrochar with 0.5 mol/L, 1.0 mol/L, 1.5 mol/L, 2.0 mol/L, 2.5 mol/L KOH and 1.0 mol/L HCl on the adsorption capacity (qe (mg/g) and removal efficiency for phenolics.

	Removal efficiency %				Adsorption capacity (mg/g)			
Activation agent	Vanillyl alcohol	Resorcinol	Phenol	Guaiacol	Vanillyl alcohol	Resorcinol	Phenol	Guaiacol
STDEV	±1.40	±1.72	±0.93	±0.65	± 4.67	± 3.79	±3.89	±15.14
not activated	46	46	38	45	154.2	106.1	108.4	3540.6
1.0 mol/L HCl	70	71	46	57	237.7	164.5	131.6	4491.2
0.5 mol/L KOH	48	51	65	36	164.4	118.1	184.7	2884.1
1.0 mol/L KOH	77	77	79	75	261.5	177.8	225.8	5922.9
1.5 mol/L KOH	71	59	58	49	241.8	136.5	164.9	3885.1
2.0 mol/L KOH	45	48	49	46	156.0	109.9	140.3	3598.4
2.5 mol/L KOH	48	51	52	46	165.5	116.9	146.5	3607.3

Experimental conditions: total volume of solution 100 mL solution pH; 10.6; hydrochar dosage:1g, temperature: 273 K; shaker 2.5 Hz; initial phenolics concentration: vanillyl alcohol 530 mg/L, resorcinol 330 mg/L, phenol 250 mg/L and guaiacol 113mL/L for 120 minutes.

4.3.2 Composition of filtrates from activation of hydrochar

The filtrates obtained from the hydrochar wash with HCL and KOH were analysed to determine the removed minerals and phenolics.

Table 4.6 below shows the metal composition in mg/L from ICP-OES, the elemental composition (%) with oxygen content (R) as the percentage difference of C, H and N from 100 %, total phenols (g/L) from Folin-Calteau and monomeric phenols (g/L) analysed by HPLC.

Table 4.6: Composition of filtrates from base and acid activation of hydrochar

Hydrochar activation method		0.5 mol/L KOH	1.0 mol/L KOH	1.5 mol/L KOH	2.0 mol/L KOH	2.5 mol/L KOH	1.0 mol/L HCL	STDEV
ICP-OES (mg/L)	K^+	807.0	-207.4	-1356.3	-1911.6	-3297.4	319.1	± 14.04
	Ca^{2+}	3.0	4.0	5.1	6.2	7.0	885.5	± 0.29
	Mg^{2+}	-	-	-	-	-	69.0	± 0.97
	Na^+	95.0	119.2	208.2	269.2	320.1	27.5	± 2.47
	Ti^{3+}/Ti^{4+}	1.6	-	-	-	-	2.2	± 0.03
	Pb^{2+}	-	-	-	-	-	1.2	
	Fe^{2+}	-	-	-	-	-	9.0	
	Mn	-	-	-	-	-	2.1	
	Ba^{2+}	-	-	-	-	-	1.8	
	Ni^{2+}	-	-	-	-	-	1.0	
	Al^{3+}	3.9	3.0	4.0	4.9	4.0	8.0	
	Zn^{2+}	-	-	1.1	1.2	1.2	1.7	
	As^{3+}	-	1.9	-	-	2.2	2.1	
Elemental Analysis (%)	C	1.9	1.0	0.4	0.4	2.1	0.9	± 0.031
	H	11.0	12.0	10.5	11.4	10.7	11.5	± 0.09
	N	1.5	0.2	0.8	0.4	2.1	0.3	± 0.01
	R	85.6	86.8	83.4	87.8	85.1	87.0	± 1.47

Total Phenols concentration (g/L)		0.3	0.4	0.3	0.3	0.4	0.1	± 0.01
HPLC Phenolics Concentration (g/L)	Vanillyl alcohol	0.51	0.41	0.60	5.50	12.29	-	± 0.01
	Resorcinol	0.26	1.65	-	-	-	-	± 0.01
	Vanillic acid	0.03	-	-	-	-	-	

The ICP-OES results indicated metals removed by the acid wash arranged from the highest to the lowest thus, Ca^{2+}>K^{+}> Mg^{2+}>Na^{+}>Fe^{2+}> Al^{3+}>Ti^{3+}/Ti^{4+}, Mn^{2+}, Ba^{2+}, Zn^{2+}> Ni^{2+} and Pb^{2+} with Ti^{3+}/Ti^{4+}, Mn^{2+}, Ba^{2+} and Zn^{2+} having equal concentration. HCl protonates the hydrochar (substituted metal cation M^{n+} connected to functional hydrochar groups (e.g., COO-M to COO-H)) and therefore facilitates the desorption of metal ions on the surface. No phenolic components were released by acid wash because phenols are weak acids and are stable at lower pH; hence remain attached to hydrochar. Upon base wash, the OH-dominated negative surfaces favour metal adsorption. Thus, fewer metals accumulate in the filtrate. However, the base seemed effective in removing alkali metals K^{+} and Na^{+} than acid because of their persistent alkali hydroxides present in their ionic form. The potassium (K^{+}) washed from the char was calculated as the concentration in the filtrate minus the blank initial concentration of the activation solution before adding char. The concentration of K^{+} removed was calculated by subtracting the initial KOH wash concentration before adding the char (blank) from the resultant concentration (filtrate concentration). The 0.5 mol/L base wash removed the most K^{+} (807.0 mg/L), however as the concentration of the base increase the values become negative. Negative values e.g., -207.4 mg/L for the 1.0 M KOH base wash shows that adsorption was occurring instead of desorption and the value show 207.4 mg/L of K^{+} adsorbed on to the char. The elemental analysis shows a significant C and hydrogen and is attributed to the washed off phenols. The total phenol is very low (0.01-0.04 g), and HPLC shows that monomeric phenolics are dominant. Vanillyl alcohol, resorcinol and vanillic acid were washed off the hydrochar using a base KOH, and the removed concentration increased with an increase in KOH concentration because the free hydroxyl in the solution displaces the hydrochar hydrogen-bonded phenolic compound. Therefore, it can be concluded that

activation of hydrochar with acids or bases exposes the binding sites of hydrochar, thus improving the adsorption of metals and phenolics. It is more economic to use 1.0 mol/L over 2.0 mol/L when the effect is similar. Therefore, the 1.0 mol/L KOH wash is ideal for both metals and phenolics; hence it was used for further adsorption experiments of metals and labelled bWHc.

4.3.3 Characterisation of unwashed and washed hydrochar

The quality and characteristics of unwashed and washed hydrochar were assessed by proximate analyses, elemental analysis and the results are presented in Table 4.7 below.

Table 4.7: Proximate analysis, elemental analysis, and higher heating value (HHV) of the hydrochars

Characterisation of hydrochar		Raw/ unwashed hydrochar (RHc)	Base (KOH) washed hydrochar (bWHc)					Acid (HCl) washed hydrochar (aWHc)	STDEV
		RHc	0.5 mol/L	1.0 mol/L	1.5 mol/L	2.0 mol/L	2.5 mol/L	1.0 mol/L	
Proximate Analysis	Moisture Content %	1.9	1.9	1.6	2.5	2.4	1.8	1.7	±0.04
	Volatile Content %	48.8	46.8	45.0	45.0	44.6	45.7	50.0	±1.49
	Ash Content %	7.8	11.1	11.1	13.3	13.4	13.5	6.5	±1.07
Elemental Analysis	% C	68.8	66.4	65.3	63.7	63.1	63.9	64.0	±0.87
	% H	6.2	5.8	5.5	5.8	5.4	5.7	5.8	±0.19
	% N	3.7	4.5	3.2	4.6	3.1	4.67	5.4	±1.71
	% R	21.3	23.3	26.0	25.9	28.4	25.7	24.9	±0.63
HHV MJ/kg		27.2	27.4	27.1	26.8	26.8	28.8	29.7	±0.11

The moisture content values of the hydrochar are in the 1.6-2.5 % range. The volatile content is released volatile organic compounds (VOCs), mainly vapours and gases. The hydrochar base wash decreased the volatile content by 3-4 % because of removed organic compounds determined by running HPLC of the filtrates. The ash content consists of inorganic material remaining after combustion, e.g., silica, aluminium, calcium, magnesium, and sodium. The KOH washes have

slightly higher ash content (11-13.5 %) because KOH wash introduced K^+ to ash constituents. Unlike the KOH wash the acid wash did not remove much of the mineral as shown in Table 4.6.

The aWHc had the least ash content as most of the inorganic compounds were washed off the hydrochar, as shown in the filtrate's analysis in Table 4.6. The elemental analysis provides the basic composition of the hydrochar that is the carbon (C), hydrogen (H), nitrogen (N), and residual (R) which combination of oxygen (O), sulphur (S), halogens, inorganic compounds (those detected using ICP-OES paragraph above) content etc., as the difference of C, H and N. The residual increase The results obtained in Table 4.7 above show that acid and the base wash decreased the C % due to removing organic molecules like vanillyl alcohol, resorcinol and violinic acid which were detected in the HPLC analysis of the filtrates. The acid wash has a high HHV due to the significant reduction in ash content. Hydrochar is also a potential fuel hence the higher heating value (HHV) was analysed. HHV is the energy released when fully burning fuel, and hydrochar HHV lies in the 26 -30 MJ/kg, which the higher carbon content can explain. In addition to being a potential adsorbent, municipality waste-derived hydrochar is a potential solid fuel.

4.3.4 The pH point of zero charge (pH_{pZc}) of unwashed and washed hydrochar

Figure 4.2 shows the pH_{pZc} calculated from the plot of ΔpH (final pH –initial pH) vs initial pH. The pH_{pZc} is the pH at which the ΔpH is 0 (where the curves cross the x-axis). At the x-axis, the hydrochar is neutral, while above the x-axis, the surface of the hydrochar is positively charged, and below the x-axis, the hydrochar surface is negative.

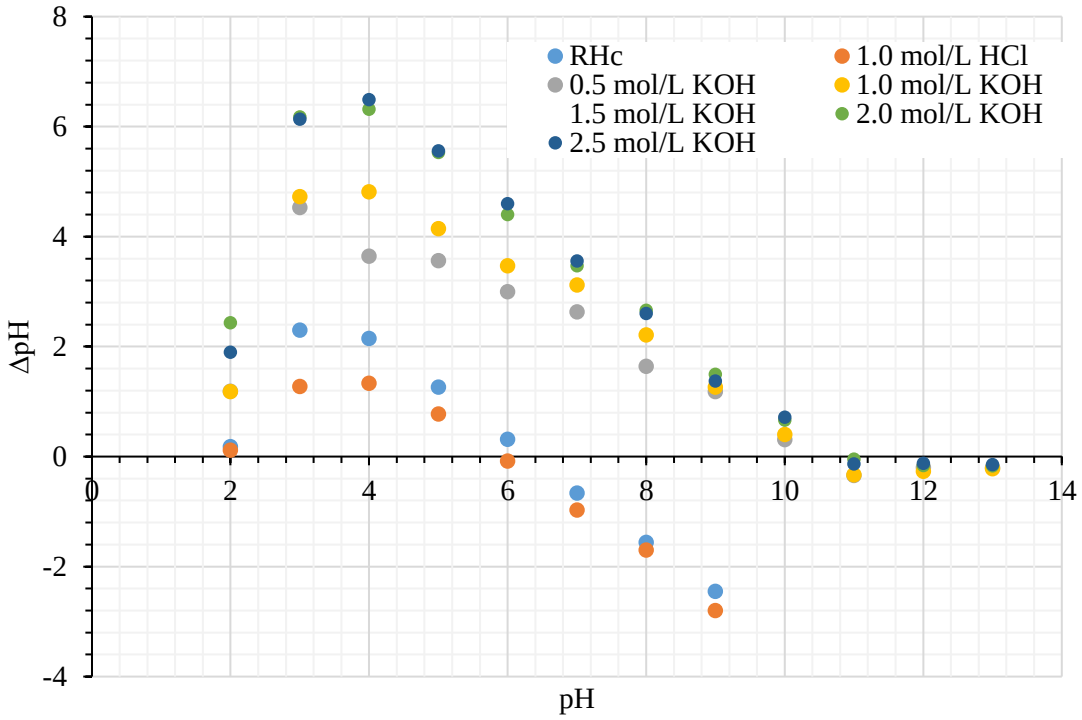

Figure 4.2: The pH point of zero charge (pH_{pZc}) of raw/ unwashed, and base- and acid-washed hydrochars

The pH_{pZc} of RHc was determined to be 6.3; thus, RHc possesses more acidic functional groups than the basic functional groups. Saha (2019) concluded that the acid wash increases the H^+ concentration on the surface, hence agreeing with pH_{pZc} of aWHc of pH 6.0. The 0.5 mol/L, 1.0 mol/L, 1.5 mol/L, 2.0 mol/L and 2.5 mol/L bWHc hydrochars have an alkaline pH_{pZc} of 10.5, 10.6, 10.8, 10,9 and 10.9 respectively because the hydroxyl neutralised the acidic functional groups Which increase with increase in KOH concentration. Furthermore, the base removed little to no metals off the hydrochar; instead, it added more K^+ to the hydrochar surface; as a result, the pH_{pZc} shifts to the alkaline region. Therefore, for further experiments, the pH of the solution will be exactly equal to the point of zero charges of the used hydrochar.

4.3.5 Hydrochar surface topography before and after adsorption

Figure 4.4 below shows the SEM images of the unwashed and washed hydrochars before (BA) and after adsorption (AA) at x10 000 magnification, from SEM analysis described in Section 3.4.2.2. The hydrochar surface was uneven, which is usually due to the incomplete carbonisation of hydrochar. The presence of OH functional groups, for example, validates the incomplete carbonisation. The hydrochar comprises spherical particles of 0.5 to 5 µm, (marked with double

arrows and the diameter size) clustered to create a porous sponge-like structure as shown in Figure 4.3 (particularly prominent for RHc BA, bWHc-BA and all after adsorption images).

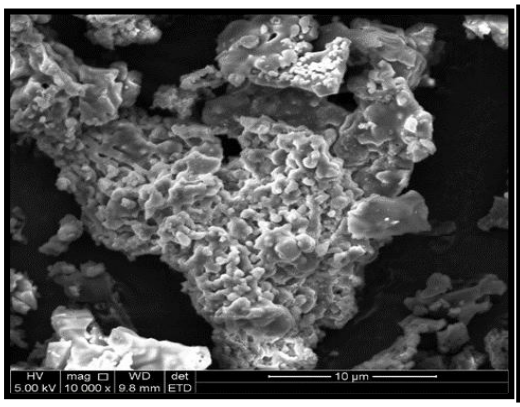

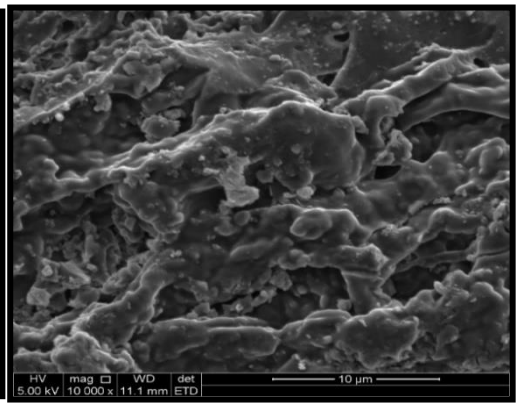

RHc- BA RHc-AA

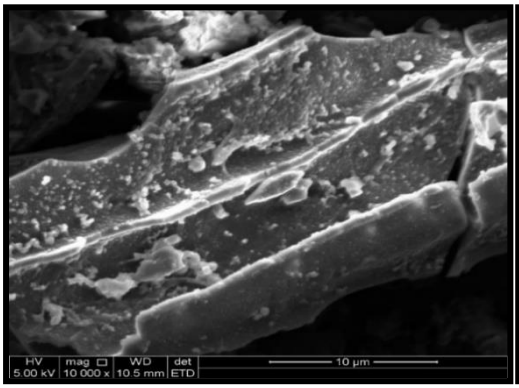

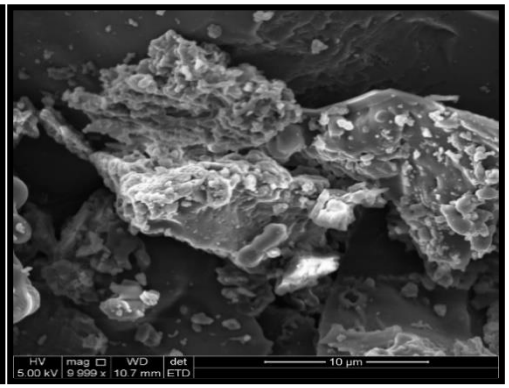

1.0 mol/L HCl aWHc- BA 1.0 mol/L HCl aWHc -AA

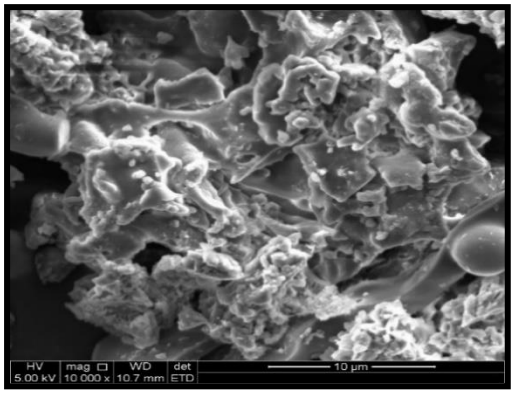

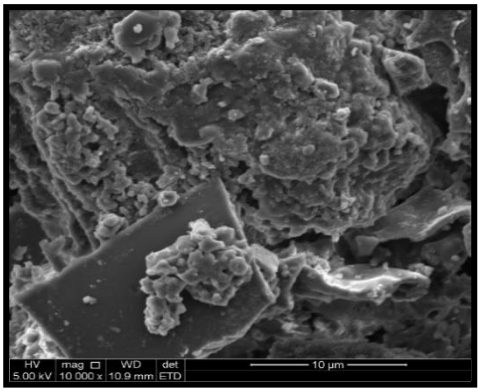

0.5 mol/L KOH bWHc- BA 0.5 mol/L KOH bWHc -AA

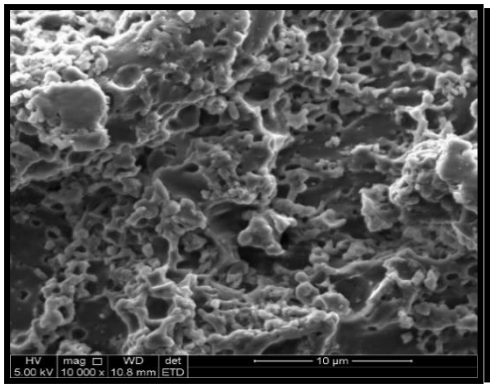

1.0 mol/L KOH bWHc- BA

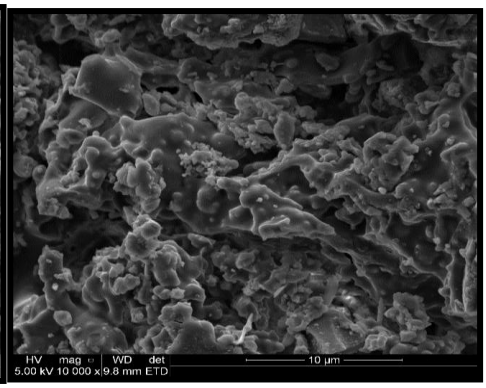

1.0 mol/L KOH bWHc –AA

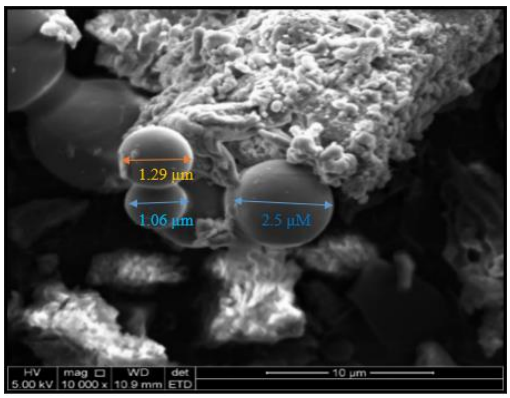

1.5 mol/L KOH bWHc- BA

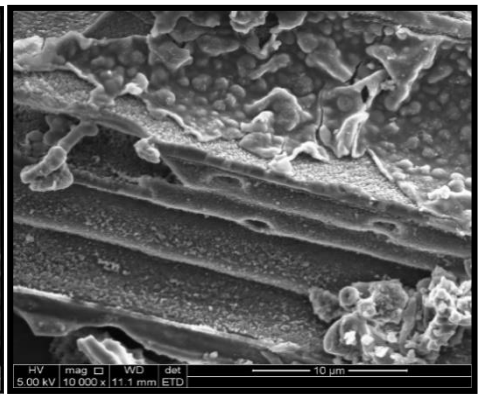

1.5 mol/L KOH bWHc -AA

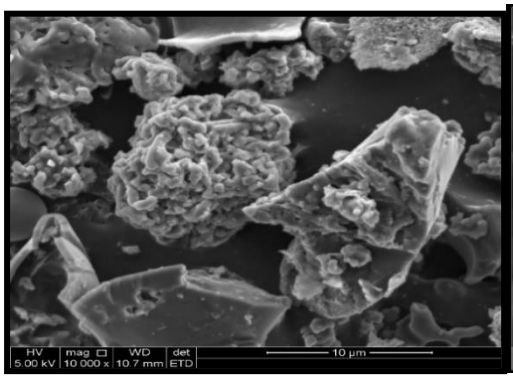

2.0 mol/L KOH bWHc- BA

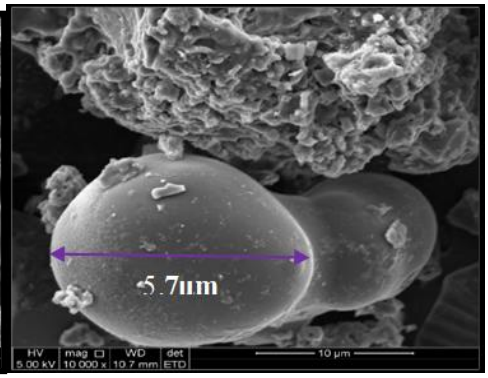

2.0 mol/L KOH bWHc -AA

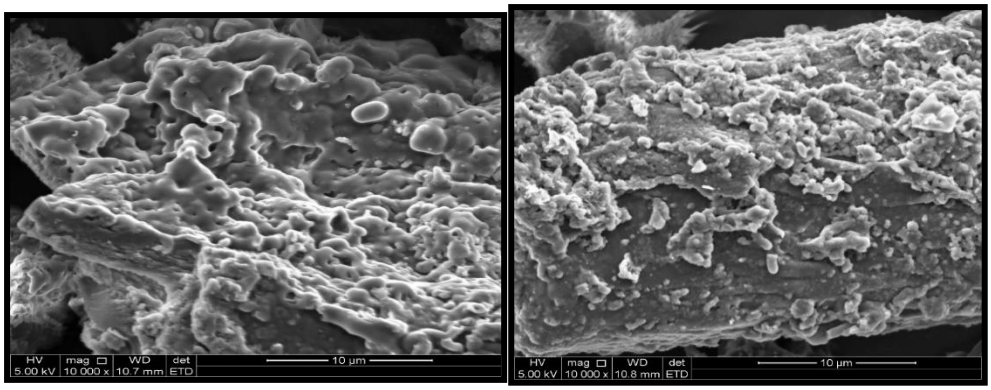

2.5 mol/L KOH bWHc- BA 2.5 mol/L KOH bWHc -AA

Figure 4.3 The SEM images of hydrochar at x10 000 magnification, before and after adsorption

Although RHc had both organic and inorganic components from the HTL of MSW, the after-adsorption images have more residues on the surface; hence adsorption occurred via complex formation and ionic interactions. The same was observed in the activated hydrochars. KOH washed hydrochars are more porous than acid-washed and unwashed hydrochar because the washing effect of KOH removes more organic compounds than metals, hence opening up the pores. By comparing the before and after images, the pores are no longer prominent suggest the phenolics pore-filling mechanism of adsorption. The pore diameter and pore volume of hydrochar were analysed using BET analysis to validate this point.

4.3.6 Hydrochar surface properties before and after adsorption

Table 4.8 below shows the BET analysis results explained in Section 3.4.2.3 as surface area in m^2/g, pore diameter (d_p) in Å and pore volume (v_p) in cm^3/g of hydrochar micropores and mesopores.

Table 4.8: Surface properties of hydrochar before and after adsorption of both metals and phenolics

	Micropore			Mesopores		
	DR-Surface Area (m^2/g)	DA-d_p (Å)	DA- v_p (cm^3/g)	BET-Surface Area (m^2/g)	BJH-d_p (Å)	BJH-v_p (cm^3/g)
Standard deviation	±2.13	±1.70	±0.0031	±0. 92	±2.47	±0.0002
RHc	53.43	19.64	0.0484	2.61	323.93	0.0182

Sample - Before adsorption	1.0 mol/L aWHc	57.86	23.25	0.0957	4.00	363.59	0.0232
	0.5 mol/L KOH bWHc	77.85	18.36	0.0612	2.51	327.49	0.0133
	1.0 mol/L KOH bWHc	75.74	19.38	0.0706	2.86	332.94	0.0169
	1.5 mol/L KOH bWHc	67.78	21.10	0.0823	2.06	379.27	0.0145
	2.0 mol/L KOH bWHc	79.38	19.64	0.0777	2.75	346.16	0.0158
	2.5 mol/L KOH bWHc	68.83	20.91	0.0810	2.03	347.33	0.0139
Sample- After adsorption	RHc	55.74	21.05	0.0059	2.07	292.65	0.0163
	1.0 mol/L HCL aWHc	78.82	18.32	0.0616	3.15	295.97	0.0206
	0.5 mol/L KOH bWHc	47.67	23.49	0.0811	2.31	310.95	0.0108
	1.0 mol/L KOH bWHc	19.40	19.10	0.0660	2.18	306.06	0.0090
	1.5 mol/L KOH bWHc	78.15	18.52	0.0633	2.33	307.15	0.0104
	2.0 mol/L KOH bWHc	78.79	19.39	0.0743	2.23	329.02	0.0130
	2.5 mol/L KOH bWHc	78.15	19.83	0.0790	2.51	339.02	0.0148

The BET analysis indicated that hydrochar consists of mesopore and micropore structures, and approximately 97 % is the microporous surface area. The mesoporous average pore diameter ranges from 292 - 380 Å (29 - 38 nm), while the microporous is 18 - 23 Å (1 - 2 nm). Most metals are small enough to diffuse into both the micropores and mesopores, but large phenolics block the pore, preventing diffusion of the smaller molecules and elements, thus reducing adsorption. KOH washes improved microporous surface area by 20.0 m^2/g because the removal of phenolics exposed the micropores. There was no significant change in the mesopore surface area upon base wash. HCl improves the micropore area by 4.0 m^2/g more than the mesopore surface of 2.0 m^2/g because the wash removed the metals occupying the micropores. Again, much as HCl washed more of the metal from the surface, the acid's corrosive nature may have destroyed the microporous

hydrochar structure, causing a loss of porosity. However, the total surface area is relatively low due to the HTL (300 ºC) lower temperatures since high operating temperatures are associated with pore formation and volatile evolution.

Additionally, mineral, and organic components on hydrochar may have also contributed to the lower surface area and pore volume. After adsorption, the surface areas and pore volume decrease due to the adsorption of metal and phenolics onto the hydrochar. Therefore, the hydrochar surface properties show that hydrochar is a potential adsorbent capable of removing metals and phenolics from wastewaters.

4.3.7 Hydrochar surface functional groups

Figure 4.4 below shows the FTIR spectra of the before and after adsorption (AD) hydrochars from the FT-IR analysis described in Section 3.4.2.4. The identified functional groups on the surface of hydrochar play an important role in the adsorption of metals and phenolics.

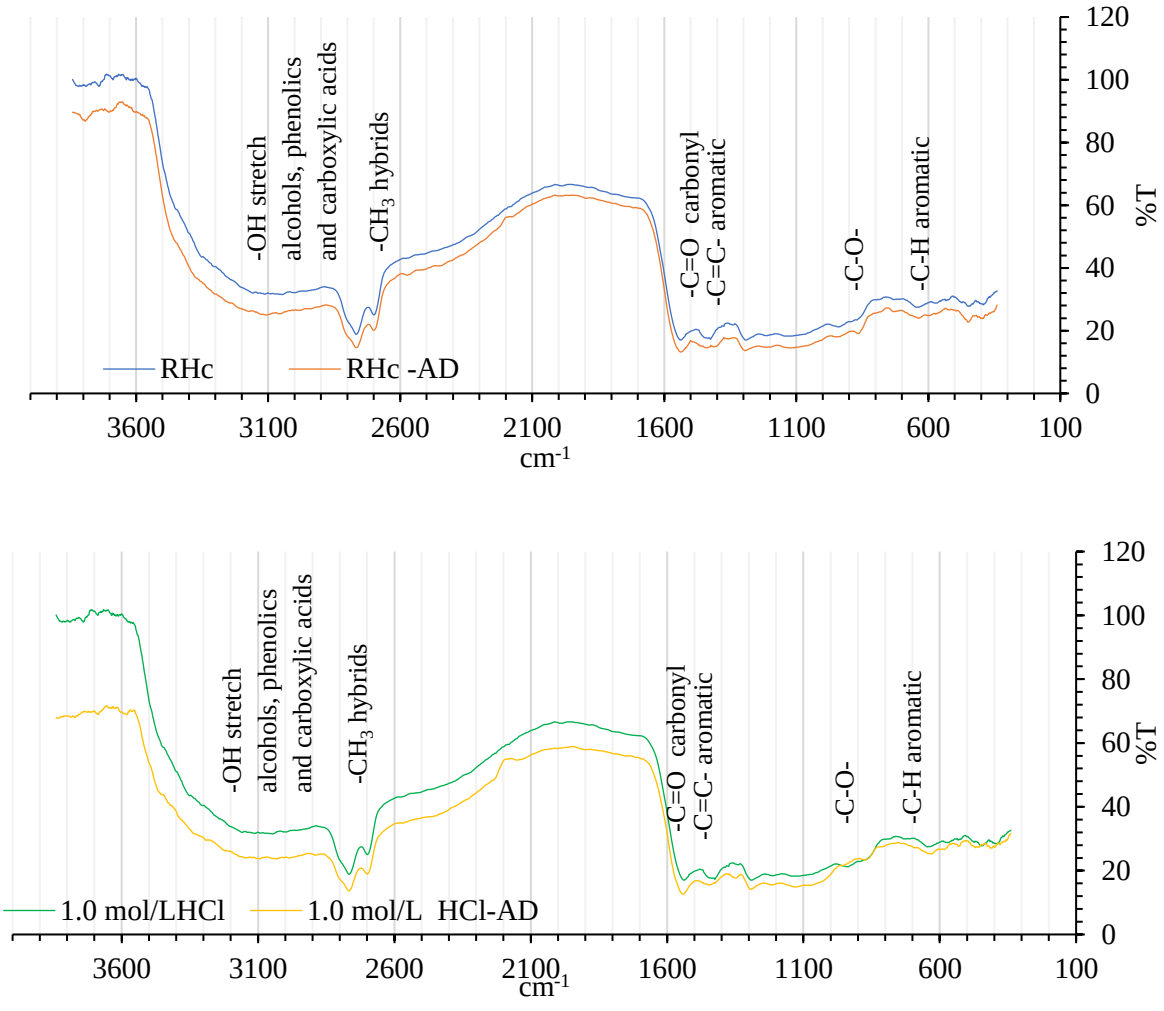

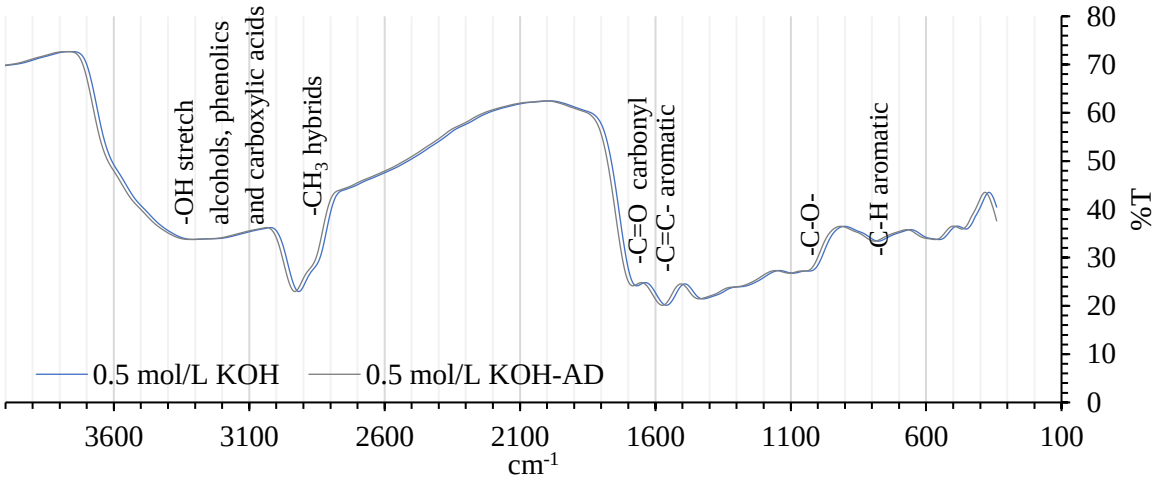
-OH stretch alcohols, phenolics and carboxylic acids
-CH3 hybrids
-C=O carbonyl
-C=C- aromatic
-C-O-
-C-H aromatic
0.5 mol/L KOH
0.5 mol/L KOH-AD
%T
cm-1

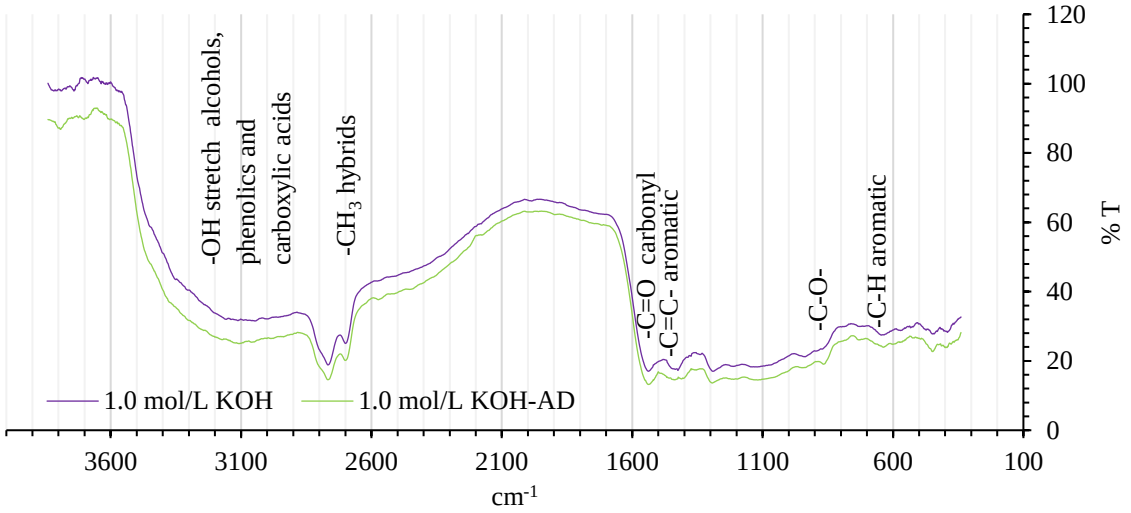
-OH stretch alcohols, phenolics and carboxylic acids
-CH3 hybrids
-C=O carbonyl
-C=C- aromatic
-C-O-
-C-H aromatic
1.0 mol/L KOH
1.0 mol/L KOH-AD
% T
cm-1

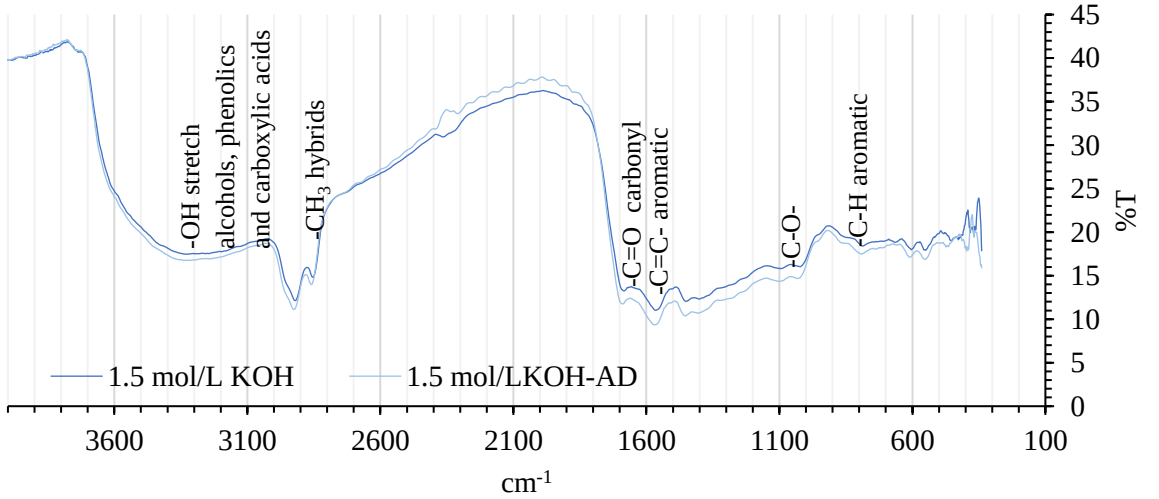
-OH stretch alcohols, phenolics and carboxylic acids
-CH3 hybrids
-C=O carbonyl
-C=C- aromatic
-C-O-
-C-H aromatic
1.5 mol/L KOH
1.5 mol/LKOH-AD
%T
cm-1

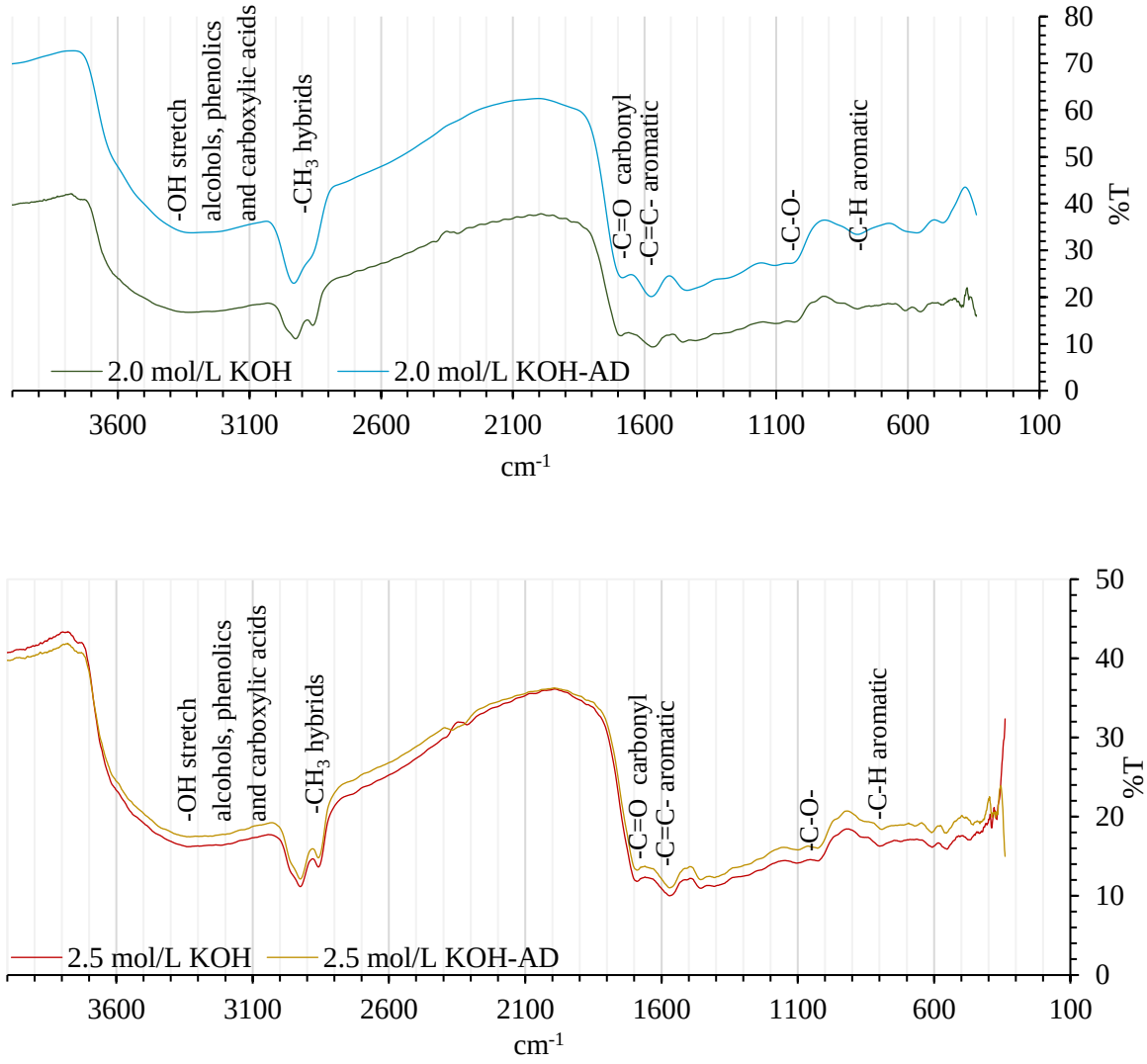

Figure 4.4: The FTIR spectra of the before adsorption and after adsorption hydrochars

The bands between 3425 and 2922 cm^{-1} indicated the O-H stretching vibrations showing hydroxyl, carboxyl and phenolic functional groups from not fully carbonised cellulose, hemicellulose, and lignin, especially when accompanied by C-H at 2900 cm^{-1} and C-O just before 1000 cm^{-1} bands. The O-H functional group could also be originating from pyranose rings found in lignin since the thermal stability of lignin is higher than that of hemicellulose and cellulose. The bands at 1710 cm^{-1} C=O originate from cellulose and hemicellulose oligomers that had undergone dehydration and decarboxylation following hydrolysis fragmentation. The 1620 cm^{-1} band attributed to C=C vibrations supported the aromatisation of sugars during the reaction. C-O stretches at 1000 – 1450 cm^{-1} (not very prominent) revealed the presence of ether and ester. The bands at 875 – 750 cm^{-1} were assigned to aromatic C-H out-of-plane bending vibrations that arise from the aromatization and polymerisation reactions. These functional groups gave hydrochar additional functionality that

serve to improve the adsorption of metals and phenolics. The functional groups generated by the HTL remained intact and more prominent after hydrochar activation, as shown in Figure 4.4 because the wash removed metals and phenolics attached to the hydrochar. Therefore, the presents of these functional groups validate hydrochar as a potential adsorbent in wastewater treatment processes.

4.4 Factors affecting the adsorption of metals and phenols onto hydrochar

The effect of different parameters; namely contact time, dosage, initial concentration, temperature, pH and combining metals and phenolics, on the adsorption of both metals and phenolics were investigated as described in Section 3.6.1, and the results are presented below. It should be noted that the metal ion charge is not in italics because Microsoft excel has no superscript function on the legend.

4.4.1 Effect of contact time on the adsorption of metals and phenolics on hydrochar

Contact time impacts an adsorbent's application and commercialisation in water remediation (Al-Qahtani. 2016; Crini *et al.*, 2019), and Figure 4.5 below demonstrates the effect of contact time on the removal efficiency (A) and adsorption capacity (B) of metals.

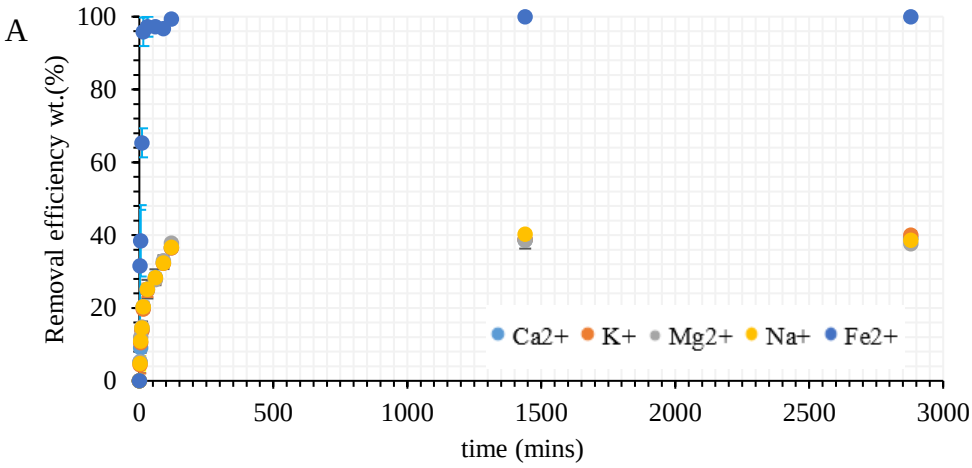

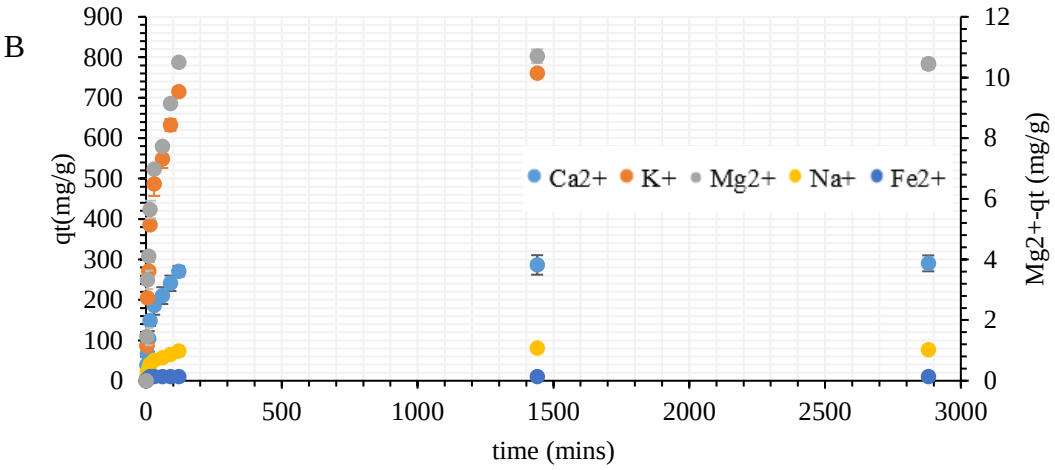

Experimental conditions: total volume of solution volume100 mL; solution pH: 10.6, bWHc dose 0.1 g; temperature: 273 K; shaker 2.5 Hz; initial metal concentration Ca^{2+} 2652 mg/L, K^{+} 3586 mg/L, Mg^{2+} 230 mg/L, Na^{+} 510 mg/L and Fe^{2+} 12 mg/L.

Figure 4.5:The effect of contact time on metal adsorption on hydrochar

Heavy metals adsorption attain equilibrium fast and, in this study, Fe^{2+} reaches equilibrium in the first 30 minutes due to their ability to form a stable complex, and with basic pH, they tend to precipitate out of solution. According to the literature, the adsorption of AAEM is completed within the first 90 minutes (Wang and Liu. 2017); however, the complexity of multi-component composition prolonged adsorption because of competition between ions of the same charge. During the first 60 minutes, metal removal was rapid because of the high concentration gradient between the medium and the hydrochar surface. After about 120 minutes, the hydrochar is saturated with the metals, and any increase in time has no impact on either adsorption capacity or removal efficiency. Hence, in further experiments, the adsorption experiment was allowed to run for 120 minutes. Figure 4.6 below shows the effect of contact time (0-2880 minutes) on removal efficiency (A) and adsorption capacity (B) of phenolics adsorption.

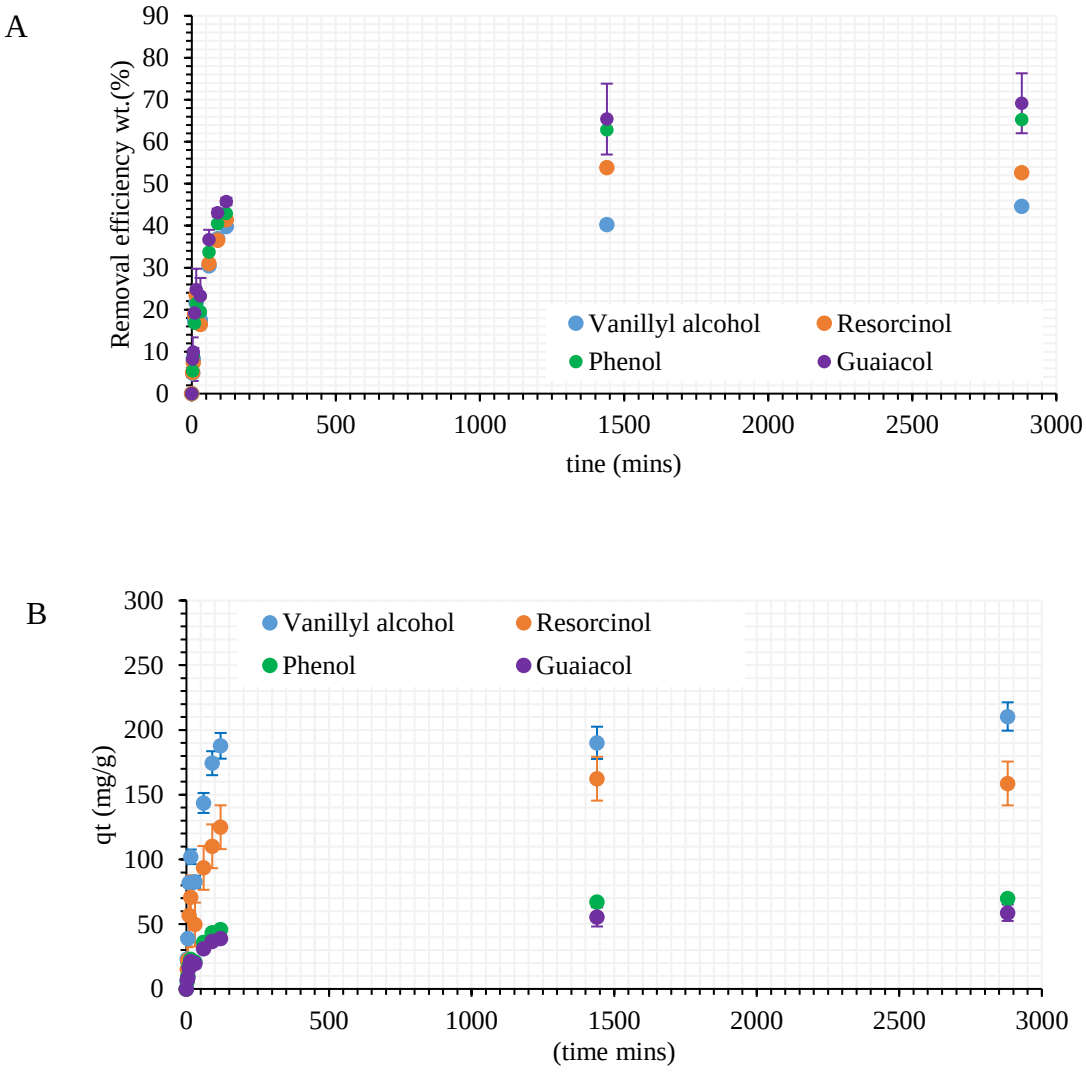

Experimental conditions: total volume of solution 100 mL, solution pH; 10.6, bWHc dose 0.1 g, temperature: 273 K; shaker 2.5 Hz; initial phenolics concentration, vanillyl alcohol 500 mg/L, resorcinol 300 mg/L, phenol 200 mg/L and guaiacol 113µL/L for 2880 minutes.

Figure 4.6: The effect of contact time on phenolic adsorption on hydrochar

The longer removal efficiencies of phenolics are ascribed to their large sizes compared to the metals as they take more time to migrate and diffuse into the hydrochar pores. Moreover, the diffusion process controls the adsorption of phenolics, which is the last step in the adsorption process. Like the removal efficiency, the adsorption capacity of hydrochar initially increases with time due to the availability of active sites, and after 120 minutes, the sites are rare; hence, more time is required for the adsorbate to find an unoccupied site. Therefore, further experiments on the adsorption of phenolics were allowed to run for 120 minutes.

4.4.2 Effect of the initial concentration on the adsorption of metals and phenolic compounds

The effect of adsorbate initial concentration on adsorption capacity and removal efficiency varying concentrations and Figure 4.7 below shows the effect of initial concentration on the adsorption of metals with qt (on the left) and removal efficiency (on the right) as a function of time at various concentrations.

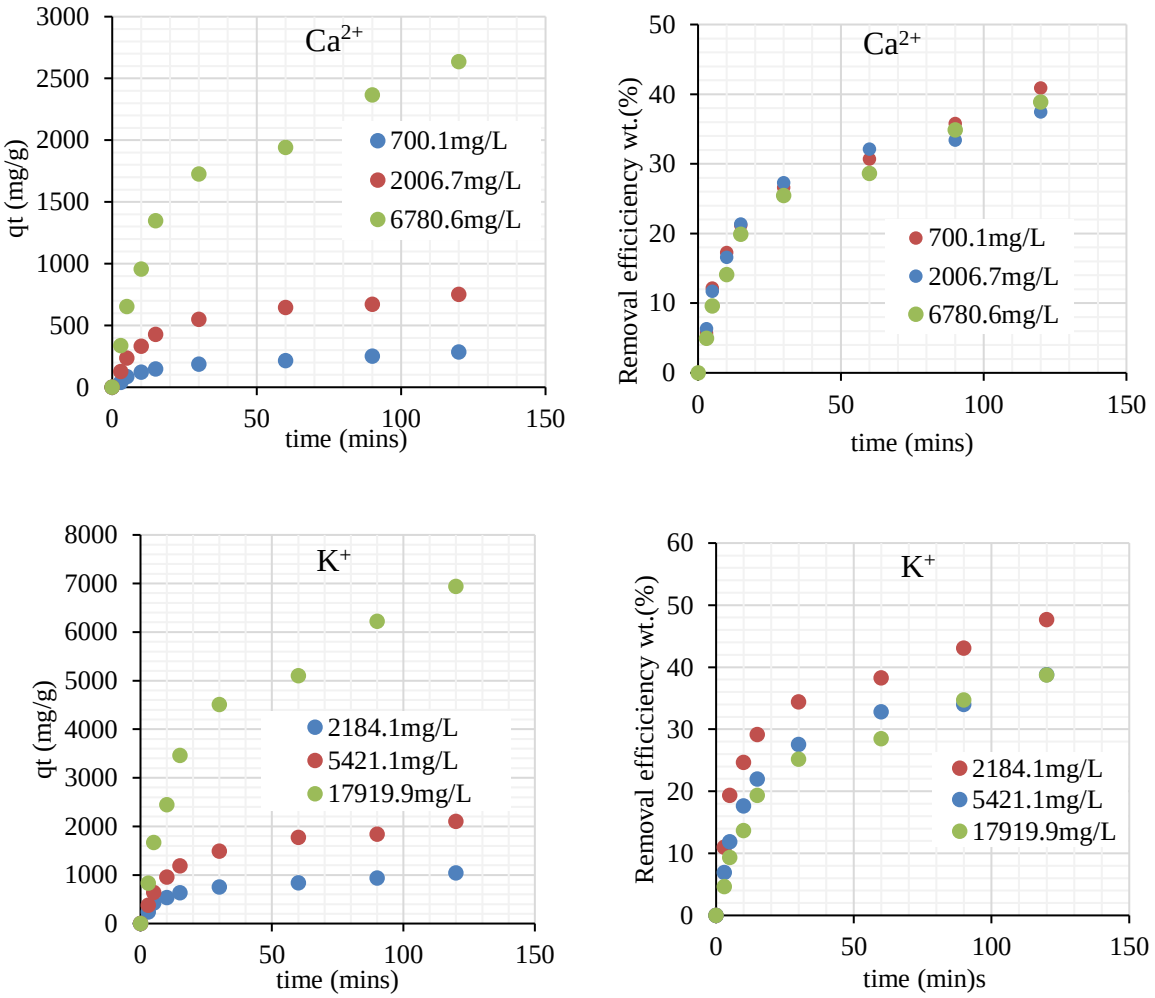

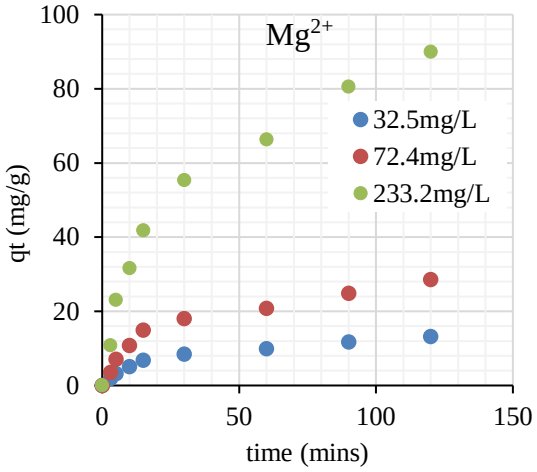

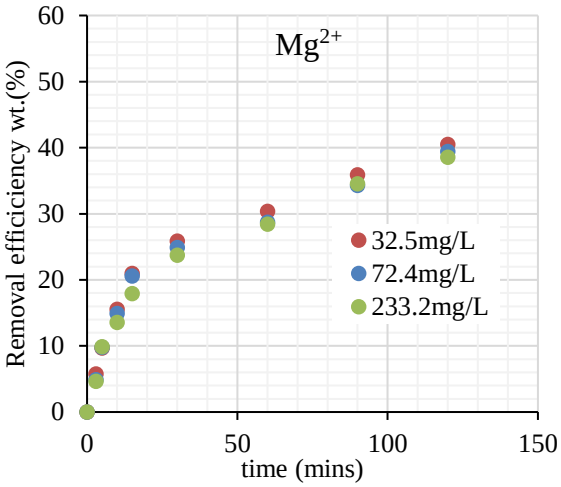

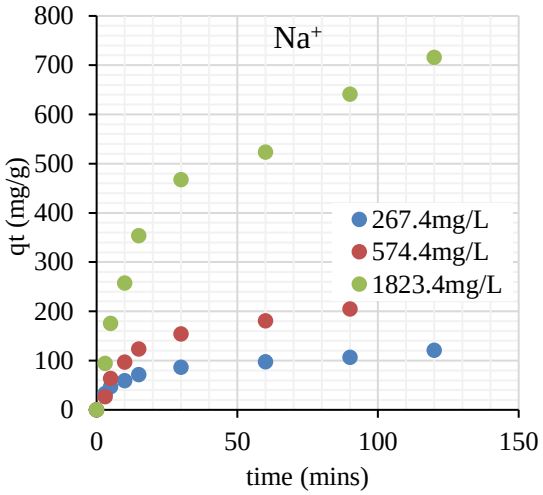

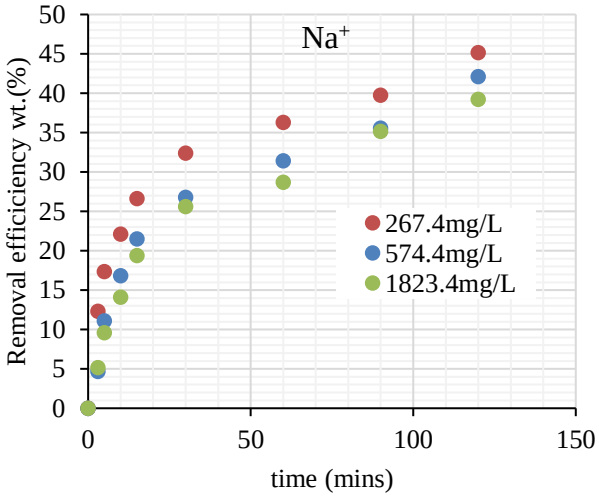

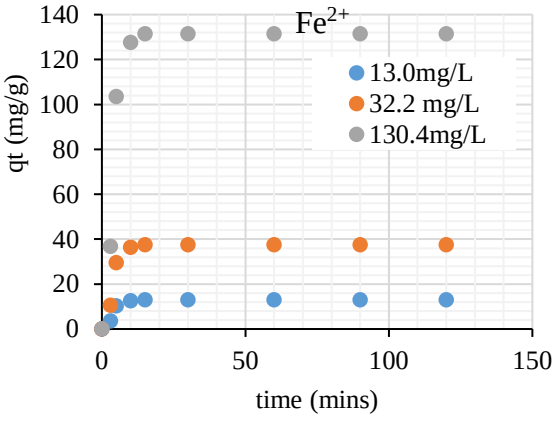

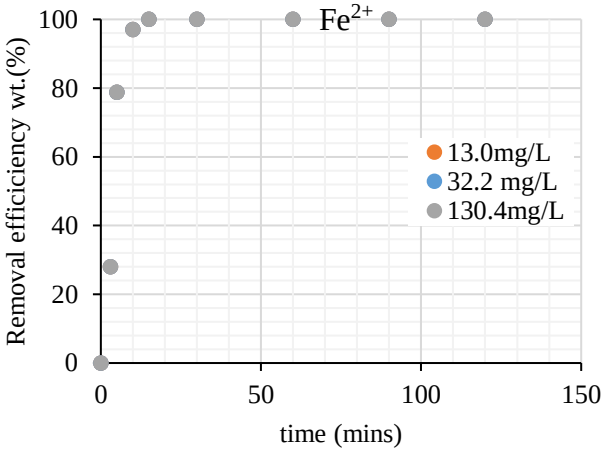

Experimental conditions: total volume of solution 100 mL, solution pH: 10.6 (pH_{pZc} of bWHc), hydrochar dose: 0.1 g, temperature: 273 K; shaker 2.5 Hz for 120 minutes.

Figure 4.7: Effect of initial metal concentration on metal adsorption on hydrochar

The adsorption capacity increased with an increase in initial concentration due to enhanced collision frequencies between the metals and the hydrochar. The observation is also attributed to improved driving force from the steep concentration gradient and the overcoming of resistance to mass transfer. The removal efficiency of the metals decreases with increased initial concentration, with K and Na^+ showing a great difference because of the fixed hydrochar dosage; thus, the binding sites become scarce at high initial concentrations. Therefore, hydrochar is ideal for the removal of metal pollutants of varying concentration, even for those at low concentrations.

Figure 4.8 below shows the effect of initial concentration on the adsorption of phenolic compounds with qt (on the left) and removal efficiency (on the right) as a function of time at various concentrations, as described in Section 3.6.1.

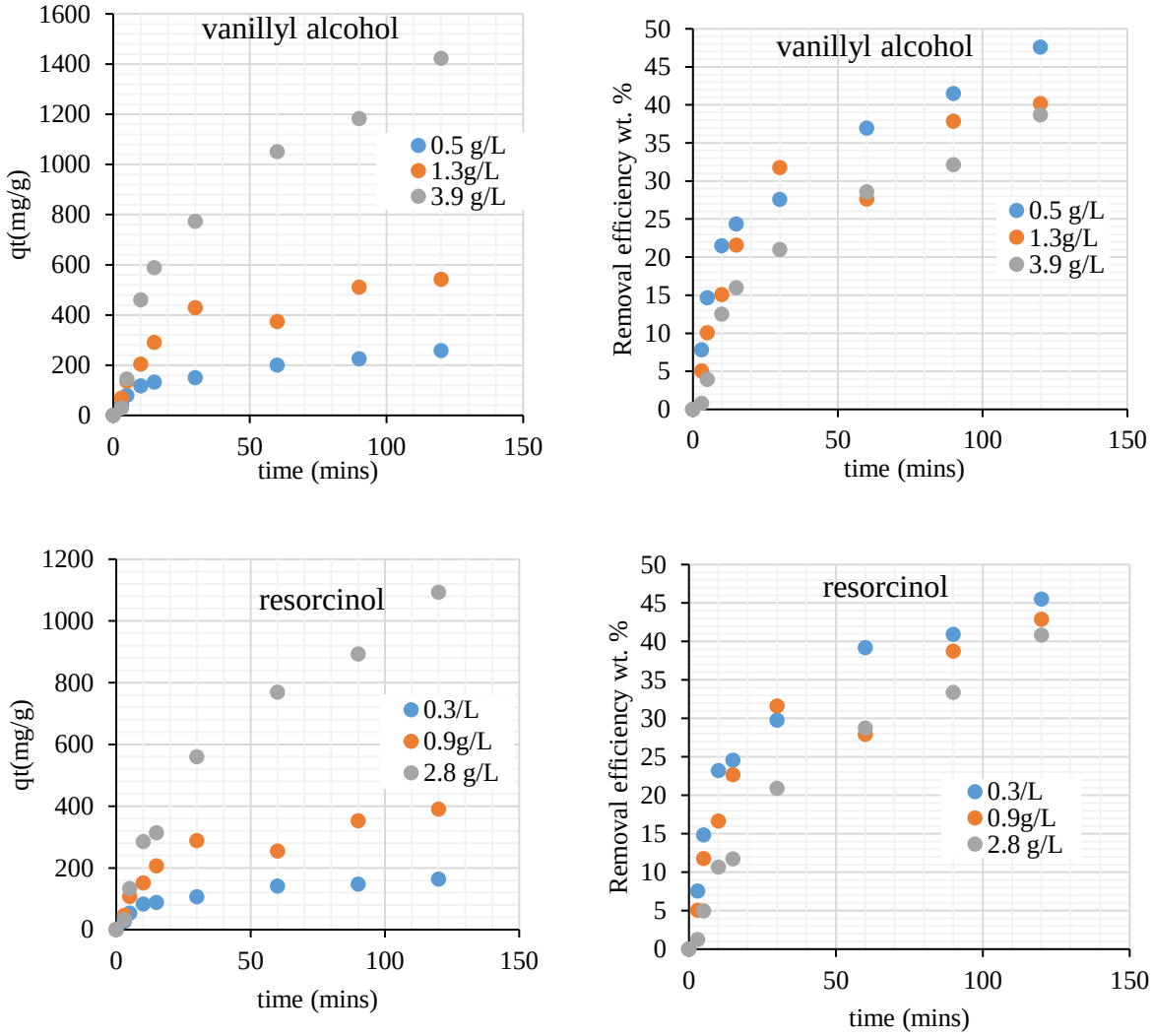

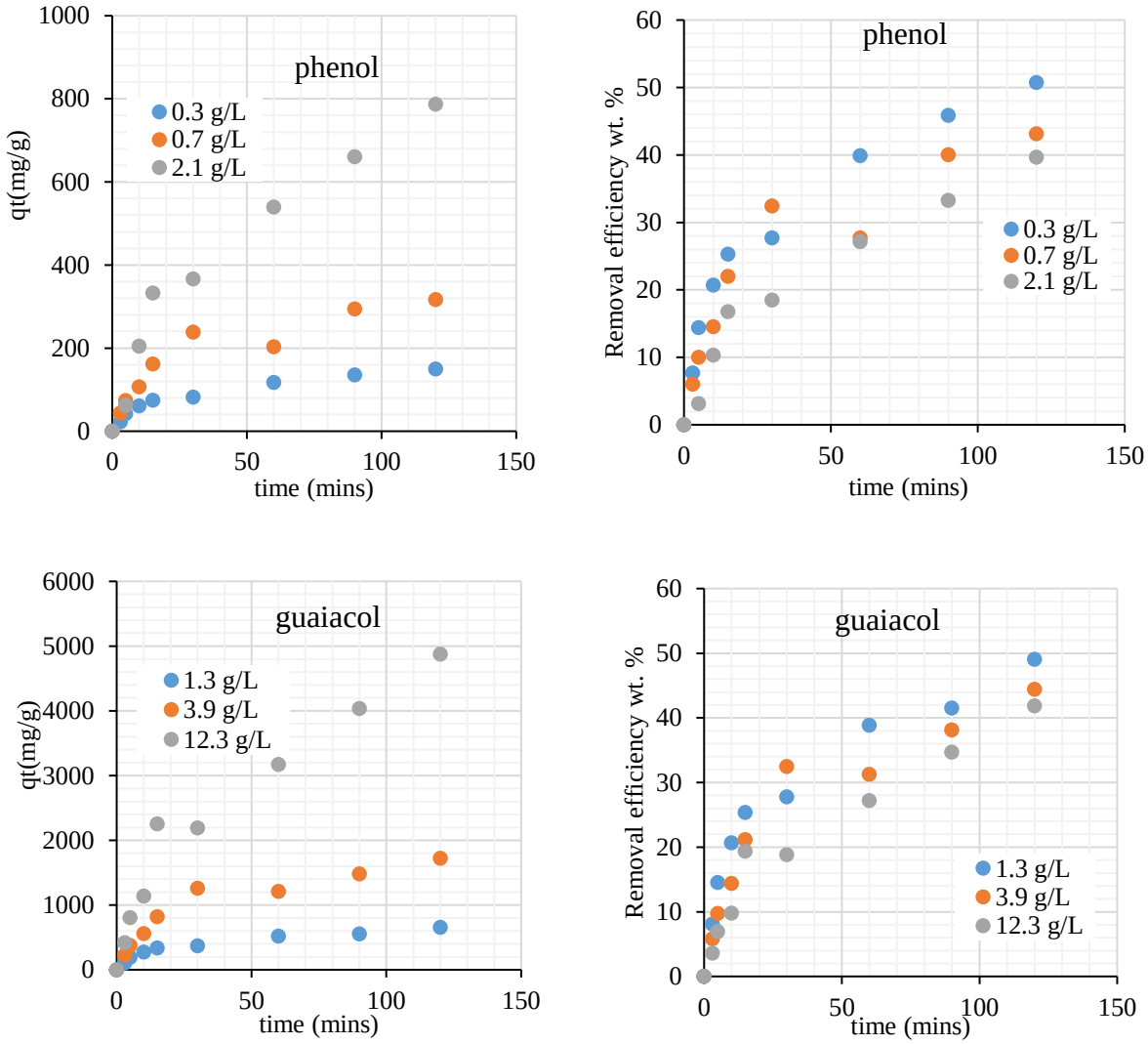

Experimental conditions: total volume of solution 100 mL, solution pH; 10.6, bWHc dose 0.1 g, temperature: 273 K; shaker; 2.5 Hz for 120 minutes.

Figure 4.8: Effect of initial phenolics concentration on phenolics adsorption

The removal efficiency decreases with an increase in the initial concentration because both the surface area and adsorption sites are abundant at low concentrations, improving the chance of the phenolic compounds to find an unoccupied site. Adsorption capacity increase with an increase in initial concentration This surge is attributed to the high surface area and active sites, which become saturated with further initial concentration. The removal efficiency decrease because its . Therefore, hydrochar is an effective adsorbent for removing lower concentration metals and phenolics hence ideal for wastewater with lower pollutant concentrations but above the recommended values for potable water (see Section 2.2.3.1).

4.4.3 Effect of hydrochar dose on the adsorption of metals and phenolics

The dose of an adsorbent effectively impacts its adsorption efficiency and capacity, which influences the cost-effectiveness of hydrochar in the adsorption of pollutants. Figure 4.9 below shows the effect of dose (0.1 g, 0.5 g, 0.75 g, 1.0 g and 2.0 g) on the removal efficiency (A) of the metals and the adsorption capacity (B) of the hydrochar on metals.

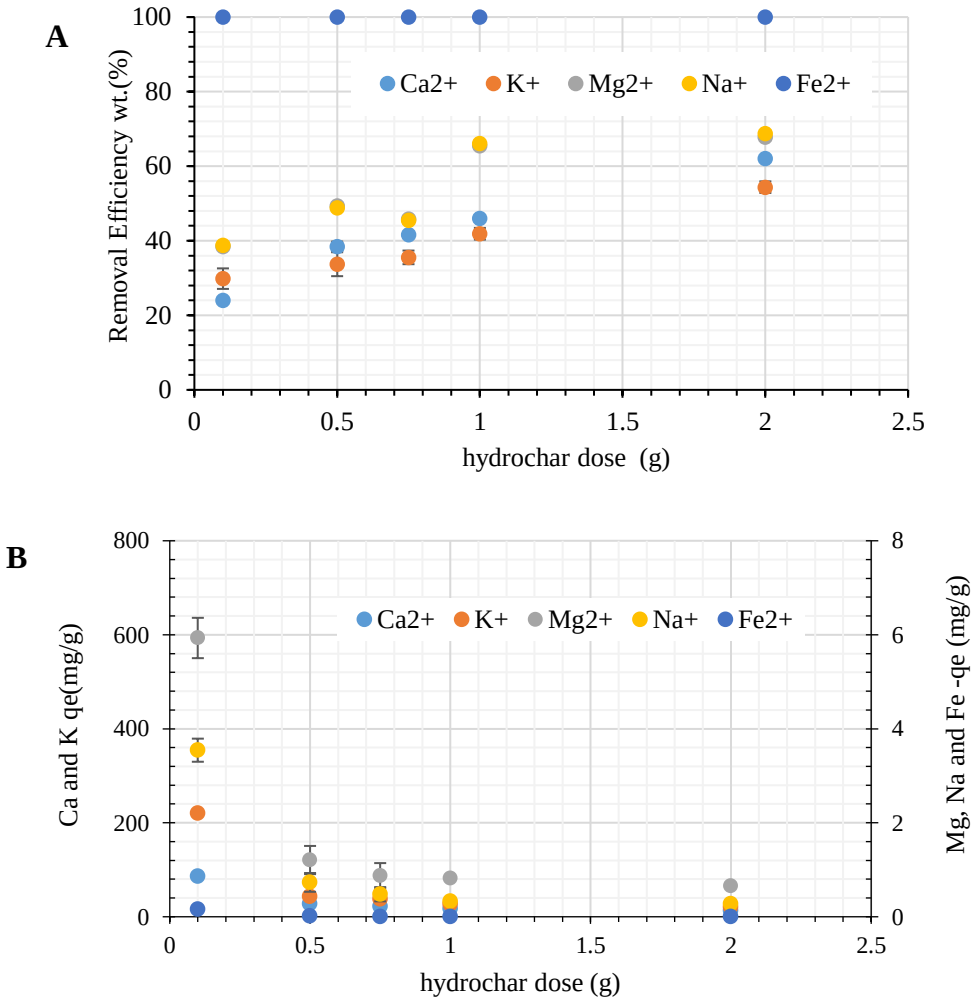

Experiential conditions: total volume of solution 100 mL pH: 10.6, temperature: 273 K; shaker 2.5 Hz; initial metal concentration Ca^{2+} 2652 mg/L, K^{+} 3586 mg/L, Mg^{2+} 230 mg/L, Na^{+} 510 mg/L and Fe^{2+} 12 mg/L for 120 minutes.

Figure 4.9: Effect of hydrochar dose on metal adsorption.

The removal efficiency of metals increases with the dose from 0,1 g-1 g and is attributed to more available active sites for the metals to bind, increasing the adsorbent-adsorbate interactions and increasing adsorbates adsorbed. From 1.0 g, the removal efficiency of Na^{+} and Mg^{2+}, Figure 4.9A,

become constant due to the scarcity of adsorption sites, hence poor adsorbate-adsorbent interactions. Additionally, the removal efficiency of Ca^{2+} and K^{+} do not level up; hence, K^{+} and Ca^{2+} require more than 2 g of hydrochar to reach maximum removal efficiency. Fe^{2+} was not affected by the dosage, and it achieved 100 % removal because it is heavy metal at a very low concentration, preferential discharge AAEM on the hydrochar by cation exchange. In addition to that it forms hydroxides precipitate at basic pH which supports its removal from the solution.

Figure 4.10 below shows the removal efficiency of phenolic compounds (A) and the adsorption capacity of the hydrochar on phenolic compounds (B).

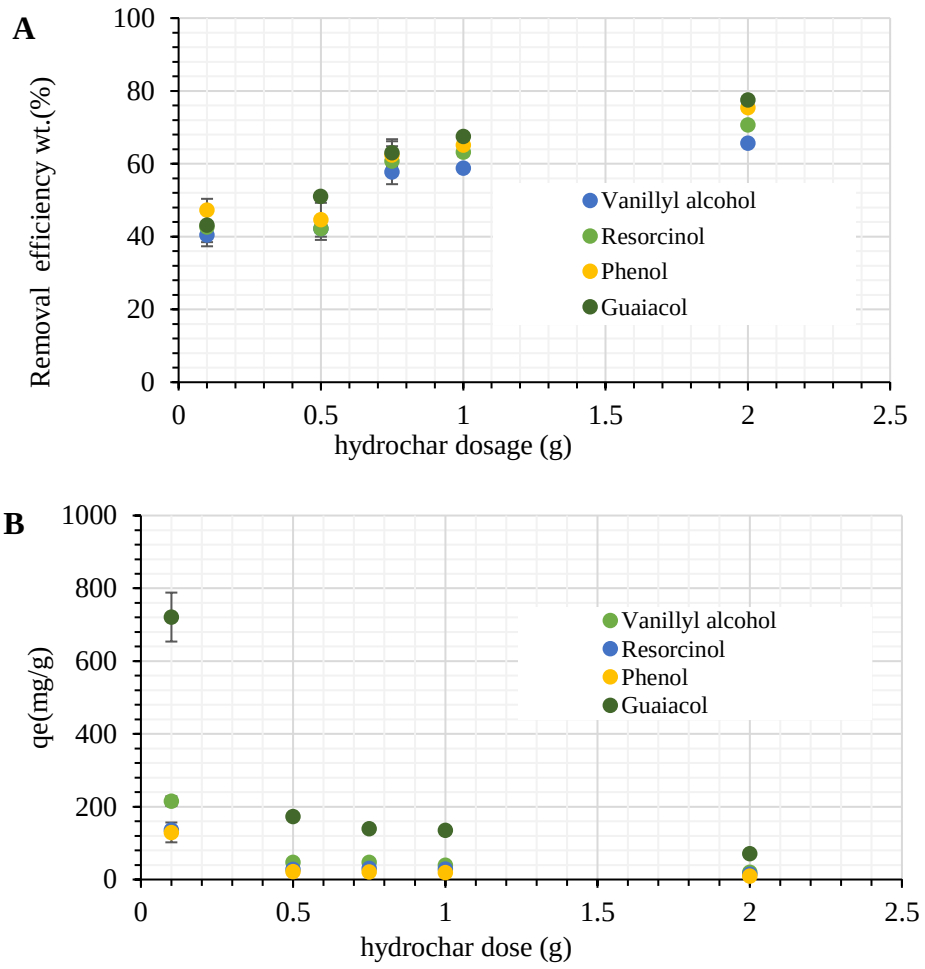

Experimental conditions: total volume of solution 100 mL, pH;10.6, temperature; 273 K shaker 2.5 Hz; initial phenolics concentration, vanillyl alcohol 500 mg/L, resorcinol 300 mg/L, phenol 200 mg/L and guaiacol 113 µL/L for 120 minutes

Figure 4.10: Effect of hydrochar dose on phenolics adsorption

The removal efficiency of phenolic compounds in Figure 4.10 increases with an increase in dosage due to binding sites, and more than 2 g of hydrochar is required for phenolics to reach maximum adsorption. The adsorption capacity (qe) decreases with a dosage decrease, as shown in Figure 4.10-B because the increase division factor from the equation.

$$qe = \frac{(C_o - C_e)V}{m} \qquad 4.1$$

Considering hydrochar cost-effectiveness as an adsorbent, increasing 1 g of hydrochar to the solution results in less than a 10 % increase in removal efficiency; therefore, the ideal dose is 1 g for adsorption of both metals and phenolics.

4.4.4 Effect of temperature on the adsorption of metals and phenolics on hydrochar

Figure 4.12 shows the effect of temperature on removal efficiency (A) and adsorption capacity (B). Both pollutant removal efficiency and hydrochar adsorption capacity are influenced by temperature. Increasing temperature tends to increase the kinetic energy of adsorbates, consequently increasing the probability of the adsorbate accessing an active site. However, the same film energy can cause the previously bound adsorbate to desorb through bond vibration.

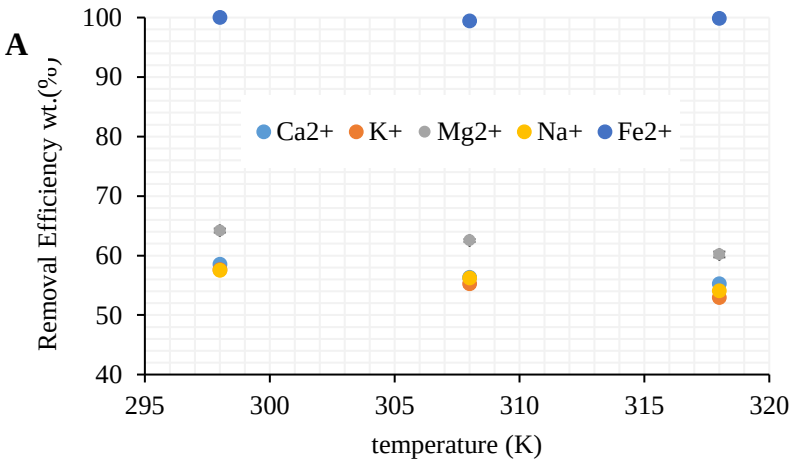

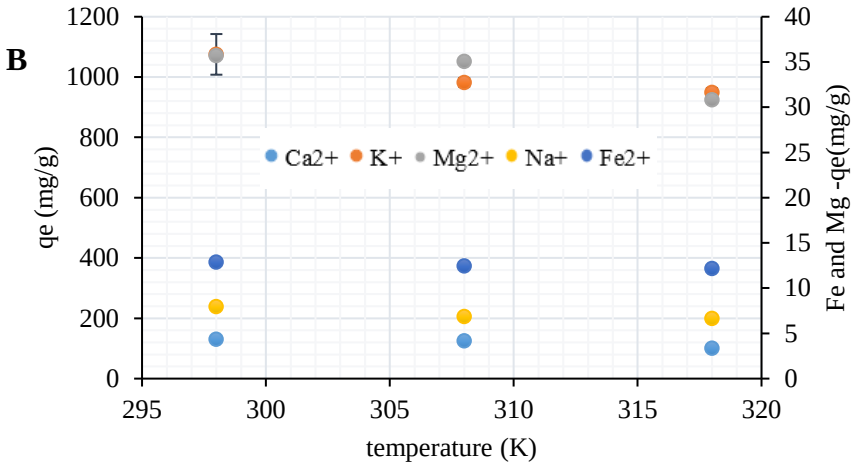

Experimental conditions; total volume of solution 100 mL, solution pH: 10.6, bWHc dosage: 1 g, 2.5 Hz, initial metal concentration Ca^{2+} 2652 mg/L, K^{+} 3586 mg/L, Mg^{2+} 230 mg/L, Na^{+} 510 mg/L and Fe^{2+} 12 mg/L for 120 minutes.

Figure 4.11: Effect of temperature on metal adsorption on hydrochar

The results exhibit a slightly higher removal efficiency at 298K and marginally decline with the rise in temperature because as the temperature increases, the bond vibration of the already bound metals also increases, causing desorption of metals. Taşar and Özer (2020) concluded that adsorption of Pb^{2+} on peanut derived biochar is exothermic as it is associated with further weakening of the Van der Waals forces between the biochar and the Pb^{2+}. Begum *et al.* (2021) also concluded the same on the 15% decrease in removal efficiency of ammonium ions with an increase in temperature by 10 degrees. Therefore, lower temperatures favour the adsorption of metals onto the hydrochar. The effect of temperature on phenolic compounds adsorption was also investigated (Figure 4.12).

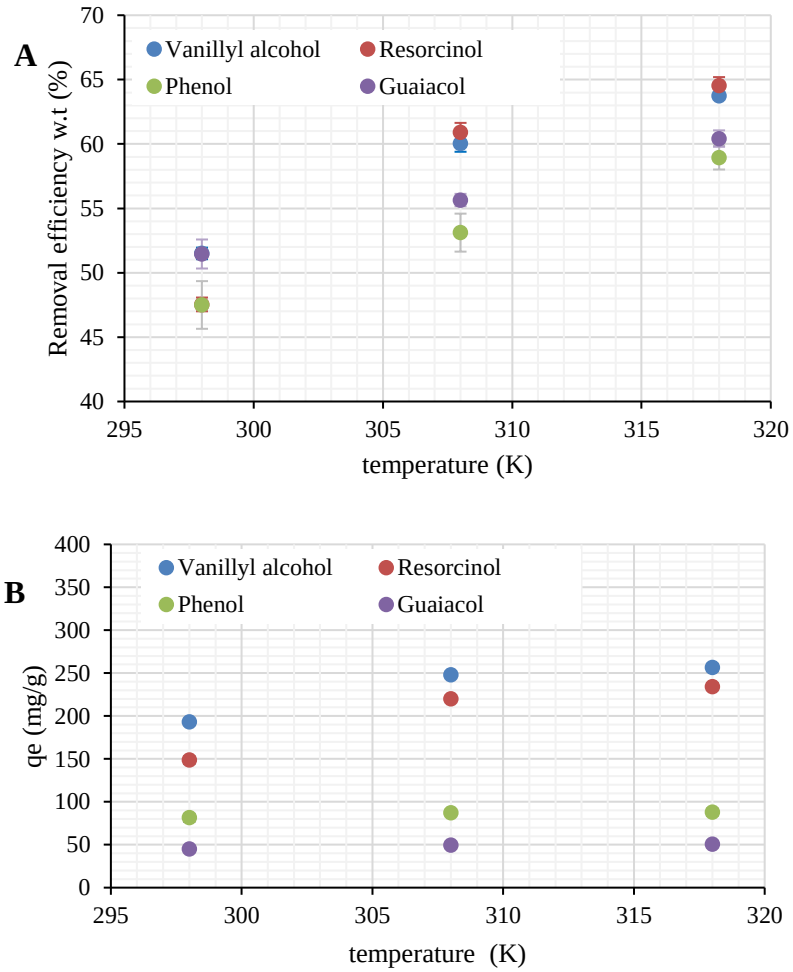

Experimental conditions: total volume of solution 100 mL, solution pH; 10.6, bWHc dose; 1 g, shaker 2.5 Hz; initial phenolics concentration, vanillyl alcohol 500 mg/L, resorcinol 300 mg/L, phenol 200 mg/L and guaiacol 113µL/L for 120 minutes.

Figure 4.12: Effect of temperature on adsorption of phenolics on the hydrochar

Removal efficiency and adsorption capacity increase with an increase in temperature because as the temperature increases, the hydrogen bonding between phenolics in solution and hydrogen bonding between the phenolics and water is weakened, making the phenolics less soluble. Therefore, they display a high tendency to adsorb to the hydrochar surface than being in solution. Furthermore, the temperature contributes to the swelling effect within the internal structure of the hydrochar, thus allowing the phenolics to penetrate further.

Temperature affects the adsorption of metals and phenolics antagonistically so to accommodate both a temperature of 298 K was considered be ideal. Moreover, treatment of wastewater can be done at room temperature thus reducing energy costs.

4.4.5 Effect of pH on the adsorption of metals and phenolics on hydrochar

Changes in pH impact principally the adsorbent functional surface (see Section 2.4.3.2), which subsequently alters adsorbent-metal interaction (Clemente *et al.*, 2017; Tong *et al.*, 2011). Figure 4.13 below shows the effect of pH on the removal efficiency (A), adsorption capacity (B) and final pH of the solution after adsorption shown in graphs as green diamonds.

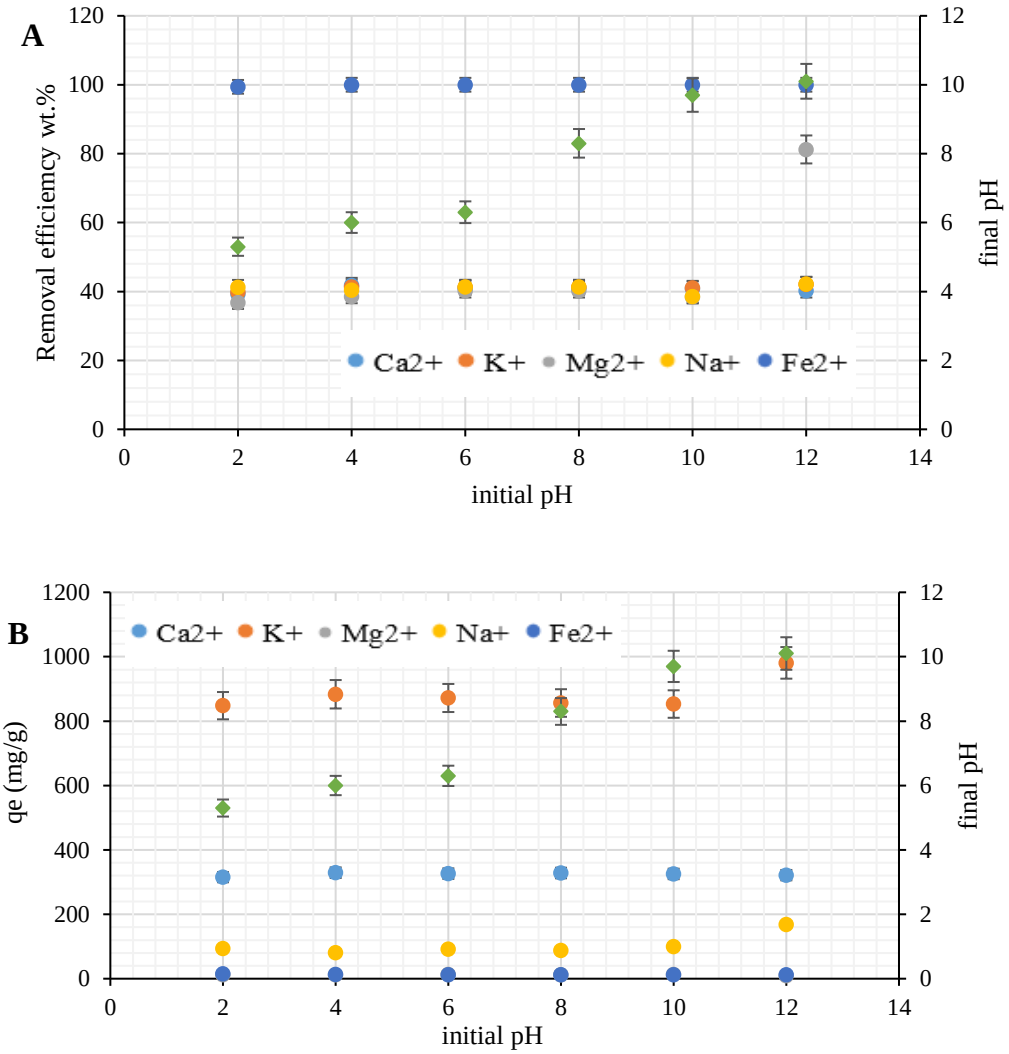

Experimental conditions: total volume of solution 100 mL, temperature; 298 K, RHc dose: 1 g/L, shaker 2.5 Hz; initial metal concentration Ca^{2+} 2652 mg/L, K^{+} 3586 mg/L, Mg^{2+} 230 mg/L, Na^{+} 510 mg/L and Fe^{2+} 12 mg/L for 120 minutes.

Figure 4.13: Effect of pH (2-12) on qe (A) and removal efficiency (B) of metals by adsorption.

Figure 4.13 below shows that pH has no significant effect on the adsorption of metals. It is also observed that the adsorption efficiency of Mg2+ increases rapidly from pH 10-12, and it is attributed to the fact that Mg (OH)2 is a precipitate with lower solubility hence aids to the high removal efficiency. Figure 4.13-A and B concludes that there is no significant effect of pH on the adsorption on Ca2+ , K+ and Na+. The final pH (in green diamonds) demonstrates the exchange of metals one of the mechanisms of adsorption (see Section 2.3.6.1).

Recent studies show that phenolic adsorption is limited by both adsorbent acid-base characteristics and micro-porosity (Mu'azu et al.,2017). The effect of pH was examined at pH 2, 4, 6, 8, 10 and 12 with all the parameters kept constant and Figure 4.14 below represents (A) removal efficiency, (B) adsorption capacity as a function of pH and change in pH after adsorption shown as black diamonds on the graphs.

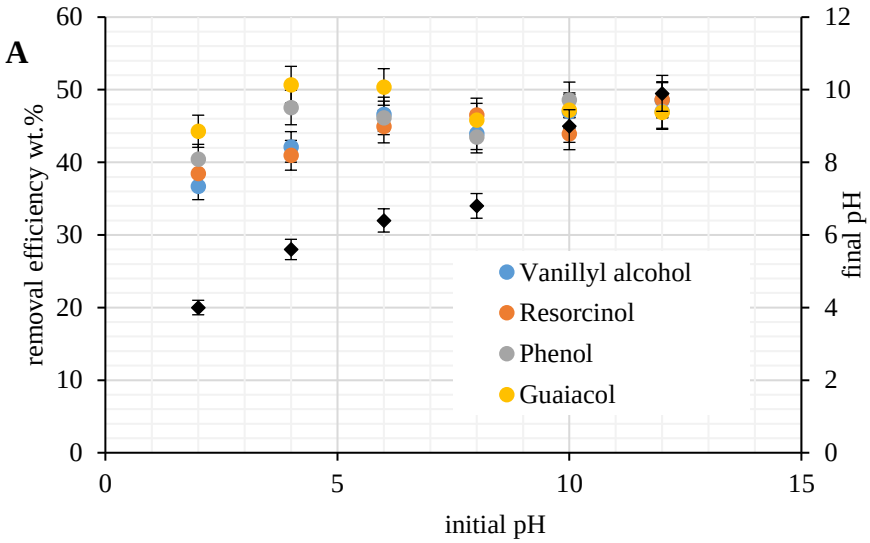

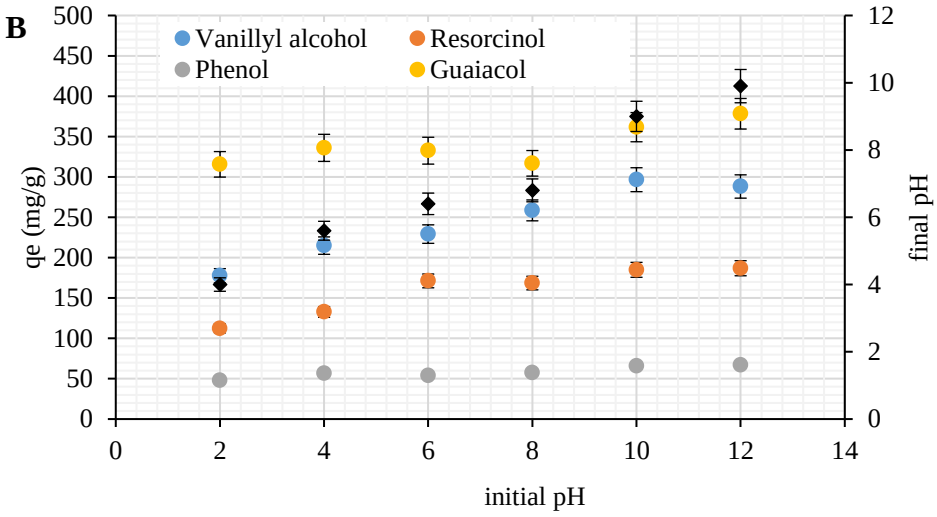

Experimental conditions: total volume of solution 100 mL, bWHc dose: 1g/L, temperature: 273 K; shaker 2.5 Hz; initial phenolics concentration, vanillyl alcohol 500 mg/L, resorcinol 300 mg/L, phenol 200 mg/L and guaiacol 113µL/L for 120 minutes.

Figure 4.14: Effect of pH (2-12) on qe (A) and removal efficiency (B) of adsorption of phenolic compounds on hydrochar

Figure 4.14 shows that from pH 2-4, the removal efficiency of all the phenolics improved because the water clusters that reduce binding sites decrease as the pH increase. At pH above 4, the removal efficiency is at its maximum and adsorption capacity is still rising. The observation is because the oxonium ion prevents the dissociation of the surface functional groups, promoting hydrogen bonding and π-π interaction between the phenolic adsorbates and the sorbent surface (Lee *et al.*, 2019). At pH above the pK_a 9.75, 9.81, 9.95 and 9.98 of vanillyl alcohol, resorcinol, phenol and guaiacol, respectively, both the hydrochar and the phenolics are negatively charged, resulting in electrostatic repulsive forces which tend to lower the adsorption process. To prevent the effect of the hydrochar pH from interfering the adsorption of phenolics, the pH_{pZc} of the hydrochars which is 10.6 was used as the pH of the solution in the adsorption experiments as it also favours the adsorption of phenolic compounds.

4.4.6 Effect of combining metals and phenols on their adsorption on hydrochar

The effect of adsorption on multi-component wastewaters was tested by performing an adsorption experiment using a phenolic synthetic mixture (PSM) / metal synthetic mixture (MSM) and combined metals and phenolics synthetic mixture (CSM) described in Section 3.5, and the results are presented in Figure 4.15.

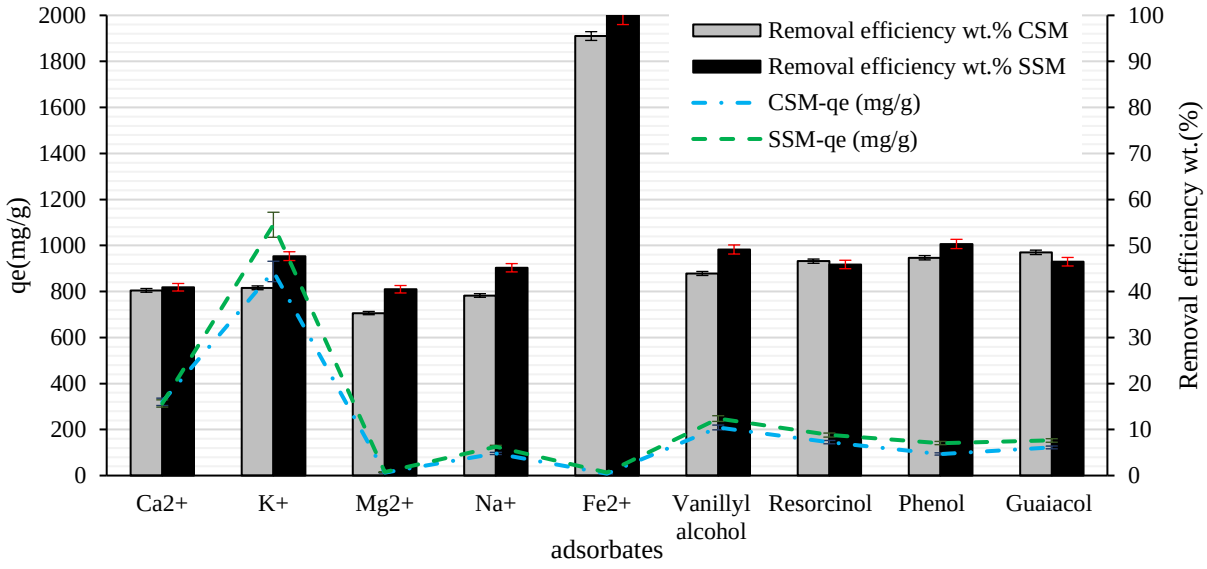

*CSM Combined Synthetic mixture

*SSM Separate synthetic mixtures (metal synthetic mixture / phenolic synthetic mixture)

Experimental conditions: total volume of solution 100 mL, solution pH; 10.6, bWHc concentration; 1g/L, temperature: 273 K; shaker 2.5 Hz; initial phenolics concentration, vanillyl alcohol 500 mg/L, resorcinol 300 mg/L, phenol 200 mg/L and guaiacol 113 µL/L; initial metal concentration Ca^{2+} 2652 mg/L, K^{+} 3586 mg/L, Mg^{2+} 230 mg/L, Na^{+} 510 mg/L and Fe^{2+} 12 mg/L for 120 minutes.

Figure 4.15: Effect of combining metals and phenolics on adsorption of metals and phenolics on hydrochar

The results show a decrease in the adsorption capacity of both metals and phenolics in CSM. This observation show that the adsorbent is capable of adsorb to the various co-existing adsorbates. In other words, each adsorbate competes with other adsorbates to adsorb on active sites resulting in reduced adsorption capacity. In literature (Johnson, 1990; Singh *et al.*, 2017), the presence of salts in solution improved the adsorption of phenolics, and this was the case for resorcinol and guaiacol because of the salting-out effect hence adsorb to the hydrochar. Figure 4.15 shows that adsorption capacity is lower in combined mixtures and higher in separate mixtures for metals and phenolics. For metals, the large size phenolics block the micropores, thereby reducing their adsorption The decrease in the adsorption capacity of vanillyl alcohol and phenol is mainly due to the increased complexity of the simulated wastewater. The decrease in removal efficiency is less than 8 %. Therefore, metals and phenolics can be simultaneously removed from wastewater using hydrochar.

4.5 Desorption of adsorbed metals and phenolics

Some desorption reagents like deionized water, 0.1mol/L HCl, 0.1 mol/L $CaCl_2$ or a mixture of 0.1 mol/L HCl 1:1 and 0.1 mol/L $CaCl_2$ suggested by Sangi *et al.*, (2008) and Chen *et al.*, (2015) were not very efficient in this study. Hence 1.0 mol/L HCl and 1.0 mol/L KOH were selected as desorption reagents. Table 4.9 shows the mass and percentages of the metals and phenols desorbed from 2g of the BWHc from the procedure described in Section 3.6.3.

Table 4.9: Desorption of adsorbed metals and phenolics (with both 1.0M HCl and KOH)

	Ca^{2+}	K^{+}	Mg^{2+}	Na^{+}	Fe^{2+}	Vanillyl alcohol	Resorcinol	Phenol	Guaiacol
STDEV	±0.93	±1.77	±0.01	±0.08	±0.01	±1.56	±1.37	±1.19	±2.04
Mass adsorbed (mg)	15.2	41.7	0.6	17.6	0.5	38.6	33.3	17.2	21.7
Mass desorbed with HCl (mg)	7.9	21.2	0.3	2.1	0.1	0.0	0.0	0.0	0.0
Mass desorbed with KOH (mg)	3.4	8.6	0.1	1.6	0.0	9.3	14.9	9.5	14.7
Total Desorption (mg)	11.3	29.8	0.5	3.6	0.1	9.3	14.9	9.5	14.7
% Desorption	74	72	71	21	25	24	45	55	68

Experimental condition contact time 2 hrs., bWHc dose 1.0 g, temperature: 273 K; shaker 1.9 Hz and 10 mL total volume

The results above show that desorption of both metals and phenolics is possible, with metals having the highest percentage, as a result of reversible physical adsorption. Therefore, the adsorbed valuable phenolics can be repurposed, e.g., lessening the dependence on fossil-based phenolics. The results also prove hydrochar as a cost-effective hydrochar as it has a potential to be reused.

4.6 Fitting the metals and phenolics adsorption data with kinetic models

Numerous kinetic models have been applied in the adsorption studies, and in this study, the Pseudo first order, Pseudo second order, and Elovich models were fitted with the adsorption data. The rate-limiting step was evaluated using the Weber and Morris and Boyd's Intraparticle diffusion model, whilst the Biot number and the coefficient of variation determines the fitness of the model.

4.6.1 Fitting with the pseudo-first-order kinetic model

The linear equation below describes the pseudo-first-order (Section 2.5.1), and Figure 4.16 presents the plots of log (qe-qt) vs t at differing initial concentrations of the adsorption data fitted with the pseudo-first-order kinetic model.

$$\ln(qe\text{-}qt) = qe^{-kt} \qquad 4.2$$

where *qe* is the adsorbate concentration at equilibrium, q_t is the adsorbate concentration at a given time is mg/g, k_1 is the rate constant (min^{-1}), and *t* is the time in minutes

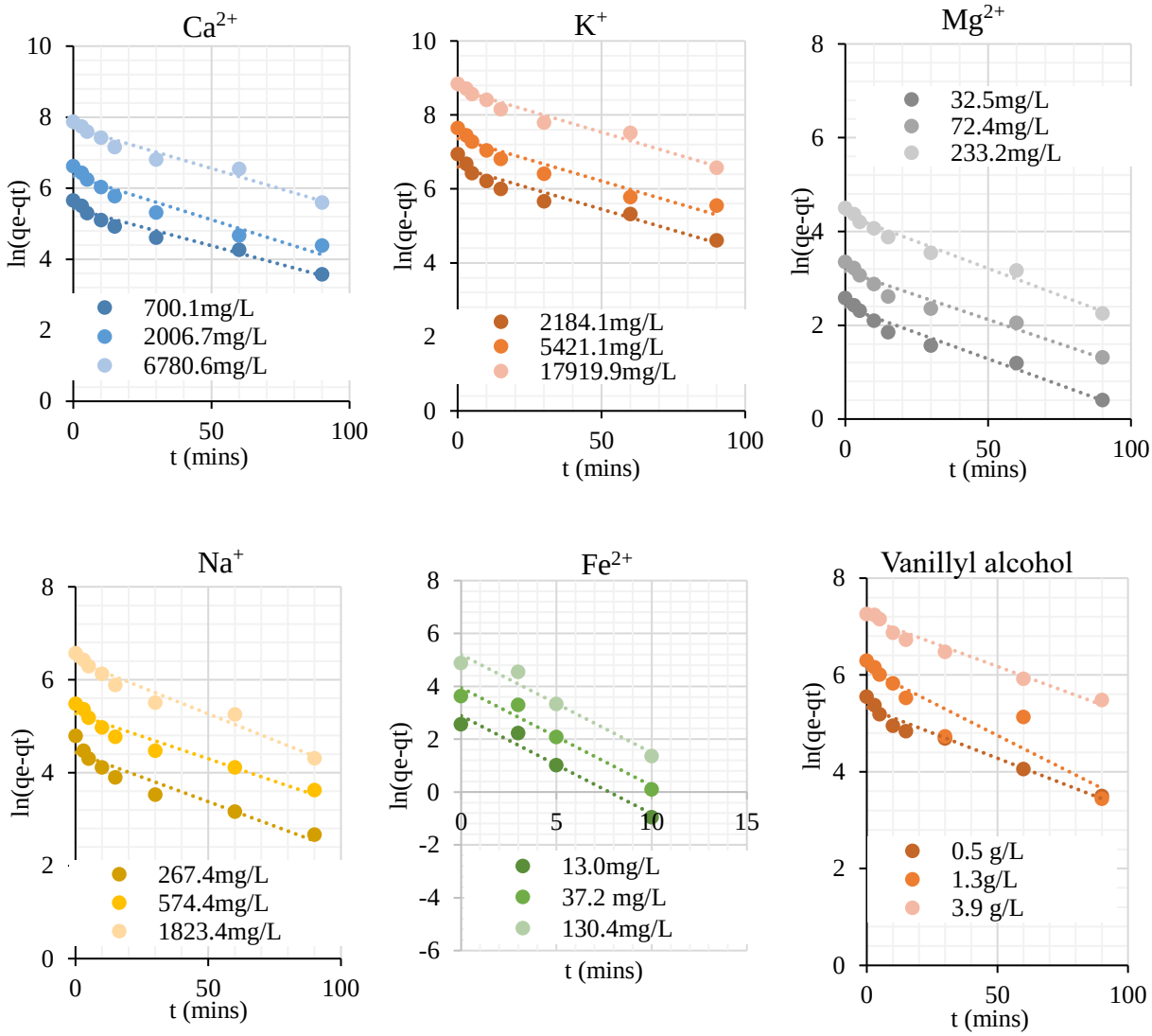

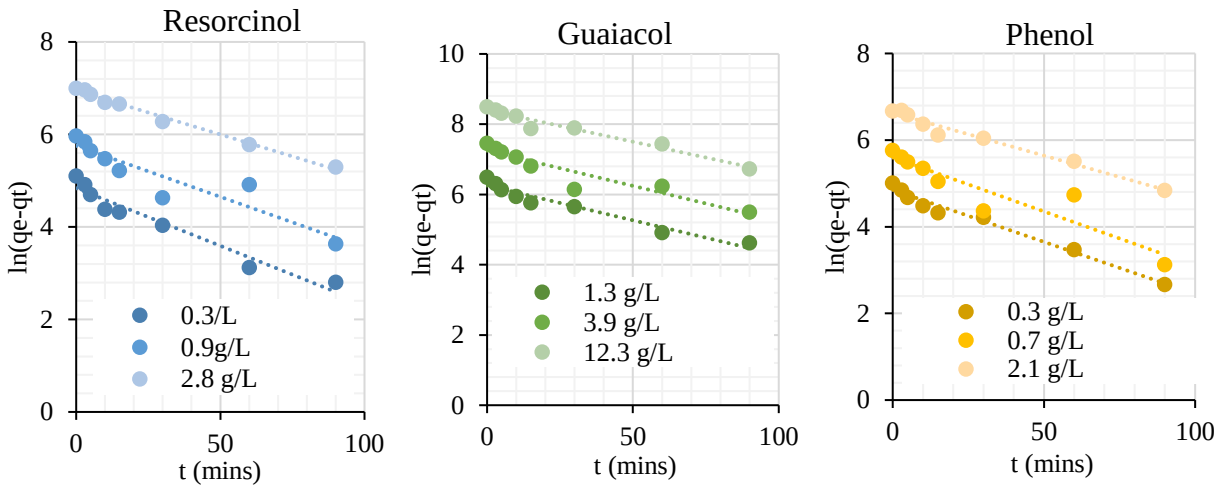

Figure 4.16:Psuedo-first-order kinetic model plots of metals and phenolic compounds at a differing initial concentration

Since the initial rate of adsorption dqt/dt depends on k_1 and (qe-qt), the pseudo first order sorption rate ($PFOS_{rate}$) adsorption rate is more precisely described by:

$$PFOS_{rate} = k_1 qe \qquad 4.3$$

Table 4.10 below shows the calculated parameters, namely the correlation coefficient R^2, the rate constant k_1, experimental $qe_{exp,}$ and calculated qe_{cal} adsorption capacity (mg/g), half-life $t^{½}$ and the pseudo-second-first order initial rate of reaction from the plots at differing initial concentration.

Table 4.10: Pseudo 1st order kinetic model calculated parameters at a differing initial concentration

PSEUDO FIRST ORDER							
Adsorbate	Initial concentration	R^2	k_1 $(min)^{-1}$	qe_{calc} (mg/g)	qe_{exp} (mg/g)	$t_{1/2}$	$PFOS_{rate}$
Vanillyl alcohol	0.5 g/L	0.962	0.021	206	258	33.1	4.3
	1.3 g/L	0.861	0.027	453	542	25.4	12.3
	3.9 g/L	0.971	0.020	1298	1422	34.9	25.8
Resorcinol	0.3 g/L	0.948	0.025	126	164	27.9	3.1
	0.9 g/L	0.859	0.022	315	391	31.4	7.0
	2.8 g/L	0.990	0.019	1040	1093	36.6	19.7
Phenol	0.3 g/L	0.979	0.024	128	150	28.8	3.1
	0.7 g/L	0.858	0.025	270	317	27.8	6.7
	2.1 g/L	0.975	0.020	756	788	35.1	14.9

Guaiacol	1.3 g/L	0.946	0.020	520	656	35.0	10.3
	3.9 g/L	0.886	0.020	1406	1725	34.5	28.2
	12.3 g/L	0.961	0.018	4449	4876	38.5	80.1
Ca^{2+}	700.1 mg/L	0.950	0.021	228	286	33.1	4.8
	2006.7 mg/L	0.928	0.025	567	751	28.2	13.9
	6780.6 mg/L	0.957	0.023	2220	2635	30.2	51.0
K^{+}	2184.1 mg/L	0.924	0.023	730	1041	30.4	16.6
	5421.1 mg/L	0.919	0.023	1571	2103	30.3	36.0
	17919.9 mg/L	0.960	0.023	5914	6940	30.1	136.0
Mg^{2+}	32.5 mg/L	0.962	0.022	11	13	31.3	0.2
	72.4 mg/L	0.949	0.021	23	29	33.6	0.5
	233.2 mg/L	0.974	0.023	78	90	30.3	1.8
Na^{+}	267.4 mg/L	0.918	0.021	84	121	32.9	1.8
	574.4 mg/L	0.938	0.019	194	242	35.8	3.8
	1823.4 mg/L	0.959	0.023	606	715	30.4	13.8
Fe^{2+}	13.0 mg/L	0.956	0.371	18	13	1.9	6.6
	37.2 mg/L	0.956	0.371	52	38	1.9	19.1
	130.4 mg/L	0.956	0.371	181	131	1.9	67.0

From the results above, the correlation coefficient of the pseudo-first-order is above 0.8, a little change in $t^{½}$, and PFOS rate increase with initial concentration; hence the adsorption of both metals and phenols increases with an increase in initial concentration. The experimental qe with the fitted qe in Table 4.10 are slightly different though they are of the same magnitude. This mismatch was justified by the presence of a boundary layer that control the adsorption process (see Section 2.4.2.2). Despite the justification, most of the correlation coefficients are lower than 0.96. Thus, the pseudo-first-order does not describe metals and phenolics' adsorption; hence, the pseudo 2nd order was considered.

4.6.2 Fitting with the pseudo-second-order kinetic model

The equation 2.9 below represent the linearised pseudo-second-order kinetic model, as explained in Section 2.5.2

$$\frac{1}{q_t} = \frac{1}{q^2_e k_2 t} + \frac{1}{qe} \qquad 4.4$$

where q_e is the equilibrium adsorption capacity and q_t is the adsorption capacity at a given time, and k_2 is the adsorption constant in gmin^{-1}. Figure 4.17 below shows the plots of t/qt (min. g/mg) vs time t (minutes) of the adsorption data fitted with pseudo-seccond-order kinetic model at differing initial concentrations.

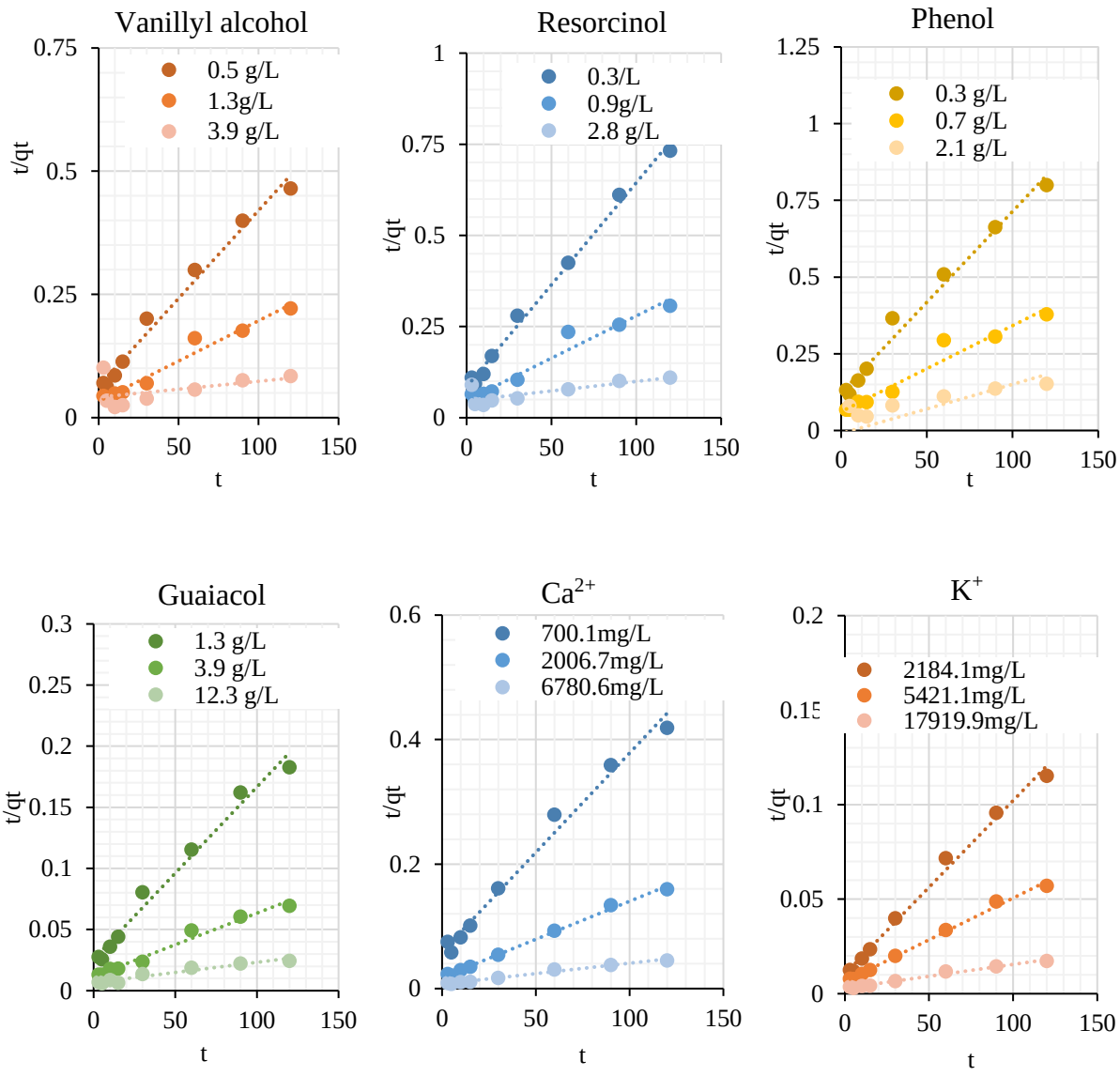

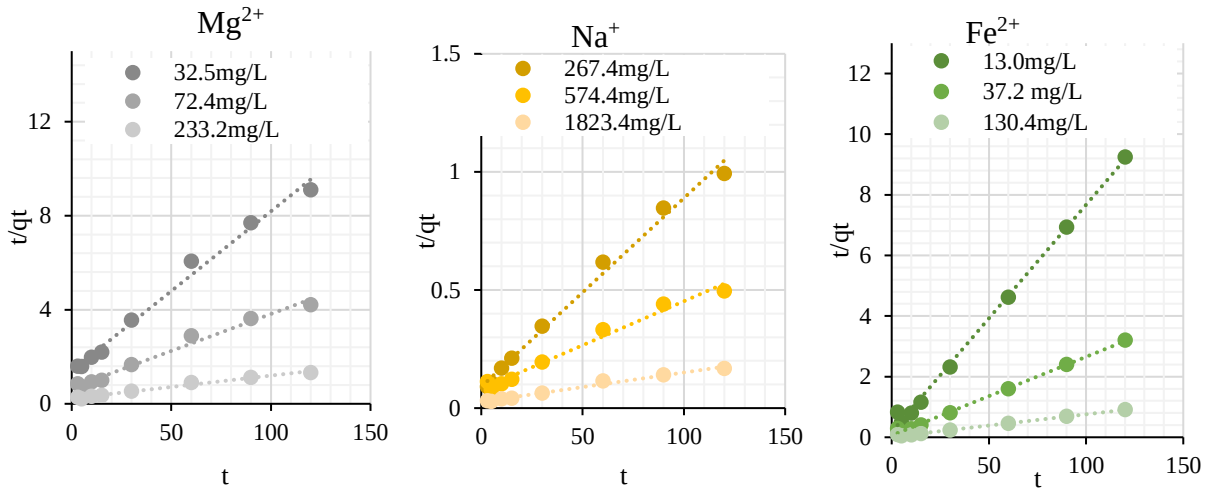

Figure 4.17 Pseudo-second-order kinetic model plots of metals and phenolic compounds at a differing initial concentration

Like k_1 in PFO, k_2 describes the rate of adsorption, and since the rate is related to both k_2 and $(qe-qt)^{2,}$ the precise PSO rate is calculated using the following equation:

$$PSOS_{rate} = k_2(qe)^2 \qquad 4.5$$

Table 4.11 below shows the calculated parameters: correlation coefficient R^2, the constant k_2, experimental qe $_{exp}$ and calculated qe $_{cal}$ adsorption capacity (mg/g), half-life t $_{½}$ and the pseudo-second-order initial rate of reaction of the plots above.

Table 4.11: Pseudo-second-order calculated parameters

		Pseudo-second-order					
Adsorbates	Initial concentration	R^2	k_2 (g/mg.min)	qe $_{cal}$ (mg/g)	qe $_{exp}$ (mg/g)	$t_{1/2}$	PS0-S $_{rate}$ (mg/g.min)
Vanillyl alcohol	0.5 g/L	0.9811	1.9E-04	281	258	18.2	15.4
	1.3g/L	0.9655	8.7E-05	604	542	18.9	31.9
	3.9 g/L	0.9477	1.3E-05	1845	1422	42.1	43.9
Resorcinol	0.3/L	0.9930	3.9E-04	178	164	14.6	12.2
	0.9g/L	0.9539	1.3E-04	424	391	18.7	22.7
	2.8 g/L	0.9780	1.3E-05	1478	1093	50.5	29.3
Phenol	0.3 g/L	0.9806	2.8E-04	170	150	21.2	8.0

	0.7 g/L	0.9462	1.3E-04	358	317	22.2	16.1
	2.1 g/L	0.8837	1.5E-05	1140	788	59.5	19.2
Guaiacol	1.3 g/L	0.9792	7.4E-05	714	656	18.9	37.8
	3.9 g/L	0.9739	2.3E-05	1936	1725	22.8	84.8
	12.3 g/L	0.9368	4.1E-06	6033	4876	40.0	150.8
Ca^{2+}	700.1 mg/L	0.9858	1.7E-04	313	286	18.5	16.9
	2006.7 mg/L	0.9961	8.3E-05	817	751	14.7	55.5
	6780.6 mg/L	0.9868	1.5E-05	2985	2635	21.8	136.8
K^{+}	2184.1 mg/L	0.9921	8.1E-05	1090	1041	11.4	95.8
	5421.1 mg/L	0.9945	3.0E-05	2264	2103	14.5	155.6
	17919.9 mg/L	0.9867	5.5E-06	7938	6940	23.0	344.4
Mg^{2+}	32.5 mg/L	0.9891	3.3E-03	15	13	20.7	0.7
	72.4 mg/L	0.9832	1.5E-03	32	29	21.5	1.5
	233.2 mg/L	0.9864	4.1E-04	103	90	23.8	4.3
Na^{+}	267.4 mg/L	0.9907	7.0E-04	125	121	11.3	11.0
	574.4 mg/L	0.9808	1.7E-04	268	242	21.4	12.6
	1823.4 mg/L	0.9867	5.6E-05	810	715	22.0	36.8
Fe^{2+}	13.0 mg/L	0.9968	3.2E-02	13	13	2.3	5.7
	37.2 mg/L	0.9968	1.1E-02	39	38	2.3	16.5
	130.4 mg/L	0.9968	3.2E-03	135	131	2.3	57.8

Figure 4.17 and Table 4.11 above show a k_2 decrease with an increase in initial concentration as the adsorption process depends on the qe. It is observed that the qe $_{calc}$ and qe $_{exp}$ of metals are close to each other hence better suitability of the kinetic order. Like with pseudo 1st order, the $PSOS_{rate}$ increases with an increase change in t½ is insignificant as the initial concentration increases. The plots of both phenolics and metals have correlation coefficients above 0.95 and 0.99, respectively. Therefore, metal adsorption is better described by pseudo-second-order than and the diffusion process limits the adsorption of metals into a network of small pores.

4.6.3 Fitting with the Elovich kinetic model

The Elovich model was described in Section 2.5.3 and is given by the equation (Peers, 1965):

$$qt = \frac{1}{\beta}\ln \propto \beta + \frac{1}{\beta}\ln t \qquad 4.6$$

where qt = the amount of adsorbate adsorbed mg/g, at time t, α = the initial adsorbate sorption rate, mg/g, min, β = the desorption constant, g/mg,

The constants $\frac{1}{\beta}$ and $\frac{1}{\beta} ln\, \alpha$ were calculated from the slope and intercept respectively of the plot of qt vs lnt. Figure 4.18 shows plots of the data fitted with the Elovich model.

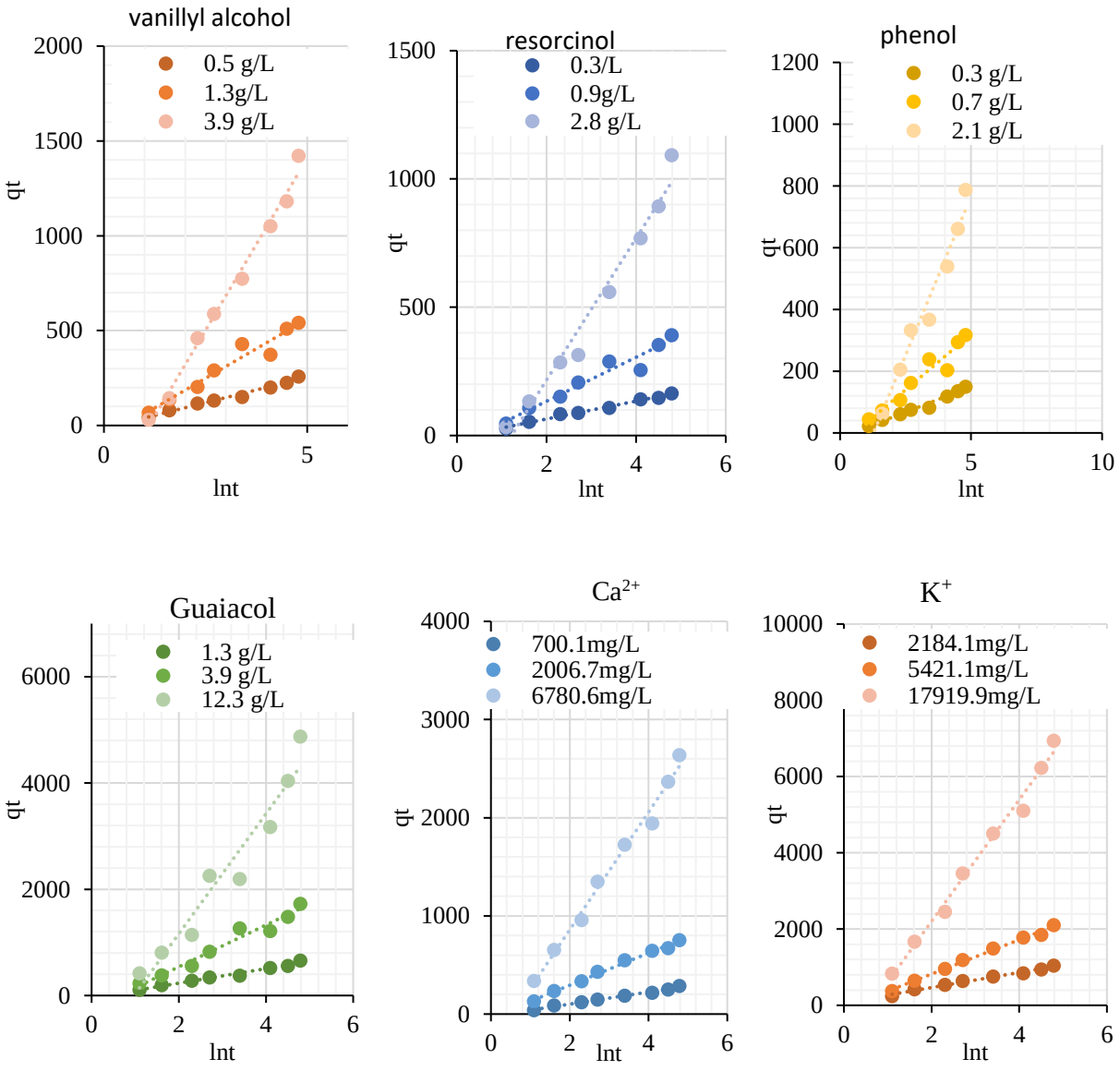

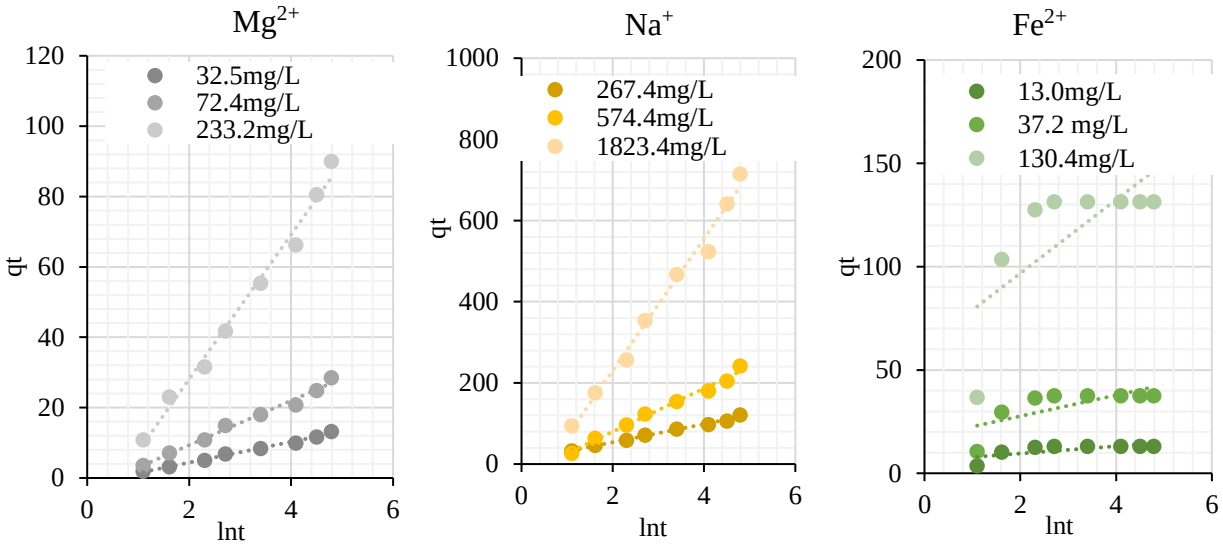

Figure 4.18: Elovich model plots of the adsorption of metals and phenolics at a different initial concentration

The Elovich kinetic adsorption model is more compatible with chemisorption, and Figure 4.18 indicates the Elovich plots with the $R^2 > 0.94$ except for Fe^{2+} slightly above 0.5. The parameters from the model were calculated and are presented in Table 4.12 below. According to the correlation coefficients, the data fits with the model, therefore, implying the transfer of electrons may control the rate-limiting step. However, the constant desorption β shows significant desorption, which is not a chemisorption characteristic. Therefore, it is concluded that the rate-limiting step is not controlled by chemisorption

Table 4.12: Elovich kinetic model calculated parameters

Adsor-bate	C_0 (mg/L)	R^2	β (mg/g)	α (mg /g.min)		C_0 (g/L)	R^2	β (mg/g)	α (mg /g.min)
Ca^{2+}	700.1	0.9887	1.60E-02	41	Vanillyl	0.5	0.9806	1.90E-02	283
	2006.7	0.9926	6.10E-03	75	alcohol	1.3	0.9478	8.00E-03	378
	6780.6	0.9883	1.70E-03	119		3.9	0.9896	2.80E-03	860
K^+	2184.1	0.9854	5.10E-03	30	resorcinol	0.3	0.9882	2.90E-02	2
	5421.1	0.9933	2.20E-03	55		0.9	0.9467	1.20E-02	4
	17919.9	0.9888	6.30E-04	82		2.8	0.9715	3.60E-03	11
Mg^{2+}	32.5	0.9911	3.40E-01	21	Phenol	0.3	0.9779	3.00E-02	34
	72.4	0.9861	1.60E-01	41		0.7	0.9377	1.40E-02	32

	233.2	0.9878	4.90E-02	57		2.1	0.9771	4.90E-03	91
Na^+	267.4	0.9916	4.50E-02	101	Guaiacol	1.3	0.9788	7.30E-03	55
	574.4	0.9875	1.90E-02	210		3.9	0.9647	2.50E-03	158
	1823.4	0.9879	6.20E-03	427		12.3	0.9399	8.90E-04	552
Fe^{2+}	13.0	0.5266	5.70E-01	43					
	37.2	0.5266	2.00E-01	133					
	130.4	0.5266	5.60E-02	340					

The high coefficients of determination (R^2) and closer proximity between the experimental capacities at equilibrium and the calculated capacities from the model indicate that the pseudo-second-order model fits the experimental data quite well; hence the adsorption of metals and phenolics occur on heterogeneous surfaces of hydrochars.

4.7 Mass transfers during adsorption of metals and phenolics

4.7.1 Fitting with Weber and Morris intraparticle diffusion model

The adsorption process of organic and inorganic pollutants on biochars proceed via solute external mass transport, diffusional mass transfer of solute within internal and external pores of the biochar, or a combination of both (Kara and Demirbel, 2012). Figure 4.19 below shows the fitting of the data with the Weber and Morris intraparticle diffusion model plot of qt against $\sqrt{t}$.

$$qt = K_{ipd} t^{\frac{1}{2}} + C \qquad 4.7$$

where *qt* is the amount of dye adsorbed onto the adsorbent at time *t* (mg/g), *C* is the intercept, and K_{ipd} is the intra-particle diffusion rate constant (mg /g. min).

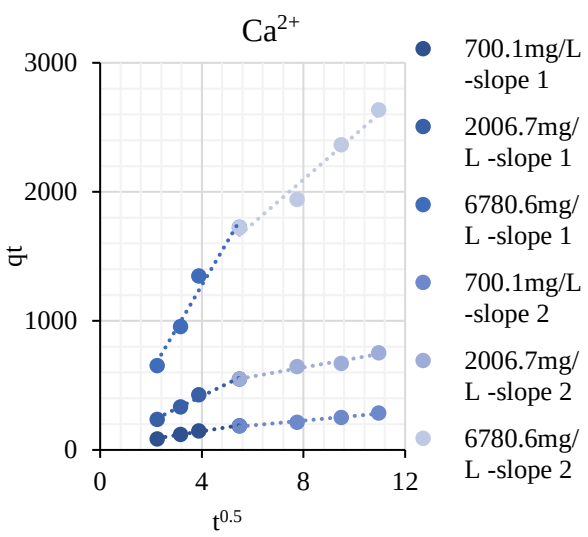
Ca2+
3000
2000
1000
0
qt
0
4
8
12
t0.5
700.1mg/L -slope 1
2006.7mg/L -slope 1
6780.6mg/L -slope 1
700.1mg/L -slope 2
2006.7mg/L -slope 2
6780.6mg/L -slope 2

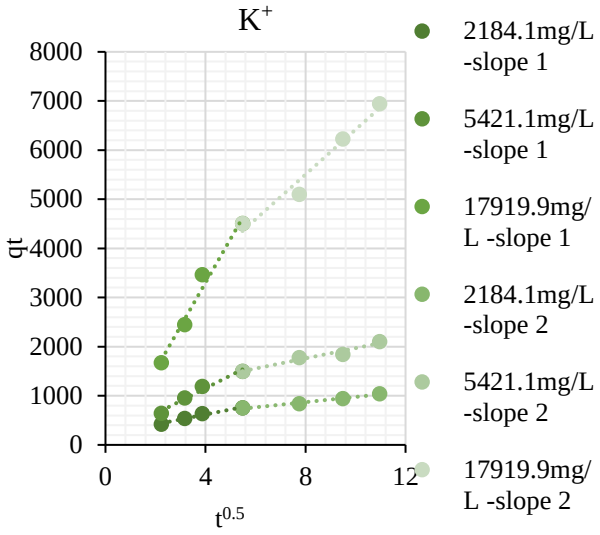
K+
8000
7000
6000
5000
4000
3000
2000
1000
0
qt
0
4
8
12
t0.5
2184.1mg/L -slope 1
5421.1mg/L -slope 1
17919.9mg/L -slope 1
2184.1mg/L -slope 2
5421.1mg/L -slope 2
17919.9mg/L -slope 2

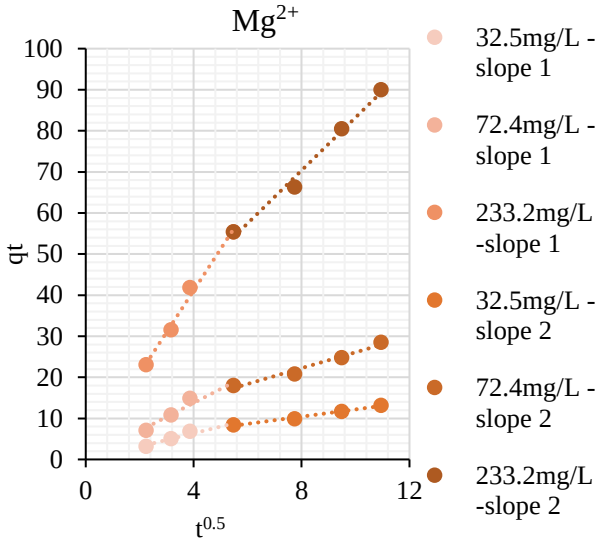
Mg2+
100
90
80
70
60
50
40
30
20
10
0
qt
0
4
8
12
t0.5
32.5mg/L -slope 1
72.4mg/L -slope 1
233.2mg/L -slope 1
32.5mg/L -slope 2
72.4mg/L -slope 2
233.2mg/L -slope 2

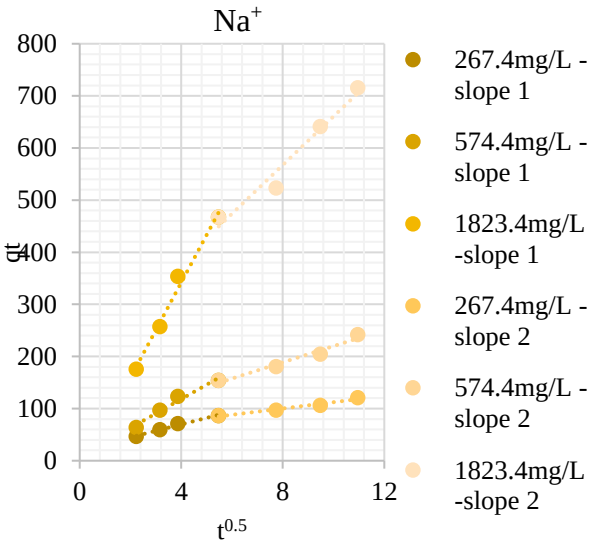
Na+
800
700
600
500
400
300
200
100
0
qt
0
4
8
12
t0.5
267.4mg/L -slope 1
574.4mg/L -slope 1
1823.4mg/L -slope 1
267.4mg/L -slope 2
574.4mg/L -slope 2
1823.4mg/L -slope 2

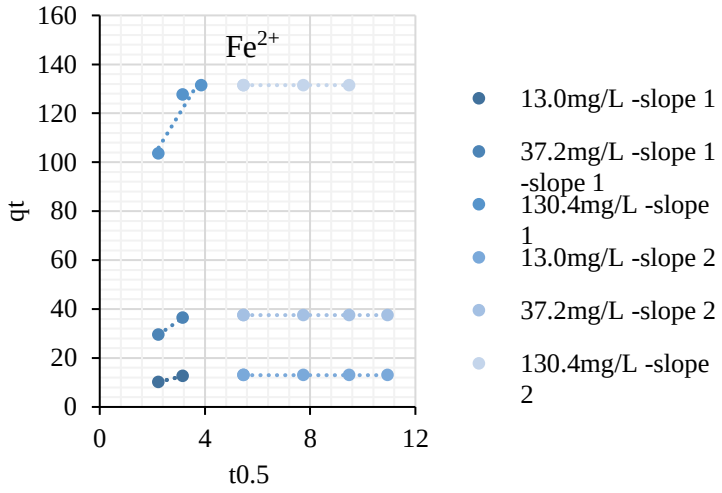
Fe2+
160
140
120
100
80
60
40
20
0
qt
0
4
8
12
t0.5
13.0mg/L -slope 1
37.2mg/L -slope 1 -slope 1
130.4mg/L -slope 1
13.0mg/L -slope 2
37.2mg/L -slope 2
130.4mg/L -slope 2

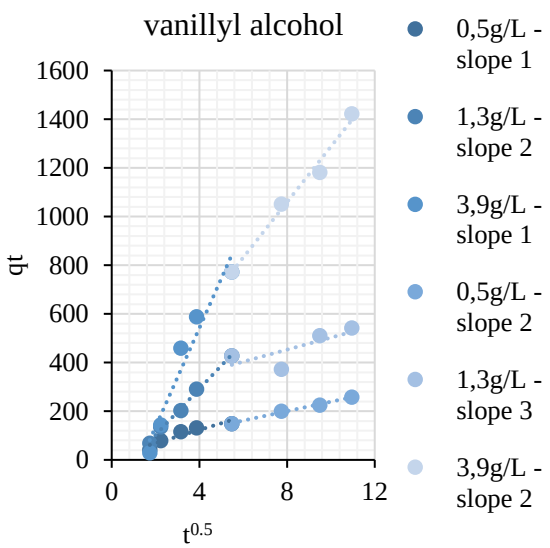
vanillyl alcohol
1600
1400
1200
1000
800
600
400
200
0
qt
0
4
8
12
t0.5
0,5g/L - slope 1
1,3g/L - slope 2
3,9g/L - slope 1
0,5g/L - slope 2
1,3g/L - slope 3
3,9g/L - slope 2

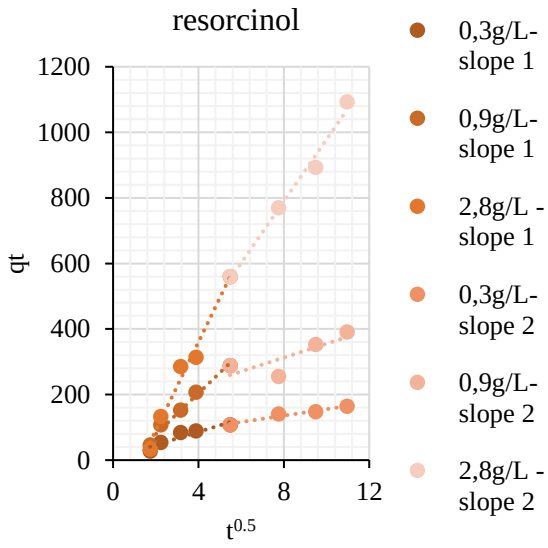
resorcinol
1200
1000
800
600
400
200
0
qt
0
4
8
12
t0.5
0,3g/L- slope 1
0,9g/L- slope 1
2,8g/L - slope 1
0,3g/L- slope 2
0,9g/L- slope 2
2,8g/L - slope 2

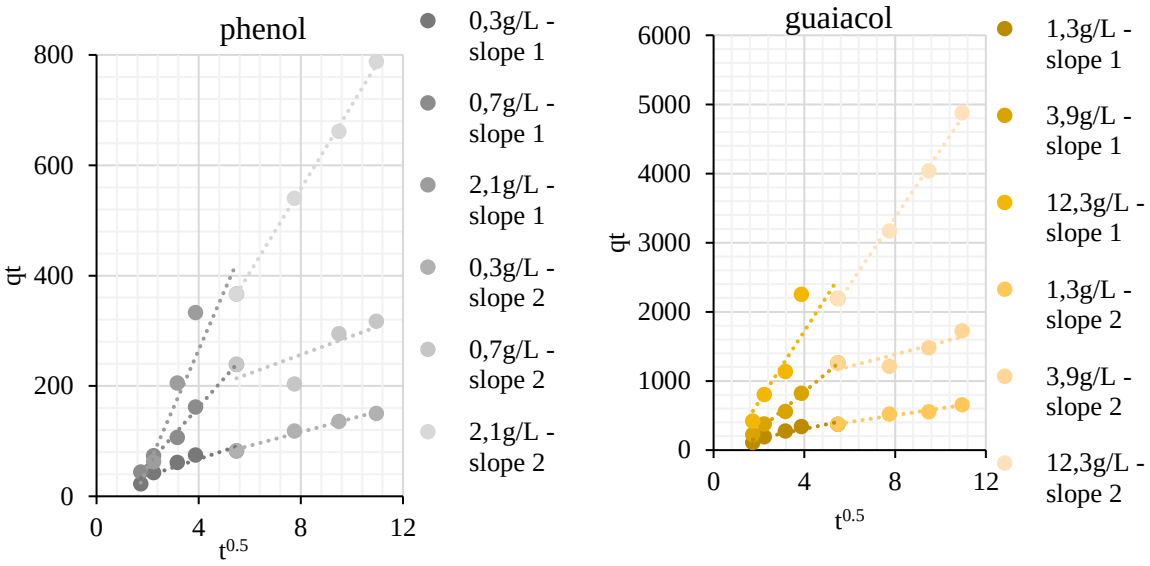

Figure 4.19: adsorption data fitted with Weber and Morris intraparticle diffusion model at different initial adsorbate concentrations (shown in the legends).

*In the legends slope 1 and slope 2 refers to different adsorption mechanism at that given concentration

Figure 4.19. illustrates that the data exhibits two linear regions corresponding to two different mechanisms. The first mechanism is bulky transfer and final mechanism is adsorbate attachment on the hydrochar binding sites are believed fast and are not considered during kinetic system engineering designs (Girish and Murty, 2016) hence the two slopes are assumed to be film diffusion and intraparticle diffusion. Table 4.13 below shows the calculated parameters from this model, which enable understanding the nature of the rate-limiting step.

Table 4.13: Weber and Morris' intraparticle diffusion calculated parameters

	diffusion model	Weber and Morris intraparticle diffusion model				
		Slope 1		Slope 2		Film diffusion layer
Adsorbates	Initial concentration	R^2	Kp (mg/g.min)	R^2	Kp (mg/g.min)	
Vanillyl alcohol	0.5 g/L	0.9529	41	0.9928	19	23
	1.3g/L	0.9870	99	0.5747	25	37
	3.9 g/L	0.9867	273	0.9851	114	222
Resorcinol	0.3/L	0.9219	29	0.9489	10	18

	0.9g/L	0.9731	70	0.6548	21	31
	2.8 g/L	0.9453	134	0.9863	94	131
	0.3 g/L	0.9754	23	0.9840	12	9
	0.7 g/L	0.9756	52	0.5959	17	17
Phenol	2.1 g/L	0.9986	162	0.9987	76	94
	1.3 g/L	0.9792	104	0.9666	49	53
	3.9 g/L	0.9832	266	0.7610	87	76
Guaiacol	12.3 g/L	0.9098	790	0.9960	488	764
	700.1mg/L	1.0000	38	0.9774	18	23
	2006.7 mg/L	0.9949	117	0.9656	35	81
Ca^{2+}	6780.6 mg/L	0.9780	421	0.9648	171	162
	2184.1 mg/L	0.9995	131	0.9805	53	172
	5421.1 mg/L	1.0000	335	0.9559	104	233
K^{+}	17919.9 mg/L	0.9771	1081	0.9677	456	471
	32.5 mg/L	0.9968	2	0.9872	1	1
	72.4 mg/L	0.9897	5	0.9717	2	2
Mg^{2+}	233.2 mg/L	0.9834	11	0.9883	6	5
	267.4 mg/L	0.9965	15	0.9668	6	20
	574.4 mg/L	0.9997	37	0.9648	16	15
Na^{+}	1823.4 mg/L	0.9847	108	0.9610	47	48
	13.0 mg/L	0.9017	2			6
	13.2 mg/L	0.9017	5			16
Fe^{2+}	13.4 mg/L	0.9017	18			65

The film boundary increases with an increase in initial concentration due to increased adsorbate competition. The rate-limiting process is associated with a slower initial adsorption rate, and Table 4.13 shows that slope 1 has a higher initial rate than slope 2, thus faster film diffusion and slow intraparticle diffusion. Boyd's intraparticle diffusion was applied to validate intraparticle diffusion as the rate-limiting step.

4.7.2 Fitting with Boyd intraparticle diffusion model

The Boyd's intraparticle diffusion described in Section 2.6.2 is given by the equation 4.5, and Bt is calculated under the following given conditions:

$$F = 1\text{-}\frac{6}{\pi^2}1\infty\left(\frac{1}{n^2}\right)e\text{-}n2Bt \qquad 4.8$$

where F is the fraction of solute adsorbed at time t and Bt is the mathematical function of F

$$F = \frac{q_t}{q_\infty} \qquad 4.9$$

where qt is mass adsorbed at a given time and q_e is solute adsorbed at an infinite time (t>24hrs). It is difficult to calculate the values of Bt using the equation above but easy from the integrated Fourier transformation of equation 2.13 and equation 2.14 and the following given conditions

$$0 \leq F \leq 0 \cdot 85; \quad Bt = 2\pi - \frac{\pi^2 F}{3} - 2\pi\sqrt{1 - \frac{\pi F}{3}} \qquad 4.10$$

$$0.86 \leq F \leq 1: B_t = -0.4977 - \ln 1 - F \qquad 4.11$$

Figure 4.20 shows the plots of Bt as a function of time at differing concentrations.

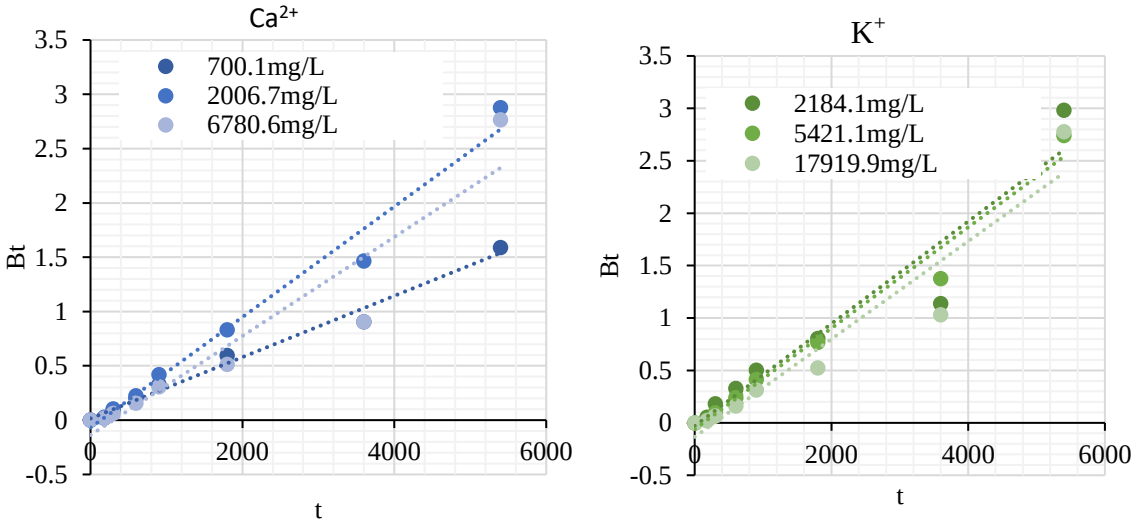

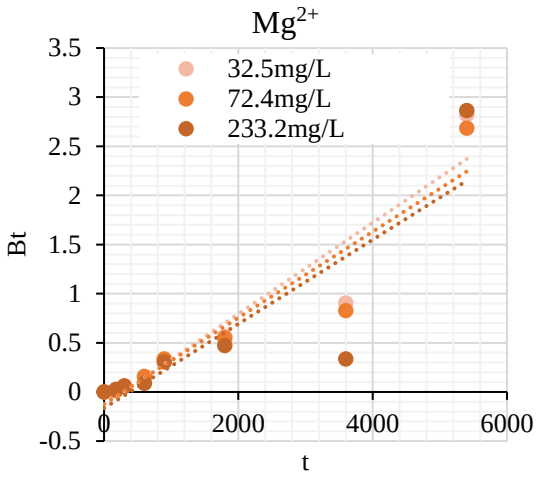
Mg2+
32.5mg/L
72.4mg/L
233.2mg/L
Bt
t

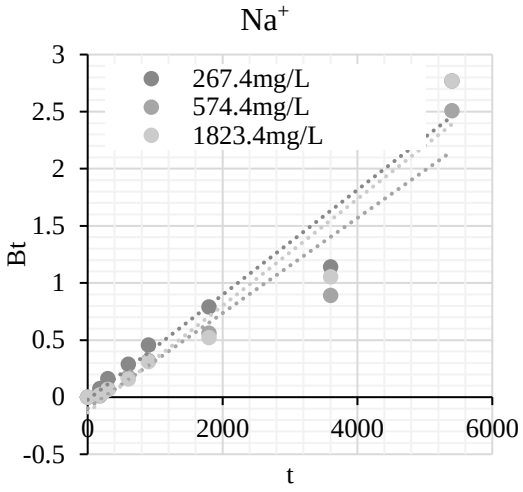
Na+
267.4mg/L
574.4mg/L
1823.4mg/L
Bt
t

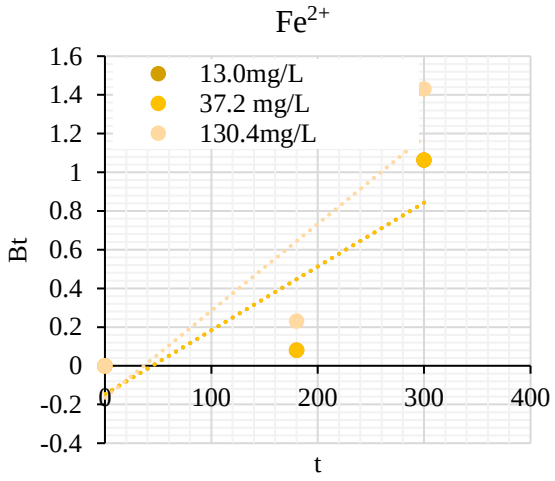
Fe2+
13.0mg/L
37.2 mg/L
130.4mg/L
Bt
t

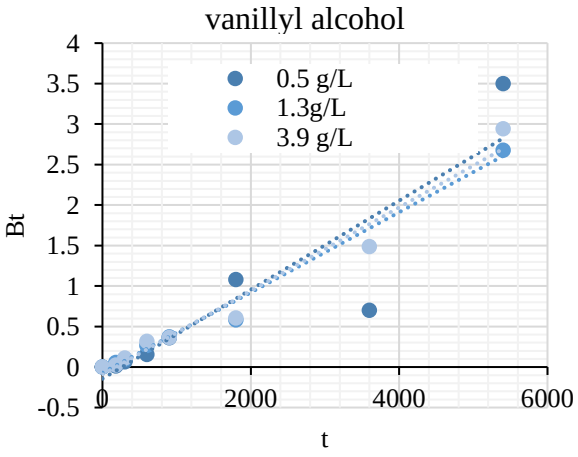
vanillyl alcohol
0.5 g/L
1.3g/L
3.9 g/L
Bt
t

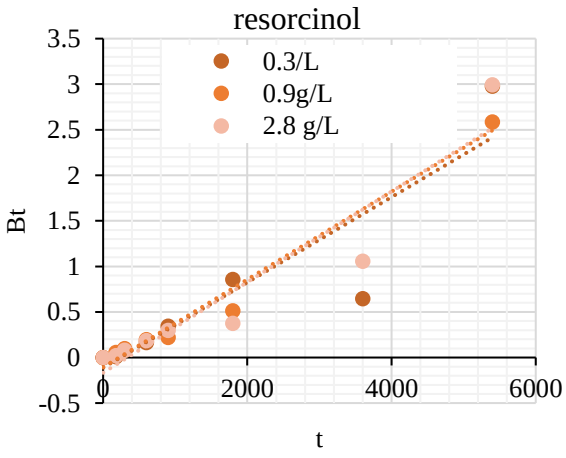
resorcinol
0.3/L
0.9g/L
2.8 g/L
Bt
t

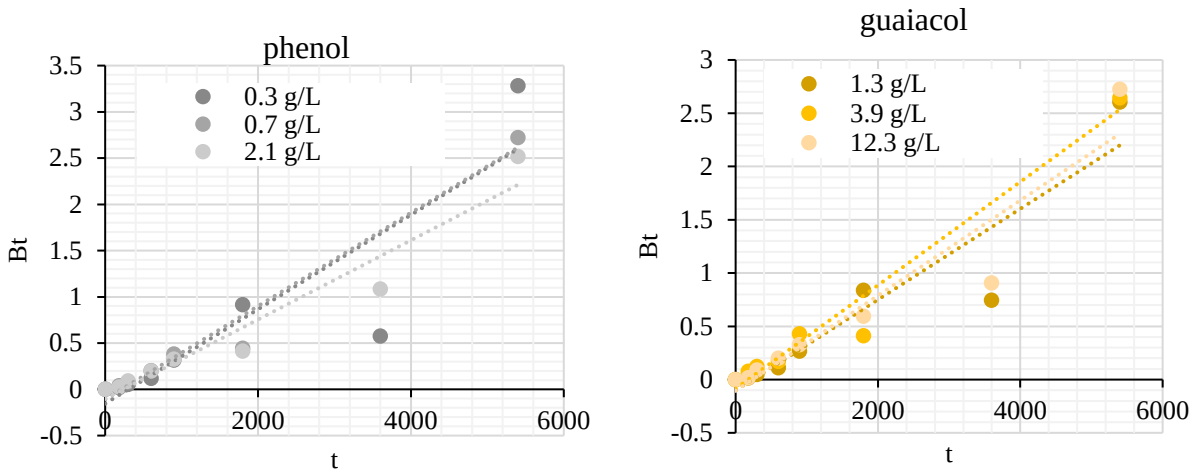

Figure 4.20: Boyd's intraparticle diffusion plots at different concentrations of metals and phenolic compounds.

Figure 4.20 above represents a linear relationship with a correlation coefficient in the range 0.88-0.99, and Table 4.14 below shows the calculated parameters.

Table 4.14:Boyd's intraparticle diffusion calculated parameters

Boyd Intraparticle Diffusion Model							
Metals	c_0	R^2	C	Phenolics	c_0	R^2	C
Ca^{2+}	700.1 mg/L	0.9658	-0.1	Vanillyl	0.5 g/L	0.9152	-0.1
	2006.7 mg/L	0.9814	-0.1	alcohol	1.3g/L	0.9961	-0.1
	6780.6 mg/L	0.8813	-0.1		3.9 g/L	0.9139	-0.2
K^+	2184.1mg/L	0.9246	0	resorcinol	0.3/L	0.9490	-0.1
	5421.1 mg/L	0.9789	-0.1		0.9g/L	0.9970	-0.1
	17919.9 mg/L	0.8812	-0.2		2.8 g/L	0.8901	-0.2
Mg^{2+}	32.5 mg/L	0.8982	-0.1	Phenol	0.3 g/L	0.9003	-0.2
	72.4 mg/L	0.8888	-0.1		0.7 g/L	0.9943	-0.1
	233.2 mg/L	0.8837	-0.2		2.1 g/L	0.8607	-0.2
Na^+	267.4 mg/L	0.9411	0	Guaiacol	1.3 g/L	0.9404	-0.1
	574.4 mg/L	0.9174	-0.1		3.9 g/L	0.9949	-0.1
	1823.4 mg/L	0.8787	-0.1		12.3 g/L	0.8347	-0.2
Fe^{2+}	13.0 mg/L	0.8970	-0.7				
	37.2 mg/L	0.8970	-0.7				

	130.4 mg/L	0.8970	-0.7

The rate-limiting step is intraparticle diffusion if the curve approximates y=mx+02; otherwise, the film diffusion model governs the process (Viegas et al., 2014). Figure 4-23 and Table 4.11 show the calculated intercepts of phenolics and AAEM to be 0.1-0.2 hence, the rate-limiting step is mainly limited intraparticle diffusion. However, Fe^{2+} has an intercept of -0.7 hence adsorption of Fe^{2+} is limited by film diffusion.

4.7.3 Mass transfer behaviour using Biot number

The dimensionless Biot number (Bi), which gives the relationship between the transfer from liquid and intraparticle transfer. It describes the mass transfer behaviour and is the ratio of the rate of transport across the liquid layer to the rate of intraparticle mass transfer.

$$B_i = \frac{k_f d_p}{De} \qquad 4.12$$

where kf (m/s) is the film mass transfer constant and is obtained as a slope of $\frac{C_t}{C_i}$ (fractional adsorbate content) vs time *t*, d_p (m) is the average hydrochar particle, and D_e (m^2/s) is the effective intraparticle diffusion coefficient. parameters.

Table 4.14 below depicts the k_f and k_d values obtained and subsequently used to calculate the dimensionless Biot number.

Table 4.15: The dimensionless Biot number parameters

Adsorbate	Initial Concentration	R^2	kf (cm/s)	R^2	kd(cm2/s)	Bi
Ca^{2+}	700.1 mg/L	0.8145	4.8E-05	0.9663	2.5E-09	145
	2006.7 mg/L	0.7568	4.3E-05	0.9805	2.3E-09	143
	6780.6 mg/L	0.8330	4.7E-05	0.8812	2.1E-09	166
K^+	2184.1 mg/L	0.7266	5.1E-05	0.9245	2.2E-09	174
	5421.1 mg/L	0.7620	4.4E-05	0.9783	2.2E-09	155
	17919.9 mg/L	0.8401	4.7E-05	0.8812	2.1E-09	167
Mg^{2+}	32.5 mg/L	0.8326	4.9E-05	0.8977	2.1E-09	176
	72.4 mg/L	0.8619	4.7E-05	0.8890	2.0E-09	182
	233.2 mg/L	0.8307	4.7E-05	0.8808	2.1E-09	166

Na^+	267.4 mg/L	0.7444	4.8E-05	0.9413	2.1E-09	174
	574.4 mg/L	0.8198	5.0E-05	0.9171	1.9E-09	199
	1823.4 mg/L	0.8408	4.8E-05	0.8790	2.1E-09	169
Fe^{2+}	13.0 mg/L	0.8841	1.7E-03	0.8968	3.3E-08	382
	37.2 mg/L	0.8841	1.7E-03	0.8968	3.3E-08	382
	130.4 mg/L	0.9488	2.2E-06	0.8968	3.3E-08	382
Vanillyl a	0.5 g/L	0.8287	5.5E-05	0.9153	2.0E-09	205
alcohol	1.3 g/L	0.7670	4.9E-05	0.9955	3.0E-09	121
	3.9 g/L	0.8764	5.1E-05	0.9132	1.8E-09	207
Resorcinol	0.3 g/L	0.7723	5.3E-05	0.9487	2.7E-09	146
	0.9 g/L	0.7826	5.0E-05	0.9967	2.5E-09	149
	2.8 g/L	0.9276	5.5E-05	0.8904	1.8E-09	232
Phenol	0.3 g/L	0.8552	6.1E-05	0.8998	2.2E-09	206
	0.7 g/L	0.7967	5.2E-05	0.9939	2.8E-09	140
	2.1 g/L	0.9002	5.3E-05	0.8605	1.8E-09	221
Guaiacol	1.3 g/L	0.8324	5.7E-05	0.9402	1.9E-09	222
	3.9 g/L	0.8132	5.4E-05	0.9950	2.2E-09	180
	12.3 g/L	0.9144	5.3E-05	0.8354	1.7E-09	230

Girish and Murty (2016) conclude that when Bi< 100, film diffusion is dominant, and when Bi >100, internal diffusion is dominant. From Table 4.15, the calculated Bi is in the range 145< Bi< 389; therefore, it can be concluded that the adsorption process of Ca^{2+}, K^+, Mg^{2+}, Na^+, vanillyl alcohol, resorcinol, phenol and guaiacol is limited by intraparticle diffusion.

4.8 Fitting metal and phenolic adsorption data with adsorption isotherms

Isotherms are mathematical models that describe the distribution of adsorbate and adsorbent based on a series of assumptions related to heterogeneity or homogeneity of adsorbent, and the possibility of interaction between the adsorbate species. In this study, the data were fitted with Henry's law, Langmuir, Freundlich, Temkin and Dubinin-Radushkevich isotherms described in Section 2.7.

4.9 Fitting with Henry's law

The simplest adsorption in which the amount of the adsorbate is proportional to the adsorbate concentration at equilibrium and is given equation 2.18 below, and Figure 4.21 shows the fitted data by plotting qe (mg/g) vs Ce (mg/L).

$$q_e = k_{HE} c_e \quad 4.13$$

where q_e is amounts of adsorbate adsorbed, C_e is the adsorbate concentration at equilibrium, K_{HE} is Henry's constant

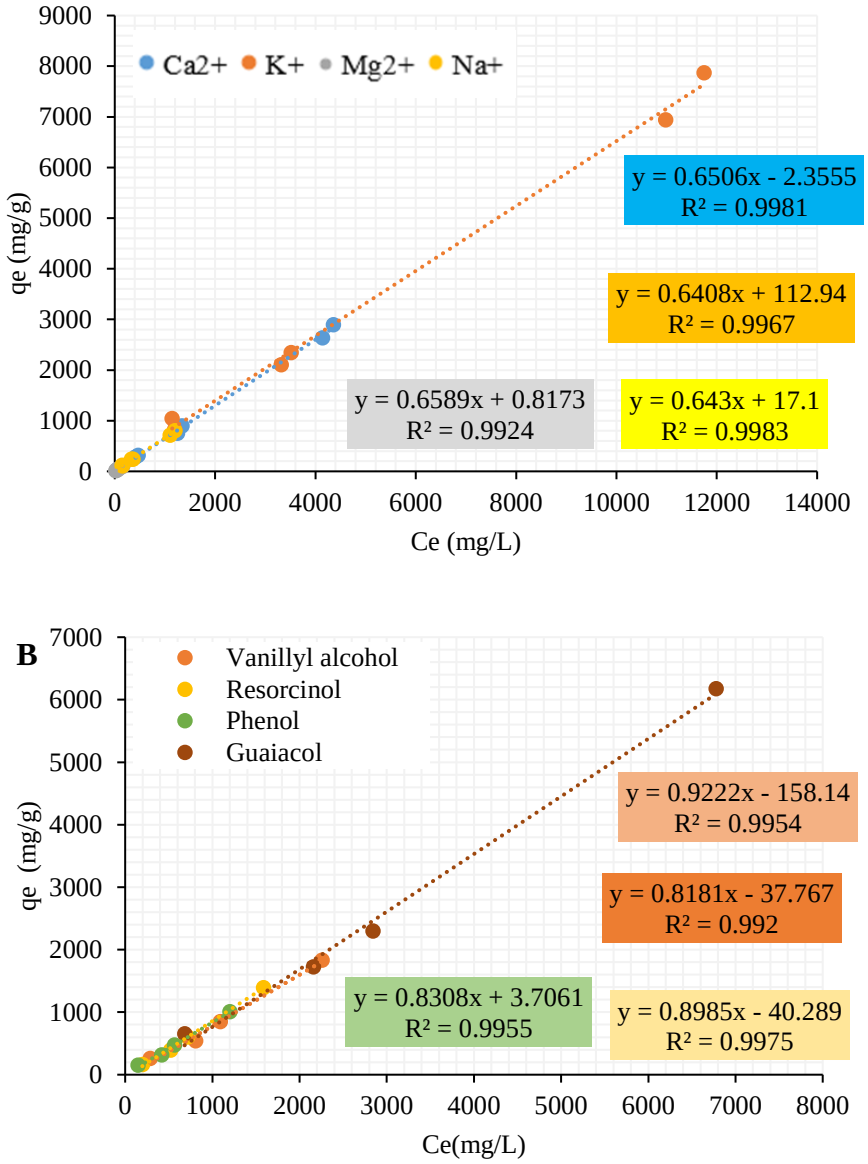

Figure 4.21: The Henry isotherm plots of metals (A) and phenolics (B)

The correlation coefficient of metals and phenols is above 0.99, as shown in Figure 4.21. When comparing the qe $_{cal}$ and qe $_{exp}$, Table 4.16 shows that Mg^{2+}, resorcinol, vanillyl alcohol, phenol, and Na^{+} correlates well with the isotherm. The magnitude of c (the intercept) is considered in the fitting. The closer the c value to 0, the better the fitting and only Mg^{2+}, Ca^{2+}, and phenol are close to zero. It can be concluded that the amount of phenol, resorcinol, and alkaline earth metals, Mg^{2+}

and Ca^{2+}, adsorbed onto the hydrochar is directly proportional to the adsorbate concentration at equilibrium.

4.9.1 Fitting with Langmuir isotherm

The experimental data were fitted Langmuir isotherm described in Section 2.7.2 by plotting the curve of $\frac{1}{q_e}$ vs $\frac{1}{C_e}$ show in Figure 4.22 . The constants $\frac{1}{q_{max.K_L}}$ and $\frac{1}{q_{max}}$ were calculated from the slope and the intercept, respectively.

$$qe = \frac{q_{max}\, K_L\, C_e}{1+K_L C_e} \qquad 4.14$$

where q_e amount of metal adsorbed, C_e is the adsorbate concentration at equilibrium, K_L is Langmuir's constant which shows the degree of adsorption affinity, q_{max} (l/g) is the constant related to the overall solute adsorptivity.

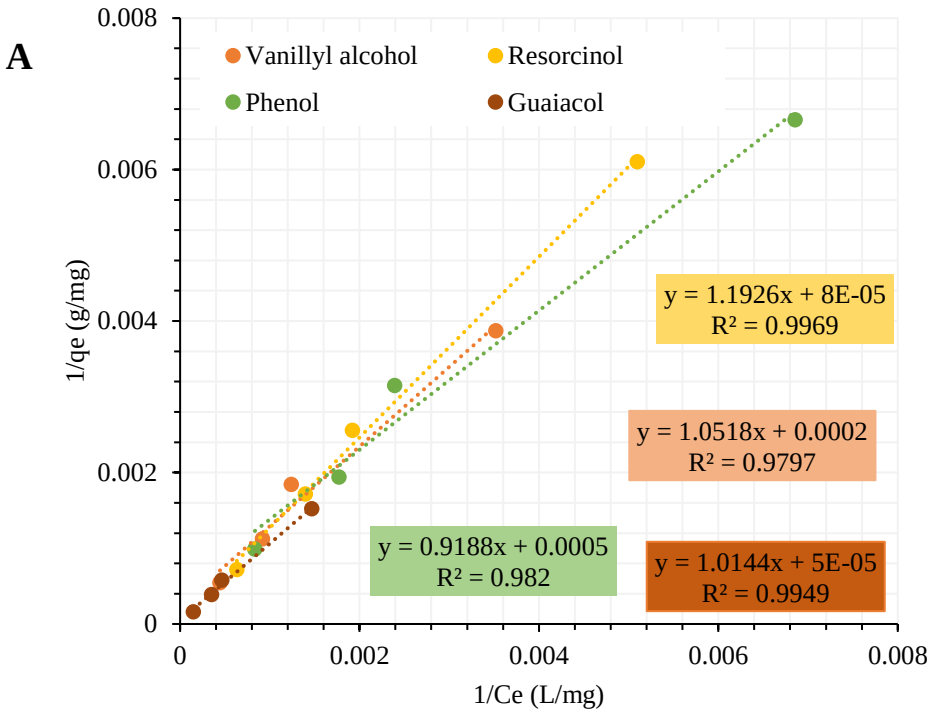

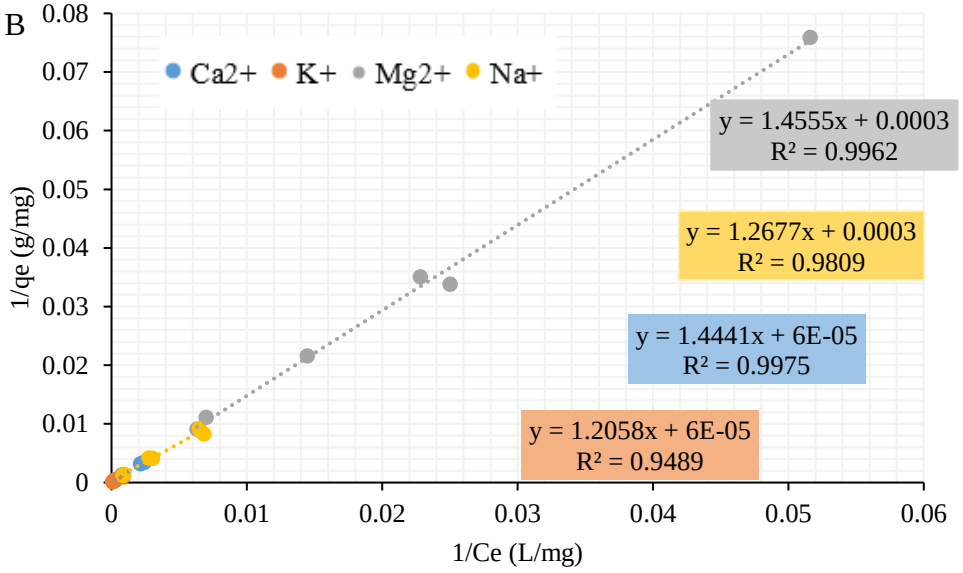

Figure 4.22:Linearised Langmuir plots of 1/qe vs 1/Ce for (A) phenolics and (B) metals.

The above results show that the Langmuir isotherms fit with data with all the R^2 values above 0.97 except for K^+ with 0.94 hence the linear curves were used to calculate the parameters Table 4.16. again, the data fits better at low concentration because the isotherm is valid at lower concentrations. Table 4.16 below shows that the regression coefficient for all the metals and phenolic compounds above 0.978 hence a better fit. The K_L value indicates the extent of interaction between the hydrochar and metals or phenolics. High K_L values are associated with the adsorbent surface area and pore volume and the affinity of the adsorbate to the adsorbent. The K_L value of metals Na^+> Mg^{2+} > K^+> Ca^{2+} and phenols phenol> vanillyl alcohol >resorcinol> guaiacol indicating the order of strength of their interaction with the hydrochar. The q_{max} shows the correct value in which the thermodynamic saturation is achieved. The q_{max} and the qe_{exp} are close for K^+, Na^+, vanillyl alcohol, phenol and guaiacol; hence, they form a monolayer on the hydrochar surface. The q_{max} for Ca^{2+}, Mg^{2+} and resorcinol are over 3-fold higher than the qe_{exp} hence not a perfect fit. The separation factor $R_L = \frac{1}{1+K_L \cdot C0}$ was also calculated. From the parameters in Table 4.16 shows that the R_L of both metal and phenolic compounds is in the 0 – 1 range and changes with initial concentration. Therefore, it can be concluded that the adsorption of both metals and phenolics is favourable.

4.9.2 Fitting with Freundlich isotherm

This model is realistic for multi-layer adsorption, with homogeneous heat adsorption and affinities distributed across a heterogeneous surface. The data were fitted to the equation 2.23, and the constants $\ln K_F$ and $\frac{1}{n}$ were obtained for the slope and intercepts of the plot of lnqe vs lnCe, respectively.

$$\ln qe = \ln k_f + \frac{1}{n}\ln Ce \qquad 4.15$$

where q_e is amount of adsorbate adsorbed, C_e is the adsorbate concentration at equilibrium, K_F adsorption capacity, $1/n$ is adsorption intensity, and value n indicates how favourable the adsorption process is. The prediction of the adsorption process based on the calculated n value is illustrated in the Table 2.2. Figure 4.23 shows the linearized Freundlich isotherm.

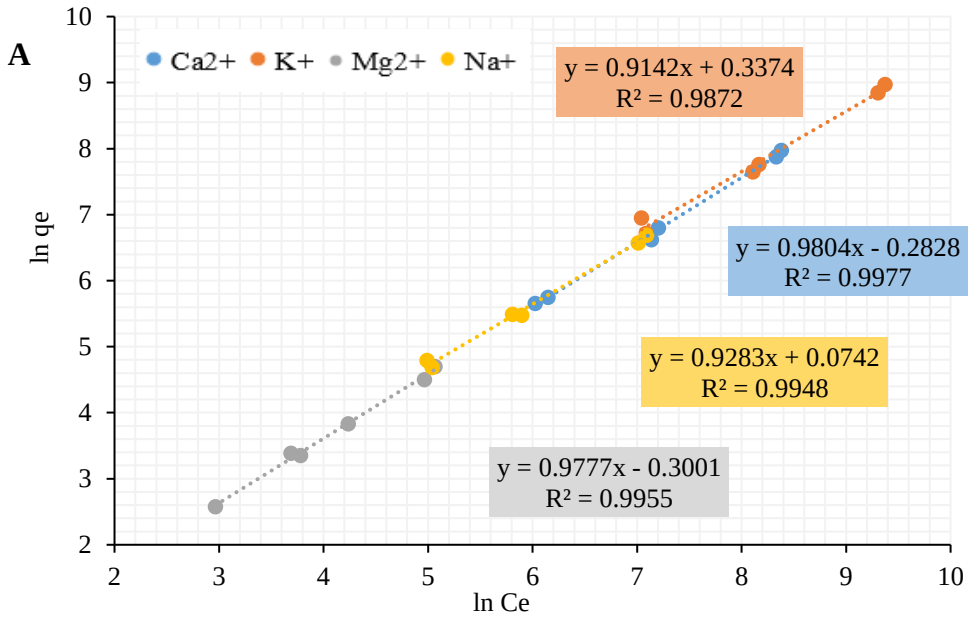

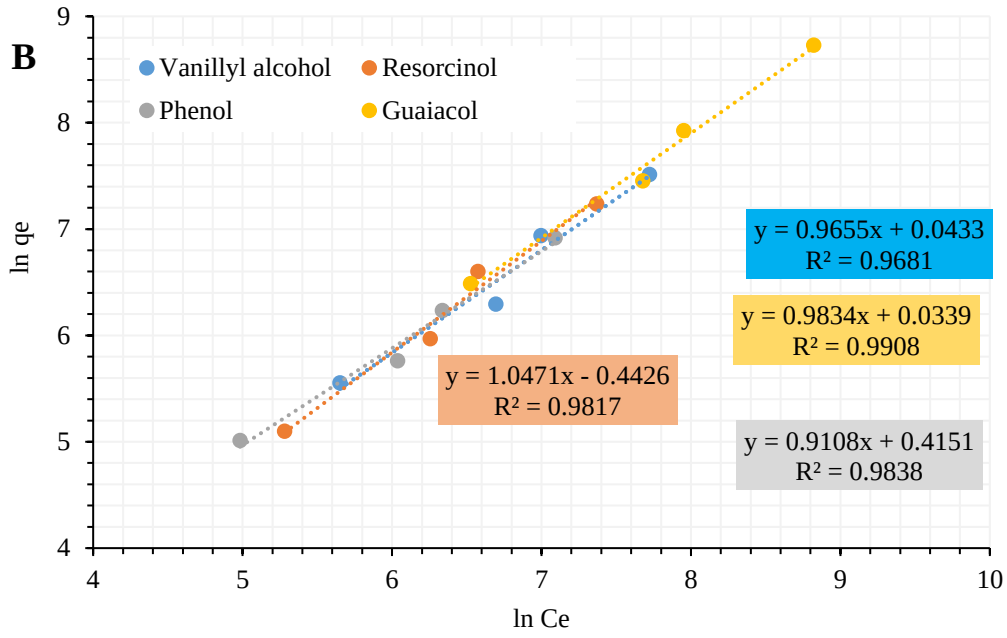

Figure 4.23: Linearised Freundlich plots of ln qe vs ln Ce for (A) phenolics and (B) metals.

The regression coefficient is above 0.97 for all the metals and the phenolic compounds showing that the data fits the isotherm hence parameters were calculated from the graphs and recorded in Table 4.16. The K_F implies energy of adsorption on heterogeneous surfaces, and the larger the value, the better the hydrochar adsorption performance. Table 4.16 shows that the K_F of metals is lower than that of phenolics. Therefore, the phenolics adsorb better than metals on the hydrochar. The n is the heterogeneity factor, which measures adsorption intensity and indicates feasibility, strength, and favourability. Komkiene and Baltrenaite, (2016) and Kumar *et al.*,(2006a) stated that values in the range 1–10 represent excellent adsorption characteristics. Table 4.16 shows that the values of n are in the range 1.03-1.27 that's n>1; hence the adsorption of both phenolic and metal is favourable. The 1/n value represents adsorption intensity and is related to surface heterogeneity 1/n <1 indicates normal adsorption and 1/n > 1 indicates cooperative adsorption. Table 4.10 below shows that 1/n <1 implies favourable adsorption for metals and phenolics. The correlation coefficient of phenolics is higher than metals, hence better fitting, also supported by the heterogeneity factor >1.

4.9.3 Fitting with Temkin isotherm

The model suggests that the heat adsorption (temperature function) of all layer molecules is lowered linearly rather than logarithmically, except in the case of extremely low and high

concentrations. This isotherm is valid only for an intermediate range of concentrations and is given by the following equation:

$$qe = \frac{RT}{b_T} \ln(A_T C_e) \quad 4.16$$

where A_T =Temkin isotherm equilibrium binding constant (L/g), b_T = Temkin isotherm constant related to heat of sorption (J/mol), R= universal gas constant (8.314J/mol/K), T= temperature at 298K.

Temkin isotherm parameters were calculated from the plot of qe vs lnCe. The b_T value indicates whether the process is physisorption or chemical sorption. Values above 80 kJ/mol indicate chemical adsorption while less than 4 kJ/mol present physisorption (Ionel *et al.,* 2003; Kara and Demirbel, 2012). Table 4.16 below shows that b_T is less than the 80 kJ/mol; hence the process indicates a physical process. However, the correlation coefficient is 0.89-0.93 lower than Langmuir and Freundlich isotherms, hence not a perfect fit.

4.9.4 Fitting with Dubinin-Radushkevich isotherm

The Dubinin-Radushkevich isotherm estimates the energy of adsorption. It assumes the Gaussian distribution for the characteristic curve and is expressed by the equation:

$$Inqe = \ln q_{DR} - K\varepsilon^2 \quad 4.17$$

where *qe* = amount of adsorbed adsorbate at equilibrium (mg/g); q_{DR} is theoretical isotherm saturation capacity (mg/g); *K* is Dubinin–Radushkevich isotherm constant (mol^2/kJ^2). The ε is given by the equation:

$$\varepsilon = RT\ ln\left(1 + \frac{1}{Ce}\right) \quad 4.18$$

where R, T and Ce represent the gas constant (8.314 J/mol K), absolute temperature (K) and adsorbate equilibrium concentration (mg/L), respectively.

The isotherm is not only suggested for continuous or homogeneous adsorption potential but also for heterogeneous adsorbents. Free sorption energy E_s is used to determine the nature of adsorption and the equation 4.16 expresses this.

$$E_S = \frac{1}{\sqrt{2B}}. \quad 4.19$$

where *B* is denoted as the isotherm constant *(-K*).

The R^2 in the Dubinin-Radushkevich fitting is quite low hence the adsorption of both metals and phenolics do not follow this isotherm. Despite the low R^2 his model normally differentiates between chemical and physical adsorption by considering calculate E_s value from equation 4.19 above. The adsorption process is considered chemical when E_s value is in the range of 8.0 to16.0 kJ/mol and physical when E_s is less than 8.0 kJ/mol (Dubinin, 1960). Table 4.16 below shows that the E_s values 0.005-0.3 J/mol are thus lower than 8.0 kJ/mol with the lowest correlation coefficient hence validating that the adsorption of both metals and the phenolics follow a physical process. Table 4.16 shows E_s value less than 8.0 kJ/mol with the values 0.12, 0.30, 0.01, 0.04, 3.49, 4.76, 6.87, 1.36 kJ/mol for Ca^{2+}, K^+, Mg^{2+}, Na^+, vanillyl alcohol, resorcinol, phenol and guaiacol, respectively. Hence concluding a physical adsorption process for both metals and phenolics.

Table 4.16:Isotherm calculated parameters

Isotherm	parameters	Ca^{2+}	K^+	Mg^{2+}	Na^+	Vanillyl alcohol	Resorcinol	Phenol	Guaiacol
Henry	R^2	0.9977	0.9959	0.9905	0.9979	0.9920	0.9975	0.9955	0.9954
	K_{HE}(L/g)	0.651	0.641	0.659	0.643	0.898	0.831	0.922	1.089
	c	-2	113	1	17	-38	-40	4	-158
	qe_{cal}(mg/g)	269	732	13	94	255	163	135	451
	qe_{exp}(mg/g)	286	1041	13	121	258	164	150	656
Langmuir	q_{max} (mg/g)	5729.1	6727.7	1256.9	1142.6	2414.8	2816	1201.9	7153
	qe_{exp}(mg/g)	2897.9	7869.5	109.8	802.3	2255.5	1583.6	1199.4	6775.9
	k_L (L/mg)	5.88E-05	6.55E-05	2.64E-04	3.60E-04	3.65E-04	2.74E-04	8.52E-04	1.29E-04
	R_L	0.78	0.53	0.96	0.67	0.40	0.63	0.36	0.49
	R^2	0.9921	0.8837	0.9901	0.9530	0.9914	0.9979	0.9898	0.9897
Freundlich	k_F (mg/g) $(l/mg)^{1/n}$	0.390	1.033	0.379	0.696	2.105	1.287	2.572	2.075
	n	1.03	1.15	1.04	1.13	1.21	1.12	1.27	1.17
	R^2	0.9327	0.9400	0.9180	0.9541	0.9965	0.9995	0.9966	0.9927
Temkin	k_T (L/g)	1.92E-03	7.79E-04	4.16E-02	6.58E-03	4.52E-03	6.06E-03	9.15E-03	1.65E-03
	b_T (J/mol)	3.84	1.48	91.41	13.07	4.69	6.10	8.66	1.48

	B= RT/b_T	645	1672	27	190	528	406	286	1671
	R^2	0.9039	0.8898	0.9042	0.9343	0.9216	0.9302	0.9243	0.8900
D-R	q_{DR} (mg/g)	1714	4615	66	522	993	763	561	3241
	B (mol. J)^2	5.60E-02	3.70E-01	1.20E-04	5.90E-03	1.80E-02	1.00E-02	4.80E-03	1.20E-01
	E (kJ/mol)	0.12	0.30	0.01	0.04	3.49	4.76	6.87	1.36
	R^2	0.7719	0.7389	0.7281	0.7729	0.7687	0.8088	0.7866	0.8008

4.9.5 The isotherm fitting curves

The adsorption data of each metal and each phenolic compound fitted with all the isotherms was also presented by the plots of *qe* (mg/g) versus *Ce* (mg/L) on the same curve. The Figure 4.24 below shows the fitting of the adsorption data of metals and phenolics fitted with Henry isotherm, Langmuir isotherm, Freundlich isotherm, Temkin isotherm and Dubinin-Radushkevich isotherm.

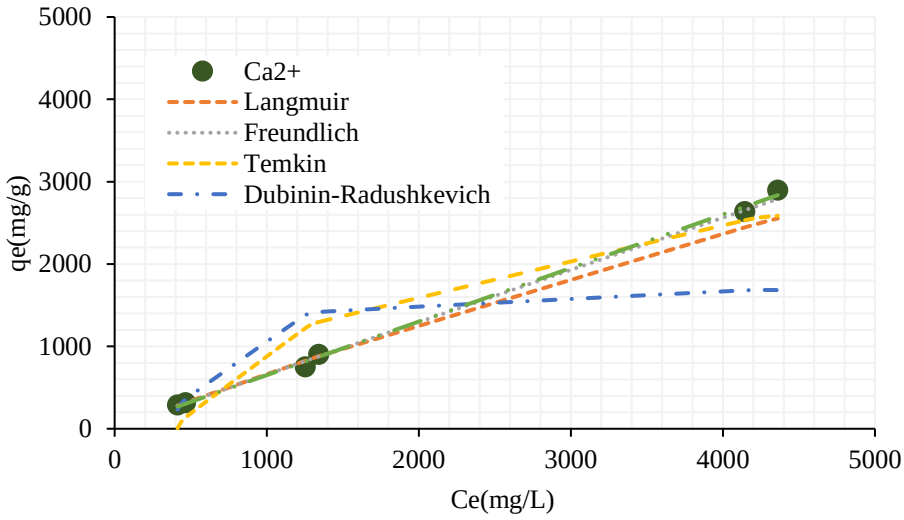

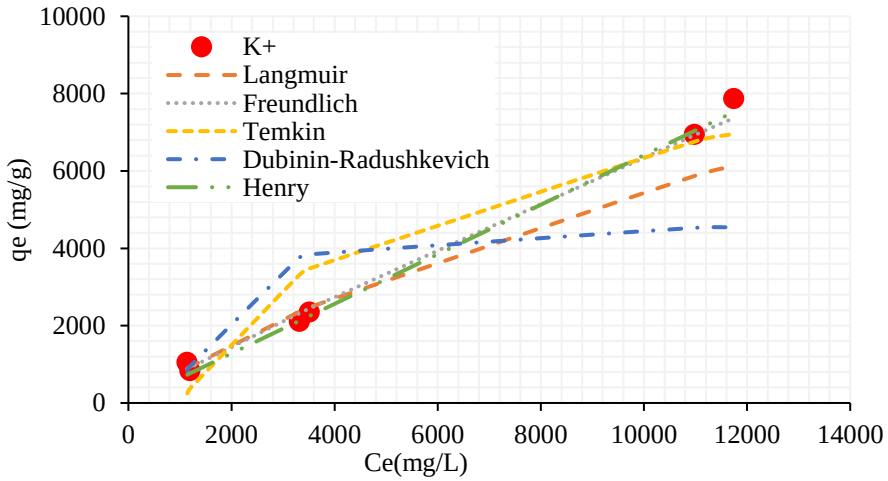

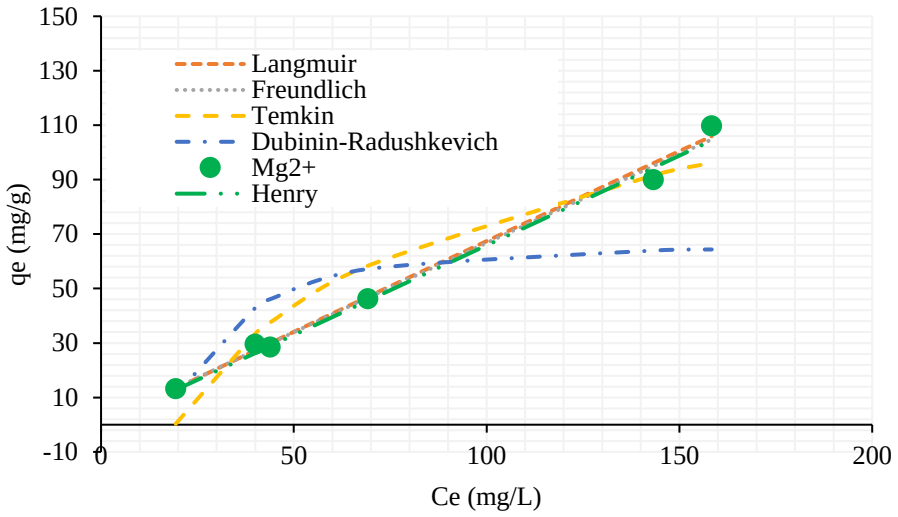
150
130
110
90
70
50
30
10
-10
0
50
100
150
200
qe (mg/g)
Ce (mg/L)
Langmuir
Freundlich
Temkin
Dubinin-Radushkevich
Mg2+
Henry

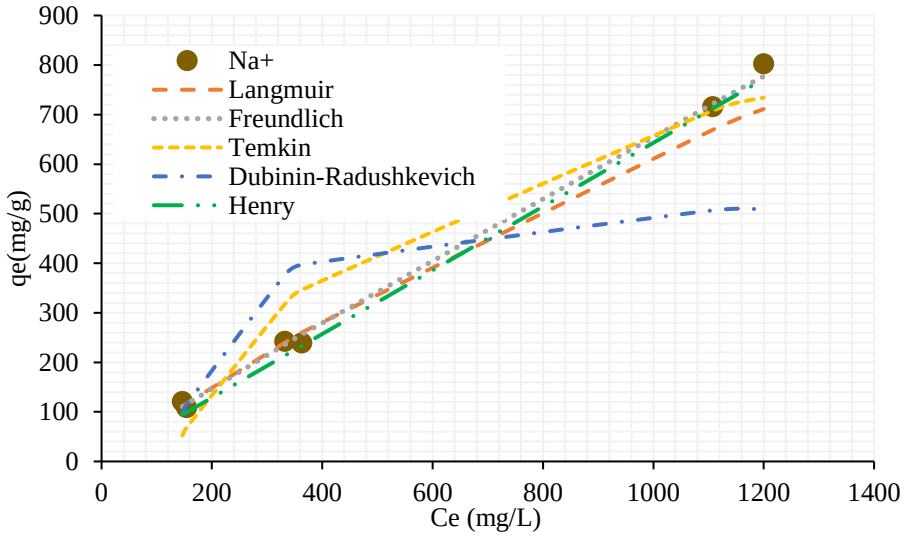
900
800
700
600
500
400
300
200
100
0
0
200
400
600
800
1000
1200
1400
qe(mg/g)
Ce (mg/L)
Na+
Langmuir
Freundlich
Temkin
Dubinin-Radushkevich
Henry

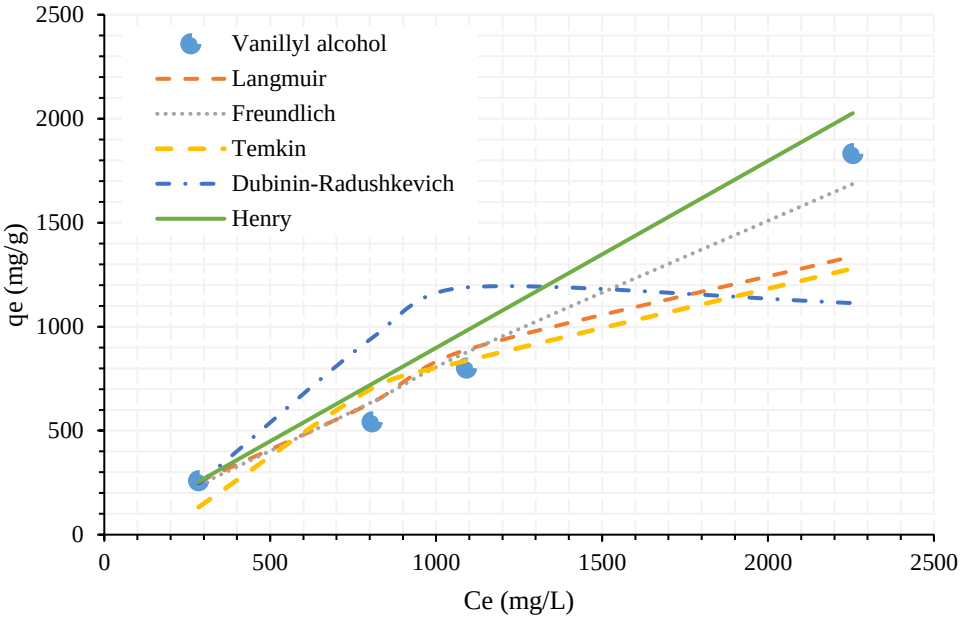
Vanillyl alcohol
Langmuir
Freundlich
Temkin
Dubinin-Radushkevich
Henry
qe (mg/g)
Ce (mg/L)
0
500
1000
1500
2000
2500

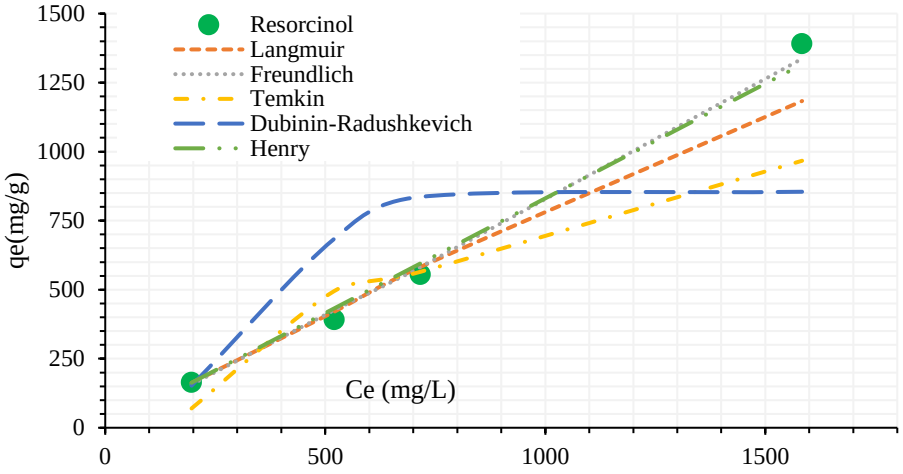
Resorcinol
Langmuir
Freundlich
Temkin
Dubinin-Radushkevich
Henry
qe(mg/g)
Ce (mg/L)
0
250
500
750
1000
1250
1500

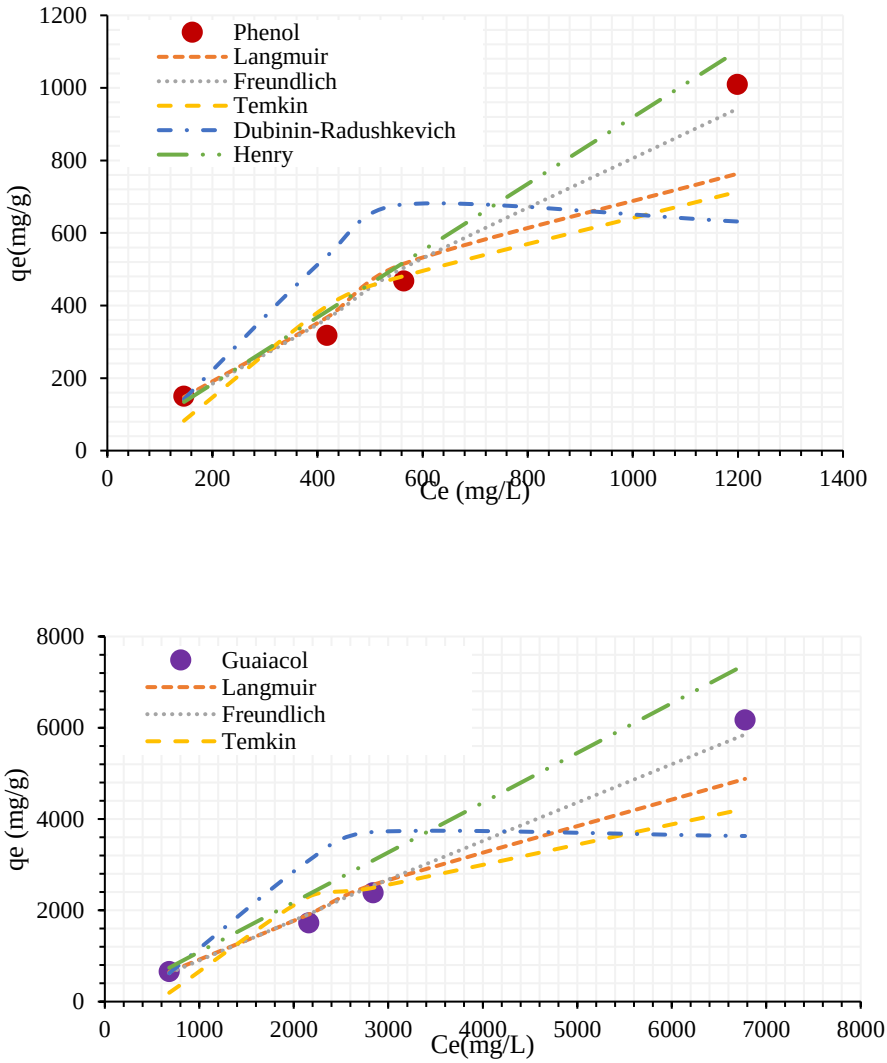

Figure 4.24: Fitted isotherms to experimental equilibrium adsorption data of phenolic components

A perfect fit for each adsorbent was analysed by comparing the alignment of qe_{exp} (dotted line) and qec_{al} (dots) from Henry's law, Langmuir and Freundlich Temkin and Dubinin-Radushkevich isotherm. Adsorption of phenol, Ca^{2+}, and Mg^{2+} fits well with Henry's law considering the R^2 value, the qe_{cal} and the intercept c. Henceforth, a linear relationship between the fluid phase and the adsorbed phase (Mendoza-castillo, 2017). K^+ and Na^+ show can be described by the Langmuir isotherm considering the q_{max} and Freundlich when considering the R^2 and a larger (compared to Ca^{2+} and Mg^{2+}) heterogeneity factor; consequently, the data fits well with the Freundlich isotherm better than the Langmuir isotherm. Vanillyl alcohol, phenol and guaiacol agrees with the Langmuir isotherm based on the q_{max} values. Henry's law also describes the resorcinol and phenol-based on qe_{cal}, the intercept c and R^2. Freundlich isotherm seems to describe the adsorption based on the correlation coefficient. The same was concluded for catechol and phenol adsorption on Scots pine

(*Pinus sylvestris L.*) biochar and Silver birch (*Betula pendula)* derived biochar (Komkiene and Baltrenaite, 2016). In consideration of the heterogeneity of the hydrochars in physical-chemical properties (e.g., surface functional groups and elemental compositions), it is reasonable that the Freundlich model gives a better description of the isotherm curve. Temkin and Dubinin-Radushkevich isotherms concluded that the adsorption of metals and phenolics is a physical process.

4.10 Thermodynamics of metal and phenolics adsorption

4.10.1 Calculated Enthalpy Change (ΔH), Gibbs Free Energy (ΔG) and Entropy Change (ΔS) from the adsorption data

The nature of adsorption can be more fully understood by calculating the thermodynamic parameters like enthalpy change ΔH, Gibbs free energy ΔG and entropy change ΔS using the equilibrium constants under varying temperatures. The equations below are used to estimate these thermodynamic parameters.

$$K_e = \frac{q_e}{C_e} \quad (4.20)$$

$$\ln Ke = \frac{\Delta S}{R} - \frac{\Delta H}{RT} \quad (4.21)$$

$$\Delta G = \Delta H - T\Delta S \quad (4.22)$$

ΔS and ΔH are determined from the intercept and the slope of $\ln K_e$ vs, $\frac{1}{T}$. The slope and the intercept of the curves correspond to -ΔH/R and ΔS/R, respectively, as shown in Figure *4.25* below.

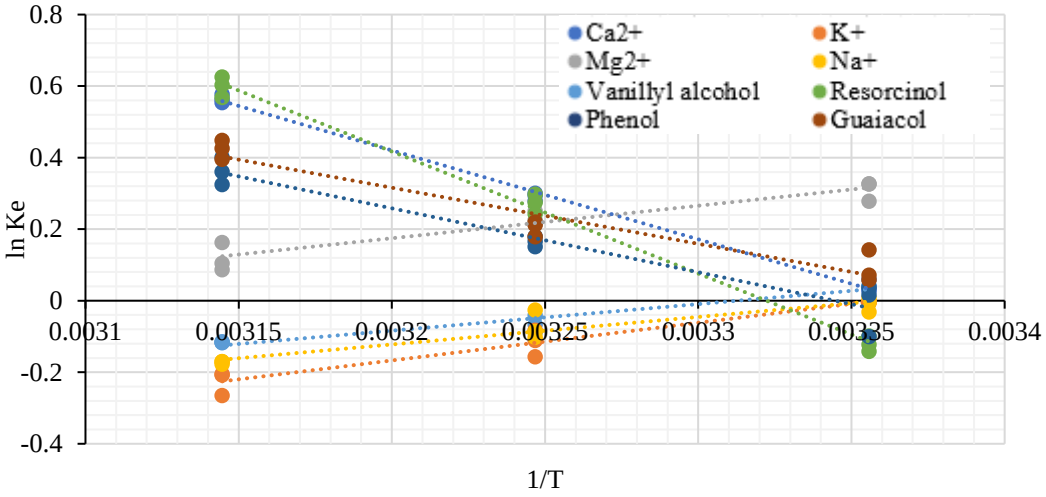

Figure 4.25: Van't Hoff plot w.r.t. Ke for both metal adsorption and phenolics adsorption

The linear curves in Figure 4.25 and parameter values in Table 4.17 show R^2 values (R^2>0.9) except for Na^+ with slightly lower R^2 value of 0.88 which indicates that the thermodynamic properties can appropriately be determined using the Van't Hoff equation. The observed plots show a positive slope for metals and a negative for phenolic compounds. The Gibbs free energy of a significant adsorption process must be negative. However, the ΔG can become dependent on temperature if both entropy and enthalpy are positive or negative. The results obtained in the adsorption of all the metals is spontaneous at all temperatures with alkaline earth metals Ca^{2+} and Mg^{2+} are more spontaneous when compared to the alkali earth metals because of their more negative ΔG. Figure 4.26 below show the effect of temperature on the Gibbs free energy for the adsorption of both phenolics and metals.

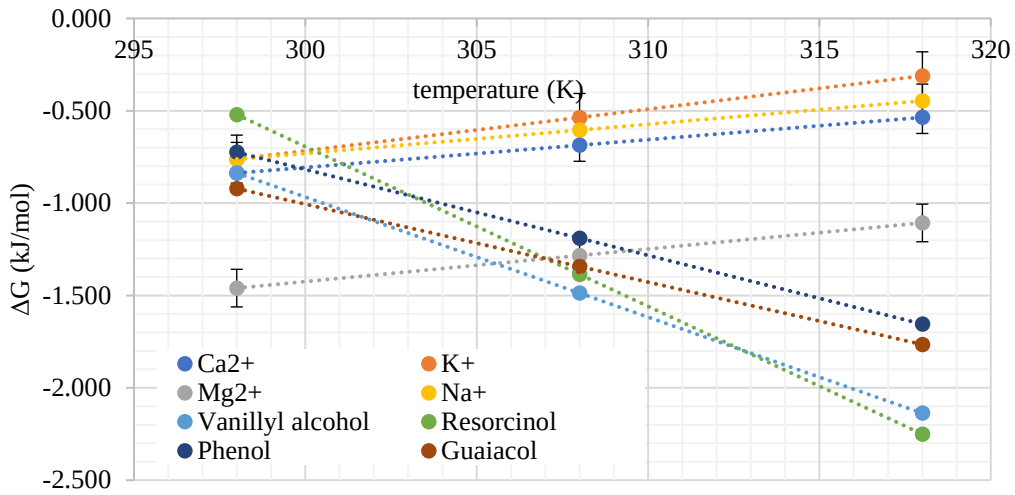

Figure 4.26:The plot of Gibbs free energy vs temperature to show the feasibility of the adsorption process of the metal and phenolic compounds

From the above results, it is noted that the ΔG increases with an increase in temperature for metals; hence the metal adsorption becomes less spontaneous. As opposed to the metals, the spontaneity of phenolic compounds increases with an increase in temperature, as shown in Figure 4.26. The same was observed by Ahmed and Theydan, (2012) for the adsorption of phenol and n-nitrophenol on date stones. Table 4.17 below show the calculated Gibbs free energy ΔG (kJ/mol), enthalpy ΔH (kJ/mol), and entropy ΔS (kJ/mol. K) of the adsorption of both metals and phenolics.

Table 4.17: Thermodynamic parameters for the adsorption of metals and phenolic compounds on hydrochar

Adsorbates	Temperature (K)	Ca^{2+}	K^{+}	Mg^{2+}	Na^{+}	Vanillyl alcohol	Resorcinol	Phenol	Guaiacol
R^2		0.9400	0.9357	0.9006	0.8855	0.9950	0.9870	0.9160	0.9410
ΔH (kJ/mol)		-5.3	-7.5	-6.7	-5.5	18.5	25.2	13.1	11.7
ΔS (kJ/mol. K)		-0.02	-0.02	-0.02	-0.02	0.07	0.09	0.05	0.04
ΔG (kJ/mol)	318	-0.5	-0.3	-1.1	-0.5	-2.1	-2.3	-1.7	-1.8
ΔG (kJ/mol)	308	-0.7	-0.5	-1.3	-0.6	-1.5	-1.4	-1.2	-1.3
ΔG (kJ/mol)	298	-0.8	-0.8	-1.5	-0.8	-0.8	-0.5	-0.7	-0.9

The value of ΔH gives information about the exothermicity or endothermicity of the adsorption process. Table 4.17 shows that ΔH of Ca^{2+}, K^{+}, Mg^{2+} and Na^{+} are negative, hence an exothermic reaction, while vanillyl alcohol, resorcinol, phenol, and guaiacol are positive, suggesting an endothermic process. The magnitude of ΔH denotes the type of sorption. In physical adsorption, the heat evolved is similar to the heats of condensation, i.e., 2.1–20.9 kJ mol^{-1}, while that chemisorption mostly falls into a range of 80–200 $kJmol^{-1}$ (Chowdhury, 2017). The results in Table 4.17 show that metals, phenol, and guaiacol are adsorbed through physical adsorption, while vanillyl alcohol adsorbs through a combination of physical and chemical adsorption.

The positive entropy indicates the adsorbent's affinity for adsorbate and structural changes in the adsorbent and the adsorbent at the solid /solution interface. Table 4.17 above shows positive entropy for phenolic compounds, hence corresponding to an increase in the degree of freedom of the phenolics solid-liquid interphase during the adsorption process.

Generally, a -ΔG and a +ΔS denotes a spontaneous reaction (noted in phenolic adsorption calculated parameters). Therefore, it can be concluded that the adsorption process of phenolic compounds is entropy-driven, not enthalpy. A negative entropy for metals decreased disorder at the solid/liquid interface during the adsorption process, causing the adsorbate ions/molecules to escape from the solid phase to the liquid phase, which also explains the low removal efficiency of metals. The adsorption process of metal is enthalpy driven rather than entropy implying that the spontaneity of the reaction, the TΔS being small relative to ΔH, so that ΔG is negative.

4.10.2 Activation energy

The activation energy is calculated using the Arrhenius equation below:

$$\ln k = \frac{E_a}{RT} + \ln A \qquad 4.23$$

The plot of ln k versus 1/T gives values of E_a and A from the slope and the intercept. Figure 4.27 below shows the Arrhenius plot using Pseudo-first-order kinetic constant.

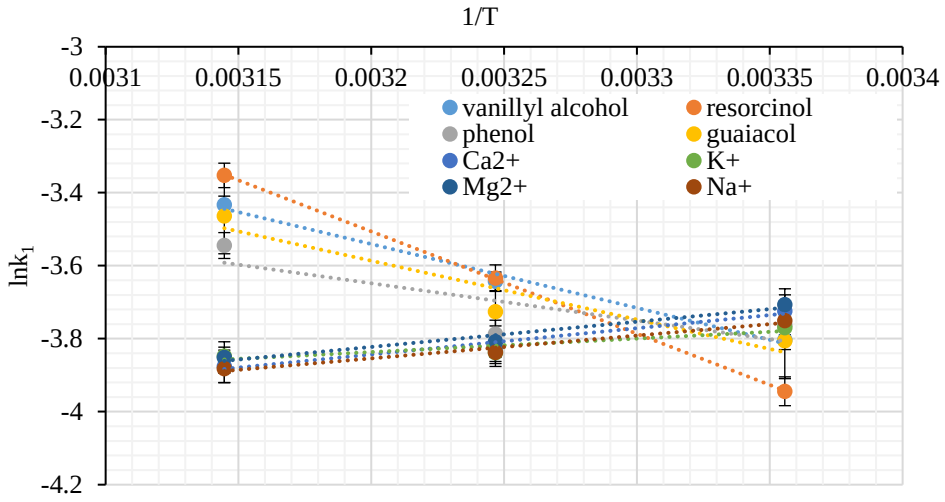

Figure 4.27: Arrhenius plots w.r.t k_1 for metals and phenolic compounds

From the plot above, the AAEM and phenolics' activation energy is below 40 kJ/mol, suggesting physisorption. Because chemisorption is associated with bond breaking and bond formation, activation is mostly high above 40 kJ/mol while physisorption is less than 40 kJ/mol. The $E_{a.}$ of phenolics is higher than that of metals, which agrees that phenolic adsorption requires external heat energy in an endothermic adsorption process while metals is an exothermic reaction.

Table 4.18: Activation energy of metals and phenolic compounds on bWHc.

Adsorbate	Ca^{2+}	K^+	Mg^{2+}	Na^+	Vanillyl Alcohol	Resorcinol	Phenol	Guaiacol
R^2	0.9612	0.8269	0.9401	0.9599	0.9910	0.9999	0.6493	0.9027
A	0.23	0.07	0.21	0.16	7.82	236.50	0.68	4.80
Ea (kJ/mol)	5.94	3.03	5.69	5.17	14.54	23.31	8.47	13.40

4.11 Adsorption experiments using HTL aqueous phase (wastewater)

4.11.1 Adsorption of metals and phenolics from real wastewater

Figure 4.28 below depicts the removal efficiency of the metals present in the HTL aqueous phase.

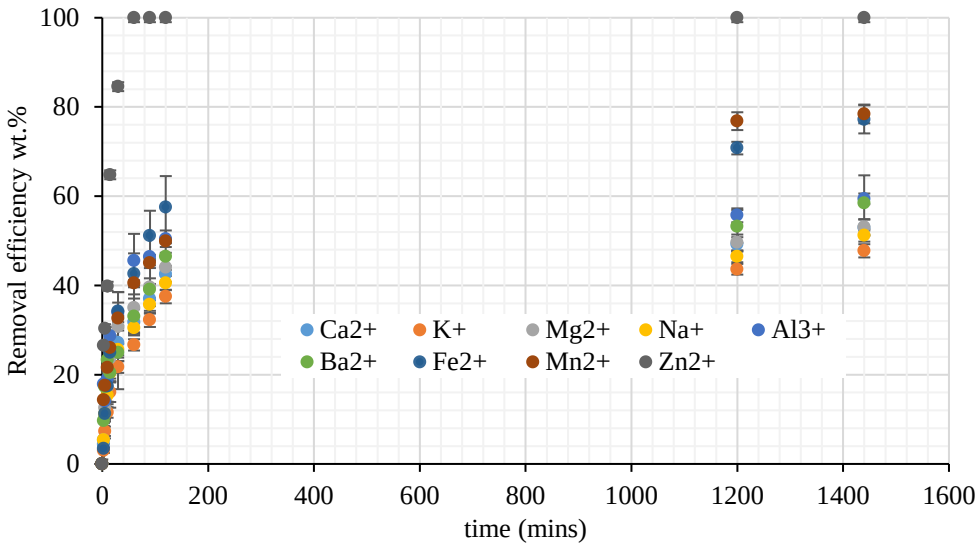

Experimental conditions; total volume of solution 100ml, contact time 24 hrs, pH = pZc of bWHc: 10.6, bWHc dose: 1.0 g, temperature: 273 K; shaker 2.5Hz.

Figure 4.28: Removal efficiency of metals present in HTL aqueous phase

From the results above, the efficiency is expected to decrease by almost 10% compared to synthetic mixtures due to the complexity of the mixture, e.g., the unidentified organic acids, anions, and large molecules like oligomers. However, using a high dose of 1g of hydrochar increases the removal efficiency instead, as discussed in Section 4.4.3. The pH adjustment to match the point of zero charges of the hydrochar contributes to increased removal efficiency because of the precipitation of heavy metals like Pb^{2+}, Sr^{2+}, Co^{2+} and about 33 % of Fe^{2+} and Mn^{2+} detected in Section 4.2.1. This was achieved by concentration of these metals before and after pH adjustment but before the adding hydrochar. The organic acids detected in Section 4.2.3 were all neutralised with the pH adjustment. Figure 4.29 below shows the adsorption capacity of the hydrochar on HTL aqueous phase metals.

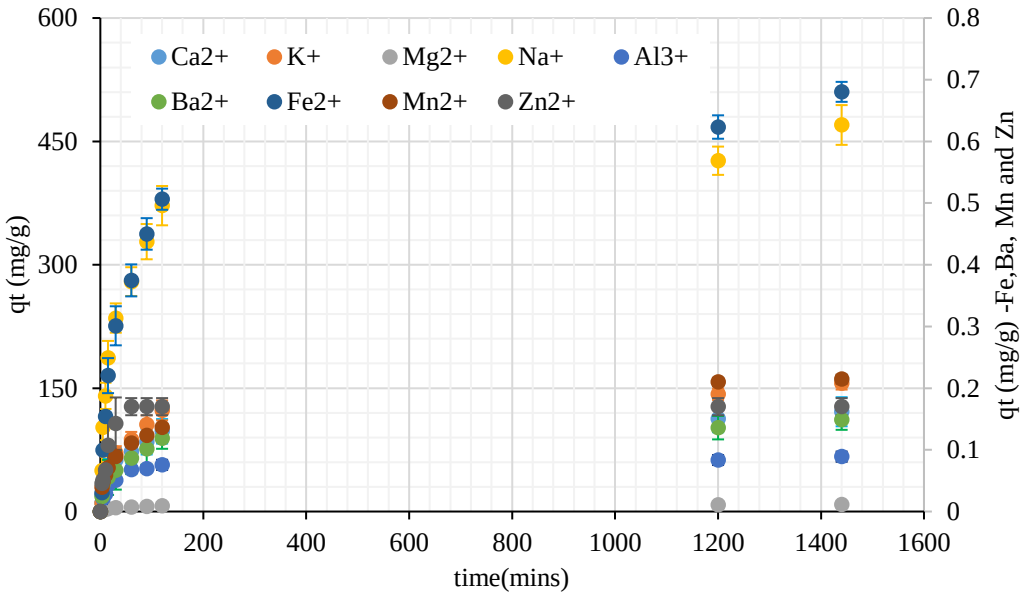

Experimental conditions; total volume of solution 100 ml, contact time 24 hrs, pH = pZc of bWHc: 10.6, bWHc dose: 1.0 g, temperature: 273 K; shaker 2.5 Hz.

Figure 4.29: Adsorption capacity of hydrochar on the metals present in HTL aqueous phase

It is noted that the adsorption capacity decreased in real wastewater compared to the synthetic mixtures due to increased dose. The adsorption of phenolics in the real wastewater was also investigated, and Figure 4.30 below shows the removal efficiency wt. (%) of the phenolics from wastewater

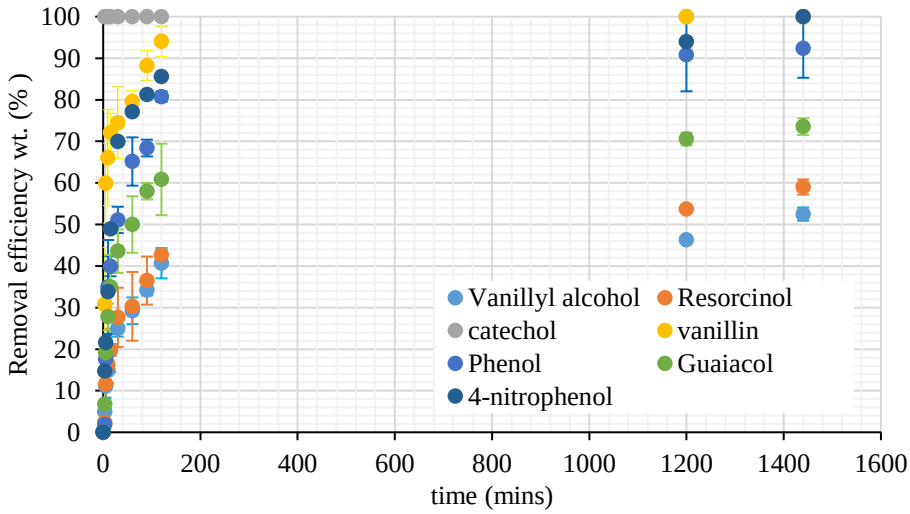

Experimental conditions; total volume of solution 100 ml, contact time 24 hrs, pH = pZc of bWHc: 10.6, bWHc dose: 1.0 g, temperature: 273 K; shaker 2.5 Hz.

Figure 4.30: Removal efficiency of phenolic compounds present in HTL aqueous phase

From Figure 4.30 above, the removal efficiency of vanillyl alcohol and resorcinol decreased by 8 % due to presence of other phenolics like catechol, vanillin, and 4-nitrophenol and other wastewater components like unidentified organic acids, phenolics, and oligomers. Phenol adsorption increased by over 15 %, while that of guaiacol by 8% because of the salting effect associated with more NaOH pH adjustment in the presence of organic acids and oligomers. Again, the increase in dosage contributed to the high removal efficiencies. The adsorption capacity of the hydrochar on phenolic compounds adsorption was also investigated, and Figure 4.31 below shows the adsorption capacity over time. As observed in Figure 4.29, hydrochar adsorption capacity decreases with an increase in dose from 1 g/L to 10 g/L of adsorption solution. Again, the presence of adsorbents of differing chemistries also decreases their hydrochar capacity.

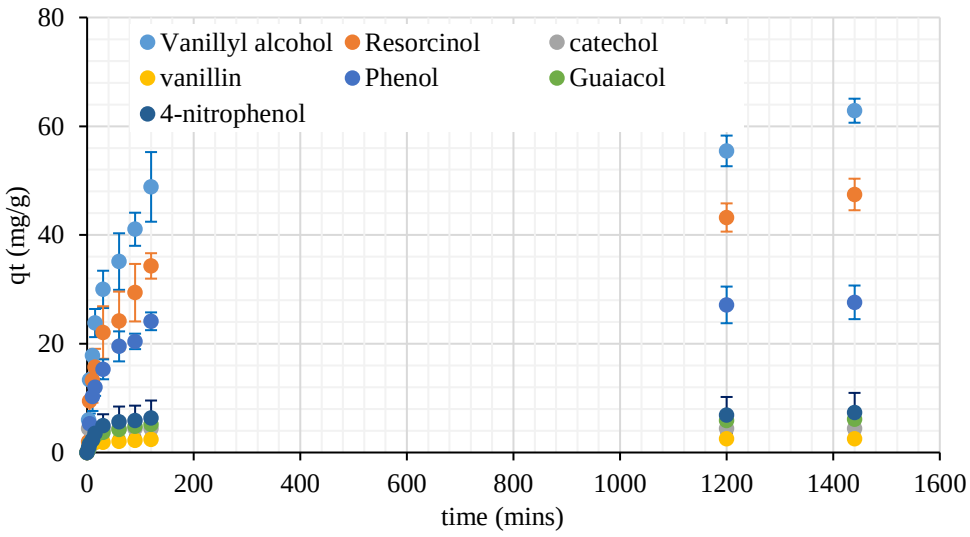

Experimental conditions; total volume of solution 100 ml, contact time 24 hrs, pH = pZc of bWHc: 10.6, bWHc dose: 1.0 g, temperature: 273 K; shaker 2.5 Hz.

Figure 4.31: Adsorption capacity of the phenolic compounds present in HTL aqueous phase

4.11.2 Recovery of adsorbed metals and phenolics

Recovery of adsorbed material on the hydrochar is crucial, especially for lignin-based phenolics, potentially reducing the dependence on fossil-based phenolics; hence the adsorbed components were recovered via adsorption-desorption experiments as described in Section 3.6.3. Table 4.19

below shows the mass of desorbed metal and the calculated percentage desorption from the equation.

$$\text{Desorption efficiency} = \frac{\text{amount of metal or phenolics desorbed}}{\text{amount of metal and phenolics adsorbed}} \quad 4.24$$

$$\% \text{ Desorption} = \text{desorption efficiency X } 100 \quad 4.25$$

Table 4.19: Desorption of metals

Adsorbate	Ca^{2+}	K^{+}	Mg^{2+}	Na^{+}	Al^{3+}	Ba^{2+}	Fe^{2+}	Mn^{2+}	Zn^{2+}
STDEV	±1.63	±2.45	±0.87	±7.13	±0.01	±0.03	±0.03	±0.02	±0.01
Mass adsorbed (mg)	250.89	312.64	22.96	888.50	0.05	0.29	0.87	0.28	0.15
Mass desorbed with 1M HCl (mg)	171.50	125.21	13.19	16.10	0.05	0.27	1.67	0.34	0.16
Mass desorbed with 1M KOH (mg)	0.61	-	0.11	33.45	0.09	0.01	0.03	-	-
Total desorption (mg)	172.11	125.21	13.30	49.55	0.14	0.27	1.70	0.34	0.16
% Desorption	69	40	58	6	287	96	195	124	104

Experimental condition contact time 2 hrs., bWHc dose 1.0 g, temperature: 273 K; shaker 1.9 Hz and 10 mL total volume

The 1.0 mol/L HCl efficiently desorbs over 50 % of the desorbed metals while the remaining(total desorption – base desorption) with were desorbed by1.0 mol/L KOH. The same was realised during the activation of hydrochar, as explained in Sections 4.3.1 and 4.3.2. Al^{3+}, Fe^{2+}, Mn^{2+}, Zn^{2+} and K^{+} have a desorption percentage of over 100 % due to desorption of already bound metals since the hydrochar used is base activated. The KOH based desorption also introduced the extra K^{+}. By comparing synthetic desorption and real wastewater desorption, the presence of other metals and organic acids tends to lower both the adsorption and desorption of the metals. Therefore, it can be concluded that 50 % of the metals are recovered using 1.0 mol/L HCl; hence, the hydrochar is achievable. Table 4.20 below shows the mass of desorbed phenolics and the calculated desorption percentage.

Table 4.20:Desorption of phenolic compounds

Adsorbate	Vanillyl alcohol	Resorcinol	catechol	vanillin	Phenol	Guaiacol	4-nitrophenol
STDEV	±0.48	±0.87	±0.16	±0.09	±0.02	±0.13	±0.11

Mass adsorbed (mg)	104.19	69.05	3.96	2.45	28.88	8.82	8.17
Mass desorbed with 1M HCl (mg)	0.00	0.00	0.00	0.00	0.00	0.00	0.00
Mass desorbed with 1M KOH (mg)	33.12	18.44	1.33	0.38	10.86	2.78	1.96
Total desorption (mg)	33.12	18.44	1.33	0.38	10.86	2.78	1.96
% Desorption	32	27	34	16	38	32	24

Experimental conditions contact time 2 hrs, bWHc dose: 1.0 g, temperature: 273 K; shaker 1.9 Hz and 10 ml total volume.

The desorption of phenols is quite low due to the reduced salting-out effect in the presence of other organic molecules but achievable. Therefore, recovery of phenolic compounds is possible, and optimisation is required. Hence the recovered phenolics can reduce the dependency of industries, e.g., pharmaceutical companies, on fossil-based phenolic compounds with the hope of completely replacing them.

4.11.3 Reusability of the hydrochar

The hydrochar reusability and regeneration were determined by performing adsorption and desorption experiments on the same hydrochar described in Section 3.7.2. Figure 4.32 below shows percentages of metals adsorbed and adsorbed calculated from the mass adsorbed and desorbed in Annexure A: for the six cycles performed.

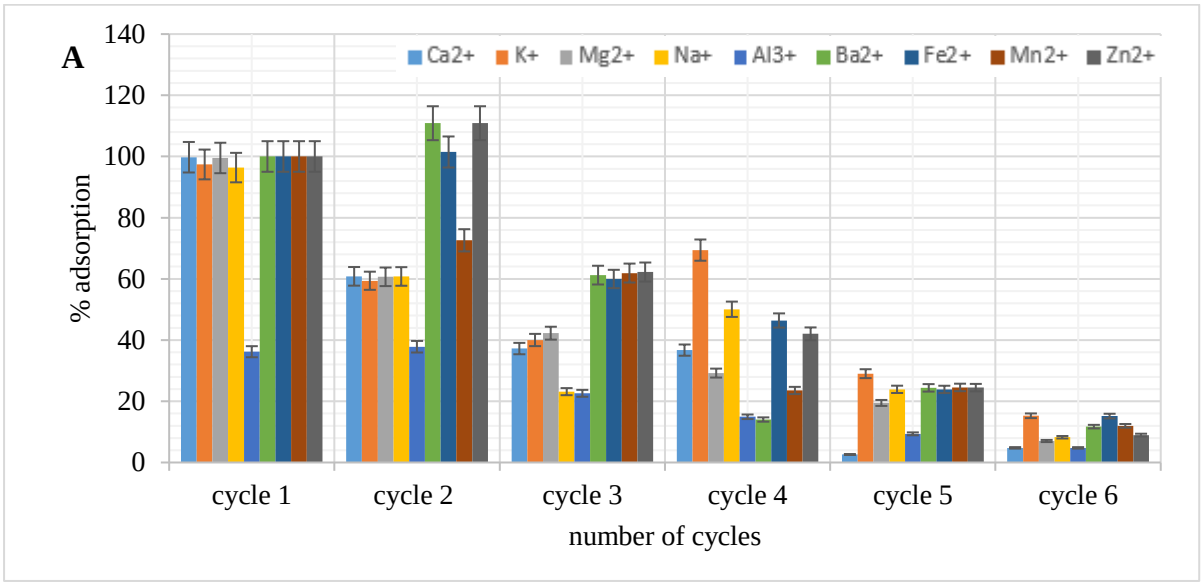

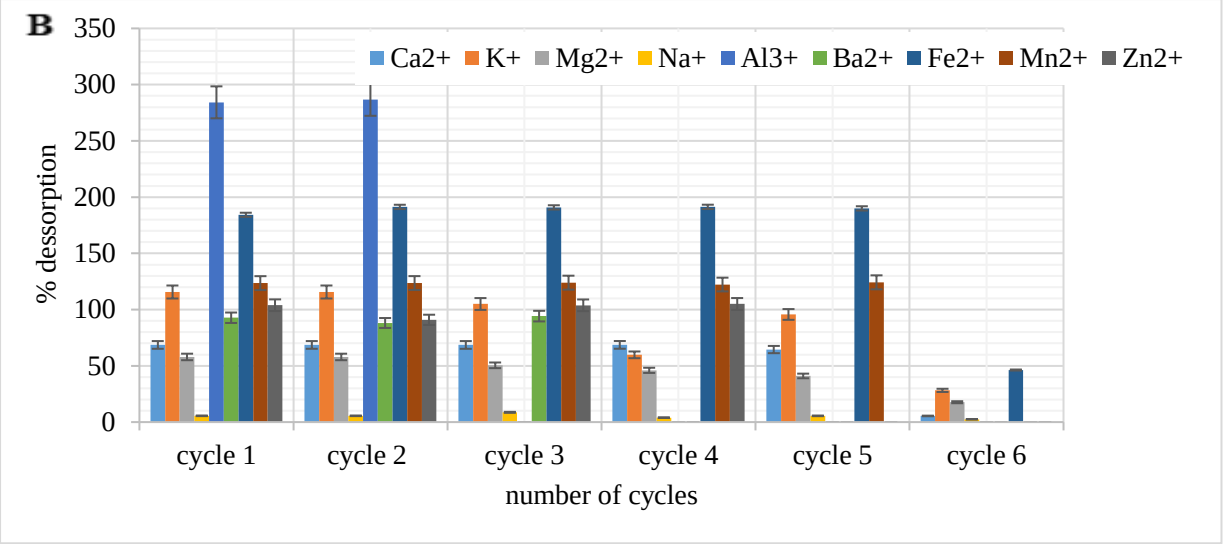

Experimental conditions contact time 2 hrs, bWHc dose: 10.0 g, temperature: 273 K; shaker 1.9 Hz and 50 ml total volume

Figure 4.32: Percentages of metal adsorbed (A) and desorbed (B) per given cycle

As the number of cycles increases, the percentage of adsorption decreases because the since desorption is not 100 %, some metals are still bound to the hydrochar, preventing further adsorption. The percentage desorption is low because the desorption reagent removed the bound metals from the previous and current cycle. Since the hydrochar used was base activated, most metals remained bound to the hydrochar, and upon desorption, they were washed off with the acid HCl. Thus, K^+, Al^{3+} and all the heavy metals percentage desorption of over 100 %. The desorption reagent KOH further introduced more K^+ onto the hydrochar hence increasing the number of metals desorbed. After the third cycle, the desorption efficiency drops below 10 % because of poor adsorption and continued desorption. Furthermore, the adsorption and desorption cycles continue to wear out the adsorbent. However, five cycles are achievable for significant adsorption and desorption of adsorbates; hence hydrochar is a cost-effective adsorbed that can be reused for at least four cycles.

Figure 4.33 below illustrates the percentage adsorption and desorption of phenolic compounds per adsorption-desorption cycle.

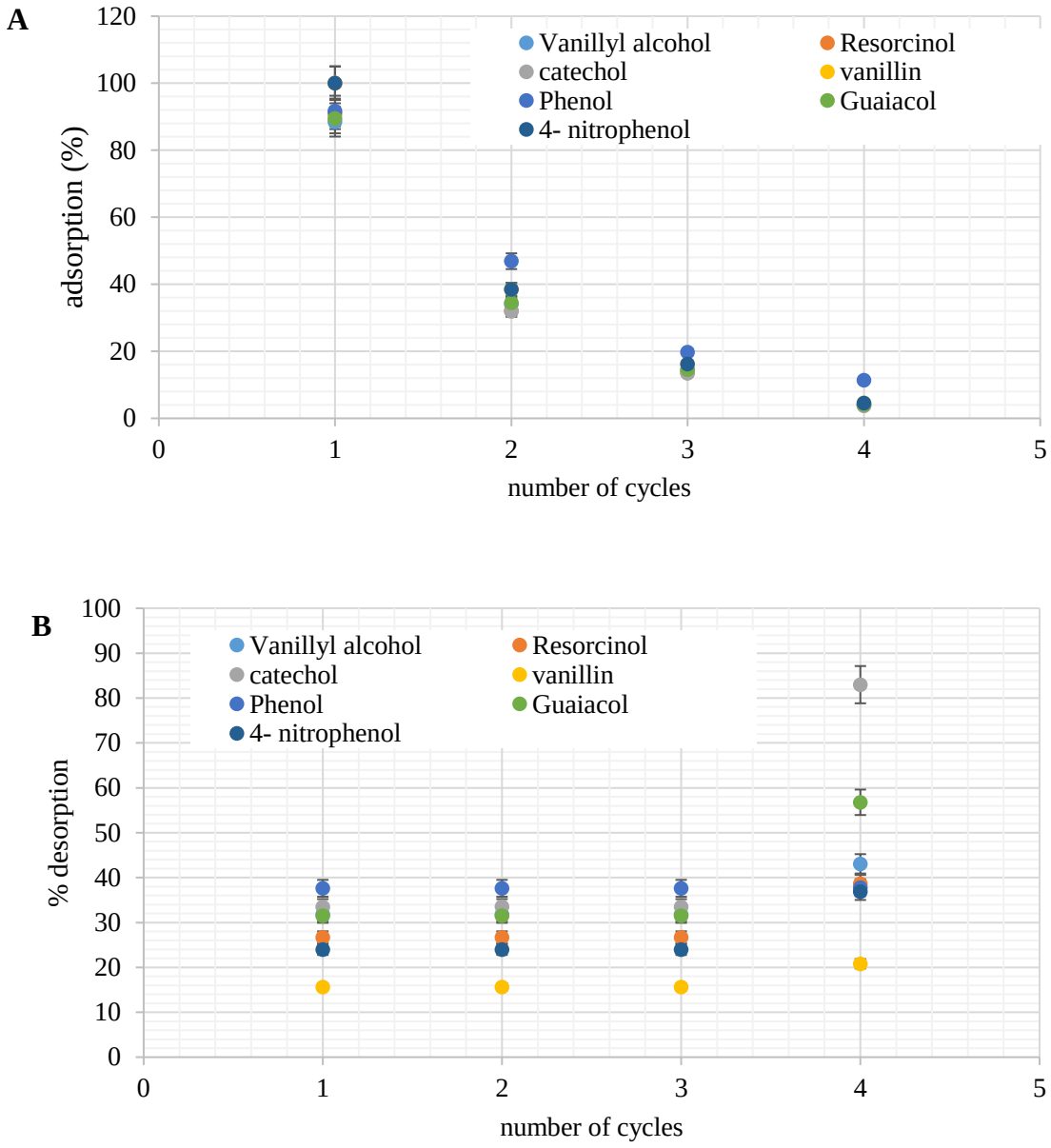

Experimental conditions: contact time 2hrs, bWHc dose: 10.0 g, temperature: 273 K; shaker 1.9 Hz and 50 ml total volume

Figure 4.33: Percentages of phenolic compounds adsorbed (A) and desorbed (B) per given cycle

The same trend is noted in phenolics as in metals. However, the adsorption and desorption of phenolics are less efficient because of their bulky size hence more efficient in blocking the pores and preventing further adsorption. And it can be concluded that in this study, a significant amount of both adsorption and desorption is only effective in three cycles. Therefore, it can be concluded that hydrochar is a cost-effective adsorbent in the recovery of valuable phenolics in the HTL

aqueous phase that have potential use in pharmaceuticals and food industries. However, in future the desorption process requires optimisation and (or) other desorption reagent should be explored for a much more higher percentage desorption.

REFERENCES

Aharoni, C. and Tompkins, F.C. 1970. Kinetics of Adsorption and Desorption and the Elovich Equation. *Advances in Catalysis*. 21(C):1–49.

Ahmed, M.J. and Theydan, S.K. 2012. Equilibrium isotherms, kinetics and thermodynamics studies of phenolic compounds adsorption on palm-tree fruit stones. *Ecotoxicology and Environmental Safety*. 84:39–45.

Al-Qahtani, K.M. 2016. Water purification using different waste fruit cortexes for the removal of heavy metals. *Journal of Taibah University for Science*. 10:700–708.

Begum, S.A., Golam Hyder, A.H.M., Hicklen, Q., Crocker, T. and Oni, B. 2021. Adsorption characteristics of ammonium onto biochar from an aqueous solution. *Journal of Water Supply: Research and Technology - AQUA*. 70(1).

Chen, K., Lyu, H., Hao, S., Luo, G., Zhang, S. and Chen, J. 2015. Separation of phenolic compounds with modified adsorption resin from aqueous phase products of hydrothermal liquefaction of rice straw. *Bioresource Technology*. 182:160–168.

Clemente, J.S., Beauchemin, S., MacKinnon, T., Martin, J., Johnston, C.T. and Joern, B. 2017. Initial biochar properties related to the removal of As, Se, Pb, Cd, Cu, Ni, and Zn from an acidic suspension. *Chemosphere*. 170:216–224.

Crini, G., Lichtfouse, E., Wilson, L.D. and Morin-Crini, N. 2019. Conventional and non-conventional adsorbents for wastewater treatment. *Environmental Chemistry Letters*. 17(1):195–213.

Girish, C.R. and Murty, V.R. 2016. Mass transfer studies on adsorption of phenol from wastewater using Lantana camara, forest waste. *International Journal of Chemical Engineering*. 2016.

Johnson, B.B. 1990. Effect of pH, Temperature, and Concentration on the Adsorption of Cadmium on Goethite. https://pubs.acs.org/sharingguidelines Date of access: 23 Mar. 2021.

Komkiene, J. and Baltrenaite, E. 2016. Biochar as adsorbent for removal of heavy metal ions [Cadmium (II), Copper (II), Lead (II), Zinc (II)] from aqueous phase. International Journal of Environmental Science and Technology. 3:13.

Lv, Z., Yang, S., Liu, Y., Zhou, J., Xing, L. and Chen, L. 2018. The novel PEI-modified biochars and their application for the efficient elimination of Cr (VI) from aqueous solutions. *Water Science and Technology*. 77(8):2045–2056.

Marais, H.B., Marx, S. and Venter, R.J. 2019. Valorisation of waste lignin for phenolic derivative compounds using hydrothermal liquefaction. 27th European Biomass Conference and Exhibition, 27-30 May 2019, Lisbon, Portugal

Marx, S., Venter, R.J., Stols, C. and Bartlett, D. 2019. Predictive model for fuels from hydrothermal liquefaction. 27th European Biomass Conference and Exhibition, 27-30 May 2019, Lisbon, Portugal (May):27–30.

Mendoza-castillo, D.I. 2017. Adsorption Processes for Water Treatment and Purification. H. Elizabeth and Reynel-Ávila, eds. 1st ed. Cham, Switzerland: Springer International Publishing.

Peers, A.M. 1965. Elovich adsorption kinetics and the heterogeneous surface. *Journal of Catalysis*. 4(4):499–503.

Sangi, M.R., Shahmoradi, A., Zolgharnein, J., Azimi, G.H. and Ghorbandoost, M. 2008. Removal and recovery of heavy metals from aqueous solution using Ulmus carpinifolia and Fraxinus excelsior tree leaves. *Journal of Hazardous Materials*. 155(3):513–522.

Singh, P.K., Banerjee, S., Srivastava, A.L. and Chandra Sharma, Y. 2017. Kinetic and equilibrium modeling for removal of nitrate from aqueous solutions and drinking water by a potential adsorbent, hydrous bismuth oxide. Department of Civil Engineering, University of Allahabad, Allaha. Mumbai, India.

Taşar, Ş. and Özer, A. 2020. A thermodynamic and kinetic evaluation of the adsorption of Pb (II) ions using peanut (Arachis hypogaea) shell-based biochar from aqueous media. *Polish Journal of Environmental Studies*. 29(1):3571-3579

Tong, X.J., Li, J.Y., Yuan, J.H. and Xu, R.-K. 2011. Adsorption of Cu (II) by biochars generated from three crop straws. *Chemical Engineering Journal*. 172(2–3):828–834.

Viegas, R.M.C., Campinas, M., Costa, H. and Rosa, M.J. 2014. How do the HSDM and Boyd's model compare for estimating intraparticle diffusion coefficients in adsorption processes. *Adsorption.* 20(5–6):737–746.

Wang, Y. and Liu, R. 2017. Comparison of characteristics of twenty-one types of biochar and their ability to remove multi-heavy metals and methylene blue in solution. *Fuel.* 160:55–63.

Watson, J., Wang, T., Si, B., Chen, W.T., Aierzhati, A. and Zhang, Y. 2020. Valorization of hydrothermal liquefaction aqueous phase: pathways towards commercial viability. *Progress in Energy and Combustion Science*. 77:100819.

Wu, S.Y., Peng, W.C., Wu, Y.Q., Gao, J.S., Qin, X.G. and Nie, L. 2013. Characteristics of liquid products from hydrothermal liquefaction of typical crop straws under CO atmosphere. *Journal of the Energy Institute*. 86(3):134–139.

5.1.1 Conclusion

The HTL of the organic phase of municipal solid waste was successfully synthesised the potential adsorbent hydrochar and a complex wastewater HTL-aqueous phase. The HTL-AQ contained alkali, alkaline earth metals, heavy metals, phenolic chemicals, organic acids, and oligomers, which completely reflect most industrial wastewaters. Hydrochar was discovered to be a possible low-cost adsorbent with over 63 % carbon content, porous surface topography with a pore diameter in the range of 1-34 nm. The hydrochar also has a high surface area above 50 m^2/g surface area and oxygen containing functional groups (-COOH, -OH, -CO-). Post hydrochar treatment, washing with 1.0 mol/L HCl and 1.0 mol/L KOH removed some of the metal and phenolics attached to the hydrochar, improving the adsorption of metals and phenolic compounds onto the hydrochar. The pH of hydrochar did not affect the adsorption process as the pZc of RHc pH 6.0, aWHc 6.3 and bWHc 10.6 were used in batch adsorption experiments. The hydrochar was fully saturated with metals and phenolics in 120 minutes. The 1.0 g was an economic hydrochar dose that supported adsorption of metals and phenolics and was an efficient even at lower adsorbate concentrations. Elevated temperatures (318K) improve adsorption of phenolics by 12 %, while that of metals decreases by 5%. The basic pH had little effect on metal adsorption. However, the basic pH favours phenolic adsorption and precipitation of metals e.g., Mg^{2+}. Hydrochar allowed co-adsorption of metals and phenolics; hence the two were simultaneously and effectively removed from wastewaters.

Metal and phenolic compounds adsorption was best described by pseudo-second-order kinetics, which suggest the adsorption on heterogeneous surfaces and the process is limited by diffusion into small pores. The intraparticle diffusion is the rate limiting step in metal and phenolics adsorption onto the hydrochar. The adsorption of phenol Ca^{2+} and Mg^{2+} was best described with Henry's isotherm recommending a linear relationship between the fluid and adsorbed phases. Guaiacol, vanillyl alcohol, resorcinol, K^+ and Na^+ by the Freundlich isotherm propose adsorption on heterogeneity surface. Both Temkin and Dubinin-Radushkevich confirm a physisorption process. The adsorption of metals and phenolics is a feasible process (negative Gibbs free energy values), with phenolic adsorption as an endothermic process while metal adsorption is an exothermic process. The presents of multiple adsorbates (in HTL aqueous phase) lowered the removal of both metals and phenolics by 8-15 %. The 1.0 mol/L KOH recovered adsorbed

phenolics, whereas 1.0 mol/L HCl recovered adsorbed metal, regenerating the hydrochar. The hydrochar was competently reused for metal and phenolics adsorption up to the fourth and third cycles, respectively. Hydrochar is a cost-effective adsorbent applicable in recovering valuable compounds, e.g., bio-based phenolics that can replace fossil-based phenolics. Therefore, the study concludes that hydrochar is an excellent adsorbent that can simultaneously remove metals and phenolics from complex wastewaters (HTL aqueous phase).

5.1.2 Recommendations

The activation of hydrochar with both HCl and KOH is recommended for further improved adsorption for both metals and phenolics since both effectively remove already bound metal and phenolics, which negatively affect the adsorption process.

The hydrochar assessment on its environmental interaction at its different life stages presents a further understanding of the whole adsorption process. Its uses, disposal, energy inputs and output emissions are analysed, thus providing adsorbent competencies and limitations. Singh *et al.,* 2019 and Shakoor *et al.,*2020) results indicated that hydrochar has lower energy demands and global warming potential impacts when compared to ACs. With several proposed adsorbents in water remediation, their environmental impacts are insufficiently provided. Therefore, their industrialisation and commercialisation are debatable. On this basis, improper discharge of exhausted hydrochar could compromise the cost of the whole wastewater treatment; hence further studies are required on hydrochar discharge techniques. It is mandatory to assess the novel adsorbent advantages and limitations, environmental and economic perspectives using the life cycle analysis.

Further studies on the identification and synthesis routes development of the industrial adsorbent with outstanding water remediation properties are still required.

ANNEXURE A: CALIBRATION DATA

HPLC CALIBRATION DOCUMENTS

https://1drv.ms/u/s!Ao-u6CeUBCQ2gokUBAeG_UcM_Pvv0Q?e=Q9ySBb

ANNEXURE B: FACTORS AFFECTING ADSORPTION PROCESS RAW DATA

Effect of dose on Metal adsorption

		Concentration (ppm)					**Time (min)**	**Volume (ml)**	**Mass removed(mg)**				
Sample ID	0	Ca^{2+}	K^{+}	Mg^{2+}	Na^{+}	Fe^{2+}			Ca^{2+}	K^{+}	Mg^{2+}	Na^{+}	Fe^{2+}
0.1g	run 1	375.5	2142.2	23.4	590.2	36.4	0.0	100.0	0.0	0.0	0.0	0.0	0.0
0.1g		325.8	1961.6	19.3	588.0	0.0	3.0	95.0	6.6	27.9	0.5	3.2	3.6
0.1g		356.1	1927.0	19.5	610.5	0.0	5.0	90.0	5.5	40.8	0.6	4.1	3.6
0.1g		351.9	1987.6	19.1	606.5	0.0	10.0	85.0	7.6	45.3	0.7	7.5	3.6
0.1g		342.9	1950.5	17.7	606.8	0.0	15.0	80.0	10.1	58.2	0.9	10.5	3.6
0.1g		333.9	1892.6	15.1	604.5	0.0	30.0	75.0	12.5	72.3	1.2	13.7	3.6
0.1g		346.9	1904.5	14.3	601.8	0.0	60.0	70.0	13.3	80.9	1.3	16.9	3.6
0.1g		331.0	1980.2	14.4	633.2	0.0	90.0	65.0	16.0	85.5	1.4	17.9	3.6
0.1g		332.1	1943.3	16.9	608.1	0.0	120.0	60.0	17.6	97.6	1.3	22.5	3.6

0.1g	run 2	350.5	2004.0	19.0	610.3	3.8	0.0	100.0	0.0	0.0	0.0	0.0	0.0
0.1g		339.9	1972.2	13.4	606.1	0.0	3.0	95.0	2.8	13.0	0.6	3.5	0.4
0.1g		344.7	1885.3	13.4	595.7	0.0	5.0	90.0	4.0	30.7	0.7	7.4	0.4
0.1g		352.9	1892.6	18.9	603.8	0.0	10.0	85.0	5.1	39.5	0.3	9.7	0.4
0.1g		346.3	1913.2	18.7	602.3	0.0	15.0	80.0	7.3	47.3	0.4	12.9	0.4
0.1g		340.9	1905.4	18.4	593.3	0.0	30.0	75.0	9.5	57.5	0.5	16.5	0.4
0.1g		331.1	1889.3	18.1	605.9	0.0	60.0	70.0	11.9	68.2	0.6	18.6	0.4
0.1g		322.8	1992.8	12.3	601.0	0.0	90.0	65.0	14.1	70.9	1.1	22.0	0.4
0.1g		328.3	1936.1	17.6	605.9	0.0	120.0	60.0	15.4	84.2	0.8	24.7	0.4
0.1g	run 3	346.8	2015.0	17.4	596.1	6.1	0.0	100.0	0.0	0.0	0.0	0.0	0.0
0.1g		348.3	1898.8	14.2	591.4	0.0	3.0	95.0	1.6	21.1	0.4	3.4	0.6
0.1g		336.4	1824.0	18.8	637.6	0.0	5.0	90.0	4.4	37.3	0.0	2.2	0.6
0.1g		315.0	1799.4	12.6	578.9	0.0	10.0	85.0	7.9	48.5	0.7	10.4	0.6
0.1g		343.1	1900.8	17.9	600.6	0.0	15.0	80.0	7.2	49.4	0.3	11.6	0.6
0.1g		317.9	1877.4	17.2	593.1	0.0	30.0	75.0	10.8	60.7	0.4	15.1	0.6
0.1g		328.3	1822.9	17.2	586.4	0.0	60.0	70.0	11.7	73.9	0.5	18.6	0.6
0.1g		321.6	1894.1	13.7	586.8	0.0	90.0	65.0	13.8	78.4	0.8	21.5	0.6
0.1g		309.0	1806.1	17.0	577.3	0.0	120.0	60.0	16.1	93.1	0.7	25.0	0.6
0.5g	run 1	368.6	1832.4	21.8	608.2	20.4	0.0	100.0	0.0	0.0	0.0	0.0	0.0
0.5g		283.7	1909.9	17.0	598.9	0.0	3.0	95.0	9.9	1.8	0.6	3.9	2.0

0.5g		307.8	1894.2	14.7	599.6	0.0	5.0	90.0	9.2	12.8	0.9	6.8	2.0
0.5g		300.2	1866.5	17.8	599.9	0.0	10.0	85.0	11.3	24.6	0.7	9.8	2.0
0.5g		290.4	1850.1	18.8	600.5	0.0	15.0	80.0	13.6	35.2	0.7	12.8	2.0
0.5g		278.0	1865.9	15.7	589.9	0.0	30.0	75.0	16.0	43.3	1.0	16.6	2.0
0.5g		258.5	1920.1	16.0	598.5	0.0	60.0	70.0	18.8	48.8	1.1	18.9	2.0
0.5g		255.3	1936.7	14.4	593.3	0.0	90.0	65.0	20.3	57.4	1.2	22.2	2.0
0.5g		246.6	1921.0	12.8	583.7	0.0	120.0	60.0	22.1	68.0	1.4	25.8	2.0
0.5g	run 2	338.6	1786.8	16.2	586.4	2.8	0.0	100.0	0.0	0.0	0.0	0.0	0.0
0.5g		280.2	1856.4	16.2	577.9	0.0	3.0	95.0	7.2	2.3	0.1	3.7	0.3
0.5g		279.2	1863.2	15.3	582.6	0.0	5.0	90.0	8.7	11.0	0.2	6.2	0.3
0.5g		286.9	1886.0	13.3	580.1	0.0	10.0	85.0	9.5	18.4	0.5	9.3	0.3
0.5g		266.8	1908.6	14.5	575.8	0.0	15.0	80.0	12.5	26.0	0.5	12.6	0.3
0.5g		287.3	1882.7	16.4	584.4	0.0	30.0	75.0	12.3	37.5	0.4	14.8	0.3
0.5g		254.2	1908.7	13.5	599.4	0.0	60.0	70.0	16.1	45.1	0.7	16.7	0.3
0.5g		273.7	1885.3	13.5	609.3	0.0	90.0	65.0	16.1	56.1	0.7	19.0	0.3
0.5g		255.9	2027.4	14.2	629.5	0.0	120.0	60.0	18.5	57.0	0.8	20.9	0.3
0.5g	run 3	347.2	1811.0	16.9	622.1	1.9	0.0	100.0	0.0	0.0	0.0	0.0	0.0
0.5g		312.5	1878.4	17.3	621.5	0.0	3.0	95.0	5.0	2.6	0.0	3.2	0.2
0.5g		287.2	1931.8	15.0	616.1	0.0	5.0	90.0	8.9	7.2	0.3	6.8	0.2
0.5g		276.7	1870.2	15.8	602.2	0.0	10.0	85.0	11.2	22.1	0.3	11.0	0.2

0.5g		276.1	1851.9	14.5	605.5	0.0	15.0	80.0	12.6	32.9	0.5	13.8	0.2
0.5g		294.9	1897.8	19.7	603.5	0.0	30.0	75.0	12.6	38.8	0.2	16.9	0.2
0.5g		274.1	1872.6	18.2	602.2	0.0	60.0	70.0	15.5	50.0	0.4	20.1	0.2
0.5g		272.7	1905.8	18.1	607.0	0.0	90.0	65.0	17.0	57.2	0.5	22.8	0.2
0.5g		268.0	1897.3	13.5	602.7	0.0	120.0	60.0	18.6	67.3	0.9	26.1	0.2
0.75g	run 1	361.0	1829.6	23.7	552.2	5.8	0.0	100.0	0.0	0.0	0.0	0.0	0.0
0.75g		319.7	1891.8	17.1	544.5	0.0	3.0	95.0	5.7	3.2	0.7	3.5	0.6
0.75g		309.7	1915.7	18.0	544.1	0.0	5.0	90.0	8.2	10.5	0.7	6.2	0.6
0.75g		298.5	1935.5	13.8	561.7	0.0	10.0	85.0	10.7	18.4	1.2	7.5	0.6
0.75g		294.7	1946.4	14.8	553.8	0.0	15.0	80.0	12.5	27.2	1.2	10.9	0.6
0.75g		276.2	1988.9	14.7	554.2	0.0	30.0	75.0	15.4	33.8	1.3	13.7	0.6
0.75g		253.6	2018.5	7.3	544.6	0.0	60.0	70.0	18.3	41.7	1.9	17.1	0.6
0.75g		253.9	1965.5	7.2	545.2	0.0	90.0	65.0	19.6	55.2	1.9	19.8	0.6
0.75g		237.6	2073.9	10.2	544.3	0.0	120.0	60.0	21.8	58.5	1.8	22.6	0.6
0.75g	run 2	368.1	1863.5	10.1	543.8	15.5	0.0	100.0	0.0	0.0	0.0	0.0	0.0
0.75g		297.8	1955.4	7.1	529.7	0.0	3.0	95.0	8.5	0.6	0.3	4.1	1.6
0.75g		286.6	1956.8	6.2	521.4	0.0	5.0	90.0	11.0	10.2	0.5	7.4	1.6
0.75g		289.6	1997.5	7.0	526.9	0.0	10.0	85.0	12.2	16.6	0.4	9.6	1.6
0.75g		277.4	1985.9	6.0	523.9	0.0	15.0	80.0	14.6	27.5	0.5	12.5	1.6
0.75g		267.0	2074.9	6.7	515.0	0.0	30.0	75.0	16.8	30.7	0.5	15.8	1.6

0.75g		240.2	2015.4	6.5	512.1	0.0	60.0	70.0	20.0	45.3	0.6	18.5	1.6
0.75g		236.2	2027.6	8.9	515.7	0.0	90.0	65.0	21.5	54.6	0.4	20.9	1.6
0.75g		226.3	2033.6	5.9	519.9	0.0	120.0	60.0	23.2	64.3	0.7	23.2	1.6
0.75g	run 3	343.7	1976.3	9.3	517.9	2.8	0.0	100.0	0.0	0.0	0.0	0.0	0.0
0.75g		289.4	2017.0	7.3	506.9	0.0	3.0	95.0	6.9	6.0	0.2	3.6	0.3
0.75g		290.6	1932.6	9.3	506.3	0.0	5.0	90.0	8.2	23.7	0.1	6.2	0.3
0.75g		280.9	1931.3	5.8	504.9	0.0	10.0	85.0	10.5	33.5	0.4	8.9	0.3
0.75g		269.6	1950.3	7.0	509.7	0.0	15.0	80.0	12.8	41.6	0.4	11.0	0.3
0.75g		264.4	1970.4	6.6	506.4	0.0	30.0	75.0	14.5	49.8	0.4	13.8	0.3
0.75g		230.1	1942.8	7.3	498.4	0.0	60.0	70.0	18.3	61.6	0.4	16.9	0.3
0.75g		222.8	1945.8	7.1	498.6	0.0	90.0	65.0	19.9	71.1	0.5	19.4	0.3
0.75g		225.4	1985.5	7.4	516.1	0.0	120.0	60.0	20.9	78.5	0.5	20.8	0.3
1.0g	run 1	405.7	1812.3	23.6	391.7	1.3	0.0	100.0	0.0	0.0	0.0	0.0	0.0
1.0g		354.6	1954.0	21.9	397.2	0.0	3.0	95.0	6.9	-4.4	0.3	1.4	0.1
1.0g		349.7	1955.6	21.8	397.7	0.0	5.0	90.0	9.1	5.2	0.4	3.4	0.1
1.0g		336.6	1938.6	20.3	396.6	0.0	10.0	85.0	12.0	16.5	0.6	5.5	0.1
1.0g		331.5	1972.1	21.1	394.9	0.0	15.0	80.0	14.1	23.5	0.7	7.6	0.1
1.0g		320.9	1980.1	21.3	401.4	0.0	30.0	75.0	16.5	32.7	0.8	9.1	0.1
1.0g		305.6	2020.7	20.8	401.3	0.0	60.0	70.0	19.2	39.8	0.9	11.1	0.1
1.0g		293.9	1979.1	20.3	406.5	0.0	90.0	65.0	21.5	52.6	1.0	12.7	0.1

1.0g		285.1	2023.4	19.8	404.7	0.0	120.0	60.0	23.5	59.8	1.2	14.9	0.1
1.0g	run 2	413.5	1872.6	23.6	407.0	2.8	0.0	100.0	0.0	0.0	0.0	0.0	0.0
1.0g		363.8	1975.8	21.9	403.0	0.0	3.0	95.0	6.8	-0.4	0.3	2.4	0.3
1.0g		353.5	1966.3	21.3	402.0	0.0	5.0	90.0	9.5	10.3	0.4	4.5	0.3
1.0g		343.9	1978.8	21.0	403.3	0.0	10.0	85.0	12.1	19.1	0.6	6.4	0.3
1.0g		336.1	1969.4	20.7	400.6	0.0	15.0	80.0	14.5	29.7	0.7	8.7	0.3
1.0g		319.0	2008.2	20.6	401.5	0.0	30.0	75.0	17.4	36.6	0.8	10.6	0.3
1.0g		304.2	2032.0	20.0	403.5	0.0	60.0	70.0	20.1	45.0	1.0	12.5	0.3
1.0g		287.5	1992.9	19.3	400.2	0.0	90.0	65.0	22.7	57.7	1.1	14.7	0.3
1.0g		281.2	2009.0	19.8	396.8	0.0	120.0	60.0	24.5	66.7	1.2	16.9	0.3
1.0g	run 3	413.8	1824.6	23.9	403.8	3.5	0.0	100.0	0.0	0.0	0.0	0.0	0.0
1.0g		350.3	1922.9	21.5	389.5	0.0	3.0	95.0	8.1	-0.2	0.3	3.4	0.4
1.0g		346.4	1968.8	20.6	396.6	0.0	5.0	90.0	10.2	5.3	0.5	4.7	0.4
1.0g		336.6	1977.2	20.5	395.1	0.0	10.0	85.0	12.8	14.4	0.6	6.8	0.4
1.0g		332.2	1902.8	21.3	397.8	0.0	15.0	80.0	14.8	30.2	0.7	8.6	0.4
1.0g		318.7	1975.0	20.9	399.9	0.0	30.0	75.0	17.5	34.3	0.8	10.4	0.4
1.0g		304.1	1976.8	20.1	396.7	0.0	60.0	70.0	20.1	44.1	1.0	12.6	0.4
1.0g		289.3	1980.0	20.1	406.6	0.0	90.0	65.0	22.6	53.8	1.1	14.0	0.4
1.0g		290.3	2049.3	20.1	408.2	0.0	120.0	60.0	24.0	59.5	1.2	15.9	0.4

2.0g	run 1	428.0	1827.9	24.9	414.5	4.1	0.0	100.0	0.0	0.0	0.0	0.0	0.0
2.0g		324.2	2084.3	20.9	403.5	0.0	3.0	95.0	12.0	-15.2	0.5	3.1	0.4
2.0g		309.5	2078.9	20.5	398.4	0.0	5.0	90.0	14.9	-4.3	0.6	5.6	0.4
2.0g		289.0	2120.3	19.8	409.7	0.0	10.0	85.0	18.2	2.6	0.8	6.6	0.4
2.0g		271.8	2181.9	19.0	405.6	0.0	15.0	80.0	21.1	8.2	1.0	9.0	0.4
2.0g		245.4	2193.1	19.1	400.2	0.0	30.0	75.0	24.4	18.3	1.1	11.4	0.4
2.0g		221.9	2216.7	18.9	408.0	0.0	60.0	70.0	27.3	27.6	1.2	12.9	0.4
2.0g		200.7	2164.5	18.1	402.4	0.0	90.0	65.0	29.8	42.1	1.3	15.3	0.4
2.0g		191.6	2210.4	17.8	400.8	0.0	120.0	60.0	31.3	50.2	1.4	17.4	0.4
2.0g	run 2	420.9	1853.2	25.9	413.4	3.5	0.0	100.0	0.0	0.0	0.0	0.0	0.0
2.0g		316.9	1901.6	21.1	389.4	0.0	3.0	95.0	12.0	4.7	0.6	4.3	0.3
2.0g		299.9	2110.2	20.5	409.8	4.1	5.0	90.0	15.1	-4.6	0.7	4.5	0.0
2.0g		284.1	2109.2	20.8	390.5	0.0	10.0	85.0	17.9	6.0	0.8	8.1	0.3
2.0g		281.6	2150.1	20.9	410.0	0.0	15.0	80.0	19.6	13.3	0.9	8.5	0.3
2.0g		248.4	2123.7	19.5	399.9	0.0	30.0	75.0	23.5	26.0	1.1	11.4	0.3
2.0g		220.3	2188.3	18.1	419.3	0.0	60.0	70.0	26.7	32.1	1.3	12.0	0.3
2.0g		198.0	2160.7	17.8	401.1	0.0	90.0	65.0	29.2	44.9	1.4	15.3	0.3
2.0g		190.0	2124.8	17.8	401.1	0.0	120.0	60.0	30.7	57.8	1.5	17.3	0.3
2.0g	run 3	418.0	1785.9	24.0	410.0	2.5	0.0	100.0	0.0	0.0	0.0	0.0	0.0

2.0g		322.0	2103.0	21.3	399.3	0.0	3.0	95.0	11.2	-21.2	0.4	3.1	0.2
2.0g		310.5	2174.5	21.0	404.9	0.0	5.0	90.0	13.9	-17.1	0.5	4.6	0.2
2.0g		286.1	2159.7	20.0	396.7	0.0	10.0	85.0	17.5	-5.0	0.7	7.3	0.2
2.0g		271.9	2189.3	19.7	393.4	0.0	15.0	80.0	20.1	3.4	0.8	9.5	0.2
2.0g		242.6	2236.5	19.0	396.2	0.0	30.0	75.0	23.6	10.9	1.0	11.3	0.2
2.0g		216.4	2233.3	18.2	394.6	0.0	60.0	70.0	26.7	22.3	1.1	13.4	0.2
2.0g		200.5	2225.6	18.5	399.6	0.0	90.0	65.0	28.8	33.9	1.2	15.0	0.2
2.0g		190.4	2236.3	17.1	401.5	0.0	120.0	60.0	30.4	44.4	1.4	16.9	0.2

Effect of dose on phenolic compounds adsorption

	Areas							**Mass removed mg**			
dose	Gallic acid	Vanillyl alcohol	Resorcinol	Phenol	Guaiacol	Time mins	volume ml	Vanillyl alcohol	Resorcinol	Phenol	Guaiacol
0.1g bWHc	3929	1369	841	322	3288	0	100	0	0	0	0
0.1g bWHc	3133	1118	740	245	2009	3	95	2	0	11	30
0.1g bWHc	3650	1297	851	291	2399	5	90	5	3	12	35
0.1g bWHc	3558	1366	842	281	2315	10	85	4	4	13	44
0.1g bWHc	3445	1294	782	278	2243	15	80	8	7	14	51
0.1g bWHc	3464	1344	828	291	2292	30	75	9	7	15	57
0.1g bWHc	3411	1322	794	282	2302	60	70	13	10	16	63
0.1g bWHc	3425	1369	836	288	2407	90	65	14	11	17	66

0.1g bWHc	3401	1315	841	288	2369	120	60	19	12	18	76
0.1g bWHc 1	3923	1374	834	320	3284	0	100	0	0	0	0
0.1g bWHc 1	3016	1060	634	235	2299	3	95	3	2	2	27
0.1g bWHc 1	3589	1246	729	276	2701	5	90	6	5	4	38
0.1g bWHc 1	3796	1207	830	265	2953	10	85	13	4	7	41
0.1g bWHc 1	3973	1226	761	252	3175	15	80	17	9	9	47
0.1g bWHc 1	4028	1263	765	272	3149	30	75	19	11	9	59
0.1g bWHc 1	3561	1151	669	250	2824	60	70	20	13	10	66
0.1g bWHc 1	4143	1369	823	287	3198	90	65	22	13	11	79
0.1g bWHc 1	3771	1304	816	278	3085	120	60	23	13	11	82
0.1g bWHc 2	3969	1249	781	275	2272	0	100	0	0	0	0
0.1g bWHc 2	3447	1060	647	235	1969	3	95	4	3	1	7
0.1g bWHc 2	4375	1310	812	270	2249	5	90	7	5	4	26
0.1g bWHc 2	4147	1219	733	266	2219	10	85	11	7	4	28
0.1g bWHc 2	4258	1195	745	254	2122	15	80	15	9	7	41
0.1g bWHc 2	4306	1241	839	272	2249	30	75	16	8	7	43
0.1g bWHc 2	4232	1201	754	263	2189	60	70	19	11	8	50
0.1g bWHc 2	4454	1294	728	281	2320	90	65	20	14	9	55
0.1g bWHc 2	4285	1265	722	275	2296	120	60	22	15	9	59
0.5g bWHc	3966	1459	938	394	2971	0	100	0	0	0	0
0.5g bWHc	3664	1182	707	261	2150	3	95	10	8	10	45
0.5g bWHc	3627	1199	755	284	2293	5	90	11	8	9	42

0.5g bWHc	3661	1220	749	264	2189	10	85	14	10	11	57
0.5g bWHc	3756	1292	823	273	2196	15	80	15	10	12	66
0.5g bWHc	3727	1285	837	258	2111	30	75	18	11	14	76
0.5g bWHc	3547	1238	794	258	2065	60	70	20	13	15	81
0.5g bWHc	3490	1211	787	267	2082	90	65	23	14	15	85
0.5g bWHc	3204	1113	661	245	1981	120	60	26	18	16	89
0.5g bWHc 1	4313	1365	789	277	2790	0	100	0	0	0	0
0.5g bWHc 1	4061	1143	687	252	2119	3	95	8	4	2	36
0.5g bWHc 1	4176	1248	773	266	2238	5	90	8	3	2	39
0.5g bWHc 1	4282	1275	826	269	2215	10	85	10	3	3	49
0.5g bWHc 1	4232	1285	822	273	2196	15	80	12	4	4	55
0.5g bWHc 1	4142	1237	737	264	2114	30	75	15	8	5	62
0.5g bWHc 1	4163	1234	791	257	2120	60	70	18	8	6	68
0.5g bWHc 1	4125	1201	762	244	2022	90	65	21	10	8	77
0.5g bWHc 1	3883	1163	685	244	2022	120	60	22	12	8	79
0.5g bWHc 2	3771	1363	804	280	2896	0	100	0	0	0	0
0.5g bWHc 2	3754	1272	788	273	2241	3	95	6	2	2	47
0.5g bWHc 2	3746	1301	807	269	2252	5	90	8	3	3	54
0.5g bWHc 2	3645	1267	799	265	2199	10	85	11	4	4	60
0.5g bWHc 2	3654	1264	798	271	2190	15	80	14	6	5	68
0.5g bWHc 2	3745	1295	822	268	2254	30	75	17	8	6	75
0.5g bWHc 2	3514	1205	783	259	2119	60	70	20	9	7	82

0.5g bWHc 2	3389	1203	747	265	2120	90	65	21	11	7	85
0.5g bWHc 2	3240	1173	727	246	2036	120	60	23	13	9	92
0.75g bWHc	3527	1189	761	272	2265	0	100	0	0	0	0
0.75g bWHc	4312	1238	774	267	2221	3	95	10	7	6	36
0.75g bWHc	4267	1170	703	254	2112	5	90	15	11	7	46
0.75g bWHc	4596	1228	776	260	2148	10	85	18	12	9	58
0.75g bWHc	4886	1184	717	255	2129	15	80	23	16	11	69
0.75g bWHc	5568	1243	788	244	2065	30	75	28	17	13	86
0.75g bWHc	5747	1246	802	249	2028	60	70	30	19	14	93
0.75g bWHc	5874	1157	696	243	1973	90	65	34	22	15	100
0.75g bWHc	5827	1162	653	225	1841	120	60	35	24	16	107
0.75g bWHc 1	2989	1226	789	280	2302	0	100	0	0	0	0
0.75g bWHc 1	3631	1264	821	271	2255	3	95	13	8	7	42
0.75g bWHc 1	3863	1254	805	265	2201	5	90	19	12	10	61
0.75g bWHc 1	3389	1219	796	255	2118	10	85	17	10	9	56
0.75g bWHc 1	4019	1218	780	253	2099	15	80	27	17	13	83
0.75g bWHc 1	3928	1249	791	260	2120	30	75	28	18	13	86
0.75g bWHc 1	3739	1177	724	246	1992	60	70	31	20	14	94
0.75g bWHc 1	3670	1215	780	241	1950	90	65	32	20	15	100
0.75g bWHc 1	3729	1164	697	243	1933	120	60	36	24	16	108
0.75g bWHc 2	3214	1259	802	283	2310	0	100	0	0	0	0
0.75g bWHc 2	3761	1236	801	269	2198	3	95	13	7	6	39

0.75g bWHc 2	3291	1272	811	262	2191	5	90	7	4	5	28
0.75g bWHc 2	4215	1180	707	261	2127	10	85	25	17	11	68
0.75g bWHc 2	4063	1203	731	257	2136	15	80	25	17	11	70
0.75g bWHc 2	3968	1234	780	257	2118	30	75	26	16	12	75
0.75g bWHc 2	4204	1185	712	252	2074	60	70	32	21	14	88
0.75g bWHc 2	3221	1197	710	238	1971	90	65	24	17	12	76
0.75g bWHc 2	4062	1209	743	245	1997	120	60	35	22	16	100
1g bWHc	2606	1065	776	265	2166	0	100	0	0	0	0
1g bWHc	3326	1223	805	248	2041	3	95	10	11	9	58
1g bWHc	3294	1164	742	241	1975	5	90	15	15	11	69
1g bWHc	4263	714	474	140	1146	10	85	43	32	22	142
1g bWHc	3785	1192	782	235	1931	15	80	25	21	16	100
1g bWHc	3852	1133	736	223	1823	30	75	31	25	18	112
1g bWHc	3848	1122	725	217	1779	60	70	33	26	19	120
1g bWHc	4050	1096	710	212	1728	90	65	38	29	20	131
1g bWHc	3831	1074	659	214	1723	120	60	39	31	21	132
1g bWHc 1	3278	1360	942	315	2799	0	100	0	0	0	0
1g bWHc 1	3306	1212	790	246	2056	3	95	11	10	8	62
1g bWHc 1	3519	1251	769	232	1921	5	90	15	14	11	86
1g bWHc 1	3858	751	509	151	1227	10	85	41	28	19	138
1g bWHc 1	3514	1146	724	235	1935	15	80	25	20	13	97
1g bWHc 1	3737	1195	784	233	1897	30	75	29	21	15	112

1g bWHc 1	3675	1137	743	216	1750	60	70	32	23	17	123
1g bWHc 1	3650	1061	705	205	1688	90	65	37	26	18	130
1g bWHc 1	3874	1097	694	214	1734	120	60	40	29	19	138
1g bWHc 2	2753	1192	788	268	2391	0	100	0	0	0	0
1g bWHc 2	3264	1289	848	259	2071	3	95	9	6	7	63
1g bWHc 2	3391	1260	827	243	1989	5	90	16	11	10	80
1g bWHc 2	3496	1035	684	205	1652	10	85	30	19	14	110
1g bWHc 2	3526	1178	777	231	1937	15	80	27	18	13	101
1g bWHc 2	3751	1165	764	221	1972	30	75	33	21	16	112
1g bWHc 2	3436	1150	760	214	1738	60	70	32	21	16	121
1g bWHc 2	3311	1046	677	205	1668	90	65	37	24	17	128
1g bWHc 2	3496	1049	641	209	1700	120	60	41	28	19	136
2g bWHc	3781	1391	999	319	2922	0	100	0	0	0	0
2g bWHc	4293	1148	745	217	1839	3	95	19	16	11	86
2g bWHc	4282	1165	755	227	1916	5	90	20	17	11	87
2g bWHc	4590	1054	644	192	1619	10	85	28	23	15	112
2g bWHc	4844	1105	709	199	1685	15	80	30	23	16	117
2g bWHc	6825	1286	834	206	1701	30	75	37	28	19	138
2g bWHc	5316	1215	727	196	1587	60	70	34	27	18	133
2g bWHc	5697	975	572	166	1346	90	65	42	32	20	146
2g bWHc	4916	1018	620	163	1313	120	60	40	30	19	144
2g bWHc 1	3655	1427	986	331	2822	0	100	0	0	0	0

2g bWHc 1	4293	1141	747	221	1872	3	95	22	17	13	84
2g bWHc 1	4064	1146	742	216	1822	5	90	22	17	13	87
2g bWHc 1	3903	1150	739	210	1752	10	85	23	17	14	92
2g bWHc 1	4057	1109	713	191	1637	15	80	28	21	16	106
2g bWHc 1	4401	1090	687	187	1542	30	75	33	24	18	120
2g bWHc 1	4387	1026	623	174	1424	60	70	37	27	19	128
2g bWHc 1	4764	972	601	158	1297	90	65	42	30	21	140
2g bWHc 1	4610	1024	624	166	1343	120	60	42	30	21	141
2g bWHc 2	4132	1575	1150	343	3249	0	100	0	0	0	0
2g bWHc 2	4098	1160	749	216	1840	3	95	18	17	10	85
2g bWHc 2	4027	1089	685	210	1781	5	90	22	20	11	92
2g bWHc 2	4317	1088	671	205	1722	10	85	27	23	13	105
2g bWHc 2	4733	1097	681	202	1689	15	80	32	26	15	118
2g bWHc 2	4962	1083	674	183	1555	30	75	35	28	17	130
2g bWHc 2	4407	1022	645	169	1498	60	70	36	28	17	129
2g bWHc 2	4491	1052	642	167	1462	90	65	37	30	18	135
2g bWHc 2	4523	1011	615	164	1420	120	60	35	31	19	136

Effect of temperature on metal adsorption

		Concentration (mg/g)					**Time**	**volume**	**Mass removed(mg)**				
Sample ID		Ca^{2+}	K^{+}	Mg^{2+}	Na^{+}	Fe^{2+}	**(mins)**	**(ml)**	Ca^{2+}	K^{+}	Mg^{2+}	Na^{+}	Fe^{2+}
298K	RUN 1	659.5	1867.7	54.3	418.9	3.4	0.0	100.0	0.0	0.0	0.0	0.0	0.0

298K		659.5	1896.5	44.6	408.3	0.0	3.0	93.0	4.6	10.4	1.3	3.9	0.3
298K		657.5	1835.9	43.2	406.4	0.0	5.0	86.0	9.4	28.9	1.7	6.9	0.3
298K		659.7	1819.2	44.5	423.0	0.0	10.0	79.0	13.8	43.1	1.9	8.5	0.3
298K		651.4	1836.9	44.5	418.5	0.0	15.0	72.0	19.1	54.5	2.2	11.8	0.3
298K		649.9	1836.9	45.1	416.2	0.0	30.0	65.0	23.7	67.4	2.5	14.8	0.3
298K		651.4	1844.4	45.1	421.1	0.0	60.0	58.0	28.2	79.8	2.8	17.5	0.3
298K		633.8	1826.0	42.4	421.6	0.0	90.0	51.0	33.6	93.6	3.3	20.4	0.3
298K		621.4	1801.2	43.8	409.2	0.0	120.0	44.0	38.6	107.5	3.5	23.9	0.3
298K	RUN 2	659.5	1867.7	54.3	418.9	3.4	0.0	100.0	0.0	0.0	0.0	0.0	0.0
298K		655.5	1837.0	44.6	414.4	0.0	3.0	93.0	5.0	15.9	1.3	3.3	0.3
298K		657.5	1820.3	43.2	410.3	0.0	5.0	86.0	9.4	30.2	1.7	6.6	0.3
298K		661.7	1838.0	44.5	411.6	0.0	10.0	79.0	13.7	41.6	1.9	9.4	0.3
298K		641.4	1838.1	44.5	414.0	0.0	15.0	72.0	19.8	54.4	2.2	12.1	0.3
298K		654.9	1845.6	45.1	396.5	0.0	30.0	65.0	23.4	66.8	2.5	16.1	0.3
298K		653.4	1827.2	45.1	395.8	0.0	60.0	58.0	28.1	80.8	2.8	18.9	0.3
298K		635.8	1802.3	42.4	406.8	0.0	90.0	51.0	33.5	94.8	3.3	21.1	0.3
298K		622.4	1796.9	43.8	401.1	0.0	120.0	44.0	38.6	107.7	3.5	24.2	0.3
298K	RUN 3	659.5	1867.7	54.3	418.9	3.4	0.0	100.0	0.0	0.0	0.0	0.0	0.0
298K		654.0	1838.5	45.8	410.2	0.0	3.0	93.0	5.1	15.8	1.2	3.7	0.3
298K		656.0	1821.8	44.5	409.4	0.0	5.0	86.0	9.5	30.1	1.6	6.7	0.3
298K		660.2	1839.6	45.7	410.1	0.0	10.0	79.0	13.8	41.4	1.8	9.5	0.3
298K		639.9	1839.6	45.7	410.7	0.0	15.0	72.0	19.9	54.3	2.1	12.3	0.3

298K		653.4	1847.1	46.4	409.6	0.0	30.0	65.0	23.5	66.7	2.4	15.3	0.3
298K		651.9	1828.7	46.4	409.6	0.0	60.0	58.0	28.1	80.7	2.7	18.1	0.3
298K		634.3	1803.9	43.6	410.7	0.0	90.0	51.0	33.6	94.8	3.2	20.9	0.3
298K		620.9	1798.4	45.0	403.8	0.0	120.0	44.0	38.6	107.6	3.5	24.1	0.3
308K	RUN 1	668.8	1806.1	56.7	371.1	4.2	0.0	100.0	0.0	0.0	0.0	0.0	0.0
308K		664.7	1829.9	48.8	363.8	0.0	3.0	93.0	5.1	10.4	1.1	3.3	0.4
308K		663.8	1832.7	48.8	367.2	0.0	5.0	86.0	9.8	23.0	1.5	5.5	0.4
308K		672.2	1845.1	49.2	369.7	0.0	10.0	79.0	13.8	34.8	1.8	7.9	0.4
308K		669.9	1842.0	48.9	369.4	0.0	15.0	72.0	18.6	48.0	2.1	10.5	0.4
308K		665.5	1854.7	48.8	366.8	0.1	30.0	65.0	23.6	60.1	2.5	13.3	0.4
308K		663.2	1840.9	48.6	368.6	0.0	60.0	58.0	28.4	73.8	2.9	15.7	0.4
308K		663.3	1857.6	48.0	370.3	0.0	90.0	51.0	33.1	85.9	3.2	18.2	0.4
308K		671.4	1872.6	47.7	375.0	0.2	120.0	44.0	37.3	98.2	3.6	20.6	0.4
308K	RUN 2	668.8	1806.1	56.7	371.1	4.2	0.0	100.0	0.0	0.0	0.0	0.0	0.0
308K		679.1	1886.0	48.7	372.3	0.1	3.0	93.0	3.7	5.2	1.1	2.5	0.4
308K		670.0	1874.5	48.9	371.6	0.0	5.0	86.0	9.3	19.4	1.5	5.1	0.4
308K		667.6	1858.4	48.4	367.7	0.0	10.0	79.0	14.1	33.8	1.8	8.1	0.4
308K		673.6	1867.5	49.1	370.8	0.0	15.0	72.0	18.4	46.2	2.1	10.4	0.4
308K		671.7	1867.9	48.6	372.5	0.0	30.0	65.0	23.2	59.2	2.5	12.9	0.4
308K		668.9	1859.0	48.5	370.3	0.0	60.0	58.0	28.1	72.8	2.9	15.6	0.4
308K		662.5	1832.0	48.6	371.0	0.1	90.0	51.0	33.1	87.2	3.2	18.2	0.4
308K		664.6	1832.9	48.7	372.1	0.0	120.0	44.0	37.6	100.0	3.5	20.7	0.4

308K	RUN 3	668.8	1806.1	56.7	371.1	4.2	0.0	100.0	0.0	0.0	0.0	0.0	0.0
308K		676.0	1825.0	46.5	367.5	0.0	3.0	93.0	4.0	10.9	1.4	2.9	0.4
308K		671.4	1834.2	48.5	366.7	0.0	5.0	86.0	9.1	22.9	1.5	5.6	0.4
308K		672.7	1824.2	48.2	367.7	0.0	10.0	79.0	13.7	36.5	1.9	8.1	0.4
308K		677.1	1837.5	48.9	372.6	0.0	15.0	72.0	18.1	48.3	2.2	10.3	0.4
308K		670.2	1824.9	48.8	370.3	0.0	30.0	65.0	23.3	62.0	2.5	13.0	0.4
308K		666.7	1806.8	48.8	368.8	0.0	60.0	58.0	28.2	75.8	2.8	15.7	0.4
308K		659.6	1813.7	48.7	364.9	0.0	90.0	51.0	33.2	88.1	3.2	18.5	0.4
308K		656.3	1807.9	48.4	361.4	0.0	120.0	44.0	38.0	101.1	3.5	21.2	0.4
318K	RUN 1	660.7	1780.4	50.4	368.4	4.4	0.0	100.0	0.0	0.0	0.0	0.0	0.0
318K		671.7	1818.9	46.4	369.4	0.0	3.0	93.0	3.6	8.9	0.7	2.5	0.4
318K		670.7	1821.3	46.1	368.9	0.0	5.0	86.0	8.4	21.4	1.1	5.1	0.4
318K		684.8	1835.6	46.7	371.1	0.0	10.0	79.0	12.0	33.0	1.4	7.5	0.4
318K		683.8	1841.0	46.8	374.2	0.1	15.0	72.0	16.8	45.5	1.7	9.9	0.4
318K		679.2	1902.9	45.3	374.7	0.0	30.0	65.0	21.9	54.3	2.1	12.5	0.4
318K		679.4	1928.6	46.4	374.9	0.0	60.0	58.0	26.7	66.2	2.4	15.1	0.4
318K		675.6	1896.6	46.3	370.4	0.0	90.0	51.0	31.6	81.3	2.7	17.9	0.4
318K		672.3	1888.9	44.6	384.3	0.0	120.0	44.0	36.5	94.9	3.1	19.9	0.4
318K	RUN 2	661.7	1785.4	50.8	368.4	4.4	0.0	100.0	0.0	0.0	0.0	0.0	0.0
318K		676.2	1874.4	46.1	369.4	0.0	3.0	93.0	3.3	4.2	0.8	2.5	0.4
318K		671.4	1914.1	46.1	368.9	0.0	5.0	86.0	8.4	13.9	1.1	5.1	0.4
318K		673.2	1908.3	46.1	371.1	0.1	10.0	79.0	13.0	27.8	1.4	7.5	0.4

318K		676.1	1968.6	44.9	374.2	0.1	15.0	72.0	17.5	36.8	1.9	9.9	0.4
318K		646.1	1926.8	45.3	374.7	0.1	30.0	65.0	24.2	53.3	2.1	12.5	0.4
318K		646.8	1903.7	46.2	374.9	0.1	60.0	58.0	28.7	68.1	2.4	15.1	0.4
318K		665.5	1930.4	46.3	370.4	0.1	90.0	51.0	32.2	80.1	2.7	17.9	0.4
318K		672.7	1943.3	46.8	384.3	0.0	120.0	44.0	36.6	93.0	3.0	19.9	0.4
318K	RUN 3	662.7	1787.4	50.6	368.4	4.4	0.0	100.0	0.0	0.0	0.0	0.0	0.0
318K		681.6	1979.0	46.3	370.6	0.1	3.0	93.0	2.9	-5.3	0.8	2.4	0.4
318K		678.2	1918.9	46.7	370.2	0.0	5.0	86.0	7.9	13.7	1.1	5.0	0.4
318K		678.1	1876.7	46.0	372.4	0.0	10.0	79.0	12.7	30.5	1.4	7.4	0.4
318K		676.0	1895.0	47.0	375.4	0.1	15.0	72.0	17.6	42.3	1.7	9.8	0.4
318K		673.7	1949.5	46.8	375.9	0.0	30.0	65.0	22.5	52.0	2.0	12.4	0.4
318K		675.8	1909.4	46.2	376.2	0.0	60.0	58.0	27.1	68.0	2.4	15.0	0.4
318K		671.2	1881.4	46.8	371.7	0.0	90.0	51.0	32.0	82.8	2.7	17.9	0.4
318K		674.7	1894.1	46.2	385.5	0.0	120.0	44.0	36.6	95.4	3.0	19.9	0.4

Effect of temperature on phenolic adsorption

Sample ID		Areas					t mins	Volume(ml)	mass removed mg			
		Gallic acid	Vanillyl alcohol	Resorcinol	Phenol	Guai acol			Vanillyl alcohol	Resor-cinol	Phenol	Guai acol
298K	Run 1	5440.96	1257.68	1076.55	299.18	194.95	0	100	0.00	0.00	0.00	0.00
298K		5538.82	1241.32	1075.57	272.40	188.74	3	93	3.70	2.75	2.79	0.00
298K		5477.53	1288.73	1090.06	254.50	190.47	5	86	4.69	4.26	4.53	0.98
298K		5111.09	1131.23	1047.91	244.73	174.31	10	79	9.16	5.73	5.17	1.40
298K		5190.01	1127.33	1069.63	244.75	169.67	15	72	12.17	7.89	6.34	2.09
298K		4943.78	1130.90	1116.77	241.99	169.73	30	65	13.42	8.14	6.99	2.90
298K		4980.25	1104.48	1026.51	236.09	170.15	60	58	16.69	12.49	8.29	3.19
298K		5117.91	1110.94	1054.72	263.12	169.15	90	51	19.61	14.80	8.67	3.77
298K		5024.18	1099.38	1014.38	263.49	166.93	120	44	21.95	17.39	9.62	4.47
298K	Run 2	5535.99	1272.71	1081.58	302.21	199.98	0	100	0.00	0.00	0.00	5.00
298K		5533.85	1236.35	1090.60	267.43	183.77	3	93	3.60	1.93	2.91	0.00
298K		5472.56	1183.76	1085.09	249.53	185.50	5	86	7.14	3.96	4.64	1.24
298K		5106.12	1126.26	1032.94	239.76	169.34	10	79	9.06	5.67	5.28	1.64
298K		5185.04	1122.36	1064.66	239.78	164.70	15	72	12.05	7.58	6.42	2.34
298K		4938.81	1125.93	1111.80	237.02	164.76	30	65	13.30	7.82	7.05	3.12
298K		4975.28	1099.51	1021.54	231.12	165.18	60	58	16.56	12.17	8.34	3.40
298K		5112.94	1105.97	1049.75	258.15	164.18	90	51	19.46	14.46	8.70	3.98

298K		5019.21	1094.41	1009.41	258.52	161.96	120	44	21.81	17.05	9.63	4.65
298K	Run 3	5449.27	1285.99	1097.66	291.49	203.26	0	100	0.00	0.00	0.00	5.17
298K		5547.13	1249.63	1093.88	280.71	197.05	3	93	4.31	2.88	1.94	0.00
298K		5485.84	1197.04	1088.37	262.81	198.78	5	86	7.87	4.92	3.71	1.01
298K		5119.40	1139.54	1036.22	253.04	182.62	10	79	9.79	6.62	4.36	1.45
298K		5198.32	1135.64	1077.94	253.06	177.98	15	72	12.81	8.32	5.56	2.15
298K		4952.09	1139.21	1125.08	250.30	178.04	30	65	14.07	8.58	6.22	2.98
298K		4988.56	1112.79	1034.82	244.40	178.46	60	58	17.35	12.94	7.56	3.28
298K		5126.22	1119.25	1063.03	271.43	177.46	90	51	20.29	15.26	7.99	3.90
298K		5032.49	1107.69	1022.69	271.80	175.24	120	44	22.65	17.87	8.96	4.63
308K	Run 1	4469.21	1190.20	1099.17	240.91	177.98	0	100	0.00	0.00	0.00	5.18
308K		4402.16	1140.30	1088.88	236.91	172.66	3	93	4.14	2.54	1.16	0.00
308K		4913.01	1298.87	1085.88	241.13	171.70	5	86	6.34	8.91	3.53	0.79
308K		4393.86	1001.87	824.22	185.55	135.25	10	79	14.03	15.59	6.19	2.30
308K		4700.98	1158.93	1146.72	247.13	193.51	15	72	14.46	11.22	4.84	3.66
308K		4246.52	1001.60	993.60	205.04	163.67	30	65	18.39	14.97	6.79	2.40
308K		4581.70	1101.86	1014.61	219.27	169.60	60	58	20.64	18.74	7.88	3.48
308K		5182.11	1102.66	1053.99	241.30	172.37	90	51	25.68	22.69	9.09	4.33
308K		5256.91	1149.62	1093.39	251.91	179.22	120	44	27.69	24.63	9.90	5.39
308K	Run 2	4482.73	1194.38	1086.07	243.65	178.73	0	100	0.00	0.00	0.00	5.85
308K		4672.19	1218.36	1135.91	246.85	179.65	3	93	3.89	2.58	1.57	0.00
308K		4466.74	1193.08	1016.37	216.60	154.16	5	86	5.98	7.43	3.81	0.97

308K		4752.14	1146.25	919.03	204.53	143.77	10	79	12.35	14.28	6.14	2.40
308K		4311.49	1048.24	1069.24	245.38	174.28	15	72	14.88	10.16	4.03	3.76
308K		4888.94	1132.79	1116.86	238.12	180.43	30	65	18.85	14.96	6.84	2.54
308K		4729.43	1095.51	959.81	234.91	168.17	60	58	21.50	19.87	7.70	3.74
308K		5249.04	1113.63	1023.09	245.78	176.53	90	51	25.76	22.79	9.19	4.54
308K		5328.31	1161.74	1071.71	255.38	182.75	120	44	27.75	24.53	10.03	5.36
308K	Run 3	4724.83	1254.16	1137.60	245.21	174.69	0	100	0.00	0.00	0.00	5.84
308K		4449.42	1147.21	1078.96	232.40	159.91	3	93	4.18	2.43	1.00	0.00
308K		4578.56	1187.69	1035.97	214.89	145.13	5	86	6.89	7.37	3.48	0.84
308K		4995.31	1171.34	914.76	199.18	136.25	10	79	13.05	15.33	6.15	2.29
308K		4462.66	1112.05	1077.52	245.60	168.22	15	72	14.00	10.68	3.70	3.64
308K		4561.70	1084.90	1049.39	197.76	151.97	30	65	18.04	14.56	7.15	2.32
308K		4273.53	1001.64	938.53	204.43	144.19	60	58	21.08	18.09	7.28	3.61
308K		5168.55	1096.31	947.48	244.56	159.14	90	51	25.60	23.49	8.37	4.10
308K		4117.27	905.08	812.45	187.03	133.35	120	44	27.46	24.56	9.62	5.01
318K	Run 1	5222.36	1299.55	1199.03	269.86	182.32	0	100	0.00	0.00	0.00	5.36
318K		4840.47	1169.66	1054.26	252.25	174.69	3	93	3.93	4.31	0.97	0.00
318K		4940.21	1150.89	1106.77	238.41	171.98	5	86	7.89	5.89	3.07	0.32
318K		4885.53	1056.09	1016.75	222.80	143.97	10	79	12.71	10.40	4.72	1.17
318K		5815.88	1163.55	1086.81	250.59	171.55	15	72	17.06	15.16	6.23	2.74
318K		6294.52	1126.88	1036.52	239.66	166.91	30	65	21.56	19.55	8.12	3.22
318K		6964.39	1116.76	996.59	234.09	155.69	60	58	25.37	23.39	9.70	4.17

318K		6883.16	1084.15	952.06	253.23	174.42	90	51	27.43	25.37	9.92	5.17
318K		6305.39	1084.80	984.49	251.31	165.02	120	44	28.18	25.67	10.29	5.18
318K	Run 2	5011.15	1280.47	1183.69	244.68	178.21	0	100	0.00	0.00	0.00	5.51
318K		4824.86	1162.68	1083.37	233.06	170.25	3	93	5.11	4.37	1.18	0.00
318K		4880.31	1169.18	1086.14	218.80	173.40	5	86	8.06	7.15	3.10	0.65
318K		4993.19	1093.06	1022.03	216.25	145.65	10	79	13.44	11.89	4.41	1.18
318K		5871.45	1135.10	1085.65	236.67	171.35	15	72	18.94	16.44	5.97	2.95
318K		6043.86	1137.94	999.33	228.21	169.18	30	65	21.67	20.54	7.32	3.43
318K		6328.74	1118.11	1006.08	223.01	156.24	60	58	24.91	22.97	8.56	4.09
318K		6562.22	1091.97	977.44	239.45	164.69	90	51	27.78	25.56	9.11	5.01
318K		5899.59	1058.31	934.33	232.46	162.39	120	44	28.75	26.57	9.49	5.37
318K	Run 3	5032.29	1285.08	1179.38	240.75	180.81	0	100	0.00	0.00	0.00	5.53
318K		4856.01	1147.83	1056.76	229.34	177.05	3	93	5.79	5.10	1.18	0.00
318K		4958.21	1145.52	983.59	221.24	168.38	5	86	9.23	10.17	2.85	0.48
318K		4905.38	1064.34	1026.17	201.55	141.30	10	79	13.67	11.02	4.64	1.59
318K		5910.36	1137.49	1049.91	232.00	176.97	15	72	19.01	16.98	5.90	3.11
318K		5911.93	1119.83	1013.10	212.08	172.86	30	65	21.53	19.62	7.39	3.39
318K		5906.31	1082.68	999.84	215.82	160.88	60	58	24.26	21.72	8.03	3.99
318K		6516.72	1161.66	1039.53	247.58	183.93	90	51	26.77	24.41	8.58	4.75
318K		6053.68	1078.89	986.97	228.85	165.26	120	44	28.80	25.94	9.41	5.08

Effect of initial concentration on metal and phenolic adsorption of hydrochar

		Areas				Time	volume ml	Remaining mass (mg)			
	Area of Gallic acid	Vanillyl alcohol area	Resorcinol area	Phenol area	Guaiacol	mins	ml	Vanillyl alcohol	Resorcinol	Phenol	Guaiacol
x1	3763.04	1187.39	803.91	349.86	2021.92	0	100	51	34	28	127
	3790.70	1225.61	832.21	361.67	2080.54	3	97	51	34	28	125
	3873.78	1224.21	827.02	361.75	2087.92	5	94	48	32	26	119
	3832.78	1179.68	781.30	351.11	2030.00	10	91	46	30	25	114
	3887.37	1225.06	826.84	356.55	2058.60	15	88	45	30	24	110
	3749.65	1206.74	792.31	354.83	2048.46	30	85	45	29	24	109
	3861.11	999.20	656.70	295.62	1713.86	60	82	35	22	19	86
	3855.23	1256.41	820.71	355.16	1969.06	90	79	42	27	22	95
	3825.87	1213.46	804.17	358.48	2043.14	120	76	39	25	21	96
x3	3776.01	3128.75	2156.60	921.50	6222.92	0	100	135	91	74	388
	3729.81	3088.65	2128.94	900.71	6092.25	3	97	131	88	71	373
	3656.75	3027.10	2047.14	892.18	6043.91	5	94	127	84	69	366
	3630.19	3005.07	2032.66	890.80	6026.64	10	91	123	81	67	356
	3787.67	3076.85	2090.63	901.16	6153.34	15	88	116	77	63	337
	3829.23	2886.82	1993.85	841.66	5683.13	30	85	104	71	56	297
	3750.08	3211.94	2204.70	945.27	6371.00	60	82	114	77	62	328
	3795.89	3007.55	2043.05	884.46	5953.70	90	79	102	68	56	292
	3789.54	3131.56	2059.66	906.45	5986.61	120	76	102	66	55	283
x10	3792.68	9021.04	6699.35	2631.28	19736.97	0	100	387	282	209	1227
	3793.64	8950.02	6617.10	2651.60	19032.07	3	97	373	270	204	1147
	3726.97	8989.31	6602.74	2642.82	19055.90	5	94	369	266	201	1133
	3788.83	8812.32	6682.49	2634.26	19879.97	10	91	345	256	191	1126
	2391.54	5673.99	4427.92	1639.78	11919.56	15	88	340	260	182	1034
	3432.65	8168.02	6074.04	2459.35	18366.09	30	85	329	240	184	1072
	3627.01	8362.12	6194.68	2486.90	18642.72	60	82	308	223	170	994

	3586.54	8459.5	6169.55	2426.45	17819.12	90	79	303	217	161	925
	3694.61	8863.21	6278.36	2415.62	18179.84	120	76	297	206	150	882

	Sample ID	Ca^{2+}	K^{+}	Mg^{2+}	Na^{+}	Fe^{2+}	time	volume	Ca^{2+}	K^{+}	Mg^{2+}	Na^{+}	Fe^{2+}
		mg/l	mg/l	mg/l	mg/l	mg/l	mins	ml	mg	mg	mg	mg	mg
ICP-OES	X1 0Min	700.162	2184.12	32.5499	267.402	12.9884	0	100	0	0	0	0	0
	X1 3Min	695.059	2046.34	32.289	246.799	9.8462	3	97	3	20	0	3	0
	X1 5Min	683.133	1957.75	32.6679	245.479	3.0673	5	94	6	34	0	4	1
	X1 10Min	681.41	1935.45	32.3515	244.965	0.452	10	91	8	42	0	4	1
	X1 15Min	689.924	1934.98	32.148	245.286	0	15	88	9	48	0	5	1
	X1 30Min	685.133	1909.8	32.1868	241.023	0	30	85	12	56	1	6	1
	X1 60Min	693.323	1925.33	32.3757	243.325	0	60	82	13	61	1	7	1
	X1 90Min	691.537	1913.05	32.1084	247.833	0	90	79	15	67	1	7	1
	X1 120Min	689.441	1904.78	32.2882	244.424	0	120	76	18	74	1	8	1
IC	X1 0Min	780.86	2021.31	69.53	262.56	3877.64	0	100	0	0	0	0	0
	X1 3Min	774.78	1986.54	67.09	256.14	3805.1	3	97	3	9	0	1	19
	X1 5Min	776.89	1987.08	29.55	256.65	3818.57	5	94	5	15	4	2	29
	X1 10Min	775.95	1988.56	66.78	255.21	3810.99	10	91	7	21	1	3	41
	X1 15Min	773.65	1985.34	66.78	255.87	3803.92	15	88	10	27	1	4	53
	X1 30Min	770.76	1978.36	66.36	254.82	3794.85	30	85	13	34	1	5	65
	X1 60Min	770.88	1978.44	66.68	254.78	3782.97	60	82	15	40	1	5	78
	X1 90Min	769.61	1970.39	29.53	256.23	3773.07	90	79	17	46	5	6	90
	X1 120Min	779.1	1992.84	66.63	256.87	3807.66	120	76	19	51	2	7	98
ICP-OES	X3 0Min	2006.71	5421.11	72.3575	574.447	13.2258	0	100	0	0	0	0	0

	X3 3Min	1978.03	5311.18	72.4331	576.445	7.6972	3	97	9	27	0	2	1
	X3 5Min	1967.88	5308.08	72.5501	567.488	2.1529	5	94	16	43	0	4	1
	X3 10Min	1969.26	5251.94	72.4191	561.971	0.8653	10	91	21	64	1	6	1
	X3 15Min	1972.7	5286.8	71.8337	563.491	0	15	88	27	77	1	8	1
	X3 30Min	1944.58	5236.35	72.4623	560.589	0	30	85	35	97	1	10	1
	X3 60Min	1945.17	5204.99	73.7041	562.798	0	60	82	41	115	1	11	1
	X3 90Min	2055.32	5504.12	73.1589	569.277	0	90	79	38	107	1	12	1
	X3 120Min	2092.04	5530.87	73.0691	554.123	0	120	76	42	122	2	15	1
IC	X3 0Min	2242.93	5859.01	115.47	601.97	11337.28	0	100	0	0	0	0	0
	X3 3Min	2202.59	5820.9	106.38	607.8	11424.09	3	97	11	21	1	1	26
	X3 5Min	2249.1	5866.96	115.4	607.55	11383.59	5	94	13	34	1	3	64
	X3 10Min	2244.23	5840.75	115.15	605.26	11327.67	10	91	20	54	1	5	103
	X3 15Min	2241.63	5849.08	115.09	606.92	11346.1	15	88	27	71	1	7	135
	X3 30Min	2260.5	5891.81	115.8	611.59	11420.57	30	85	32	85	2	8	163
	X3 60Min	2259.24	5889.51	115.99	611.63	11406.42	60	82	39	103	2	10	198
	X3 90Min	2273.6	5901.67	116.13	612.1	11481.92	90	79	45	120	2	12	227
	X3 120Min	2238.96	5860.87	115.32	605.43	11411.18	120	76	54	0	3	14	266
ICP-OES	X10 0Min	6780.58	17919.9	233.235	1823.41	13.3856	0	100	0	0	0	0	0
	X10 3Min	6783.98	17985.5	234.097	1819.99	8.3798	3	97	20	47	1	6	1
	X10 5Min	6809.24	18053.9	233.535	1831.22	3.5973	5	94	38	95	1	10	1
	X10 10Min	6851.96	18201.8	237.259	1842.79	1.1528	10	91	55	136	2	15	1
	X10 15Min	6789.89	18072.5	239.282	1837.19	0.4762	15	88	81	202	2	21	1
	X10 30Min	6740	17882	237.169	1808.23	0	30	85	105	272	3	29	1
	X10 60Min	6915.02	18312.5	238.502	1857.45	0	60	82	111	290	4	30	1

	X10 90Min	6792.11	17993.6	234.967	1819.13	0	90	79	141	370	5	39	1
	X10 120Min	6908.53	18299.8	238.786	1846.71	0	120	76	153	401	5	42	1
IC	X10 0Min	7257.63	19617.86	268.16	2002.19	0	0	100	0	0	0	0	0
	X10 3Min	7204.3	19430.98	262.61	1982.82	47682.85	3	97	27	77	1	8	253
	X10 5Min	7259.4	19560.72	267.82	1995.89	47391.55	5	94	43	123	2	13	630
	X10 10Min	7252.95	19551.32	277.56	1996.45	47356.18	10	91	66	183	2	19	1018
	X10 15Min	7251.42	19523.43	266.15	1994.75	47245.02	15	88	88	244	3	25	1338
	X10 30Min	7297.98	19652	270.13	2007.23	47872.97	30	85	105	291	4	30	1612
	X10 60Min	7264.72	19252.5	301.14	1959.83	47659.91	60	82	130	383	2	40	1962
	X10 90Min	7244.8	19512.11	262.06	1993.97	47470.54	90	79	153	420	6	43	2241
	X10 120Min	7267.94	19580.68	263.99	1999.9	47527.43	120	76	173	474	7	48	2635

Effect of pH on metal and phenolic adsorption

		Areas						Remaining mass (mg)			
	Area of Gallic acid	Vanillyl alcohol area	Resorcinol area	Phenol area	Guaiacol	Time mins	volume ml	Vanillyl alcohol	Resorcinol	Phenol	Guaiacol
pH2	3944	1004.4	676.5	137.8	984.7	0	100	0.00	0.00	0.00	0.00
	3774	974.2	635	133.1	956.1	3	97	0.70	1.30	0.20	0.90

	4019.9	982.7	644.9	135.5	965.9	5	94	4.00	3.30	1.00	5.60
	4272.4	1018.6	665.8	137.7	1000	10	91	6.10	4.70	1.70	8.60
	3814.3	983.4	643.2	133.9	948.7	15	88	4.50	3.70	1.20	7.30
	4446.1	1253.2	849.4	164.6	1142.7	30	85	2.50	1.50	1.00	7.40
	4773.5	1294.2	898	188	1179.6	60	82	5.30	2.80	0.80	11.10
	4119.1	1015	690	130.6	892.1	90	79	9.80	6.30	3.00	18.50
	4989.8	1340.8	877.5	173	1156.8	120	76	8.20	6.00	2.60	17.30
pH4	3977.3	1174.8	769.4	148.5	1061.4	0	100	0.00	0.00	0.00	0.00
	4184	1098.2	714.8	136.7	979.1	3	97	6.60	4.40	1.70	9.40
	3167.1	826.4	561	100.6	711.9	5	94	8.20	4.30	2.30	13.10
	3806.3	1049.4	684.9	131	933	10	91	7.20	4.70	1.80	10.30
	4100.9	1093.4	714.8	135.9	967.3	15	88	9.90	6.40	2.50	14.00
	4556.4	1282.2	838.4	155.2	1086.2	30	85	9.10	5.90	2.50	15.10
	3999	1100	745.1	135.9	948.3	60	82	11.40	6.50	2.90	17.10
	4304.4	1147.5	772.6	133.5	922.7	90	79	13.80	8.20	3.90	23.00
	3814.5	1086.8	725.9	124.5	836.6	120	76	12.80	7.80	3.80	23.60
pH6	3864.5	996.4	654.4	126.2	903.6	0	100	0.00	0.00	0.00	0.00
	4197.3	1038.9	681	131.4	938.2	3	97	2.90	1.90	0.70	4.00
	4369.5	1146.1	796	146.6	1048.4	5	94	1.80	-0.30	0.30	2.00
	4359.7	1143.1	771.2	140	997.6	10	91	3.10	1.30	1.00	6.00
	4906.7	1256.6	826.9	157.2	1124	15	88	5.30	3.40	1.30	7.60
	3908.8	1000.1	677.9	119.7	888.2	30	85	6.60	3.50	2.00	9.60
	4824.6	1050.6	691.7	126.2	852.3	60	82	12.90	8.30	3.40	21.00
	4630.2	1108.7	728.4	136.1	942.8	90	79	11.20	7.20	2.80	17.20
	4383.7	1005.2	681.4	128.5	847.6	120	76	13.60	8.20	3.10	20.50
pH 8	4129.7	1119.5	794.7	140.9	1021	0	100	0.00	0.00	0.00	0.00
	4013.7	1089.2	767.2	136	978.1	3	97	1.30	1.10	0.40	2.60
	4026.8	1072.4	738.3	138.8	991.5	5	94	3.40	3.20	0.50	3.70

	4137.1	1087.1	767.4	136.3	981.4	10	91	5.20	3.80	1.20	7.40
	4910.7	1291.6	921.2	164.2	1175.9	15	88	6.50	4.40	1.40	8.60
	4333.6	1125.2	771.7	142.2	1027.6	30	85	8.20	6.60	1.90	10.80
	4333.1	1109.2	765.9	140.2	1003.5	60	82	10.00	7.60	2.30	13.50
	4518.7	1138.2	804.9	138.6	998.9	90	79	11.70	8.20	3.00	17.10
	3761.6	933.3	637.3	119.2	834	120	76	13.40	10.20	3.00	18.60
pH 10	3807.1	1102.2	753	146.1	1020.3	0	100	0.00	0.00	0.00	0.00
	3827	1118.9	765.2	139.3	921.6	3	97	1.00	0.60	0.90	8.10
	4432.8	1333	901.6	170.6	1232.1	5	94	1.10	1.10	0.70	1.60
	3594.6	1088.8	760.6	134.8	972.1	10	91	2.30	0.80	1.30	5.20
	4572.4	1311.7	908.3	164.8	1191.2	15	88	6.00	3.70	2.00	9.10
	4096.7	1065.1	722.6	134.6	965	30	85	11.20	7.60	3.10	16.00
	3707.8	915.1	645	112.1	798.3	60	82	14.20	8.80	4.10	21.60
	4385.4	1120.6	792.2	139.2	997.9	90	79	14.30	8.80	4.00	20.80
	4361.4	1115.6	806	143.3	1028.7	120	76	15.50	9.10	4.00	20.90
pH12	3183.7	1081.3	719.6	134.2	968.7	0	100	0.00	0.00	0.00	0.00
	3507.9	1157.4	776.4	147.2	1066.8	3	97	3.20	1.80	0.40	2.20
	3595.2	1113.6	756.7	142.1	1016.8	5	94	7.90	4.50	1.50	9.10
	3492.9	1100.5	727.6	140.4	1015.5	10	91	8.60	5.80	1.70	9.40
	3664.4	1140.5	790.4	142.4	1032.1	15	88	10.70	5.80	2.40	13.30
	3774.4	1133.4	776.7	141.6	1019.1	30	85	13.70	8.20	3.10	17.60
	3762.2	1136.8	786	143.6	1021.7	60	82	14.90	8.70	3.30	19.20
	3402.3	1015.2	698.9	126.5	918	90	79	16.90	10.20	3.90	21.50
	3934.9	1146	761	146.4	1059.8	120	76	19.30	12.60	4.20	23.50

Sample ID	Ca^{2+}	K^{+}	Mg^{2+}	Na^{+}	Fe^{2+}	volume	Ca^{2+}	K^{+}	Mg^{2+}	Na^{+}
	mg/l	mg/l	mg/l	mg/l	mins	ml	mg	mg	mg	mg
pH 2	676.44	1806.38	26.83	202.81	0	100	0	0	0	0
	650.71	1748.84	26.34	193.17	3	97	4.53	11	0.13	1.54
	688.1	1836.81	27.78	200.63	8	94	2.96	7.98	0.07	1.42
	695.78	1831.58	27.7	201.28	11	91	4.33	13.96	0.16	1.96
	696.89	1852.25	27.89	201.27	16	88	6.32	17.64	0.23	2.57
	702.98	1832.91	28.19	202.63	30	85	7.89	24.84	0.29	3.06
	683.82	1804.87	27.96	202.21	60	82	11.57	32.64	0.39	3.7
	676.41	1795.58	26.35	197.73	90	79	14.21	38.79	0.6	4.66
	684.23	1811.74	28.27	198.46	120	76	15.64	42.95	0.53	5.2
pH 4	694.07	1838.81	27.41	197.58	0	100	0	0	0	0
	686.68	1845.36	27.16	225.32	3	97	2.8	4.88	0.11	-2.1
	697.67	1861.23	27.91	199.16	5	94	3.83	8.93	0.12	1.04
	705.31	1867.91	27.89	197.67	10	91	5.22	13.9	0.2	1.77
	690.23	1833.46	27.9	197.41	15	88	8.67	22.54	0.29	2.39
	680.44	1827.79	27.33	195.96	30	85	11.57	28.52	0.42	3.1
	677.56	1808.72	28.25	197.14	60	82	13.85	35.57	0.42	3.59
	678.79	1805.38	28.01	196.62	90	79	15.78	41.26	0.53	4.23
	672.64	1796.41	28.09	196.33	120	76	18.29	47.35	0.61	4.84
pH 6	669.55	1798.15	27.68	195.03	0	100	0	0	0	0
	669.26	1795.79	27.93	194.45	3	97	2.04	5.62	0.06	0.64
	662.43	1775.77	28.18	192.94	8	94	4.69	12.89	0.12	1.37
	683.27	1796.67	28.03	189.56	11	91	4.78	16.32	0.22	2.25
	667.38	1779.93	28	189.66	16	88	8.23	23.18	0.3	2.81
	662.74	1773.78	28.14	195.13	30	85	10.62	29.04	0.38	2.92

	661.47	1763.03	27.76	192.76	60	82	12.71	35.25	0.49	3.7
	653.19	1744.31	27.84	192.32	90	79	15.35	42.01	0.57	4.31
	658.27	1760.15	27.56	190.73	120	76	16.93	46.04	0.67	5.01
pH 8	731.49	1922	26.31	200.97	0	100	0	0	0	0
	739.12	1932.84	26.76	200.91	3	97	1.45	4.71	0.03	0.61
	719.21	1879.8	26.5	200.61	5	94	5.54	15.5	0.14	1.24
	709.56	1863.29	26.51	199.89	10	91	8.58	22.64	0.22	1.91
	726.68	1906.6	26.7	199.7	15	88	9.2	24.42	0.28	2.52
	728.47	1915.64	26.8	202.61	30	85	11.23	29.37	0.35	2.87
	728	1909.05	26.88	200.62	60	82	13.45	35.66	0.43	3.65
	749.91	1966.3	26.6	199.8	90	79	13.91	36.86	0.53	4.31
	720.74	1889.07	26.99	205.73	120	76	18.37	48.63	0.58	4.46
pH 8	752.44	1935.76	60.55	211.54	0	100	0	0	0	0
	758.93	1942.48	59.47	212.08	3	97	1.63	5.16	0.29	0.58
	765.08	1956.51	57.5	214.02	5	94	3.33	9.66	0.65	1.04
	762.44	1655.23	55.12	180.49	10	91	5.86	42.95	1.04	4.73
	758.31	1932.98	59.08	211.32	15	88	8.51	23.47	0.86	2.56
	759.85	1938.62	59.35	212.02	30	85	10.66	28.79	1.01	3.13
	760.98	1940.28	59.62	213.15	60	82	12.84	34.47	1.17	3.68
	759.77	1941.11	59.82	212.13	90	79	15.22	40.23	1.33	4.4
	765.58	1944.93	59.58	213.12	120	76	17.06	45.76	1.53	4.96
pH 10	720.83	1890.26	27.18	205.43	0	100	0	0	0	0
	708.94	1857.44	27.12	201.04	3	97	3.32	8.85	0.09	1.04
	719.82	1887.69	27.4	204.44	8	94	4.42	11.58	0.14	1.33
	706.92	1854.86	27.26	202.8	11	91	7.75	20.23	0.24	2.09
	713.34	1869.14	27.03	202	16	88	9.31	24.54	0.34	2.77
	712.79	1868.32	27.27	202.41	30	85	11.5	30.22	0.4	3.34
	708.35	1857.95	27.2	199.45	60	82	14	36.67	0.49	4.19

	705.07	1845.96	27.19	199.23	90	79	16.38	43.2	0.57	4.8
	733.77	1924.88	27.16	198.19	120	76	16.32	42.74	0.65	5.48
pH 10	766.25	1964.59	59.54	212.21	0	100	0	0	0	0
	762.37	1958.38	59.51	213.43	3	97	2.68	6.5	0.18	0.52
	758.52	1938.22	59.51	211.73	8	94	5.32	14.27	0.36	1.32
	758.45	1937.08	59.5	210.2	11	91	7.61	20.18	0.54	2.09
	764.85	1953.76	59.81	212.12	16	88	9.32	24.53	0.69	2.55
	731.78	1875.29	58.51	201.77	30	85	14.42	37.06	0.98	4.07
	757.62	1925.38	29.51	208.14	60	82	14.5	38.58	3.53	4.15
	756.61	1931.01	29.58	210.64	90	79	16.85	43.91	3.62	4.58
	754.06	1916.74	59.31	208.73	120	76	19.32	50.79	1.45	5.36
pH 12	638.94	1976	10.93	370.37	0	100	0	0	0	0
	646.5	1948.11	0.14	358.49	3	97	1.18	8.63	1.08	2.26
	638.93	1913.54	0.13	357.17	5	94	3.83	17.73	1.08	3.46
	634.99	1905.69	0.19	355.72	10	91	6.11	24.18	1.08	4.67
	626.63	1877.94	0.17	358.37	15	88	8.75	32.34	1.08	5.5
	638.07	1920.18	0.2	357.96	30	85	9.66	34.38	1.08	6.61
	2.36	6.95	0.16	340.9	60	82	63.7	197.03	1.08	9.08
	639.23	1910.68	1.35	360.09	90	79	13.4	46.66	0.99	8.59
	636.24	1906.06	3.42	357.14	120	76	15.54	52.74	0.83	9.89
pH 12	670.21	1913.93	45.64	386.6	0	100	0	0	0	0
	636.15	1939.87	30.12	392.08	3	97	5.31	3.23	1.64	0.63
	666.71	1931.97	29.51	391.56	8	94	4.35	9.79	1.79	1.85
	651.78	1918.68	29.95	386.59	11	91	7.71	16.79	1.84	3.48
	656.22	1893.5	29.81	382.22	16	88	9.27	24.77	1.94	5.02
	664.09	1934.66	29.51	390.33	30	85	10.57	26.95	2.06	5.48
	660.98	1929.88	30.07	330.38	60	82	12.82	33.14	2.1	11.57
	669.2	1925.77	31.03	394.91	90	79	14.15	39.26	2.11	7.46

	652.23	1893.38	29.57	383.09	120	76	17.45	47.5	2.32	9.55

ANNEXURE C: ADSORPTION WITH REAL WASTEWATER (HTL-AQ)

Adsorption of phenolics from HTL-AQ

		Areas									Mass		
	Area of Gallic acid	Vanillyl alcohol	Resor-cinol	catechol	Vanil-lin	Phenol	Guaiacol	4 nitro phenol	time	Volu-me (ml)	Vanillyl alcohol	Resor-cinol	catech
Run 1	4870.20	3748.77	2548.92	139.62	173.95	440.10	139.52	87.41	0	100	0.00	0.00	0.00
	4754.87	3643.80	2600.64	0.00	70.21	459.33	134.50	67.42	3	95	6.79	0.60	4.67
	5113.62	3768.33	2439.18	0.00	60.33	435.42	131.65	73.01	5	90	17.34	15.01	4.67
	5586.15	4323.30	2847.65	0.00	66.43	321.55	129.20	65.33	10	85	18.21	14.37	4.67
	4778.01	3626.71	2626.47	0.00	55.39	335.13	125.54	51.53	15	80	26.45	13.34	4.67
	5015.56	3775.53	2559.82	0.00	53.39	302.89	119.40	28.69	30	75	33.40	22.43	4.67
	4256.05	3165.42	2314.26	0.00	43.60	212.50	100.72	23.26	60	70	40.55	22.77	4.67
	4978.29	3801.43	2669.42	0.00	42.86	213.16	93.91	19.98	90	65	44.50	27.89	4.67
	3583.64	2534.39	1798.99	0.00	0.00	99.02	83.51	19.56	120	60	56.22	35.44	4.67
	5277.82	3930.98	2280.88	0.00	0.00	87.39	80.29	13.07	1200	55	58.61	45.57	4.67
	5504.69	4123.18	2435.87	0.00	0.00	88.73	79.49	0.00	1440	50	64.33	48.19	4.67
Run 2	5168.77	3694.88	2646.98	142.58	211.10	530.37	184.89	290.32	0	100	0.00	0.00	0.00
	5007.90	3595.39	2532.77	0.00	98.58	502.37	174.02	236.35	3	95	5.34	5.05	4.50
	5081.00	3699.80	2714.34	0.00	88.67	439.51	168.90	235.49	5	90	9.69	5.00	4.50
	5168.40	3670.89	2476.80	0.00	76.56	400.77	162.90	221.40	10	85	18.09	16.71	4.50

	5089.63	3715.88	2688.17	0.00	58.04	395.99	132.86	201.72	15	80	21.29	14.29	4.5
	4789.91	3524.45	2586.85	0.00	51.48	336.09	124.58	143.08	30	75	26.53	17.08	4.5
	4859.22	3675.09	2702.25	0.00	51.58	200.64	112.98	83.80	60	70	30.18	19.60	4.5
	4661.83	3366.88	2087.18	0.00	0.00	221.68	101.98	85.22	90	65	39.95	35.27	4.5
	4952.49	3632.63	2370.78	0.00	0.00	157.93	95.37	65.68	120	60	44.72	35.88	4.5
	4924.10	3475.24	2135.02	0.00	0.00	148.64	89.79	52.46	1200	55	53.18	43.65	4.5
	4617.02	3179.38	1839.71	0.00	0.00	125.67	83.86	0.00	1440	50	60.31	49.91	4.5
Run 3	5396.04	3902.76	2570.85	131.01	196.54	563.70	225.59	236.35	0	100	0.00	0.00	0.0
	5060.12	3662.51	2527.23	0.00	238.21	556.21	208.37	235.49	3	95	5.80	0.31	3.9
	5086.81	3634.17	2397.59	0.00	107.10	511.17	184.82	221.40	5	90	13.07	8.33	3.9
	4996.16	3628.56	2479.11	0.00	91.40	470.98	179.65	201.72	10	85	17.24	8.72	3.9
	5362.42	3872.41	2372.08	0.00	86.26	401.87	177.20	143.08	15	80	23.69	19.55	3.9
	5434.52	3902.49	2239.20	0.00	90.87	342.94	158.63	83.80	30	75	30.06	26.71	3.9
	5256.56	3833.94	2158.35	0.00	62.93	295.80	146.59	85.22	60	70	34.62	30.15	3.9
	4748.21	3545.45	2334.50	0.00	52.47	258.63	132.64	65.68	90	65	38.73	25.02	3.9
	4922.52	3635.91	2282.49	0.00	53.34	177.36	124.69	39.23	120	60	45.59	31.62	3.9
	4998.70	3524.34	2026.54	0.00	0.00	165.98	118.07	0.00	1200	55	54.61	40.43	3.9
	4989.34	3298.29	1986.12	0.00	0.00	145.63	119.99	0.00	1440	50	63.93	44.25	3.9

Adsorption of metals from real wastewater

	Concentration in mg/L	Time	Volume	Mass removed mg

										Min	ml								
Run 1	Ca^{2+}	K^{+}	Mg^{2+}	Na^{2+}	Al^{3+}	Ba^{2+}	Fe^{2+}	Mn^{2+}	Zn^{2+}			Ca^{2+}	K^{+}	Mg^{2+}	Na^{2+}	Al^{3+}	Ba^{2+}	Fe^{2+}	Mn^{2+}	Zn^{2+}
	1980.74	3489.56	40.18	9385.07	1.56	1.99	8.56	2.74	1.78	0	100	0.00	0.00	0.00	0.00	0.00	0.00	0.00	0.00	0.00
	2085.64	3401.44	39.98	9253.17	1.26	1.87	8.79	2.47	1.29	3	95	0.06	25.82	0.22	59.46	0.04	0.02	0.02	0.04	0.06
	2090.03	3607.73	38.35	9313.57	1.46	1.75	8.58	2.52	1.42	5	90	9.97	24.26	0.57	100.29	0.02	0.04	0.08	0.05	0.05
	1985.75	3628.72	37.95	9349.60	1.49	1.60	8.28	2.53	1.34	10	85	29.29	40.51	0.79	143.79	0.03	0.06	0.15	0.06	0.06
	1927.49	3604.18	35.73	9248.90	1.39	2.20	8.39	2.54	1.25	15	80	43.87	60.62	1.16	198.60	0.04	0.02	0.18	0.07	0.08
	1984.67	3592.13	32.52	9174.69	1.40	2.24	7.90	2.47	1.10	30	75	49.22	79.55	1.58	250.41	0.05	0.03	0.26	0.09	0.10
	1980.04	3587.92	33.86	9212.04	1.29	2.03	7.18	2.31	0.00	60	70	59.47	97.80	1.65	293.66	0.07	0.06	0.35	0.11	0.18
	1939.60	3561.58	34.55	9134.95	1.28	1.95	6.79	2.30	0.00	90	65	72.00	117.45	1.77	344.74	0.07	0.07	0.41	0.12	0.18
	1925.57	3553.05	35.35	9125.77	1.26	1.66	6.72	2.27	0.00	120	60	82.54	135.77	1.90	390.96	0.08	0.10	0.45	0.14	0.18
	1857.88	3640.85	36.10	9268.30	1.26	1.54	4.80	1.04	0.00	1200	55	95.89	148.71	2.03	428.75	0.09	0.11	0.59	0.22	0.18
	1899.53	3729.67	37.47	9043.20	1.25	1.37	4.52	1.05	0.00	1440	50	103.10	162.47	2.14	486.35	0.09	0.13	0.63	0.22	0.18
Run 2																				
	2365.29	3115.42	221.78	8912.53	1.56	2.84	8.78	2.69	1.78	0	100	0.00	0.00	0.00	0.00	0.00	0.00	0.00	0.00	0.00
	2400.40	3290.36	226.12	9061.96	1.26	2.75	8.92	2.47	1.29	3	95	8.49	-1.04	0.70	30.37	0.04	0.02	0.03	0.03	0.06
	2286.31	3236.30	222.62	8925.50	1.46	2.70	8.70	2.52	1.42	5	90	30.76	20.28	2.14	87.96	0.02	0.04	0.10	0.04	0.05
	2370.71	3287.16	225.69	9033.79	1.49	2.75	8.76	2.53	1.25	10	85	35.02	32.13	2.99	123.38	0.03	0.05	0.13	0.05	0.07
	2384.84	3367.07	226.18	9105.95	1.39	2.72	7.97	2.54	1.10	15	80	45.74	42.18	4.08	162.78	0.04	0.07	0.24	0.07	0.09
	2344.59	3312.50	224.30	9008.23	1.40	2.71	7.14	2.47	0.00	30	75	60.68	63.10	5.36	215.64	0.05	0.08	0.34	0.08	0.18

	2362.87	3315.10	221.46	9017.74	1.29	2.65	6.56	2.31	0.00	60	70	71.13	79.49	6.68	260.01	0.07	0.10	0.42	0.11	0.18
	2398.95	3327.73	219.70	9035.86	1.28	2.61	5.73	2.30	0.00	90	65	80.60	95.24	7.90	303.92	0.07	0.11	0.51	0.12	0.18
	2312.86	3328.42	219.21	9103.17	1.26	2.64	5.04	2.27	0.00	120	60	97.76	111.84	9.03	345.06	0.08	0.13	0.58	0.13	0.18
	2230.98	3210.59	211.45	8780.92	1.21	2.55	4.56	1.19	0.00	1200	55	113.83	134.96	10.55	408.30	0.09	0.14	0.63	0.20	0.18
	2281.64	3283.49	216.25	8980.28	1.24	2.60	3.73	1.24	0.00	1440	50	122.45	147.37	11.37	442.24	0.09	0.15	0.69	0.21	0.18
Run 3																				
	2514.96	3210.09	230.74	9219.46	1.37	2.90	9.07	2.78	1.54	0	100	0.00	0.00	0.00	0.00	0.00	0.00	0.00	0.00	0.00
	2396.20	3315.72	224.48	9076.43	1.34	2.74	9.12	2.46	1.34	3	95	23.86	6.02	1.75	59.69	0.01	0.03	0.04	0.04	0.03
	2365.10	3263.19	220.92	8918.04	1.36	2.69	8.74	2.48	1.12	5	90	38.64	27.32	3.19	119.32	0.01	0.05	0.12	0.05	0.05
	2349.13	3298.38	221.19	9025.79	1.30	2.71	8.60	2.51	1.03	10	85	51.82	40.65	4.27	154.75	0.03	0.06	0.18	0.06	0.07
	2322.45	3318.66	220.00	9039.68	1.22	2.67	8.39	2.51	0.00	15	80	65.70	55.52	5.47	198.77	0.04	0.08	0.24	0.08	0.15
	2314.14	3334.14	218.66	9096.86	1.16	2.67	8.13	2.43	0.00	30	75	77.94	70.95	6.67	239.68	0.05	0.09	0.30	0.10	0.15
	2329.92	3370.77	217.75	9099.38	0.93	2.65	7.93	2.35	0.00	60	70	88.40	85.06	7.83	284.99	0.07	0.10	0.35	0.11	0.15
	2297.54	3331.45	215.95	9019.60	1.14	2.64	7.34	2.34	0.00	90	65	102.16	104.46	9.04	335.67	0.06	0.12	0.43	0.13	0.15
	2320.14	3330.85	214.32	9037.78	1.18	2.64	6.94	2.31	0.00	120	60	112.29	121.16	10.21	379.68	0.07	0.13	0.49	0.14	0.15
	2238.01	3212.94	206.74	8717.84	1.14	2.55	4.66	1.23	0.00	1200	55	128.41	144.30	11.70	442.46	0.07	0.15	0.65	0.21	0.15
	2262.14	3247.58	208.96	8811.84	1.15	2.57	3.75	1.25	0.00	1440	50	138.39	158.63	12.63	481.35	0.08	0.16	0.72	0.22	0.15

Reusability and regeneration data

Metals regeneration and reusability data

	Adsorbate	Cycle 1	Cycle 2	Cycle 3	Cycle 4	Cycle 5	Cycle 6
Mass of metals adsorbed	Ca^{2+}	250.89	152.98	93.64	92.34	6.56	12.03
	K^{+}	312.64	190.64	128.50	222.73	93.26	49.03
	Mg^{2+}	22.96	14.00	9.75	6.74	4.50	1.62
	Na^{+}	888.50	560.49	213.45	461.59	220.62	76.05
	Al^{3+}	0.05	0.05	0.03	0.02	0.01	0.01
	Ba^{2+}	0.29	0.32	0.18	0.04	0.07	0.03
	Fe^{2+}	0.91	0.92	0.54	0.42	0.22	0.14
	Mn^{2+}	0.28	0.20	0.17	0.07	0.07	0.03
	Zn^{2+}	0.15	0.17	0.10	0.06	0.04	0.01
% adsorption	Ca^{2+}	100	61	37	37	3	5
	K^{+}	97	59	40	69	29	15
	Mg^{2+}	100	61	42	29	19	7
	Na^{+}	96	61	23	50	24	8
	Al^{3+}	36	38	23	15	9	5
	Ba^{2+}	100	111	61	14	24	12
	Fe^{2+}	100	101	60	46	24	15
	Mn^{2+}	100	73	62	24	25	12
	Zn^{2+}	100	111	62	42	24	9
Mass of metals desorbed	Ca^{2+}	172.11	104.95	64.23	63.39	4.23	0.66
	K^{+}	361.58	220.49	134.93	133.18	89.23	13.83
	Mg^{2+}	13.30	8.11	4.92	3.10	1.84	0.29
	Na^{+}	49.55	31.26	18.49	18.25	12.23	1.90
	Al^{3+}	0.14	0.15	0.00	0.00	0.00	0.00

	Ba^{2+}	0.27	0.28	0.17	0.00	0.00	0.00
	Fe^{2+}	1.67	1.76	1.04	0.81	0.41	0.06
	Mn^{2+}	0.34	0.25	0.21	0.08	0.08	0.00
	Zn^{2+}	0.16	0.16	0.10	0.07	0.00	0.00
% desorption	Ca^{2+}	69	69	69	69	64	5
	K^{+}	116	116	105	60	96	28
	Mg^{2+}	58	58	50	46	41	18
	Na^{+}	6	6	9	4	6	2
	Al^{3+}	284	287	0	0	0	0
	Ba^{2+}	93	88	94	0	0	0
	Fe^{2+}	184	191	191	191	190	46
	Mn^{2+}	124	124	124	122	124	0
	Zn^{2+}	104	91	104	105	0	0

Phenolic compound regeneration and reusability cycles

	Phenolic compound	Cycle 1	Cycle 2	Cycle 3	Cycle 4
Mass adsorbed	Vanillyl alcohol	104.19	40.43	15.19	4.97
	Resorcinol	69.05	24.57	9.23	3.02
	Catechol	3.96	1.27	0.48	0.16
	Vanillin	2.45	0.95	0.36	0.12
	Phenol	28.88	14.89	5.59	3.74
	Guaiacol	8.82	3.42	1.29	0.42
	4- nitrophenol	8.17	3.17	1.19	0.39
% adsorption	Vanillyl alcohol	89	34	14	4
	Resorcinol	91	32	14	4
	Catechol	100	32	13	4
	Vanillin	100	38	16	5
	Phenol	92	47	20	11
	Guaiacol	90	34	15	4

	4- nitrophenol	100	38	16	5
Mass desorbed	Vanillyl alcohol	33.12	12.85	4.83	2.14
	Resorcinol	18.44	6.56	2.47	1.17
	Catechol	1.33	0.43	0.16	0.13
	Vanillin	0.38	0.15	0.06	0.02
	Phenol	10.86	5.60	2.10	1.41
	Guaiacol	2.78	1.08	0.41	0.24
	4- nitrophenol	1.96	0.76	0.29	0.14
%desorption	Vanillyl alcohol	32	32	32	43
	Resorcinol	27	27	27	39
	Catechol	34	34	34	83
	Vanillin	16	16	16	21
	Phenol	38	38	38	38
	Guaiacol	32	32	32	57
	4- nitrophenol	24	24	24	37